National Library
of Canada

Bibliothèque nationale
du Canada

Canadian Theses Service

Service des thèses canadiennes

Ottawa, Canada
K1A 0N4

NOTICE

The quality of this microform is heavily dependent upon the quality of the original thesis submitted for microfilming. Every effort has been made to ensure the highest quality of reproduction possible.

If pages are missing, contact the university which granted the degree.

Some pages may have indistinct print especially if the original pages were typed with a poor typewriter ribbon or if the university sent us an inferior photocopy.

Previously copyrighted materials (journal articles, published tests, etc.) are not filmed.

Reproduction in full or in part of this microform is governed by the Canadian Copyright Act, R.S.C. 1970, c. C-30.

AVIS

La qualité de cette microforme dépend grandement de la qualité de la thèse soumise au microfilmage. Nous avons tout fait pour assurer une qualité supérieure de reproduction.

S'il manque des pages, veuillez communiquer avec l'université qui a conféré le grade.

La qualité d'impression de certaines pages peut laisser à désirer, surtout si les pages originales ont été dactylographiées à l'aide d'un ruban usé ou si l'université nous a fait parvenir une photocopie de qualité inférieure.

Les documents qui font déjà l'objet d'un droit d'auteur (articles de revue, tests publiés, etc.) ne sont pas microfilmés.

La reproduction, même partielle, de cette microforme est soumise à la Loi canadienne sur le droit d'auteur, SRC 1970, c. C-30.

NL-339 (r. 88/04)

Canada

THE UNIVERSITY OF ALBERTA

THE EFFECTS OF INFRARED LASER IRRADIATION ON ROOT CANAL WALL DENTIN IN HUMAN TEETH

by

DOUGLAS N. DEDERICH

A THESIS

SUBMITTED TO THE FACULTY OF GRADUATE STUDIES AND RESEARCH
IN PARTIAL FULFILLMENT OF THE REQUIREMENTS FOR THE DEGREE OF
DOCTOR OF PHILOSOPHY.

DEPARTMENT OF ELECTRICAL ENGINEERING

EDMONTON, ALBERTA

SPRING, 1988

Permission has been granted to the National Library of Canada to microfilm this thesis and to lend or sell copies of the film.

The author (copyright owner) has reserved other publication rights, and neither the thesis nor extensive extracts from it may be printed or otherwise reproduced without his/her written permission.

L'autorisation a été accordée à la Bibliothèque nationale du Canada de microfilmer cette thèse et de prêter ou de vendre des exemplaires du film.

L'auteur (titulaire du droit d'auteur) se réserve les autres droits de publication; ni la thèse ni de longs extraits de celle-ci ne doivent être imprimés ou autrement reproduits sans son autorisation écrite.

ISBN 0-315-42767-1

THE UNIVERSITY OF ALBERTA

RELEASE FORM

Name of Author: **DOUGLAS NORMAN DEDERICH**

Title of Thesis: **THE EFFECTS OF INFRARED LASER IRRADIATION ON ROOT CANAL WALL DENTIN IN HUMAN TEETH**

Degree: **DOCTOR OF PHILOSOPHY IN ELECTRICAL ENGINEERING**

Year This Degree Granted: 1988.

Permission is hereby granted to THE UNIVERSITY OF ALBERTA LIBRARY to reproduce single copies of this thesis and to lend or sell such copies for private, scholarly or scientific research purposes only.

The author reserves other publication rights, and neither the thesis nor extensive extracts from it may be printed or otherwise reproduced without the author's permission.

Douglas N. Dederich
(Student's Signature)

#401, 5125 Riverbend Road
(Student's Permanent Address)

Edmonton, Alberta T6H 5K5

Date: April 22, 1988

THE UNIVERSITY OF ALBERTA

FACULTY OF GRADUATE STUDIES AND RESEARCH

The undersigned certify that they have read, and recommend to the Faculty of Graduate Studies and Research for acceptance, a thesis entitled **THE EFFECTS OF INFRARED LASER IRRADIATION ON ROOT CANAL WALL DENTIN IN HUMAN TEETH** submitted by **DOUGLAS N. DEDERICH** in partial fulfillment of the requirements for the degree of **DOCTOR OF PHILOSOPHY IN ELECTRICAL ENGINEERING.**

....
(Supervisor)

....

....

D. Jones
....

....

....

Date: April 5, 1988

DEDICATION

First and foremost, this work must be dedicated to my parents, Venance and Helene. It was they who taught me the value of love, hard work and education (among so many other things), and who worked to afford me the opportunity to further myself through advanced education. Their love and support sustained me through undergraduate engineering and dental school at The University of Iowa as well as through my M.Sc. and this Ph.D program in biomedical engineering at The University of Alberta. This small dedication can only in part repay the years of unconditional love and dedication on their part from which I have so greatly benefited.

I would also like to dedicate this thesis to two colleagues and friends. First, the late Dr. Carl W. Svare, who first initiated me into dental research at The University of Iowa. Carl's integrity and allegiance to the truth in research was infectious, and profoundly influenced my development as a researcher. Most importantly, he was my friend, and I include myself among those who miss him.

Secondly, Dr. Kenneth L. Zakariasen. Without Ken's influence, I would never have moved to Edmonton to pursue advanced research training. His advise during my M.Sc. program helped to pave the way for my obtaining the background necessary for this work. On a personal level, having an advisor/partner who is also your best friend makes the whole struggle even more meaningful. Ken and his wife Paula, daughters Kristi and Stephanie, and son Ken III have enriched my life more than I deserve. Their love and generosity have touched many, and I am grateful for being one of them.

ABSTRACT

Since the advent of the laser in the early 1960's, the field of medicine has seen arise a number of applications for this technology. This is not presently so with the field of clinical dentistry, largely due to the cumbersome beam delivery apparati of current commercial laser systems. In spite of this, there have been numerous in-vitro investigations performed which point the way towards the day when technological improvements will allow efficacious use of the laser in the clinical dental setting.

Basic to the problem of the use of the laser in root canal therapy is its effect on root canal wall dentin and the surrounding periapical tissues. It has been proposed that laser energy can create a glazed, nonporous surface on dentin and thereby decrease its permeability to fluids, one of the main objectives of endodontic therapy. This thesis investigated the continuous-wave carbon dioxide, pulsed carbon dioxide, and pulsed Nd-YAG laser with respect to their relative ability to create this desired glazed surface on *in-vitro* specimens of root canal wall dentin. Furthermore, a finite element numerical analysis was performed to develop a better insight into the heat transfer and stress dynamics which occur in dentin upon laser impact.

The results indicate that the pulsed carbon dioxide and pulsed Nd-YAG lasers were not able to produce a glazed surface in any single instance, much less do so consistently. However, the continuous-wave carbon dioxide laser demonstrated the ability to reliably create this effect at a power of 15 Watts, duration of 0.2 seconds, and spot diameter of 1.0 mm. Since these settings produced the desired fracture-free fused surface, they were chosen to be modelled using the finite element numerical method. The numerical analysis results predicted the presence of fusion and tensile stresses within experimental error of empirically determined values of the tensile strength of dentin. The results also suggest that the presence of surface cracking in the dentin may be strongly related to the depth to which the maximum tensile stresses are allowed to progress rather than to the variation of the maximum tensile stresses with time.

PREFACE

By definition, the field of biomedical engineering is multidisciplinary in that it seeks to apply engineering technology to problems encountered in the clinical life sciences. As such, any work in this area must address readers with expertise in one or the other, and perhaps both, of these fields. To accommodate this diversity in readership, I have attempted to write this thesis in such a way as to allow both the engineer and dentist to understand the basic elements of this work. This may result, however, in sections of this work which appear to be elementary from either the engineering or the dental perspective. However, I believe it safe to assume that the engineers and dentists will probably not consider the same sections to be elementary.

For example, the section dealing with the developmental stages of dentin may well be redundant for those with dental training; however, this information is important to allow the readers with engineering training a general concept of the actual structure and composition of dentin. Accordingly, the information on laser output may well seem to be unnecessary to engineers, but is mandatory for those readers who are dentists to understand the effects of this radiation on the dentin.

Therefore, I would ask that consideration of the above be given when reading this work.

ACKNOWLEDGEMENT

I would like to acknowledge and thank Dr. John Tulip for his role as my advisor throughout both my M.Sc. and Ph.D. program. Without his support and technical guidance, not only would this work not have been possible, but the potential for the near-term advancement of the clinical use of the laser in dentistry would have been severely curtailed.

Also, my sincere gratitude goes out to Dr. Gordon W. Thompson, Dean of the Faculty of Dentistry. Ever since my arrival and "unofficial" residence in the Faculty of Dentistry as an engineering graduate student, Dr. Thompson has supported both me and my work beyond the call of duty. His support is in part manifested in my current appointment in the Division of Biomaterials, Faculty of Dentistry, which has provided to me an environment in which to complete this and other research.

TABLE OF CONTENTS

DEDICATION iv

ABSTRACT v

PREFACE vii

ACKNOWLEDGEMENT viii

- Introduction 1
  - The Problem 2
    - Overview 2
    - The Laser 5
  - Objectives of this Study 8
- Root Canal Wall Dentin: The Target Material 9
  - Development 9
    - Dentinogenesis: The Formation of Dentin 9
    - Structure 13
    - Composition 17
      - Inorganic Components 19
      - Organic Components 27
    - Age Related Changes. 27
  - Thermal Properties 28
    - Thermal Conductivity 29
    - Thermal Diffusivity 31
    - Specific Heat 31
  - Mechanical Properties 31
    - Modulus of Elasticity 32
    - Proportional Limit 34
    - Ultimate Tensile Strength 34

Ultimate Compressive Strength 35
Coefficient of Thermal Expansion 36
Viscoelastic Properties (Stress-Relaxation Behavior) 37
Optical Properties 37
Instrumented Canal Wall Dentin 38
The Smear Layer 39
Laser Output Parameters 40
Power 40
Wavelength 41
Mode of Operation 41
Continuous-Wave 42
Super-Pulsed 43
Q-Switched 43
Spot Size 44
TEM Mode 45
Duration 46
Laser/Tissue Interaction 47
General Interaction Phenomena 47
Qualitative Interaction 47
Quantitative Interaction 48
Thermal Effects on Living Tissue 51
Soft Tissue 51
Hard Tissue 53
Enamel 54
Dentin 58
Bone 59
Non-Thermal Effects on Living Tissue 60

Basic Heat Transfer Theory 60
Conduction 61
Convection 62
Radiation 63
Basic Thermal Stress Theory 64
Numerical Analysis: The Finite Element Method 67
CW-CO2 Laser Effects on Canal Wall Dentin 69
Introduction 69
Method and Materials 70
Results 71
Discussion 73
Conclusions 84
Pulsed CO2 Laser Effects on Canal Wall Dentin 85
Introduction 85
Method and Materials 85
Results 85
Discussion 86
Conclusion 89
Pulsed Nd-YAG Laser Effects on Root Canal Wall Dentin 90
Introduction 90
Method and Materials 91
Results 91
Discussion 92
Conclusion 95
Radiometric Surface Temperature Measurement 96
A Numerical Model: Temperature and Stress Analysis by the Finite Element Method 98

Introduction 98

ADINAT 100

    Simplifying Assumptions 100

    Method 103

ADINA 104

    Simplifying Assumptions 104

    Results 105

    Discussion 105

    Conclusions 112

Summary and Discussion 114

References 265

Appendix 284

    Experimental Data 285

LIST OF TABLES

Table I: Composition of Dentin 117

Table II: Ash Composition of Mineralized Tissues 118

Table III: Median Concentrations of Trace Elements in Enamel 119

Table IV: Organic Constituents of Dentin 120

Table V: Thermal Conductivity of Dentin 121

Table VI: Elastic Modulus of Dentin 122

Table VII: Proportional Limit of Dentin 123

Table VIII: Ultimate Tensile Strength of Dentin 124

Table IX: Ultimate Compressive Strength of Dentin 125

Table X: Thermal Coefficient of Expansion of Dentin 126

Table XI: Thermogravimetric Analysis of Dentin: A Summary of the Results 127

Table XII: Pulsed Nd-YAG Laser Exposure Parameters 128

Table XIII: Pulsed Carbon Dioxide Laser Exposure Parameters 129

Table XIV: Continuous-Wave Carbon Dioxide Laser Exposure Parameters 130

Table XV: Results of Multivariate Analysis; CW-CO_2 131

Table XVI: Duncan's MRT; Hairline; Power/Pulse Duration; CW-CO_2 132

Table XVII: Duncan's MRT; Fusion; Power/Pulse Duration; CW-CO_2 133

Table XVIII: Duncan's MRT; Wide; Power Only; CW-CO_2 134

Table XIX: Duncan's MRT; Wide; Pulse Duration Only; CW-CO_2 135

Table XX: Multiple Regression Results; CW-CO_2 136

Table XXI: Measurement Reliability Data Descriptive Statistics 137

Table XXII: Results of Multivariate Analysis; Pulsed-CO_2 138

Table XXIII: Duncan's MRT; Hairline; Pulsed-CO_2 139

Table XXIV: Duncan's MRT; Wide; Pulsed-CO_2 141

Table XXV: Duncan's MRT; Hairline; Pulsed-CO_2 143

Table XXVI: Multiple Regression Results; Pulsed-CO_2 145

Table XXVII: Results of Multivariate Analysis; Pulsed-Nd-YAG 146

Table XXVIII: Duncan's MRT; Fusion; Rate/Duration; Pulsed-Nd-YAG 150

Table XXIX: Duncan's MRT; Cratering; Rate/Duration; Pulsed-Nd-YAG 151

Table XXX: Duncan's MRT; Fusion; Power/Rate; Pulsed-Nd-YAG 152

Table XXXI: Duncan's MRT; Cratering; Power/Rate; Pulsed-Nd-YAG 153

Table XXXII: Duncan's MRT; Hairline; Power/Duration; Pulsed-Nd-YAG 154

Table XXXIII: Duncan's MRT; Fusion; Power/Duration; Pulsed-Nd-YAG 155

Table XXXIV: Duncan's MRT; Cratering; Power/Duration; Pulsed-Nd-YAG 156

Table XXXV: Duncan's MRT; Hairline; Power Only; Pulsed-Nd-YAG 157

Table XXXVI: Pearson Correlation Coefficients: Pulsed-Nd-YAG 158

Table XXXVII: Multiple Regression Results; Pulsed-Nd-YAG 159

Table XXXVIII: IRCON Optical Pyrometer Calibration Data 160

Table XXXIX: Surface Temperature Data: CW-CO_2 Laser Impact Site 161

Table XXXX: Latent Heat Values used in ADINAT 162

Table XXXXI: Mechanical Properties Used in Finite Element Model 163

Table XXXXII: Maximum Stresses Calculated in ADINA 164

LIST OF FIGURES

Figure 1: Diagram of a Human Molar and its Surrounding Structures 166

Figure 2: Schematic of Enamel and Dentin Development 167

Figure 3: Mineralization Phase of Dentinogenesis 168

Figure 4: Diagram of Intertubular and Peritubular Dentin 169

Figure 5: Diagrammatic Representation of Two Stages in Dentin Deposition 170

Figure 6: Diagram of Tubule Arrangement and Granular Layer of Tomes 171

Figure 7: Diagram of Incremental Lines in Dentin 172

Figure 8: Diagram of Interglobular Dentin 173

Figure 9: Diagram of primary and secondary dentin 174

Figure 10: Method to Separate Enamel and Dentin by Manley and Hodge 175

Figure 11: Hydroxyapatite Unit Cell 176

Figure 12: Diagram of Incident, Reflected, and Transmitted Light 177

Figure 13: Extinction Length 178

Figure 14: Diagram of Split Tooth Specimen 179

Figure 15: Chart; Hairline; Power/Duration; CW-CO_2 Laser 180

Figure 16: Chart; Wide; Power/Duration; CW-CO_2 Laser 181

Figure 17: Chart; Fusion; Power/Duration; CW-CO_2 Laser 182

Figure 18: Chart; Wide; Power Only; CW-CO_2 Laser 183

Figure 19: Chart; Wide; Duration Only; CW-CO_2 Laser 184

Figure 20: Chart; Hairline; Power/Duration; Pulsed-CO_2 Laser 185

Figure 21: Chart; Wide; Power/Duration; Pulsed-CO_2 Laser 186

Figure 22: Chart; Fusion; Power/Duration; Pulsed-CO_2 Laser 187

Figure 23: Diagram of Pulsed Nd-YAG Experimental Set-Up 188

Figure 24: Chart; Hairline; Power/Duration; Pulsed-Nd-YAG Laser 189

Figure 25: Chart; Wide; Power/Duration; Pulsed-Nd-YAG Laser 190

Figure 26: Chart; Fusion; Power/Duration; Pulsed-Nd-YAG Laser 191
Figure 27: Chart; Cratering; Power/Duration; Pulsed-Nd-YAG Laser..................... 192
Figure 28: Chart; Hairline; Power/Rate; Pulsed-Nd-YAG Laser 193
Figure 29: Chart; Wide; Power/Rate; Pulsed-Nd-YAG Laser 194
Figure 30: Chart; Fusion; Power/Rate; Pulsed-Nd-YAG Laser 195
Figure 31: Chart; Cratering; Power/Rate; Pulsed-Nd-YAG Laser..................... 196
Figure 32: Chart; Hairline; Rate/Duration; Pulsed-Nd-YAG Laser..................... 197
Figure 33: Chart; Wide; Rate/Duration; Pulsed-Nd-YAG Laser..................... 198
Figure 34: Chart; Fusion; Rate/Duration; Pulsed-Nd-YAG Laser..................... 199
Figure 35: Chart; Cratering; Rate/Duration; Pulsed-Nd-YAG Laser 200
Figure 36: Chart; Hairline; Power Only; Pulsed-Nd-YAG Laser..................... 201
Figure 37: Chart; Wide; Power Only; Pulsed-Nd-YAG Laser..................... 202
Figure 38: Chart; Fusion; Power Only; Pulsed-Nd-YAG Laser..................... 203
Figure 39: Chart; Cratering; Power Only; Pulsed-Nd-YAG Laser 204
Figure 40: Chart; Hairline; Rate Only; Pulsed-Nd-YAG Laser 205
Figure 41: Chart; Wide; Rate Only; Pulsed-Nd-YAG Laser 206
Figure 42: Chart; Fusion; Rate Only; Pulsed-Nd-YAG Laser 207
Figure 43: Chart; Cratering; Rate Only; Pulsed-Nd-YAG Laser..................... 208
Figure 44: Chart; Hairline; Duration Only; Pulsed-Nd-YAG Laser 209
Figure 45: Chart; Wide; Duration Only; Pulsed-Nd-YAG Laser 209
Figure 46: Chart; Fusion; Duration Only; Pulsed-Nd-YAG Laser 209
Figure 47: Chart; Cratering; Duration Only; Pulsed-Nd-YAG Laser..................... 209
Figure 48: Diagram of the Laser Beam Impinging on the Finite Element Mesh 211
Figure 49: Heat Energy Versus Energy Curve for Dentin..................... 214
Figure 50: ADINAT-Calculated Temperature Profiles..................... 215
Figure 51: ADINAT-Calculated Depth of Melt vs. Stefan's Equation 220
Figure 52: Time Versus Temperature Profile of the External-Most Nodes.............. 221

Figure 53: ADINA-Calculated Stress Plot for t=0.02 222
Figure 54: ADINA-Calculated Stress Plot for t=0.04 223
Figure 55: ADINA-Calculated Stress Plot for t=0.06 224
Figure 56: ADINA-Calculated Stress Plot for t=0.08 225
Figure 57: ADINA-Calculated Stress Plot for t=0.10 226
Figure 58: ADINA-Calculated Stress Plot for t=0.12 227
Figure 59: ADINA-Calculated Stress Plot for t=0.14 228
Figure 60: ADINA-Calculated Stress Plot for t=0.16 229
Figure 61: ADINA-Calculated Stress Plot for t=0.18 230
Figure 62: ADINA-Calculated Stress Plot for t=0.20 231
Figure 63: ADINA-Calculated Stress Plot for t=0.22 232
Figure 64: ADINA-Calculated Stress Plot for t=0.24 233
Figure 65: ADINA-Calculated Stress Plot for t=0.26 234
Figure 66: ADINA-Calculated Stress Plot for t=0.28 235
Figure 67: ADINA-Calculated Stress Plot for t=0.30 236
Figure 68: ADINA-Calculated Stress Plot for t=0.32 237
Figure 69: ADINA-Calculated Stress Plot for t=0.34 238
Figure 70: ADINA-Calculated Stress Plot for t=0.36 239
Figure 71: ADINA-Calculated Stress Plot for t=0.38 240
Figure 72: ADINA-Calculated Stress Plot for t=0.40 241
Figure 73: ADINA-Calculated Stress Plot for t=0.42 242
Figure 74: ADINA-Calculated Stress Plot for t=0.44 243
Figure 75: ADINA-Calculated Stress Plot for t=0.46 244
Figure 76: ADINA-Calculated Stress Plot for t=0.48 245
Figure 77: ADINA-Calculated Stress Plot for t=0.50 246
Figure 78: ADINA-Calculated Deformation Plot for t=0.02 247
Figure 79: ADINA-Calculated Deformation Plot for t=0.04 248

Figure 80: ADINA-Calculated Deformation Plot for t=0.06 249

Figure 81: ADINA-Calculated Deformation Plot for t=0.08 250

Figure 82: Transmittance Spectra from FTIR Analysis 251

LIST OF PLATES

Plate 1: SEM of Nonsclerotic, Opaque Dentin 253
Plate 2: SEM of Sclerotic, Translucent Dentin 254
Plate 3: SEM of a CW-CO_2 Laser Impact Site; No Effect 255
Plate 4: SEM of a CW-CO_2 Laser Impact Site; Hairline 256
Plate 5: SEM of a CW-CO_2 Laser Impact Site; Hairline, Wide, Fusion 257
Plate 6: SEM of a CW-CO_2 Laser Impact Site; Fracture-Free Glazing 258
Plate 7: SEM of a Pulsed-CO_2 Laser Impact Site; Hairline 259
Plate 8: SEM of a Pulsed-CO_2 Laser Impact Site; Wide, Hairline 260
Plate 9: SEM of a Pulsed-CO_2 Laser Impact Site; Hairline, Wide, Fusion 261
Plate 10: SEM of a Pulsed-Nd-YAG Laser Impact Site; No Effect 262
Plate 11: SEM of a Pulsed-Nd-YAG Laser Impact Site; Cratering 263
Plate 12: SEM of a Pulsed-Nd-YAG Laser Impact Site; Root Perforation 264

LIST OF SYMBOLS

ρ = density

c = specific heat

q = heat transfer rate

T = temperature

α = thermal diffusivity

α = statistical confidence level

α = absorption coefficient

k = thermal conductivity

I = intensity

H = Hermite polynomial

ω = frequency

ω_0 = spot size

λ = wavelength

An In-Vitro Quantitative Analysis of the Effects of Infrared Laser Irradiation on Root Canal Dentin in Human Teeth

Introduction

Since the advent of the laser in the early 1960's, the field of medicine has seen arise a number of applications for this technology. These began with the use of the laser in ocular surgery[1-3], and eventually included treatments such as: gastro-intestinal coagulation[4-6]; the removal of pigmented epithelial lesions such as tattoos, melanomas, hemangiomas, and nevi[7,8]; treatment of neoplasms utilizing hematoporphryn and low power laser energy[9,10]; stimulation of accelerated wound healing with low power laser energy[11-13]; and, most commonly, the use as a tissue ablation device, or scalpel[14-16]. Dentistry, on the other hand, presently embraces no widely practiced treatments using laser energy. This is partly because a laser delivery system which allows access to secluded corners of the mouth has only recently become available. A significant amount of research has been done involving the use of lasers in dentistry, and from this several possible uses have been postulated, even though no immediate solution to the problem of intraoral access was available. Some potentially beneficial applications of lasers in the dental setting would include use as a scalpel; as a coagulator; as an aid in hemostasis through heat denaturation and subsequent thermal shrinkage of the collagen in the blood vessel walls; as an aid in sterilization; as a preventive device for reducing the susceptibility of enamel to decay; as a welding device to aid in crown and bridge placement or orthodontic work; and as a tool used to fuse dentin and other materials in an attempt to hermetically seal the interior, apical portion of the root canal during endodontic therapy. This last application requires, as do the rest, that a groundwork of research be laid before such treatment is performed on patients. It is necessary to know whether laser exposure can accomplish the desired clinical result, and whether it can result in any negative clinical sequela as well, in order for a knowledgeable estimate of the cost/benefit ratio can be put forth to the patient. This thesis will address one basic subject which is vitally important to the use of laser energy in endodontics; namely, the effects on root canal wall dentin.

The Problem

Overview

The dental pulp is a soft tissue organ which normally resides at the center of the tooth, and from which most of the hard tissue in the tooth develops (Figure 1). After development of the tooth is complete, the pulp continues to serve as a sensory organ, capable of sensing hot, cold, pressure, and, of course, pain. It's healthy composition is characterized histologically by the presence of small blood vessels, nerves, and connective tissue. When suffering minor injury or irritation, as from restorative dental procedures, the pulp can heal and protect itself even more by depositing more dentin at the site of irritation, thus withdrawing from the source of irritation. However, the ability of the pulp to heal is limited. When the injury becomes too severe, the pathologic changes become irreversible and the pulp will die. If it is left alone, it will eventually necrose and become the source of an infection which can result in serious clinical sequela. The pulp must therefore be removed when it is identified that it is beyond the point of recovery, or, alternatively, the tooth must be extracted. Then, the space once occupied by the pulp must be filled.

The cleaning, shaping, and filling of the root canal system is referred to as *instrumentation and obturation*. The goal of instrumentation is to remove all organic debris, such as necrotic pulp tissue, from the canal space and to shape the canal in such a way as to facilitate subsequent obturation. The goal of obturation is to attain a fluid-tight, or hermetic, seal between the interior of the root canal and the externally surrounding periapical tissues. These two procedures are the keys to successful endodontic therapy. However, neither of these procedures is easily performed. This is because the root canal system as well as the oral environment in which it exists can present both morphologic and biologic complexities which make treatment difficult. Removing all organic tissues from the root canal space during instrumentation and attaining a fluid-tight seal with currently available obturation methods is easier said than done and has been demonstrated in several published articles[17-27]. Failure to completely debride the canal leaves necrotic tissue behind which may serve as substrates for bacterial growth. The failure to create a fluid-tight seal allows fluid to leak into the root canal. It can also provide a path for bacterial migration into the canal space, and for microorganisms, their by-products and other irritants to exit in the periapical tissues[28]. Since removing the pulp also removes the tooths only viable circulation, the body's blood-borne defense mechanisms cannot effectively remove remnants of necrotic tissue from the root canal. *In vivo* animal research has shown that a hollow space containing necrotic tissues and microorganisms can lead to pathologic changes in the surrounding tissue[29,30]. It therefore appears prudent to perform the most effective instrumentation and obturation possible to insure the highest rate of success.

Several things can complicate and increase the difficulty of performing endodontic therapy. For example, pulpal age and irritation can cause the canal to sclerose; that is, to calcify and decrease in size to the point where it is difficult to insert an endodontic instrument. In addition, it is frequently necessary to treat curved canals in multi-rooted posterior teeth where access is cumbersome. As a response to these and other difficulties seen in many of the teeth requiring endodontic therapy, many dentists have chosen to utilize inferior but more convenient techniques. These techniques are not supported by any biologic rationale based on the current state of knowledge, do not result in the most effective instrumentation and obturation possible, are not taught in North American dental schools, and can lead to serious pathologic sequela[31-35]. Typically, they require little precision or finesse and use tissue fixation chemicals. It has been shown that when such chemicals are used on vital pulpal tissues the remaining tissues seldom remain in or heal to a normal histologic state[36,37]. Accordingly, the substitution of a pulpal tissue fixation technique for traditional root canal therapy cannot be considered to be biologically acceptable.

Several studies have indicated that traditional endodontic therapy techniques yield a success rate ranging between 82% and more than 90%[38-41]. Thus, there seems to be room for significant improvement even over traditional techniques taught in accredited dental schools. It should be noted that the success rates mentioned here are based on studies using relatively short recall intervals. It is possible that over a longer period of time (i.e. years) these rates are actually lower than indicated.

The difficulty observed in attaining complete canal instrumentation and obturation, and the propensity of some dentists to avoid traditional therapy techniques because of their complexity accentuates the need for continued development of instruments, materials and techniques which are both more effective and less complex with respect to their application.

The Laser

Research investigating the possible applications of lasers to endodontics has not been plentiful, especially when compared to that existing for lasers in medicine. Early efforts included attempts to seal the apical root canal foramen externally at the root apex with the CO_2 laser and internally from within the root canal with the CO_2 and Nd-YAG lasers[42,43]. These attempts were not successful. Charring and "cap" formation occurred without fusion to the underlying dentin, and the foramina were not sealed. With the exception of these studies, early research into endodontic laser applications is conspicuous by its absence.

Other studies, however, have been published which examine dental hard tissue structural changes[44,45]. Of particular interest is the report by Kantola[45] of dentin recrystallization after CO_2 laser irradiation to closely resemble normal enamel hydroxyapatite crystalline structure. Melcer et al.[46] has reported similar dentin crystalline structural changes as well as microhardness increases, and sterilization of dentin. This raises the possibility that appropriate laser application may induce crystalline changes in dentin which may be beneficial in endodontic therapy by effecting a decrease in dentin permeability. As previously mentioned, little research has been published relating to the enhancement of the canal "seal" by laser irradiation. The early studies by Kantola[44,45] did not look at root canal wall dentin in particular. Also, canal wall dentin has been shown to vary both morphologically and histologically both within and between sites[47,48]. Accordingly, canal wall dentin may vary in its response to laser irradiation as a function of the location of the impact site. More recent studies[49,50] have shown that it is possible to create a smooth, continuous, and nonporous surface on canal wall dentin with Nd-YAG laser energy. This may figuratively be described as "glazing" of the dentinal surface, where the normally present microtubule openings are occluded. This occlusion is attributed to the melted inorganic component of dentin which, after vaporization of the local organic content, flows into and covers the tubule openings before recrystallization occurs. Pashley et al.[51] indicated that the surface occlusion of dentinal microtubules with debris accounted for 86% of the total measured resistance to fluid flow. Such information lends credence to the suggestion that glazing the dentinal surface would also result in reduced dentinal permeability to fluids.

Although continuous-wave Nd-YAG laser irradiation was found to be capable of creating this desired glazed surface on undyed canal wall dentin, the presence of this effect was strongly dependent on the presence of opaque colored (i.e. nonsclerotic) dentin in the target area[49]. This was because translucent or sclerotic dentin is transparent at λ=1.06μm, and therefore undergoes little or no laser-induced changes, at least at the powers used in that study. Dyeing the dentinal surface in an attempt to localize the energy on the surface regardless of the color of the underlying dentin improved the consistency and predictability of dentinal glazing. The possible existence of a trend for shorter pulse durations to results more often in less thermal cracking of the dentinal surface than longer pulse durations was indicated here[50]. This, however, was not a statistically significant trend. This was important because cracking resulting from laser-induced thermal stresses can, in theory, be considered to be a threat to the desired objective of a hermetic seal. Unfortunately, the use of dark colored dyes in the clinical setting poses serious esthetic risks to the patient. It is unlikely that they could be regularly employed to stain canal wall dentin *in vivo* without also inadvertently staining the coronal dentin and enamel as well, resulting in a darkened tooth and very unhappy patient. The need for a means of creating a smooth, nonporous, and continuous glazed surface without the need for staining is therefore obvious.

Preliminary and unpublished pilot experiments indicated that, as was expected, canal wall dentin is opaque at λ=10.6μm. It was subsequently postulated that the CO_2

laser may be able to create the desired glazing effect without the need to dye the target surface, and at the same time offer consistency and predictability of result. What was now necessary was to quantify and describe the relationship between the CW-CO_2 laser exposure parameters and their resultant dentinal effects.

Another mode of operation available with the CO_2 laser used was the pulse mode. The question of whether the pulsed waveform of the incident energy would differ in its effect on dentin, and if so, how, was an intriguing one. Whether the difference, if any, would be clinically beneficial was unknown, and hence the investigation of pulsed CO_2 laser effects on dentin became an area of interest.

Beam delivery down a narrow structure like a root canal requires that the energy be able to transit down an even smaller waveguide. The most obvious solution was to use an optical fiber as the waveguide, since sizes small enough to be fully inserted into the root canal were already available for the Nd-YAG laser. Unfortunately, CO_2 laser energy will not transit down quartz fibers. In the search for a solution to the problem of beam delivery, the question arose whether pulsed Nd-YAG laser energy would differ in its effect on dentin when compared to continuous-wave Nd-YAG laser energy. Personal experience had lead one researcher to suggest that Q-switched Nd-YAG laser pulses could interact with various materials in a significantly different way than continuous-wave Nd-YAG energy, and that, in the present application, this might involve a decrease in the depth of penetration[52]. This lead to questioning whether a normally pulsed Nd-YAG laser (which happened to be available, along with the CO_2 laser, for use in this study) might also demonstrate differences in resultant dentinal effects, and if so, whether the desired glazing of the dentinal surface was possible. The pulsed Nd-YAG laser therefore solved the delivery problem; however its ability to glaze undyed dentin was still in question.

Objectives of this Study

The objectives of this study were as follows:

1. To investigate the potential of continuous-wave CO_2 laser energy, pulsed CO_2 laser energy, and pulsed Nd-YAG laser energy to glaze* the surface of instrumented root canal wall dentin in extracted *in-vitro* human teeth.
2. If such glazing is found to occur, to identify and quantify the trends, if any, relating the combinations of laser exposure parameters (power, pulse duration, pulse rate, pulse train duration, and spot size) to their corresponding dentinal effects. The null hypotheses to be tested are that power, pulse rate, pulse duration, pulse train duration, wavelength or any relevant combination thereof have no effect on the measured dentinal effects.
3. To qualitatively describe those trends in relation with their clinical significance.
4. To put forth a mathematical model of the heat transfer and stress dynamics to better understand the phenomena underlying *in-vitro* cracking and melting of dentin.

---

*Glazing, from here on, shall refer to the presence of a smooth, continuous, and nonporous layer of recrystallized inorganic dentin on the surface with negligible or no surface cracking.

Root Canal Wall Dentin: The Target Material

Dentin is a highly calcified tissue which constitutes the greater bulk of the human tooth. Normally, the dentin is covered by enamel in the crown of the tooth and by cementum in the root area of the tooth. In the center of the tooth, dentin forms the walls of the pulp chamber and root canals within which resides the pulp. The pulp is derived developmentally from the *dental papilla*, a connective tissue organ which plays an important role in tooth development. The pulp in turn acts as a formative organ for the dentin and also serves as the pathway by which nutrition reaches the dentin.

That physical changes in a material caused by laser irradiation can depend strongly on the characteristics of the material itself is not surprising, and is readily corroborated by practical experience. For example, dentin reacts quite differently to laser irradiation than enamel or soft tissue. This section will discuss the properties of dentin which have bearing on its reaction to laser irradiation: its development, structure, and composition; its mechanical properties; its optical properties; and the effect of ageing and canal instrumentation on some of these properties.

Development

Dentinogenesis: The Formation of Dentin

Throughout life, dentinogenesis occurs in two stages. First, an unmineralized collagenous matrix, called predentin, is formed which, in the second stage, becomes mineralized at a sharp boundary, the dentin/predentin junction. If mineralization and matrix formation are normal, then the thickness of the predentin remains constant; should mineralization be delayed, the predentin increases in thickness as the rate of matrix formation outpaces that of mineralization (Figure 2).

Matrix Formation. With the light microscope, the first event which is observed in dentinogenesis is the formation of a membrane between the inner enamel epithelium (the layer of cells, called ameloblasts, responsible for the formation of enamel) and the connective tissues (i.e. tissues which binds together and is the support for body structures; it is made up of fibroblasts, fibroglia, collagen fibrils, and elastic fibrils) of the dental papilla at the junction which marks the future meeting place of the coronal enamel and dentin, the dentinoenamel junction, or DEJ. This membrane consists of fibers which dye black in color with silver containing stains, and are oriented parallel to the DEJ.

The *preodontoblasts* are the outermost cells of the dental papilla, and are also situated subjacent to the inner enamel epithelium. These cells are irregular in shape, are separated from each other by extracellular spaces, and have various internal organelles which are apparently randomly arranged[53,54]. These preodontoblasts then differentiate, or change, into *odontoblasts* (probably, the ameloblasts help to orchestrate this transformation) which are short and columnar in shape, but still are separated from each other by relatively large intracellular spaces. Later, these cells become taller and develop various organelles including an extremely complex *endoplasmic reticulum* (an internal organelle which participates in protein synthesis) which extends from the nucleus to the peripheral edge of, but not into, a long and narrow extension of the cell called the *odontoblastic process* [53-57]. The endoplasmic reticulum is the site where the protein component of the organic matrix of dentin is fabricated. Collagen fibers ranging in diameter from 200μm to 2000μm have been identified in the extracellular spaces at this stage[58,59], marking the beginning of the deposition of the organic matrix of dentin. The larger fibrils (Korff's fibers) are found only in the first layer of dentin, especially between the very young odontoblasts[60]. Once dentinogenesis is well underway, only smaller, 400μm to 1000μm fibers are deposited.

As the odontoblasts develop they form the odontoblastic process which extends in length as the matrix grows and thus permeates the entire thickness of the dentin, enclosed by a tubule. Here, the cell bodies of the odontoblasts are receding away from the DEJ and are moving toward the pulp (Figure 3). Therefore, the deposition of dentin results in a successively smaller pulp chamber. Much preliminary information obtained at the light microscope level had suggested that odontoblasts were primarily responsible for the secretion of dentin matrix. Light microscopic autoradiography has provided evidence that odontoblasts were the direct source of the collagenous component of the organic matrix[61-64]. Similar studies utilizing ^{35}S labeled sulfate and ^{14}C labeled sugars demonstrated the role of the odontoblast in elaborating the ground substance (i.e. the non-protein component of the organic matrix) of the dentin[65-67]. The primary synthetic and secretory activity was shown to occur within the odontoblastic layer; little or no such activity was demonstrated within the subodontoblastic cells of the pulp. Accordingly, the contribution of the pulpal fibroblasts in formation of the dentin matrix must be considered to be negligible. The predentinal part of the process contains numerous dense granules now known to be collagen secretion granules[68,69]. This indicates that the odontoblastic process is the secretory pole of the odontoblast. As dentin deposition continues, the odontoblasts retreat toward the pulp and the secretory cytoplasmic process elongates to extend into the dentin and predentin. Electron microscopic studies have indicated that the odontoblastic processes may not continue all the way to reach the DEJ in mature teeth[70,71].

Mineralization. The mineralization of the dentin can be observed via light microscopy as the formation of spheres of inorganic material, *calcospherites*, beginning in that part of the matrix which occupies the tip of the cusp and extending throughout the crown and into the roots. This initial mineralization occurs approximately 5 to

10μm from the odontoblastic layer. As already mentioned, there is always a band of unmineralized matrix (the predentin) between the cell membrane and the mineralization front. Several investigators have reported that the first discernible crystallites occur as small discrete foci which expand circumferentially. Dense membrane-bound bodies (0.1 to 0.2 μm in diameter) have been reported to be scattered throughout the early predentin[58,72-74]. Needle-like crystals, presumably of hydroxyapatite, first develop inside these dense bodies. Further mineralization then spreads out circumferentially to form larger globules that eventually fuse into the initial front of dentin. Later-formed crystals are preferentially aligned to the collagen fibrils. It has been hypothesized that the dentin collagen molecule, by virtue of its three-dimensional architecture and composition, can in itself nucleate the deposition of the hydroxyapatite crystal phase[75,76]. However, this gives rise to the question: Since blood, and presumably tissue fluid, is supersaturated with bone salt, what factors are unique in the mineralizing tissues which cause the deposition of minerals (i.e. calcium phosphate) in them and only in them? Two mechanisms have been put forth to explain this: 1) a "booster" mechanism such as an enzyme activity which by raising still further the concentration of calcium or phosphate ions would lead to precipitation and 2) the presence of a seeding or "nucleating" substance which, because its shape resembles that of apatite, acts as a mold or template upon which the crystals are laid down, after which crystallization proceeds automatically. During the 30 years up to 1956, discussion of the first mechanism, the "booster" theory, dominated this field; but since then the second possibility, or "seeding" theory, received most of the attention. The discovery in the late 1960's of vesicles, apparently budding from cells concerned with mineralization and containing substances which could participate both in boosting and seeding, suggests that both mechanisms may occur. However, it is not known for certain whether the first precipitate is apatite or whether some other calcium phosphate is formed and is converted later into apatite.

Structure

Mature dentin is therefore a porous material, consisting of many tubules oriented more or less in a radial direction from the pulpal surface to the external tooth surface. The numbers of dentinal tubules is very considerable, for at the pulpal surface of the dentin there are between 30,000 and 70,000 tubules/mm^2. Since the external surface of the dentin is of a considerably greater area than the pulpal surface, the tubules are more widely spaced towards the external surface, where the tubule density is approximately 15,000 tubules/mm^2.

It has been estimated that mid-way between the pulp and enamel the total cross-sectional area of the dentinal tubules corresponds to a tube of 0.3 mm in diameter for each square millimeter of dentin (or, equivalently, about 7% of the surface area is accounted for by dentinal tubule openings). This degree of porosity could allow a considerable movement of fluid within dentin and experimental work on teeth both *in vivo* and *in vitro* has supported this concept[51]. Since the tubules are fluid-filled and thus hydraulically connected to the pulp, the application of various stimuli to the surface of exposed dentin results in the outward or inward movement of fluid. Removal of fluid at the exposed surface through evaporation by an air blast, dehydration of the surface by hypertonic solutions or by absorbent material, or the application of cold all produce a net outward movement of fluid (i.e. toward the source of stimuli). Heat, applied via a heated fluid, produces an opposite net flow, away from the source of stimuli.

The dentinal tubules constitute a system in which capillary forces can act. The loss of fluid at the dentinal surface causes "replacement" fluid to be transported along the tubules by capillary action. This can occur at considerable rates; it has been found that this rate of flow can reach 2 to 4 mm/sec. The displacement of fluid in the dentinal tubules is probably related to the production of pain by the distorting effect produced on the nerve endings located either in the dentinal tubules or close to them in the pulp.

When first formed, the dentinal tubules have a diameter of several microns but this quickly is reduced to a diameter of approximately 1.5 to 2.0 µm by the deposition of a zone of very highly calcified dentin *within* the original primary tubule. This tissue is called the *peritubular dentin* from its relationship to the tubule in the mature tooth (Figure 4). The peritubular dentin shows a number of differences compared with the rest of the mineralized dentin, or *intertubular dentin.* The peritubular dentin is much more highly mineralized than the intertubular dentin. Unlike the intertubular dentin, no collagen fibrils have been demonstrated in peritubular dentin.

In the intertubular dentin, the collagen fibrils are grouped together in dense bundles or fibers. These fibers have a lattice-like arrangement, coursing in gentle curves between the tubules and their peritubular areas (Figure 4).

During the active formation of dentin, the peritubular dentin reaches to the dentin/predentin junction; but in a mature tooth which has been in the mouth for several years, the peritubular dentin usually stops short of this junction (Figure 5). The dentinal tubules generally show two shallow curvatures, called the *primary curvatures,* in their course from the pulp cavity towards the external surface of the dentin. The curvatures in the pulpal half of the dentin is directed convexly rootward, whereas the curvature in the outer half of the dentin is directed with its convexity crownwards (Figure 6). The primary curvatures are particularly marked in the coronal and cervical dentin; whereas the tubules take a relatively straight course outward from the pulp in the dentin forming the roof of the pulp chamber and the apical portion of the roots. In addition to the primary curvatures, each tubule shows numerous small *secondary* curvatures along its course. These are produced by the spiral course taken by the odontoblasts and their processes in the deposition of the dentin. At the outer dentin surface, the dentinal tubules usually show a division into two main branches. These, or further fine branches, unite with the branches of adjacent processes to form a plexus close to the outer surface of the dentin.

Certain features which are seen in histological examination of ground (undemineralized) sections of dentin are produced by variations in the pattern of mineral deposition in the organic matrix. These include *incremental lines*, *interglobular dentin*, and the *granular layer of Tomes*. Variations in mineralizations may be produced by a disturbance in calcium metabolism which is associated with certain dietary deficiencies, birth, or certain diseases.

The incremental lines run at right angles to the dentinal tubules but are not parallel to the outer surface of the dentin (Figure 7). They correspond to the position of the pulpal surface of the dentin at successive stages in its formation, and are observable because of variations in the degree of mineralization at their sites. The incremental lines in dentin are often known as the *contour lines of Owen*.

The mineral material is laid down in dentin in the form of globular concentrations, known as *calcospherites*, which normally fuse together rapidly so that a relatively homogeneous area of mineralized dentin is produced. In certain teeth, however, the fusion may not take place completely in all situations, producing areas of *interglobular dentin*. These areas represent small patches of nonmineralized organic matrix of dentin which are bounded by the rounded outlines of unfused calcospherites. Interglobular dentin is found, to some degree, in the crowns of most teeth not far from the dentinoenamel junction (Figure 6). Those dentinal tubules which traverse areas of interglobular dentin show no peritubular dentin in that part of their course (Figure 8).

Beneath the cementum, a narrow layer of dentin of a granular appearance is constantly found in ground sections (Figure 6). This is known as the *granular layer of Tomes*, and is seen in sections because of variations in the level of mineralization in the layer which give the appearance of a concentration of numerous minute areas of interglobular dentin. A number of different hypothesis have been suggested in explanation of the origin of this layer, but none appear to be completely satisfactory.

The formation of dentin may continue throughout life, though the rate can vary considerably. The dentin which produces the bulk of the tissue is called *primary* dentin. This dentin is layed down rapidly during the development of the tooth and is characterized by having a very orderly, regular arrangement of the dentinal tubules. the dentin which is laid down later is known as *secondary* dentin (Figure 9). Secondary dentin can show various degrees of structural regularity, depending on the arrangement of the dentinal tubules. In some secondary dentin, the tubules may be as numerous and as regularly arranged as in primary dentin; however, there may also be few tubules present or sometimes none at all. Secondary dentin may be classified into two groups: 1) *physiological*, that is, secondary dentin which is not produced as a response to any external stimulus, and 2) *reparative*, or dentin whose deposition is the result of the opening up of the dentinal tubules at the external surface by some agent as attrition, abrasion, caries, or restorative dental procedures. Physiological secondary dentin is usually found to have a regular structure, with the tubule morphology being quite similar to that of primary dentin. Reparative dentin, on the other hand, is characterized by an irregular structure, with very few if any tubules present.

Changes can also take place within primary dentin as a response to external stimuli. In some instances, notably in relationship to occlusal caries, the dentin reacts by the production of a sclerosed area beneath the carious area. In such an area the dentinal tubules are occluded by mineral deposits with the result that the sclerosed dentin has a more uniform refractive index than normal dentin. When viewed by transmitted light, the sclerosed dentin appears more translucent than normal dentin, thus the term *translucent dentin* has been used to describe it (Plate 1 and Plate 2). The ability to produce translucent dentin varies, but where it is well developed it presumably acts as a barrier to the rapid spread of caries towards the pulp. The production of translucent dentin in the roots of teeth occurs progressively with time, and is therefore considered to be part of the normal process of ageing.

Composition

The composition of enamel and dentin differ so much that it is essential to separate them before analysis if the results are to have any practical biologic meaning. The separation of the cementum from the dentin is less important because these two tissues have similar composition and the proportion of cementum present in the normal tooth is too small to have much influence on the composition of the mixture.

Methods of separating enamel from dentin include mechanical and floatation methods. The earliest method consisted of chipping off the enamel from the underlying dentin. This process is greatly facilitated by first thoroughly drying the tooth by heating. Other mechanical methods consist of grinding off the enamel with a bur, leaving the dentin behind, or alternatively, grinding the dentin away until only a hollow shell of enamel is left. These methods are laborious, they do not yield pure enamel or dentin, and it is not easy to completely collect the ground material because of the tendency for it to escape into the air as a fine dust.

In the floatation method[77,78], the whole tooth is ground into a fine powder in some device which prevents loss of particles escaping into the air. The principle of the separation is that when a mixture of enamel, dentin, and cementum is added to a fluid with a density of 2.70, the enamel (density 2.9-3.0) sinks, while the dentin and cementum (density 2.14 and 2.03, respectively) float*. Powdered tooth is poured into a pointed tube open at the lower end, which is fitted into a centrifuge tube containing the liquid whose density is 2.70 (Figure 10). A suitable liquid is composed of 91% bromoform and 9% acetone. After thoroughly wetting the powdered tooth with the liquid, the whole assembly is centrifuged and the enamel and dentin form distinct layers, the enamel sinks into the outer tube and the dentin and cementum float inside the inner tube. The finger is then placed over the inner tube which is removed with its contents. The dentin and enamel are then washed free of the bromoform by acetone. Dentin and cementum may be separated by treating the above mixture with a fluid of density 2.07, but this is rarely done as the composition of cementum is very similar to that of dentin[79]. The purity of the samples is about 97-99% and can be improved by several repetitions of the process with fluids of slightly different densities.

The effect of floatation methods on the composition of enamel and dentin has not been thoroughly studied, but bromoform-acetone solutions remove lipids, at least partially. An 82% aqueous solution of cadmium tungstoborate has a density of 2.70 and may be used for separation without altering the lipids or, so far as is known, the rest of the organic matrix, but does contaminate the inorganic fraction with cadmium[80].

While density separation of entire powdered teeth is rapid, it does not permit differentiation on the basis of site or origin in the tooth. To overcome this problem, thin layer samples of enamel and dentin have been collected by grinding teeth with diamond abrasive points or drills at selected sites. Chemical analyses of such samples have shown distinct concentration differences in a number of chemical constituents in different layers of enamel and dentin from individual teeth[81].

---

*Density is defined in units of mass per unit volume. The above densities are in units of grams/ml. For comparison, the densities of water, lead, and gold are 1.00, 11.35, and 19.3 respectively.

A combination of layer sampling and density fractionation has been applied to small amounts of powdered enamel and dentin from single teeth[82,83]. In coronal dentin, an increase was found in high density fractions (d>2.25 g/ml) with age; furthermore, lower density fractions predominated adjacent to the enamel and to the pulp, with heavier fractions in the middle portions. It was suggested that the heavier fractions originated from peritubular dentin.

When considering analytical figures of the composition of teeth, it is important to be clear whether they refer to moist, dry, or ashed material. The analyses themselves are almost invariably carried out on either dried material (from which water has been removed by gentle heat), or on ashed material (i.e. from which both water and organic matter have been removed by the methods described below).

Inorganic Components

Major Constituents. The overall composition of enamel and dentin in terms of inorganic and organic constituents, as well as water, is listed in Table I. The inorganic fraction may be estimated on the basis of chemical analyses for calcium, phosphate, carbonate, and other constituents[84]; or on weight loss during ashing[85]. Ashing removes the organic matter from enamel and dentin, and can be done in two different ways. (1) *Dry Ashing*. The dry tissue is heated in a crucible to a high temperature which breaks down the organic matter, but also alters the inorganic substance by liberating carbon dioxide from carbonates[86-88] and changes crystal form. (2) *Wet Ashing*. The tissue is boiled with ethylene glycol and KOH (potassium hydroxide) which removes the organic matter completely from dentin. It leaves the carbonate unaffected but apparently extracts some of the calcium and phosphorous. The reagent ethylene diamine has been found to be a more satisfactory means of removing the organic matter without altering the inorganic matter[89].

The protein content of dentin is about 20% by weight[90,91]. The water content of mineralized tissues is difficult to assess. Chemical analyses for organic material can account for only part of the weight reduction during ashing; it has been assumed that water accounts for the difference. By heating dentin, dried at 105°C, to different temperatures and measuring changes in weight (thermogravimetry)[92-95] it has been shown that water occurs in two forms: one loosely bound, probably to the organic matter, and another tightly bound, possibly as the hydration shell around the apatite crystals[96,97]. Peaks of weight loss occur at 100°C, from loosely bound water, at 350°C, from organic matter and water bound tightly to the crystals, and at 750°C, from bound carbonate[88,94,98].

The ash composition of enamel and dentin is well established[99]. The mean data are listed in Table II. Phosphate has been listed, rather than phosphorous, to illustrate better how calcium orthophosphates account for more than 90% of the inorganic composition in these tissues.

The published results of analyses of dental tissues vary too much to warrant the exact calculation of averages, but Table II gives approximate figures for the inorganic composition of enamel and dentin. The variations found by different workers are partly caused by real differences between the composition of different teeth and partly by variations in the reliability of the methods used.

The exact molecular form in which the various elements are present in the crystals of the calcified tissues is a highly technical controversy. Several structures have been suggested, but the difficulty of choosing between them arises because the empirical formula and properties such as solubilities, refractive indices, and X-ray diffraction patterns of the various suggested substances are so similar.

The two suggested structures which have received the most attention are the apatite crystal and a simple mixture. The inorganic composition of the mineralized tissues varies from place to place in each tissue and may be affected by such factors as diet and age. This suggests that the inorganic constituent must either be a mixture or a substance whose composition can vary. There is now general agreement that the main constituent is the crystalline form of calcium phosphate known as *apatite* with some amorphous calcium phosphate. Apatites are a crystalline form having the general formula $Ca_{10}(PO_4)_6X_2$ sometimes reduced to $Ca_5(PO_4)_3X$, and the most widely distributed in the biological field is *hydroxyapatite* where X is an hydroxyl group, OH. Apatites are three-dimensional ionic structures consisting of periodically repeated, identically constituted, congruent cells. The unit cell is a right prism with a four-sided, equilateral base with two angles each of 60° and 120° as shown in Figure 11. The side length of the base is 9.42 Å (referred to as the a-axis) and the height of the prism is 6.88 Å (referred to as the c-axis). To the box representing the unit cell are assigned ten calcium ions (open circles), six phosphate ions (not shown), and, in hydroxyapatite, two hydroxyl ions (solid circles). In hydroxyapatite, two hydroxyls are located on the edges, one fourth and three fourths the height over the base plane as shown. In the structure, the hydroxyls can be replaced with fluoride ions. If all hydroxyls are replaced, the crystal becomes fluorapatite. This change causes a decrease of the a-axis from 9.42 to 9.38 Å. Calcium ions are presented in two environments, namely, in vertical columns (columnar calciums, open circles with dot in center) and screw axis calciums placed around hydroxyl ions (open circles joined to a triangle in Figure 11).

Note that the screw axis calcium triangles are turned 60° in relation to each other going from one hydroxyl to the next.

The position of the carbonate ions is controversial. It has been suggested that they are in the apatite crystal lattice, thus making the crystal a mixed carbonate hydroxyapatite[100]. Alternatively, it is possible that the crystal consists of hydroxyapatite with calcium carbonate adsorbed or that calcium carbonate is present with the apatite as a simple mixture. No calcium carbonate has been identified to date by X-ray diffraction patterns, but this evidence is inconclusive since there is doubt as to whether the method is sufficiently sensitive to detect the 2-3% of carbonate present. Another method of investigating whether a substance is part of the lattice or is adsorbed, is by determining whether the substance can be dissolved separately from other constituents of the crystal. Since most workers have found that carbonate can be dissolved out of the calcified tissues at a greater rate than can phosphate, it is concluded that at least some of the carbonate is adsorbed on the lattice rather than being contained within it. Studies of the infra-red spectrum of enamel by Elliot[101] showed a more complicated pattern than can be explained by any one position of the carbonate and he concluded that part of it replaces hydroxyl ions of the apatite and the rest is adsorbed on to the crystals.

All crystals are liable to contain defects such as the absence of an ion from its place in the lattice or dislocations where a column of atoms is inserted in an incomplete and irregular manner. Crystals also vary in size. Large crystals with few defects are described as having a high crystallinity and vice versa. The presence of certain ions in the environment in which apatite is forming (especially magnesium and carbonate) tends to inhibit crystal growth and thus lead to the formation of crystals with a poor crystallinity: fluoride has the reverse effect and improves the crystallinity of apatite.

The crystallinity may have a marked effect on certain chemical and physical properties (for example, solubility and the ability to take up additional ions).

Whitlockite, or *tricalcium phosphate (TCP)*, may be obtained by igniting proper proportions of dicalcium phosphate and calcium carbonate at 1100°C[102]. Biologically occurring TCP always seems to contain magnesium, and this ion favors the precipitation of TCP *in vitro* which probably explains the positive correlation between magnesium content and TCP abundance in dental calculus[103,104]. TCP has also been identified in carious dentin and enamel[105-107] and most recently in sound peritubular dentin[108]. The structure of TCP is complex and not fully determined[109].

Octacalcium phosphate (OCP) has been studied in detail[110-112]. Biologically, OCP occurs in dental calculus with great frequency[113]. Furthermore, there is some evidence to suggest that the mineral material in tubules occluded as a response to caries (i.e. translucent dentin) is not in the form of hydroxyapatite but is present as crystallites of OCP. However, the presence of OCP in bone, dentin, or enamel has not been directly proven. The unit cell of OCP measures 9.6 × 19.9 × 6.9 Å, which is about twice the size of that of hydroxyapatite. The structure of OCP is very similar to that of HA, except that a hydrated layer is introduced in the middle of the OCP unit cell, yielding the large dimension of 19.9 Å in the unit cell. Consequently, when one unit cell has formed, it is possible that growth could continue as hydroxyapatite rather than as OCP, giving rise to interlayering of the two types of mineral in the same crystallite.

The oldest theory as to the mineral composition of teeth is that it is a simple mixture of hydroxyapatite and calcium carbonate. This theory became eclipsed when the X-ray diffraction studies unanimously suggested an apatite structure. The work of Dallemagne et al.[114] in 1956 revived this theory and provided considerable evidence for it, although many of their observations are capable of other interpretations and their views have not been generally accepted.

Minor Constituents. One of the most important findings on the lesser constituents of the enamel and dentin is that their distribution throughout these tissues is not uniform. These ions can be classified into three groups: (1) higher concentration on the surface than within (F, Pb, Zn, Fe, Sb); (2) lower concentration on the surface than within (Na Mg, CO_3); and (3) distribution approximately uniform (Sr, Cu, Al, K).

Ions which readily become attached to the apatite crystals tend to build up in those parts of the tooth which are exposed for the longest time to the body fluids, i.e. outer enamel, which is bathed in tissue fluid after mineralization and before eruption, and in saliva, food, and drinks after eruption. The outer cementum and inner dentin are also in contact with tissue fluid throughout life and tend to concentrate trace elements in the same way as outer enamel. If, on the other hand, an ion is readily dissolved out from the calcified tissues by body fluids (Cl, CO_3, Mg, Na) then the outer and most vigorously bathed layers will be low in these constituents.

Most trace elements are present throughout the bulk of the tooth in concentrations ranging from a few parts per million to less than 0.01 ppm, although in certain places, such as the outer enamel surface, the concentration may be much higher. Only strontium, fluoride, and zinc reach or exceed concentrations of 100 ppm throughout the tooth.

SODIUM. Estimates of the sodium concentration in enamel and dentin vary rather widely, but the more recent figures average about 0.7% in enamel, increasing slightly up to the dentinoenamel junction with similar concentration of sodium in dentin (wet weight) but falling as the pulp is approached[115]. The type of combination of sodium in the dental tissues is uncertain but some is probably adsorbed onto apatite or within the crystal in exchange with calcium.

POTASSIUM. There have been few analyses for potassium but recent figures range between 0.3 and 0.4% (wet weight) for both enamel and dentin, the distribution being fairly uniform throughout both tissues[115].

MAGNESIUM. Studies on the distribution of magnesium show that its concentration rises from about 0.45% on the outer layer of enamel to about 0.7% in the inner enamel with still higher values in the outer dentin (1.5%) rising further to about 2% in the innermost dentin[115,116].

MANGANESE. Manganese is present in enamel at concentrations ranging from 0.45 to 1.98 ppm in the outer enamel to 0.34 to 0.79 ppm for inner enamel[117].

CHLORIDE. Chloride has been found in both enamel and dentin and some of it can be dissolved out by water, suggesting that it originates partly from tissue fluid. The concentration in outer enamel averages about 0.6% and falls to about 0.1% at its mid-point and remains fairly constant in the inner half. This pattern is established during tooth formation as it is present in unerupted teeth[118]. The dentin contains about 0.4% (dry weight) but the published figures may be low owing to loss of chloride during the preparation of the tissue.

CARBONATE. The nature of the group in the calcified tissues from which carbon dioxide may be liberated is not definitely known. Although usually referred to as "carbonate", it may be either bicarbonate or simply carbon dioxide adsorbed as such.

TRACE ELEMENTS. Several methods have been applied to the analysis of dental tissues for trace elements, and the two which have given most comprehensive information are activation analysis and spark source mass spectroscopy. In activation analysis, the sample to be analyzed is exposed to neutron bombardment in a reactor which induces radioactivity with properties characteristic of each element. By determining the nature of the induced radioactivity and its rate of decay it is possible to estimate individual elements. Some of the elements detected spectroscopically in teeth have been estimated by this method and others not previously found have been detected; for example dentin has been found to contain tungsten and gold[119]. Arsenic in an average concentration of 0.06 ppm has been found in mixed tooth substance[120,121].

Activation analysis is limited in its ability to detect element variations over very small physical distances (i.e. has limited resolution). Spark spectroscopy is a more suitable and sensitive method for repetitive analysis for all elements. A small sample is vaporized and ionized by a high voltage spark producing an ion beam which is accelerated and the ions separated magnetically according to the ratio of their mass to charge, the resulting spectrum being recorded photographically. When applied to the estimation of 66 of the elements in 28 samples of young enamel (< 20 years) from various parts of the U.S.A., 35 elements were detected and 31 were absent or present in concentrations below detection[122,123]. The other elements were excluded either because their presence was already well established or, like the inert gases, they were of no biological significance. The results are listed in Table III. Nickel and silicon cannot be estimated by this method but both are known, from other methods, to be present in enamel.

Little is known of the significance of most of these elements in teeth and it is likely that the presence of at least some may even be due to contamination from dental fillings in neighboring teeth. Metals from fillings and inlays, especially gold, silver, and mercury, do enter the intact enamel and dentin of the teeth containing the restorations and also adjacent gingival tissues[124,125]. Although uptake by neighboring teeth does not seem to have been definitely shown it is quite likely that some slight transfer occurs via the oral fluids.

Organic Components

Tomes, as long ago as 1895, stated that dentin contained 19.6% organic matter and pointed out that previous estimates were too high. The reason for the high values is that even after drying at 100°C, dentin still contains between 5 and 8% of water chemically bound to other constituents, and, since this is driven off at high temperatures, it is included in the figure described as "organic matter" when this is estimated by measuring weight loss during incineration.

Dentin contains an average of 3.4% of nitrogen and analysis of the amino acids show that about 90% of this is present as collagen, whose nitrogen content is 18.4%. The collagen content works out, therefore, to be about 18% of the dentin dried to 100°C. The collagen is present in higher concentrations in the outer third of the dentin corresponding with the slightly lower density of this part of the dentin[126].

Dentin collagen contains *chondroitin sulfate* which has been isolated from it in amounts stated to be about 0.6%. A complex mixture of many types of lipids comprise 0.33% of the composition of dentin (by weight)[127-129]. The composition of the organic matter in dentin is further summarized in Table IV.

Age Related Changes.

The permeability of dentin has been shown to decrease with age, and several suggestions have been made to explain this observation. One is that the tubules become narrower and may eventually become completely blocked by the mineralization of the peritubular matrix. This is confirmed by chemical analysis of dentin from teeth of different ages which show a small but statistically significant increase in the mineral concentration. This increase, however, was found only in the apical region of the root. This corroborates the observation that increases in transparency or translucency are most marked in the apical region. The water content of dentin (i.e. loss of weight at 105°C) diminishes from an average of 12.1% at ages from 10-20 years to 9.7% at ages from 50-80 years[130].

Several workers have shown histologically that the tubule contents (i.e. the odontoblastic process) become smaller and the peritubular zone becomes wider with increasing age. Eventually the odontoblastic process disappears and is replaced by material which is more radioopaque (i.e. is more heavily mineralized) than the intertubular matrix. Electron micrographs have shown that this material differs in structure from the intertubular matrix[131]. This change occurs at different rates even in adjacent tubules since transverse sections may show some tubules completely occluded and others still containing a high proportion of odontoblastic process. However, the reason for some tubules remaining patent (i.e. open) when adjacent ones become obliterated is unknown.

Thermal Properties

The thermal properties of the target material are of great importance when analyzing the effects of transient laser-induced temperatures on dentin. The coefficients of thermal conductivity and thermal diffusivity are related by a factor of 1/ρc (where ρ = the density and c = the specific heat of the material), and must be known in order for any theoretical analysis of the heat flow to be possible. Thermal conductivity is defined in one dimension by

$$q = -kA\frac{\partial T}{\partial x} \qquad (1)$$

where q is the heat transfer rate, A is the surface area over which the heat transfer occurs, $\frac{\partial T}{\partial x}$ is the temperature gradient in the direction of the heat flow, and k is the thermal conductivity in units of calories/seconds/cm^2/°C/cm. Accordingly, the thermal diffusivity can then be described by

$$\alpha = \frac{k}{\rho c} \tag{2}$$

where α is the thermal diffusivity of the material. These coefficients lend themselves to experimental validation.

Thermal Conductivity

The literature currently holds experimentally determined values for the thermal conductivity of dentin which range from 0.257×10^{-3} to 2.35×10^{-3} cals/sec/cm^2/°C/cm[132-137]. This variance may in part be explained by improvements in measuring apparati with time, and by attempts in later studies to control for variables such as water content and the degree of tubule sclerosis of the dentin.

In 1950, Lisanti and Zander[132] constructed an apparatus for the determination of the thermal conductivity of dentin. The dentin samples used were discs of dentin 6.3 mm in diameter and 1.5 mm thick taken from the crown of a molar tooth. These discs were hand polished on a fine stone under water. The heat flow across the dentin sample was measured under temperature gradients of 40°, 70°, and 90° C. Seven specimens of dentin were measured at each of these temperature gradients, and the mean thermal conductivity was found to be 2.29×10^{-3} cals/sec/cm^2/°C/cm. However, it was correctly pointed out that possible confounding factors existed and included variation in the water content from specimen to specimen, and that the consistent orientation of tubules from one sample to the next might cause the obtained value to be different from the actual value of dentin with a different tubule orientation pattern.

Craig and Peyton[136] used an apparatus which was essentially a modification of that used by Lisanti and Zander[132] to arrive at a value for the thermal conductivity of dentin. Importantly, they controlled for the orientation of the tubules and thereby the variation in the thermal conductivity with tubule direction. For heat flow in a direction parallel to the dentinal tubules, they found the thermal conductivity to be 1.36×10^{-3} cals/sec/cm^2/°C/cm, and for heat flow in a direction perpendicular to the tubules, 1.39×10^{-3} cals/sec/cm^2/°C/cm.

In 1975, Fanibunda and De Sa[137] developed an apparatus which used smaller dentin discs as specimens (approximately 3.8 mm diameter versus 6.3 mm diameter used by Lisanti and Zander[132]). This made it possible for Fanibunda and De Sa to improve the resolution of the thermal conductivity estimate with respect to the original location of this smaller specimen within the tooth. The impact of this was that it became possible to obtain specimens of dentin which contained only normal, tubular dentin and other specimens which also contained reparative, translucent dentin. In addition to controlling for variations in tubular morphology, the authors measured the thermal conductivity of the specimens before and after dehydration. It was found that the mean thermal conductivity value of specimens containing reparative and transparent dentin was 29.3% higher than the corresponding normal dentin value before dehydration and 32.5% higher following dehydration. The mean thermal conductivity value of normal tubular dentin fell by 7.6% after dehydration, during which the water content of the tubules is replaced by air. The specimens containing reparative and transparent dentin, however, decreased by only 3.2% following dehydration; the fewer tubules in this type of dentin reduce the available water content. The values for these thermal conductivities found by Fanibunda and De Sa can be found in Table V along with a summary of those values found by other investigators.

Thermal Diffusivity

Data for thermal conductivity[132-137], specific heat[138], and the density of enamel and dentin[139] are available in the literature; hence values for the thermal diffusivity can be calculated. Using 1.5×10^{-3} cals/sec/cm^2/°C/cm as the thermal conductivity of dentin, Braden (1964)[140] calculated the thermal diffusivity of dentin to be 2.6×10^{-3} cm^2/sec. Here, Braden used a specific heat value of 0.28 cal gm^{-1}°C^{-1}, and a density value of 2.1 g/cm^3.

Specific Heat

The specific heat of a substance may be considered as the quantity of heat needed to raise the temperature of a unit mass one degree centigrade. Usually one gram of water is chosen as the standard for comparison.

A search of the dental literature indicates that only two studies describing measurements of the specific heat of tooth structure; Henchel (1943)[141] has determined the specific heat of dentin to be 0.3 cal gm^{-1}°C^{-1}, which is in agreement with the value of 0.28 cal gm^{-1}°C^{-1} reported by Peyton and Simeral (1954)[138].

Mechanical Properties

The mechanical properties of tooth structure have influenced the development of dental restorative techniques to a great degree since the beginning days of dentistry. As a necessary part of the search for better restorative materials, an improved understanding of the physical and mechanical properties of enamel and dentin was sought by the investigators in this field. This has resulted in a substantial body of work which spans close to 100 years in time[142-159,161-162].

As they relate to dental restorations, these properties allow the tooth to retain amalgam and gold fillings in function for long periods of time. This is no small feat when one considers the complex and hostile environment of the mouth; here the tooth and restoration see heavy and multidirectional occlusal forces, temperature cycling, and a corrosive environment. With respect to the application of laser energy to the canal wall surface, these properties largely influence the degree of surface cracking seen upon irradiation.

The literature contains information on, and this work will cover, the following properties of dentin: modulus of elasticity, proportional limit, tensile strength, compressive strength, coefficient of thermal expansion, and stress-relaxation behavior.

Modulus of Elasticity

The *modulus of elasticity* of a material may, in general terms, be thought of as the ratio of an applied stress in a known direction divided by the dimensional change along that direction caused by the applied stress. Symbolically, this can be stated as

$$E = \frac{\sigma}{\varepsilon} \tag{3}$$

where E = the modulus of elasticity, σ = the stress, and ε = the strain. Here, stress is measured in units of force per unit area, and strain (i.e. the change in length/the length of the body) in percent[160].

The modulus of elasticity can, and should, be thought of as the slope of the initial linear portion of a typical stress-strain curve. It is a constant, which is unique for a particular material, and is a measure of the *stiffness* of the material. Since $\Delta\varepsilon$ is usually many orders of magnitude smaller than $\Delta\sigma$, the modulus E is usually a relatively large number; for example, it is 30×10^6 psi for steel and 10×10^6 psi for aluminum.

The literature holds experimentally determined values for the modulus of elasticity of dentin which range from 0.8 to 2.8×10^6 psi[142-145,147,148,150,152]. This range of values is indicative of the possibility that the physical properties of dentin are influenced by physiologic differences in the teeth tested, directional effects in tooth structure, rate of stress application, and the length/diameter ratio of the test specimen[143]. Furthermore, improvements in measuring apparati with time may also contribute to the variance seen in the reported values. Of particular interest are the studies by Stanford et al.[150] and Tyldesley[148] where it was found that the properties of the modulus of elasticity, proportional limit, and compressive strength do *not* depend on the orientation of the dentinal tubules; i.e. that dentin behaves isotropically with respect to its mechanical properties. Furthermore, Stanford et al.[150] found no difference in these three properties between vital and pulpless incisors. Tyldesley[148] found that the average value of the elastic modulus of dentin is unaffected by the age or sex of the subject and by whether caries are present in other locations on the tooth. He also found it to be the same in molars as in canines and incisors, and that the fracture of both dentin and enamel takes place along planes determined by the distribution of stresses rather than by the structure of the materials. Interestingly, 17 years later in 1976 Rasmussen et al.[158] found that dentin has anisotropic fracture properties, with the easiest fracture occurring perpendicular (i.e. in cross section) to the dentinal tubules. This apparent inconsistency suggests that both the stress distribution and the anisotropic properties of dentin may play a role in determining the reaction of dentin to stress. A summary of the values for the modulus of elasticity of dentin is shown in Table VI.

Proportional Limit

It is generally true that for dentin, and other hard tissues of the body as well, the modulus of elasticity demonstrates linearity for early portions of the stress-strain curve. The *proportional limit* is defined as the stress corresponding to the first point at which the curve deviates from the initial straight, or linear, portion of the curve[160]. In practice, it is often used synonymously with the term *elastic limit* because in most cases these two values are very similar. However, the elastic limit is determined by a different testing method, and represents the greatest stress which does not cause permanent deformation in a given specimen. In theory, then, these two properties can not be considered identical.

The literature reveals several experimentally determined values for the proportional limit of dentin which range from 9,600 psi to 25,100 psi with most of them clustering in the general range from 23,000 to 25,000 psi[143,145,147,148,150]. A table summarizing these values for the proportional limit is shown in Table VII.

Ultimate Tensile Strength

In the existing dental literature, the term *tensile strength* is used to describe the stress at which fracture occurred[151-153]. Although this definition is likely to be adequate for use in those studies, a more exact description will be given here for purposes of clarity and exactness.

The *ultimate tensile strength* of a material is the maximum tensile stress the material can withstand *before* rupture in a tensile test in which the load is applied slowly[160]. It is obtained by dividing the ultimate load by the original cross-sectional area of the test specimen (measured before loading). The ultimate tensile strength is the stress corresponding to the uppermost point on the stress-strain curve, and represents an important design property for a brittle material.

The *rupture stress* is, as the name implies, the stress at the time of rupture. It is obtained by dividing the load at rupture by the original cross-sectional area of the test specimen. For a brittle material, the ultimate stress and the rupture stress are likely to have the same value. As can be seen from the literature, this approximates the case for dentin.

The experimentally determined values for the tensile strength of dentin (i.e. the ultimate tensile strength) found in the literature range from 5,800 psi to 7,500 psi[151-153]. It was also pointed out by Lehman (1967)[153] that fracture occurred at the proportional limit; in other words, in his case the proportional limit, ultimate tensile strength, and rupture strength had the same value as far as it could be measured. A summary of these values can be found in Table VIII.

Ultimate Compressive Strength

The ultimate compressive strength of a material is analogous to the ultimate tensile strength with the exception that the a compressive stress is applied rather than a tensile stress. The ultimate compressive strength is also often referred to as the *crush strength*. Therefore, the ultimate compressive strength can be defined as the maximum compressive stress a particular material can withstand before rupture in a compressive test in which the load is applied slowly.

The literature contains experimentally determined values for the ultimate compressive strength of dentin which range from 30,000 psi to 50,400 psi[142,143,145,147,148,150]. A summary of these values can be found in Table IX.

Coefficient of Thermal Expansion

The coefficient of thermal expansion is a measure of the dimensional change a material undergoes when subjected to a given change in temperature. This property has great clinical import when considering the restorative materials used in dentistry. A typical approach in the development of restorative systems is to match the coefficient of thermal expansion of the material to that of tooth structure in an attempt to maintain the continuity or integrity of the tooth-restoration margin during the temperature cycling seen during alternate eating of hot and cold foods. A slight mismatch of coefficients of thermal expansion is sometimes intentionally incorporated into ceramometal systems designed for the fabrication of porcelain fused to metal crowns, where an esthetic layer of porcelain is baked onto a metal substructure. In this case, a correct mismatch of coefficients will result in a final product where the porcelain is in a slight state of compression, and this serves to reduce the risk of fracture of the porcelain (a material which is notorious for its weakness in tension).

In this work, the coefficient of thermal expansion is important as it relates to the generation of the internal stresses upon exposure to laser-induced temperature gradients. Although the exact values for these stresses also depend on other factors such as the elastic modulus, proportional limit, and tensile strength, thermal expansion is nevertheless a requirement for the generation of these stresses in general.

The literature reveals values of the coefficient of thermal expansion of dentin which range from 7.5×10^{-6}/°C to 11.4×10^{-6}/°C[161,162]. Table X lists these values and their respective references.

Viscoelastic Properties (Stress-Relaxation Behavior)

The only information on the viscoelastic properties of human dentin available in the literature comes from a study simultaneously published in both and engineering journal[156] and a dental journal[157] in 1975. Here, stress relaxation measurements were performed on thick-walled cylinders of radicular human dentin. This involved the application of an axial compressive stress on the cylindrical specimen of dentin until a specified strain (i.e. deformation, or change in the length of the specimen) was reached. At this point, the strain was kept constant and the stress was monitored and recorded. The stresses used were of the order of 50% of the ultimate compressive strength of dentin, and were found to be able to induce permanent deformation of the dentin when applied for the periods of time used in this study (i.e. hours). This deformation was reflected by the measured permanent change in the elastic modulus, and the authors speculated that it may have been due to the collapse of dentinal tubules during the application of compressive stress.

With the strain held constant, the stress was found to decrease in an exponential manner with time, so that, in general, after about 6 hours no further reduction in stress could be measured. This, in part, lead the authors to conclude that the "relaxation" modulus (defined as the time dependent stress divided by the existing strain) showed a linear *logarithmic* dependence on time over about four decades. In addition, they found the relaxation times to be very constant from specimen to specimen for the particular orientation investigated.

Optical Properties

The optical properties of interest with respect to this thesis are the reflectance, transmittance and absorption coefficients of dentin at wavelengths of 1.06μm and 10.6μm. Unfortunately, the literature does not offer experimentally determined values of these coefficients for human root canal wall dentin, or any human dentin for that matter. However, Boehm et al.[163] states that, for enamel, reflectance values are near 50% for light in the visible region, and decrease to more desirable levels in the infrared. In spite of the obvious differences between enamel and dentin, this raises the question as to whether this is also the case for dentin.

In the absence of experimental data on these properties for dentin, it is necessary to turn to subjective observations of the interaction of these lasers with dentin. Dederich et al.[49] looked at the interaction of continuous-wave neodymium-yttrium-aluminum-garnet (Nd-YAG) laser energy with root canal wall dentin and suggested that the lack of consistency in effect was largely due to the tendency of the energy to transmit through translucent, sclerotic areas of dentin and to be more readily absorbed in the opaque, nonsclerotic areas. In theory, the degree of reflection should influence the power necessary to create a given effect; unfortunately any influence this may have had was masked by the overwhelming variation caused by the selective absorption seen with this laser. The reflectance of 1.06μm light by root canal wall dentin must therefore be an assumed value since no better information is presently available.

The 10.6μm light emitted from the CO_2 laser has absorption characteristics which are known to vary considerable from that of the Nd-YAG laser. Most applications in the literature use a reflectance coefficient of zero, and a depth of penetration of 10μm to 100μm (i.e. the depth over which 100% of the incident energy is absorbed)[164,165].

Instrumented Canal Wall Dentin

As previously mentioned, one of the cornerstones of endodontic therapy is the cleaning and shaping of the root canal prior to filling it with an inert filling material. This cleaning and shaping is usually referred to as the *instrumentation* of the canal. During instrumentation, however, the surface of the dentin is altered in such a way as to change both its appearance and its behavior. This surface alteration is known as the *smear layer*.

The Smear Layer

The smear layer is a layer of dentin chips and organic debris created by instrumentation of the canal wall. This layer is densely packed and varies from about 1µm to 5µm in thickness. The smear layer is readily distinguished from normal (i.e. untouched) canal wall dentin when viewed with a scanning electron microscope (SEM). Its SEM appearance is characterized by the absence of dentinal tubule openings, which are a major feature of untouched canal wall dentin. This is due to the packed debris, which occludes the tubule openings. Not surprisingly, Pashley et al.[166] found that the smear layer reduces the permeability of dentin to fluids when compared to dentin where the smear layer has been removed. Unfortunately, this reduction in permeability is not complete.

The effect of the presence of the smear layer on the reaction of dentin to laser irradiation is not clear. It could influence the optical properties to some degree. Also, it could facilitate the production of a continuously glazed surface by initially occluding the tubule openings, thereby reducing the size of the area to be bridged by the molten dentin during irradiation.

In this work, a smear layer was present on all irradiated surfaces. In practice, it is likely that irradiated surfaces will consist of areas where a smear layer is and is not present.

Laser Output Parameters

For clinical purposes, the output of a laser is defined by its power (peak or average), wavelength, mode of operation (e.g. continuous-wave, pulsed, Q-switched), spot size, TEM mode (i.e. spatial distribution of energy), and duration. For the purposes of this study, some of these characteristics are of greater importance than others. The following discussion will center on clinically relevant considerations rather than theoretical descriptions of these characteristics.

Power

The output power can be thought of as an instantaneous measure of the energy output; that is, power integrated over time will give the energy output during that time. It is important in a clinical sense in that it is one of the output parameters which can be controlled by the clinician. When controlled in conjunction with other output parameters (i.e. mode of operation and duration), the energy output can be precisely defined and controlled. Obviously, precise control over the energy delivered to the patient is a stringent requirement for the use of lasers in the clinical setting.

The influence that power demonstrates on laser-induced thermal effects can vary depending on the target material and other factors. For example, varying the power output of a Nd-YAG laser may not create discernible differences when irradiating translucent dentin; however, clinically apparent differences may arise when the same powers are used to irradiate pigmented tissues such as hemangiomas, nevi, tattoos, and black skin. This serves to illustrate the dependency of the laser-induced effect on the interrelation of the output parameters as a whole and the material being irradiated.

Wavelength

The wavelength (or, inversely, the frequency) of the laser output is the characteristic which predominantly determines where it is used in medicine. This is because of the strong dependency of the overall absorption characteristics of the target material on the wavelength. In general, the longer the wavelength, the higher the absorption coefficients. For example, the shorter wavelength output of the Nd-YAG laser tends to penetrate many biological tissues to a large degree, and its absorption is greatly affected by other factors such as the degree of pigmentation; on the other hand, the longer wavelength of the CO_2 laser is absorbed so well that it appears to be independent of pigmentation. In fact, analytical models in the literature commonly assume 100% CO_2 laser energy absorption on the surface or within 100μm of most materials.[164,165] The high absorption characteristic of the CO_2 laser is a very desirable thing when considering the tissue/laser interaction required for some clinical uses (e.g. scalpel), but it has made delivering the beam through an optical fiber impossible. For years various researchers have sought a solution to this beam delivery problem, without success, until the recent development of the wave-guide dental laser system at The University of Alberta by Dr. John Tulip and his team of engineers. This new dental laser system represents a break-through in laser technology, and at the same time removes the single largest roadblock to the widespread use of lasers in dentistry; i.e. the absence of a laser system which affords ease of use and convenient access to all areas of the oral cavity.

Mode of Operation

When used in this context, the word *mode* refers to the overall waveform of the laser output, and not the spatial distribution of energy (as in TEM mode). In other words, the mode of operation describes the time behavior of the laser output. The modes of operation available with current laser systems include 1) continuous-wave, 2) pulsed, and 3) Q-switched modes. Only continuous -wave and pulsed modes were used in this work; however, for purposes of comparison, all three of the above modes will be briefly described.

Continuous-Wave

When the output beam is of a relatively long duration and constant power, the laser is said to be operating *continuously*, or in the *continuous-wave* mode. In the clinical setting, the power is usually controlled by the operator. Most systems offer an on-board metering system which measures average power on demand. Conceptually, this mode of operation is probably the easiest to understand for those without a technical background.

A continuous beam can be interrupted by either internal or external means (e.g. by shuttering or by turning the laser on and off). This results in an output waveform which approximates a rectangular wave where the amplitude, duration and repetition rate of each square "pulse" can be controlled. The methods of interrupting a continuous beam are typically limited in their ability to interrupt the beam at very fast rates, and cannot approach the repetition rates seen with pulsed or Q-switched lasers. Furthermore, the power level of these flat pulses is necessarily the same as the continuous beam from which they were derived. The practice of using the word *pulse* for these rectangular waves and also for the output of super-pulsed and Q-switched lasers (and, for that matter, the word *mode* to describe more than one thing) accentuates the need to consider the context in which it is used if confusion is to be avoided.

Super-Pulsed

There are several means available to operate a laser such that the output consists of pulses of very short durations compared with those available from an interrupted continuous beam. These pulses have typical durations in the range from 100μsec to 1000μsec, and are not usually rectangular in shape. At any given average power setting, the peaks of these pulses are very much higher than the average power(generally in the thousands of watts for lasers capable of tens of watts average power). When operating in this mode, the clinician is sometimes able (depending on the laser system in use) to vary not only the average power, but also the duty cycle, pulse repetition rate, and pulse train duration. The actual shape of the pulse can vary widely depending on factors such as the type of pulsing mechanism used and the design of the laser itself. For example, in many cases the emission is not uniform but consists of many microsecond duration spikes called relaxation oscillations[167]. It is not at all clear whether either the shape of such a short pulse or the presence of relaxation oscillations within such a pulse will make a clinically significant difference when compared to a rectangular pulse of the same average power and duration. However, differences in effect on tissue between the continuous-wave and pulsed Nd-YAG laser have been observed in certain situations. This serves to point out that the effect on tissue of laser irradiation can be dependent to some degree on the output waveform.

Q-Switched

By employing the Q-switching technique, one obtains pulses in the 10-1000 nsec range. Q-switching implies the changing of the Q (or quality) of the laser resonant cavity.* Besides delivering pulses much shorter than that available with normally pulsed lasers, Q-switching also can deliver peak powers substantially higher than pulsed lasers (e.g. gigawatts). Although Q-switched lasers have been used in other investigations of the interaction of laser energy and tooth structure, one was not available and therefore not included in the present work.

Spot Size

The term *spot* is used to describe the area over which the beam is focused on the surface of the target material. This area has a direct effect on the power density, or *irradiance*, seen on the surface. Small variations in the spot size can result in significant differences in the incident power density, especially when using small spot diameters such as one millimeter or less. For example, increasing the spot radius from 0.5 mm to 1.0 mm will result in a fourfold decrease in the incident power density. This could, in some cases, cause an clinically unacceptable drop in laser-induced surface temperature. This parameter is one which should be continuously monitored for consistency.

For the purposes of this thesis, this physical definition of spot size is to be distinguished from the theoretical value, ω_0, which is also referred to as the spot size but is defined as the radius of the beam waist in a Gaussian (i.e. TEM_{00} mode) beam at

---

*The Q or quality factor of a cavity resonator is defined as the energy stored in the cavity divided by the energy lost from the cavity per cycle of the field. Thus, a high Q cavity will store energy well; a low Q cavity will emit the stored energy rapidly. Switching rapidly from a condition of high to low Q will result in rapid extraction at high power.

$z = 0$ where z is a measure of the distance in the direction of propagation[168]. The physical definition of this parameter is useful because it is usually controllable by the clinician, whereas ω_0 is determined by the design of the laser cavity, and represents the minimum spot size since the Gaussian beam will diverge as the distance from the laser source increases.

TEM Mode

The resonant cavity defined by the mirrors of a laser has certain stable configurations of the electromagnetic field called ***transverse electric and magnetic modes***, or ***TEM modes***. Each axial (or longitudinal) mode involves a standing wave with an integral number of half-wavelengths contained within the cavity. In other words, the axial modes may be regarded as field configurations in which n half-wavelengths of the light lie between the mirrors, with a node at each mirror. These modes can vary in complexity and in degree of alignment with the laser cavity. More complex (i.e. ***higher order***) TEM modes correspond to propagation of waves at slight angles to the axis of the laser system, and because of this generally suffer from higher diffraction losses. This results in a laser system which tends to operate in a small number of simpler, low order modes which, due to better alignment of the direction of propagation with the axis of the laser cavity, suffer less loss.

The power in a well-defined mode has a definite transverse spatial distribution. In theory, the mode of a resonator with the index number *qmn* (i.e., the TEM_{mn} mode) has an intensity distribution, in rectangular coordinates, given by

$$I_{m,n}(x,y) = \left\{ H_m\left(\frac{\sqrt{2x}}{\omega}\right) H_n\left(\frac{\sqrt{2x}}{\omega}\right) exp\left[-\frac{(x^2+y^2)}{\omega^2}\right]\right\}^2 \qquad (4)$$

where $I_{m,n}$ is the intensity distribution, H_m is the Hermite polynomial of order m, and ω is the previously described theoretical spot size of the beam, defined as the radius at which the intensity of the TEM_{00} mode is $1/e^2$ of its value on the axis[169].

Since the changes in biological tissue which result from laser irradiation are thermally induced[170-173] and the tissue temperature is directly related to the power, these TEM modes are important insofar as they affect the maximum power output of the laser. Operation in a single, low-order mode (e.g., TEM_{00}) is desirable because it minimizes the diffraction losses and therefore maximizes the total power input to whatever beam delivery system is being used. Furthermore, operation in a single low-order mode is desirable because it is generally possible to focus these beams to exceedingly small focal spots. This is in contrast to single or multi- higher mode operation where focusing the beam to such a small spot becomes difficult to impossible. An example of a use where an extremely small spot size is necessary is the use of the laser as a scalpel, where it is desired to keep the width of the incision to a minimum.

Duration

Duration indicates the time over which the laser output is allowed to impinge on the target tissue. In the case of continuous operation, this is merely the time from the start of the laser irradiation to when it ceases. With interrupted continuous, normally pulsed and Q-switched beams, it signifies the period over which the pulses occur in succession, and may also be referred to as the *pulse train duration.*

In simple terms, the concept of thermal diffusivity holds that time is required for heat to flow; the longer the time available, the farther the heat will flow under a given temperature gradient. The duration of laser irradiation strongly influences both the temperature gradient and the time over which this gradient exists. The duration must be of at least a certain minimum length if the target is to reach a given temperature. Contrarily, the duration must be no greater than a certain maximum length if the temperature at a certain depth in the tissue is to be kept at or below a given level. Considerations such as these are important when developing clinical applications of lasers.

Laser/Tissue Interaction

General Interaction Phenomena

In general, when electromagnetic radiation impinges on a thin layer of matter, tissues in particular, part is reflected, part is absorbed, and part is transmitted. The absorbed portion (i.e., the incident radiation less the sum of the reflected and transmitted portions) interacts with matter.

Qualitative Interaction

The qualitative nature of the interaction of electromagnetic radiation with matter depends only on the frequency, not the intensity, of the radiation[174]. Very energetic particle radiation, such as that of the γ-rays or x-rays, travel a long distance in tissues (i.e., centimeters) and ionizes and disrupts the strongest molecular bonds, thus forming reactive molecular fragments. As the wavelength of the radiation increases, its energy decreases and the interactions occur with progressively less energetic molecular bonds. In the visible portion of the electromagnetic spectrum, ionization phenomenon cease. Although many photochemical reactions essential to life (e.g., vision) take place in this wave length region, the preponderance of the interactions in the visible and farther in the infrared spectrum takes place through excitation of vibronic spectra, leading to heating. All lasers used in surgery are in either the visible or the infrared region of the electromagnetic spectrum, and their primary form of interaction with tissues leads to heating.

Quantitative Interaction

Surgery with lasers is a process of tissue vaporization or devitalization through the thermal effects of intense radiation. The quantitative nature of the surgical wound depends on the intensity of the radiation, the total energy delivered to the tissues, and the wavelength of the radiation. Other factors strongly influenced by the wavelength which also are important are the absorption, extinction length, and scattering of the radiation. It is important to note that in the following definitions of these factors, the intensity of the radiation incident on a material is assumed to be low enough to leave the material unaltered.

Absorption and Extinction Length. Consider a parallel beam of intensity I_t impinging on a thin slab of material of thickness, x (Figure 12). If I_r is the reflected and I is the transmitted portion, the absorbed portion ~~will be~~ $I_o = I_t - I$, where, for simplicity, $I_t = I_t - I_r$. In general, I and I_o are related through Beer's law:

$$I = I_o 10^{-\alpha x} \tag{5}$$

The constant α, the absorption coefficient, depends on the wave length of the radiation and the physical and chemical composition of the absorbing material. Note that when the thickness of the slab is $= \frac{1}{\alpha}$, the transmitted intensity is $I = I_o 10^{-1}$ or $0.1I_o$. In other words, 90% of the incident radiation is absorbed in a thickness $L = \frac{1}{\alpha}$ of the material. The thickness L, as α, characterizes the absorptive properties of a material, and is referred to as the *extinction length.* If the thickness is 2L, the second slab of thickness L will absorb 90% of the 10% incident on it, and 1% will be transmitted. For all practical purposes, there is no radiation present past three extinction lengths, and the bulk of the radiation is present to a depth of one extinction length (Figure 13).

More specifically, several investigators have inferred that infrared radiation is absorbed through vibrational modes of molecules, that the energy is "collision thermalized" to produce an elevation in temperature[171-176], and that the lifetime of the excited vibrational levels is smaller than 10^{-12} seconds[171]. Sagi et al.[165] consider the fact that this lifetime is extremely short compared to conventional laser pulses as being confirming evidence that the absorbed laser energy is in fact the heat source in the irradiated material.

Scattering. Light waves impinging on a material are rarely transmitted without alteration in direction. Inhomogeneities of all kinds that exist in most materials, and very pronouncedly in biological tissues, deflect the incoming radiation in all directions, and an initially parallel beam loses its parallelism and delivers the energy in a volume which is more ovoid or elliptical rather than cylindrical in shape. Scattering can also result in radiation being turned around so that it exits the material on the same side as it had entered; this is referred to as *backscattering*. In general, scattering is strong if absorption is low and the material is very inhomogeneous. Thus, inhomogeneity of the irradiated material has the effect of decreasing the extinction length.

Furthermore, if the scattered light has the same frequency as the incident light, it is referred to as *Rayleigh* scattering. However, some very weak additional frequencies may occur which are not present in the original incident spectrum. This phenomenon was discovered first by Raman and his collaborators in 1928, and is now commonly called *Raman* scattering. *Brillouin* scattering can be detected when light passes through an optical medium which is completely free of structural inhomogenieties. In this case, the scattering is due to the fluctuating dielectric inhomogenieties associated with the thermal agitation of the medium. From the classical standpoint, Brillouin scattering can be interpreted as the result of reflections, in a given direction, from the elastic waves of the material. In a sense, the heat content of a medium can be considered as a thermal source of sound (or elastic) waves within the medium[177].

Extinction Length and Scattering for the Laser Beams Used in Surgery.

CARBON DIOXIDE LASER. Radiation of this laser at λ=10.6μm is strongly absorbed by pure homogeneous water and by all biological tissues. The extinction length is approximately 0.03 mm in water and at least as short in tissues. Reflection and scattering are usually assumed to be negligible, but in certain cases can be significant.

Nd-YAG LASER. Its radiation at λ= 1.06 μm is weakly absorbed by pure water in which the extinction length is approximately 60 mm. Absorption is slightly color dependent, increasing substantially for very dark materials such as ink, darkly pigmented tissues, and carbonaceous particles. In biological tissues, strong scattering determines the extinction length, which is approximately 2 ± 1 mm[175]. Backscattering may be significant (20 to 40%).

ARGON LASER. Even though this surgical laser is not included in this work, a short description is included here for purposes of comparison. Its visible radiation at λ=0.48μm may be strongly absorbed, scattered, or reflected, depending on the specific tissue. For pure water, the extinction length is many meters. It is strongly absorbed by blood and all pigmented tissues and absorbed and reflected to varying degrees by white colored tissues such as Caucasian skin, fat, and bone.

An interesting feature of laser-tissue interaction is a conjecture held by some that the scattering process leads to higher temperatures inside the tissue than at the surface, and is thus responsible for the popcorn effect often observed when tissue is irradiated to the boiling point. This is explained by the "decrepitation" theory, which states that the maximum radiation intensity in the presence of scattering lies not at the irradiated surface, but at an interior point of the medium[178]. For Nd-YAG radiation the depth of the maximum can be on the order of 0.5 millimeters, whereas for more strongly absorbed CO_2 light, it should be much closer to the surface. Indeed, it was observed that the popcorn effect seen with the Nd-YAG laser was minimized to a great degree in the case of the CO_2 laser. An analytical proof of the general 3-dimensional version of this theory if offered by Langerholc[178]. Marchesini et al.[179] has experimentally confirmed the decrepitation theory for mucosal tissue where scattering is predominant in respect to absorption. Here, a thermographic camera was used to show that depths greater than 3 millimeters never reached the threshold temperature for coagulation when irradiated with a Nd-YAG laser. In accordance with the decrepitation theorem, the maximum temperature was shown to exist 1 millimeter beneath the surface.

Thermal Effects on Living Tissue

Soft Tissue

Within any soft tissue, heating produces a relatively predictable sequence of effects. Labile (i.e., unstable) proteins and enzymes are denatured by changes in their tertiary structure, as the weak bonds which maintain conformation are overcome by kinetic excitations. Many proteins are affected in this manner between 50 and 80°C[180-182]; in particular, human collagens denature at approximately 60°C[181] to 75°C[182]. Denaturation of collagen results in marked shrinkage along the fiber axis, such that denaturation of perivascular collagen results in partial vessel collapse[183,184].

Furthermore, denaturation increases the viscosity of blood plasma proteins, which also aids in hemostasis.

Cell survival of increased temperatures is dependent on both the cell type and the duration of heating. For example, thermophilic bacteria adapted for survival in hot springs have increased disulfide bridges that stabilize certain structural proteins and enzymes. Even these cells are incapable of active survival at temperatures much above 80°C, at which denaturation of nucleic acids occurs. Dormant spores and certain viruses survive hotter temperatures by maintenance of more rigid conformational states of their genetic material. Since mammalian soft tissue cells neither sporulate nor are particularly adapted for thermal survival, time periods of tens of milliseconds or longer at temperatures above 70 to 80°C will inactivate most mammalian cells. Some consider tissue raised to 60°C for even short periods of time to be permanently damaged[185,186]. During prolonged heating, partial injury or metabolic derangements and cell death may occur at temperatures as low as 42°C.

Tissues irradiated by a CO_2 laser beam generally do not reach a temperature greater than about 100°C[187]. At that point, the water which constitutes approximately 85% of soft tissues acts as a sink for further (i.e. latent) heat input and laser power is expended in providing latent heat for the water to boil explosively. This heat of vaporization of water is great (540 cal/g or 2,257 Joules/g), such that further energy added to the tissue after reaching 100°C results in the generation of increasing quantities of steam without necessarily much further increase in temperature. A 1670-fold volume expansion occurs when water is vaporized isobarically. If this large and rapid expansion occurs within tissue, physical separation or "cutting" occurs. During the laser pulse, the surface of the soft tissue rapidly recedes as successively deeper layers are ablated. Only the debris from ruptured cells reach significantly higher temperatures if they lie in the path of the beam. These cells are typically carbonized, and can act as a source of conductive heat at the wound edges which can, in turn, denature and coagulate the surrounding tissue, resulting in hemostasis.

The conversion of electromagnetic energy to acoustic energy can also occur when a liquid is irradiated with a pulsed infrared laser beam. These sound waves are thought to be generated by the recoil pulse produced upon evaporation at the surface and, also, by the thermal expansion due to a temperature gradient produced in the target material[188-190]. The temperature gradients which produce these sound waves have the potential of producing related stress fields in the material. In supple materials such as soft tissue, these stresses can be quickly dissipated; however, in more rigid structures such as enamel and dentin, this is not possible to the same degree.

Hard Tissue

Perhaps as a result of the fascination historically held by clinicians for the laser, many qualitative and/or preliminary investigations were performed, especially in the early years, of the general effects of lasers on hard dental tissues which were of high clinical import. These studies were necessarily diverse, and were intended to determine whether the laser held promise for clinical use in dentistry. For example, studies were performed on the production of craters in hard tissue[191-194], the "plume" associated with laser impact on teeth[195], the effect of dying the tooth surface before irradiation[196], the ability of the laser to drill cavity preparations[197,198], the ability of the laser to remove caries[199,200], the effects of laser-heating the tooth surface on the pulp[201], the potential of fusing restorative materials to tooth structure[202,203], and the lasers' ability to fuse powdered tooth structure and also other materials used in dentistry[204]. These studies also noted the ability of the laser to create a range of effects on enamel which included melting, cracking, pore formation, and vaporization.

More quantitative investigations were also done on the effects of laser irradiation on enamel, dentin, and bone, and are available in the literature. These studies will now be summarized.

Enamel

MICROSTRUCTURAL CHANGES. Even before the advent of the laser, it was known that subjecting hydroxyapatite to high temperatures (i.e. around 1400°C) would cause changes in the microstructure of the molecule; i.e. a conversion to α-calcium orthophosphate[205]. Techniques which have since been used to analyze laser-induced microstructural changes in enamel include X-ray diffraction[206-212], polarized light microscopy[191,213,214], infrared spectroscopy[212], electron probe microanalysis[213], scanning electron microscopy[212,215], microradiography[213-215], analysis of ground sections by phase-contrast microscopy[207], and microhardness testing[206,211,216]. Most of these studies used the continuous-wave CO_2 laser[207,208,211-213]; however, other studies used the pulsed CO_2 laser[216,216], pulsed ruby laser[206], a continuous-wave argon laser[209], and an oven[210] as the heat source.

Contrary to the results of subsequent investigations by other authors, Lobene and Fine[206] in 1966 found no change in the radiodensity of enamel or the hydroxyapatite configuration of enamel after ruby laser irradiation. Their report of finding no change in the microhardness of irradiated enamel was also corroborated later by Brune[211]. Furthermore, they reported that staining the surface of the enamel black helped to localize the incident energy at that surface. Their results can be explained by noting they used a ruby laser, which does not, at equivalent energies, deliver temperatures as high in enamel as the CO_2 laser, which was used with most of these other works. Lobene and Fine[206] did notice, however, a change in the birefringence of irradiated enamel which they attributed to disrupted enamel rods. This result was also corroborated in a later investigation by Lobene et al.[207], during which was also found the incineration of the odontoblastic processes underlying the irradiated enamel. Lobene et al.[207] also macroscopically described the irradiated enamel to be chalky white in color, opaque, and brittle (as did Stern et al.[215]) and to be composed of a small amount of α-calcium orthophosphate along with the major component of hydroxyapatite (which agrees with Kantola et al.[208] and Brune[211]). In accordance with the observation by Peck and Peck[191] (based on polarized light microscopy) of crystallographic changes in irradiated enamel, Kantola et al.[208] and Goodman and Kaufman[209] found not only recrystallization to have occurred in irradiated enamel (as did Stern et al.[215]), but also growth of the crystal size. Goodman and Kaufman[209] also found that enamel powder, when mixed with NaF, underwent a significant uptake of fluoride upon irradiation and resulted in a reduction of the dissolution rate in acid. In 1984, Kuroda[212] sought to more precisely determine the composition of laser-irradiated enamel. He used X-ray diffraction and infrared spectroscopy in this investigation, and found that the solidified melt of enamel consisted of minor phases of α-tricalcium phosphate, $Ca_4(PO_4)_2O$, and a major phase of modified apatite. The apatite modifications, as compared with the original, were (1) reductions in contents of water, protein, carbonate, and chloride; (2) essentially no change in apatite hydroxide content; (3) possible incorporation of oxide replacing some hydroxide ions; and (4) an uptake of traces of carbon dioxide and cyanate.

RESISTANCE TO DEMINERALIZATION. In the incipient stage of dental caries one of the most distinct microstructural features is a pronounced subsurface demineralization of the enamel, as much as 1000 μm deep, prior to the invasion and advanced destruction of the tooth structure by oral micro-organisms[217]. Early preliminary observations indicated a potential for the laser to have some effect on the degree to which this demineralization occurred in carious environments. The implication for preventive purposes was obvious, and several studies investigating this issue followed. Several lasers were used; the pulsed ruby[218,219], the pulsed CO_2[220,221], the pulsed Nd-YAG[222], and the Q-switched Nd-YAG[223]. The analytical techniques included high resolution microradiography[218,219,221-224], scanning electron microscopy[221-223,225], polarized light microscopy[225], and diffusion cell permeability analysis[220].

An overwhelming number of these papers found there to be an increase in the ability of the laser-irradiated enamel to resist subsurface demineralization in acidic environments when compared with nonirradiated control enamel[216,218,219,221-223]. Other observations included a decrease in enamel permeability with no change in solubility[219]; a microscopically smoother surface on irradiated enamel compared with unirradiated enamel[220,221,226]; a decrease in solubility in irradiated enamel compared with nonirradiated control enamel[222,223]; and a decrease in solubility in sodium acetate of enamel powder irradiated in the presence of sodium fluoride (NaF)[209]. Surprisingly enough, Borggreven et al.[220] found laser irradiation of enamel to *increase* the permeability. This contrary result can be explained by the fact that a pulsed-CO_2 laser was used to irradiate very thin sections of enamel. As will be seen later on in this thesis, the pulsed CO_2 laser appeared to create the severest thermal stresses of any of the three lasers used. The possibility that the thin enamel slices used by Borggreven underwent microcracking would seem great, especially in view of the renown tendency of enamel to demonstrate brittleness when removed from its normal underlying dentinal support. (Moreover, an account of the thermal stresses induced by the laser impact was not given.) Also, due to the translucency of enamel in the visible spectrum, such cracks may well have escaped notice when the samples were inspected for cracks with an ordinary dissecting microscope. Therefore, it would seem plausible that the increase in enamel permeability upon pulsed-CO_2 laser irradiation found by Borggreven could well be due to cracking peculiar to the geometry of the prepared specimen rather than to a change in some other factor known to influence permeability of whole, intact enamel with full dentin support, as in the case of a healthy tooth.

Given the above observations, it seemed possible that the mechanism for the increase in resistance to subsurface demineralization involved a decrease in enamel permeability due to a smoothing of the surface, and/or an actual reduction of the solubility of enamel in carious environments. However, in 1977, Newesely[210] pointed out that α-calcium orthophosphate, which had been shown to be present in small amounts after laser irradiation of enamel, is *more* soluble than hydroxyapatite in aqueous environments, and that this implied that laser-irradiated enamel should, in theory, be *less* resistant to demineralization. He explained the previous contrary results by noting their exposure of the relatively dense irradiated, "glazed" surface to the carious environment was for too short of a time period for the solubility reaction to reach equilibrium, and that if equilibrium were to have been obtained, there was no way the reaction would have yielded an increase in caries resistance over the long term. Then, in 1983, Sato[225] found that the often observed increase in resistance to subsurface demineralization occurs at temperatures around 300 to 400°C. This suggested that water and organic changes seem to be the cause of the decrease in permeability, which in turn results in the increased resistance to subsurface demineralization. These organic changes may include thermal denaturation[227], melting, and swelling. These changes seem not only to disturb the ability of enamel to rehydrate after heat desiccation as shown by Burnett and Zenewitz[228] and Carlstrom et al.[229], but also to cause closing of pathways for water penetration into enamel.

Most recently, Nelson et al.[216] were successful in inhibiting artificial lesion formation with pulsed CO_2 laser pretreatment of the enamel surface. The authors noted a certain dependency of this observed inhibition to small variations in the laser wavelength, and that rapid surface melting and recrystallization had occurred. It was also suggested that the temperature rise beneath this melted surface is large enough to affect the organic matrix of the enamel to a depth of approximately 10 μm. It would seem, then, that the decrease in permeability thought by some to be responsible for the artificial caries inhibition may be due the organic effects mentioned by Sato[225] acting in concert with the fused enamel surface.

Dentin

Similar techniques were used to analyze the effects of high temperatures on dentin as were used on enamel, and included X-ray diffraction[45,230], microradiography[44], electron probe, scanning electron microscopy[230], and thermogravimetry[86,88,92,95]. Although some of these studies did not use a laser as the heat source (for example, the thermogravimetric studies), their results may still be considered relevant to the present discussion.

In 1968, Vahl[230] made craters in dentin using a pulsed ruby laser, and collected material from the "plume" resulting from laser impact. Upon X-ray diffraction analysis of the melted dentin, the presence of tricalcium phosphate was noted. Kantola subsequently found recrystallization and crystal growth to occur in laser-melted dentin, and that this dentin closely resembled the crystalline structure of the hydroxyapatite of normal enamel[45]; and that the calcium and phosphorous contents to be higher than in nonirradiated dentin.[44] This higher calcium and phosphorous content was attributed to the fact that the organic component of the dentin being vaporized, resulting in a higher density of the remaining inorganic constituent.

Thermogravimetric analyses of dentin have yielded results which offer insight into what may actually occur during laser-heating of dentin. Loss of water occurs from 60 to 150°C; protein decomposition from 280 to 350°C; burning of protein begins at

600°C; carbonate decomposition occurs from 530 to 750°C; and decomposition of β-tricalcium phosphate at 815°C. A breakdown of these effects, their temperatures, and their references is given in Table XI. Of curious note is the assertion by Lim and Loboff that collagen in a calcified matrix melts at a higher temperature than when it is in the absence of hydroxyapatite.

On a macroscopic level, Dederich et al.[49] found that, using a continuous-wave Nd-YAG laser, canal wall dentin could be melted and recrystallized such that the microtubules were blocked off, and that this could be done without surface cracking. It was suggested that this could effect a significant decrease in dentin permeability to fluids, and therefore was of import to endodontic therapy, perhaps in conjunction with the fusion of apical plugs. This study was the precursor to this thesis.

Bone

The bulk of the literature on the effects of lasers on bone describe studies in which either the pulsed[231-233] or continuous-wave[232-238] CO_2 laser was used. These investigations were performed on rats[236], and rabbits[231-233,235]. Delayed healing was found to occur in laser-induced bone defects when compared to mechanically-induced bone defects[232,234-236] with no difference in healing being found after 60 days[235]. This delay in healing was attributed to thermal damage to the laser-cut bone edges[235]. The pulsed CO_2 laser was found to cut bone more efficiently than the continuous-wave CO_2 laser; and the healing rates of bone defects created by these two lasers were found to be similar if the charred, necrotic tissue at the wound edges were removed, the pulsed CO_2 laser-induced bone defect healing faster if it was not[233]. It was also found that irradiating bone with laser energy, *in vivo*, could create fat emboli in the bloodstream[231].

A search of the literature did not reveal any investigation into the compositional changes which occur in bone upon laser irradiation. A related study[237], however, did assert that the transformation of the hydroxyapatite in bone to β-tricalcium phosphate takes place at about 800°C, which agrees with the value obtained by Lim and Loboff[95] for dentin hydroxyapatite.

Non-Thermal Effects on Living Tissue

The reactions which occur in living tissues following laser irradiation can include (in addition to the primary thermal response) many non-thermal effects. This would include elastic recoil and pressure wave formation (mentioned earlier), tissue ionization, harmonic frequency generation (second harmonics), multiphoton absorption processes, free radical formation, inverse Bremstrahlung heating, photochemically induced photooxidation, photohydration (especially of the pyrimidine bases of nucleic acids), and, Raman and Brillouin scattering with the subsequent formation of additional frequencies and sound waves of hypersonic frequencies. However, these effects are largely limited to the effects of pulsed laser irradiation since the magnitude of the electromagnetic fields necessary for many of these non-linear effects requires field strengths well beyond the capability of any continuous-wave laser source (eg. 10^6-10^9 Volts/cm)[238]. These effects, therefore, are not expected to play a significant role in the mathematical model used in this thesis to describe the thermal and stress distribution in dentin upon continuous-wave CO_2 laser impact.

Basic Heat Transfer Theory

Heat transfer is that science which seeks to predict the energy transfer which may take place between material bodies as a result of a temperature gradient. Heat transfer differs from the science of thermodynamics in that it seeks to predict the *rate* at which this energy transfer occurs, whereas thermodynamics deals with equilibrium situations.

Thermodynamics does, however, teach that this energy transfer is defined as *heat*. Heat transfer may take place by one or more of three methods: *conduction*, *convection*, and *radiation*.

Conduction

When a temperature gradient exists in a body, there is an energy transfer from the high-temperature region to the low-temperature region. This type of energy transfer is termed *conduction*. Here, the heat transfer rate per unit area is proportional to the normal temperature gradient. Repeating Eq. (1), we have

$$q = -kA\frac{\partial T}{\partial x} \tag{1}$$

where q is the heat transfer rate, A is the area over which the heat is flowing, $\partial T/\partial x$ is the temperature gradient in the direction of the heat flow, and k is the thermal conductivity of the material. The minus sign indicates that the heat must flow downhill on the temperature gradient; that is, from higher to lower temperatures. Eq. (1) is known as Fourier's law of heat conduction. Strictly speaking, the thermal conductivity k is not constant for a particular material over a range of temperatures. However, when the range of temperature is limited, this variation in k may be neglected[239]. In fact, k is assumed to be constant in most analytical work in this area. The general three-dimensional heat conduction equation for an *isotropic* material (i.e. a material where the heat can flow in all directions equally as well) where no heat is generated from within the material itself is

$$\frac{\partial^2 T}{\partial x^2} + \frac{\partial^2 T}{\partial y^2} + \frac{\partial^2 T}{\partial z^2} = \frac{1}{\alpha}\frac{\partial T}{\partial t} \tag{6}$$

where t is time, and α is the thermal diffusivity which, as mentioned earlier, is equal to $k/\rho c$ where k is the thermal conductivity, ρ is the density of the material, and c is the specific heat of the material[240]. The larger the value of α, the faster heat will diffuse through the material. In cylindrical coordinates, this equation becomes:

$$\frac{\partial^2 T}{\partial r^2} + \frac{1}{r}\frac{\partial T}{\partial r} + \frac{1}{r^2}\frac{\partial^2 T}{\partial \phi^2} + \frac{\partial^2 T}{\partial z^2} = \frac{1}{\alpha}\frac{\partial T}{\partial t} \tag{7}$$

Convection

When one body at one temperature is in thermal contact with another body at another temperature, and at the same time is moving in relation to this other body, convective heat transfer occurs. An example is cool water flowing over a hot plate of steel. Heat transfer due to convection is described by

$$q = hA\,(T_1 - T_2) \tag{8}$$

Here, the heat transfer rate is related to the overall temperature difference between the two bodies (T_1-T_2), and the surface area of contact, A. Besides being influenced by the temperature difference, the heat transfer rate is dependent upon the velocity with which these bodies move past each other. For example, in the case of water flowing over a steel plate, the faster the flow of water the faster the heat will be transferred. Here, the velocity of the flow decreases as you get closer to the plate as a result of viscous action, and is zero at the plate. Therefore, the heat transfer which occurs at the plate is due only to *conduction*. It is nevertheless necessary to consider the velocity of the fluid because of its strong influence on the temperature gradient; the greater the velocity, the greater the temperature gradient, and the greater the rate of heat transfer.

The quantity h in Eq. (7) is called the convection heat transfer coefficient, and takes these factors into consideration. The literature holds values for h which have been determined for many materials and physical situations. Heat transfer due to convection is not likely to be of significant importance in the experimental setup used in this work.

Radiation

In contrast to the mechanisms of conduction and convection, where energy transfer through a material medium is involved, heat may also be transferred into regions where a perfect vacuum exists. The mechanism in this case is electromagnetic radiation. This discussion will be limited to electromagnetic radiation which is propagated as a result of a temperature difference, called *thermal radiation*.

Thermodynamic considerations show that an ideal radiator, or *blackbody*, will emit energy at a rate proportional to the fourth power of the absolute temperature of the body[241]. When two bodies exchange heat by radiation, the net heat exchange is then proportional to the difference in T^4. Thus

$$q = \sigma A \, (T_1^4 - T_2^4) \tag{9}$$

where σ is the proportionality constant and is called the Stefan-Boltzmann constant with the value of 5.669×10^{-8} W/m^2-K^4. Equation (9) is called the Stefan-Boltzmann law of thermal radiation, and it applies only to blackbodies. It is important to note that this equation is valid only for thermal radiation; other types of electromagnetic radiation may not be treated so simply.

The term *blackbody* is used because black surfaces (such as a piece of metal painted black) approximate this type of behavior. Other types of surfaces, like a glossy painted surface or a polished metal plate, do not radiate as much energy as the blackbody; however, the total radiation emitted by these bodies still generally follows the T^4 proportionality. To take account for the "gray" nature of these surfaces another factor is introduced called the emissivity, ε, which relates the radiation of the "gray" surface to that of an ideal black surface. In addition, it is necessary to take into account the fact that not all the radiation leaving one surface will reach the other surface since electromagnetic radiation travels in straight lines and some will be lost to the surroundings. Therefore, two new factors are introduced into Eq. (9) to take into account both situations, so that

$$q = F_{\varepsilon} F_{G}\, \sigma A\, (T_1^4 - T_2^4) \qquad (10)$$

where F_{ε} is the emissivity function and F_{G} is the geometric "view factor" function[242]. Radiation heat transfer phenomena can be exceedingly complex, and the calculations are seldom as simple as implied by Eq. (9). However, as with convection, this method of heat transfer can be considered to be negligible in the experimental setup used in this work.

Basic Thermal Stress Theory

Deformations occur when forces are applied to a material. Strain, ε, is the amount of deformation per unit length, and stress, σ, the force per unit area. With stresses less than the proportional limit, the initial strain is essentially proportional to the stress; i.e. the stress-strain curve in this area is linear. The modulus of elasticity (Young's Modulus) is the ratio between the stress and this reversible strain, and is given earlier in Equation (3).

The expansion that normally occurs during the heating of a material arises from the more intense vibrations of the atoms. To a first approximation, the increase in length, $\frac{\Delta L}{L}$, is proportional to the change in temperature, ΔT:

$$\frac{\Delta L}{L} = \alpha_L \Delta T \tag{11}$$

Closer examination shows that, for many materials, the linear coefficient of thermal expansion, α_L, increases slightly with temperature[267]. However, it is often considered to be constant for analytical purposes. The *volume* coefficient of thermal expansion, α_V, bears the same relationship between the volume change, $\frac{\Delta V}{V}$, and temperature change, ΔT. For small strains, α_V is three times the value of α_L.[*]

Note that $\frac{\Delta L}{L}$ equals the strain, ε. For physically restricted bodies,

$$\varepsilon_T = 0 \tag{12}$$

---

[*] Materials such as graphite and mica are anisotropic; i.e., their properties vary with crystal direction. Therfore, a more general statement would be that

$$a_V = a_x + a_y + a_z$$

where the x, y, and z subscripts refer to the linear expansion coefficient in the three coordinate directions. When these are equal, as is the case with many materials,

$$a_V = 3a_L \ .$$

$$= \varepsilon_\theta + \varepsilon_E \tag{13}$$

$$= \alpha_L \Delta T + \frac{\sigma}{E} \tag{14}$$

where ε_T is the total strain, $\varepsilon_\theta = \alpha_L \Delta T$ and $\varepsilon_E = \sigma/E$. In other words, the total strain consists of the strain due to thermal expansion and the strain due to applied stress. Solving for the stress, we get

$$\sigma = - E \alpha_L \Delta T \tag{15}$$

which indicates that, for a given coefficient of thermal expansion and temperature gradient, the stress is directly proportional to the elastic modulus. If we assume the convention that compressive stress has a positive sign, the stress equation then becomes

$$\sigma = E \alpha_L \Delta T \tag{16}$$

It is important to note here that this assumes the body is restricted and not allowed to expand. Although this assumption is convenient to make when using equation (16) to calculate worst-case approximations of thermally induced stresses, it does not represent the situation as it really exists. Materials are always in contact with the materials which support them or restrict them. These supporting or restricting materials have their own deformation behaviors as well. It can therefore be expected that a physically restricted material undergoing a temperature increase will be allowed to expand to some degree, relieving a certain amount of internal stress as it does so. A material which is not physically restricted and is heated uniformly will expand to its fullest possible extent, and will not develop thermal stresses. Since most real world situations fall in the midground between these two extremes, they are better dealt with using such methods as computer assisted finite element analysis, where the material properties, geometry, heat flux loading conditions, and other complexities are much more precisely accounted for.

Numerical Analysis: The Finite Element Method

The literature abounds with theoretical (i.e. analytical or mathematical) models that relate in one way or another with the situation to be analyzed in this thesis[170,175,178,243-255]. For example, analytical models have been devised for laser-induced effects on soft tissues in general[170,175,178,247,249,250,252,253], and the retina in particular[244,247,248,254]. Most of these models sought to predict the temperature distribution upon laser irradiation, with some exceptions; Papa and Sethuraman[251] sought to model laser-induced vibrations in the eye, and Feiock and Goodwin[246] the stresses in water seen upon laser impact.

Unfortunately, analytical solutions are often difficult or impossible to determine because of the mathematical complexities involved. Numerical techniques have therefore evolved which offer approximations to these solutions. With the prevalence of computers in todays' research environment, these numerical methods have become much less cumbersome to perform than in years past.

Two common numerical methods of analysis are the *finite difference method* and the *finite element method*. Models have been derived, and can be found in the literature, which utilize the finite difference method[258-260] as well as the finite element method[258-261].

The finite element method has evolved into a very effective stress analysis tool for complex structural systems[262,263], and much research has also been directed to develop finite element techniques for the analysis of field problems[262-266]. An important such problem is the analysis of heat transfer, in order to predict the temperatures and the stresses in structural systems. Analysis of the heat transfer is generally done before the stress analysis, because the stresses in a material undergoing thermal change depend directly on the temperature gradients at any given time. Also, the material properties and boundary conditions can be temperature dependent (i.e. a nonlinear heat transfer analysis may be required). In other words, the output data from a heat transfer analysis program would serve as the input to a stress analysis program. In such a case, the preparation of input data to the stress analysis program could be minimized if the same finite element model is used in both the heat transfer and the stress analyses.

The finite element program used in this work is *ADINAT** (Automatic Dynamic Incremental Nonlinear Analysis of Temperatures) which can be used for general linear and nonlinear steady-state and transient heat transfer analysis. ADINAT is compatible with the stress analysis program ADINA. Thus, the output temperature data from ADINAT can conveniently serve as the input data to ADINA.

A numerical analysis of the temperatures and stresses resulting from continuous-wave laser impact on canal wall dentin is described in the section entitled *A Numerical Model: Temperature and Stress Results by the Finite Element Method*.

---

*ADINA Engineering, Inc., 71 Elton Avenue, Watertown, Mass. 02172, U.S.A.

CW-CO_2 Laser Effects on Canal Wall Dentin

Introduction

As previously stated, the carbon dioxide laser already enjoys a high level of use in medicine, predominantly as a scalpel and tissue ablation device. The beam characteristics which make it useful in this arena also hold the potential to make this laser useful in the dental application addressed by this thesis, namely, the sealing of the internal dentinal surface of an instrumented root canal. Its characteristic of extremely high absorptivity in biological tissues translates into an ability to create extremely high surface temperatures in exceedingly short periods of time. The question then arises as to whether these laser-induced surface temperature changes can, indeed, create shallow surface melting and subsequent recrystallization of the melted material in such a way as to occlude the dentinal tubules without introducing a significant degree of thermal/stress cracking on the surface of the impact area. Not surprisingly, this has not previously been determined by other investigators, largely due to the fact that the idea of using lasers to effect endodontic treatment in this manner originated only recently[49].

Therefore, the objectives of this portion of this thesis were: 1) to determine whether continuous-wave carbon dioxide laser irradiation can consistently glaze the surface of instrumented root canal wall dentin with minimal accompanying surface cracking; and 2) to determine any trends which may be present which relate the laser exposure parameters to their corresponding dentinal effects, in the effort to find which combination of exposure parameters, if any, result in satisfactory glazing of the canal wall without the occurrence of significant surface cracking.

Method and Materials

Twenty single-rooted teeth of unknown extraction dates were stored in a water and thymol solution to maintain complete hydration and to inhibit bacterial growth. They were then split labiolingually (longitudinally in a sagittal plane) using a thin carborundum separating disc and a slow speed handpiece. This divided the root canal space in two between the resulting halves of the tooth. The root canal and pulp chamber concavities were then debrided of any remaining necrotic tissue and debris. The canal concavities were instrumented with a Gates Glidden bur to simulate the instrumentation normally accomplished *in vivo* (Figure 14). The teeth were then placed back in the thymol-water solution to await irradiation.

Individually, and randomly, each half-tooth specimen was then removed from the thymol solution, blotted dry, and irradiated at six locations along the canal length at one specific combination of power and pulse duration. A surgical binocular carbon dioxide laser was used with a 400 mm focal length lens. The beam was aimed with a movable cross-hairs image which was visibly superimposed on the field of view. The focal spot diameter was set to approximate one millimeter in diameter, and was left as such for the whole experiment. Upon completion of the exposures, the specimen was labeled and set aside. This process was repeated for each specimen until all 20 combinations of the power and pulse durations shown in Table XIV were used, resulting in a total of 120 exposures.

The specimens were then mounted on metal stubs with conductive glue, and placed in a vacuum chamber for three days to desiccate in preparation for observation with a scanning electron microscope. Upon removal from the vacuum chamber, the specimens were sputter coated with an extremely thin layer of gold in order to facilitate the electrical grounding of the specimen required during the electron bombardment seen with this form of microscopy. A scanning electron micrograph was made of each impact site (all at 55X magnification), and 8 X 10 prints were made. Opaque tape was placed over the information bar on these prints to minimize bias based on prehand knowledge of the exposure parameters used. The photographs were then randomly ordered in preparation for the measurement of laser-induced fusion (i.e. melting and recrystallization) and cracking.

Criteria were defined which identified cracking due largely to the desiccation required for scanning electron microscopic observation, and the cracks so identified were marked and thus excluded from measurement. The length of hairline cracking and the areas of wide cracking and fusion coverage were measured using the Bioquant Digitizing Morphometry Package* adapted for use on and IBM personal computer. These data were then subjected to a multivariate statistical analysis and the Duncan's multiple range test. Also, Pearson's correlation coefficients were calculated and a multiple regression procedure was performed in an effort to explain the sources of variation in the data.

Results

Pillai's multivariate tests indicated that significant differences existed in the data when the interaction of power and pulse duration was considered ($p<.001$), and also when power ($p<.001$) and duration ($p<.001$) were considered separately (see Table XV).

---

*Bioquant II Digitizing Morphometry Package by R&M Biometrics Inc., 5611 Ohio Avenue, Nashville, Tennessee 37209, U.S.A.

The MANOVA procedure indicated that the interaction of power and duration had a significant effect on hairline cracking ($p=.0333$) and on fusion coverage ($p<.0001$), assuming a confidence level of $\alpha=.05$. Furthermore, pulse duration alone was shown to significantly effect the area of wide cracking ($p=.0029$), as was power alone ($p=.0005$) (see Table XV). The results from the Duncan's multiple range tests for hairline cracking (power/duration interaction), fusion coverage (power/duration interaction), wide cracking (effect of power only), and wide cracking (effect of pulse duration only), are shown in Tables XVI through XIX, respectively.

Graphs of the mean values for hairline cracking, wide cracking, and fusion coverage can be found in Figures 15 through 19. Figures 15,16, and 17 show the effect of the interaction of power and pulse duration on hairline cracking, wide cracking, and fusion coverage, respectively; Figures 18 and 19 respectively show the effect on wide cracking of power only and pulse duration only. The Pearson correlation coefficients between the total energy in the pulse and hairline cracking, wide cracking, and area of fused surface are 0.6046 ($p<0.001$[*]), 0.4014 ($p<0.001$), and 0.8290 ($p<0.001$), respectively. The results from the multiple regression procedure are shown in Table XX. Scanning electron micrographs of laser impact sites which demonstrate the range of continuous-wave CO_2 laser-induced dentinal effects are shown in Plates 3 through 6. Plate 3 demonstrates no effect, Plate 4 hairline cracking only, Plate 5 fusion, hairline and wide cracking, and Plate 6 showing the desired result of "glazing" with minimal cracking.

---

[*] This p value represents the probability that a correlation coefficient this large would have resulted purely by chance.

Discussion

Several items require comment with regard to the method and materials section. Gates-Glidden burs are long-shanked burs with a football-shaped tip. They are one kind of bur commonly used in the instrumentation of root canals, and, like any other bur or instrument, tend to leave a smear layer of organic tissue and dentinal debris where it touches the surface of the dentin. It is unclear what effect, if any, the presence of the smear layer has on the optical properties of the dentin. It is possible that this debris, usually found already partially occluding the tubules, may facilitate the complete occlusion of these tubules during the melting and recrystallization of the dentin during and following laser impact. Such reasoning would indicate that the effect of the presence of a smear layer, if any, is a beneficial one.

When viewed at the canal wall, the orientation of the dentinal tubules is in cross-section, with the tubules arranged in a general radial direction. As previously mentioned, their numbers can be from 30,000 to 70,000 per square millimeter of canal wall surface. Since the composition, and therefore density, of this structure varies from the intertubular dentin to the peritubular dentin to the actual lumen of the tubule, an area of the size used for laser impact in this work represents a vast number of minute changes in the index of refraction. Add to that the presence of the smear layer, and the normal variation in tubular sclerosis (i.e. calcification of the lumen of the tubules; its effect is eventually to obliterate the lumen), and it becomes obvious that any description of the optical interaction of the laser beam with this microscopically inhomogeneous material must occur at a macroscopic level, because a microscopic description is impossible for practical purposes. Fortunately, since these minute variations occur with a typical resolution of around 1 to 2 μm, it is not unreasonable to consider dentin as approximating a macroscopically homogeneous material to the extent that we only differ translucent dentin from opaque dentin. However, this distinction may still be important since both areas of translucent dentin and opaque dentin may exist in any given impact site, and potentially introduce variation in the data. As has already been seen, most of the work describing the physical (i.e. mechanical) and thermal properties of dentin treated dentin as though it was a homogeneous, isotropic material, largely to avoid the experimental complexities which would arise were this assumption not made. The mathematical and numerical models of heat transport in dentin available in the literature generally assume dentin to be isotropic with respect to its thermal properties. Using a macroscopic point of view, and knowledge of the fact that the carbon dioxide laser wavelength (λ= 10.6 μm) is very efficiently absorbed by water and all biological tissues, this situation can be simplified into one of defining a value for the extinction length of the beam in the tissue.

Randomization of the teeth before laser irradiation in theory distributes the variation (or error) due to unknown and/or uncontrolled tooth-associated confounding variables equally between all groups[*]. In general, these tooth-associated confounding variables potentially include variations in micro- and macro- structure, the initial (i.e.

---

[*] A group, in this case, consists of those laser impact sites which were irradiated at identical exposure parameters. Here, there are six impact sites per group.

pre-irradiation) presence of fractures, the age of the specimen, the stress history of the specimen, variations in the thermal and mechanical properties of the specimen, the hydration history of the specimen, variations in hydration of the specimen during irradiation, and other unknown variables as well. Since controlling all pertinent variables is usually much easier said than done, randomization has become the cornerstone of good experimental design.

Blotting of the canal wall before irradiation was intended to mimic the situation *in vivo* , where the canal is partially dried with a sterile paper point (a small, conical structure of absorbent paper). Besides making the method a little more relevant to the actual clinical situation, blotting the canal wall potentially served to minimize the variation in volume of excess surface water. This surface water can affect the amount of energy required to achieve any given dentinal effect since it must first be heated and vaporized before significant changes can occur in the underlying dentin.

Measurement of the cracking and fusion was accomplished by fastening each SEM photograph, individually and in a random order, onto a digitizing pad connected to an IBM personal computer running BIOQUANT II Digitizing Morphometry software. Previously, each photograph had the visible cracks and fused areas traced with colored pens for easier identification Each hairline cracking segment was traced and then marked so as to avoid duplicate entry. This was done until all segments had been recorded. The software was then commanded to perform a summation of these values, giving the total accumulated length of hairline cracking for the photograph in question. The sequence followed for the wide cracking and fusion coverage was identical with the exception that areas were measured instead of lengths. These data were then recorded for subsequent analysis.

Since two of the three measured dependent variables (or attributes) were types of cracking, it was necessary to develop a means to minimize the confounding effect of artifactual cracking; specifically, desiccation cracking due to specimen preparation for scanning electron microscopic observation. As mentioned previously, criteria were defined by which these desiccation cracks would be identified, and then they were marked so as not to be included in the subsequent measurement process. These criteria were 1) that they be neither in a general radial nor circumferential orientation to the impact center, and 2) that they run a large percentage of the way down the root, showing no particular relationship to any given impact site. The rationale for this criteria was based on the known tendency for stress cracking in teeth due to laser impact to be either radial or circumferential in orientation[159] to the center of the impact site. However, whether those cracks identified as desiccation cracks were due solely to desiccation or were due to irradiation, or perhaps a combination of the effects of both, was not measured directly. This, therefore, remains a source of error, albeit a source minimized within the limits of the ability of the criteria to truly detect the cracks actually due solely to desiccation. It is important to note, however, that in another yet unpublished study of the effects of continuous-wave Nd-YAG laser energy on dyed canal wall dentin, the data in the irradiated group was found to have means significantly greater than that in an unirradiated control group which was only prepared for SEM observation. This suggests that artifactual cracking due to SEM desiccation is not a significant source of error, especially when the most obvious cracks are eliminated by the above criteria.

The rationale for choosing the attributes of hairline cracking, wide cracking, and fusion coverage as the measured dependent variables has to do both with their clinical significance and with their descriptive value of the temperatures and stresses which occurred during irradiation. The clinical significance relates both to dentin permeability and the objective of root canal therapy, which is to minimize or eliminate leakage to and from the root canal space. It is assumed in this work that both decreasing the amount of cracking and increasing the area of glazed surface will result in less leakage into the tubules than if the opposite were true.* Therefore, the objective would seem to be one of minimizing or eliminating surface cracking† of any kind, while, at the same time, maximizing the fusion coverage. This, of course, should occur without the creation of a crater of any significant depth (which can easily occur at the higher powers and pulse durations). This is necessary because the thickness of the dentin in the apical portions of the roots is likely to be neither sufficient to dimensionally accommodate deep craters nor to sufficiently insulate the surrounding periradicular tissues from thermal damage.

The descriptive value of the cracking and fusion lie in the manner in which they relate to the laser exposure parameters which created them. These relationships will be described in more detail shortly; but for now it can be said that the general trends for higher powers to result in more fusion coverage, and for longer pulse durations to result in more cracking, were obvious even to cursory subjective appraisals made during the actual experiment. The coincidence of severe cracking along with a large area of fusion coverage indicates a history of high temperatures for relatively long periods of time. This scenario puts the periradicular tissues at greater risk to thermal injury.

---

*Although apparati for measuring leakage directly are available at other universities, this was not done for this thesis. However, such studies are planned for a future date.

†Hairline cracking was defined as cracking with no discernable width which appeared on the scanning electron micrograph as a line of varying regularity and length, and was therefore measured in millimeters. Wide cracking was defined as cracking with a discernable width, and was measured in squared millimeters.

Several potential sources of error existed in this experiment, only some of which were theoretically controlled for by randomization of either the tooth selection or the order in which the scanning electron micrographs were evaluated. Randomization of the tooth selection process theoretically controlled for the effects of variations in the age of the teeth, the type of the tooth (i.e. incisor, premolar, cuspid, etc.), the dentinal morphology (i.e. opaque vs. translucent dentin), the degree to which the teeth were hydrated at the time of exposure, the composition, the history of trauma (i.e. prehand existence of microfractures), and possibly other unknown factors. Randomizing the order in which the scanning electron micrographs were evaluated theoretically controlled for measurement variables such as error due to operator fatigue (inaccuracies which tend to occur more often with time as the operator becomes weary of operating the electronic digitizer), inconsistencies in classifying the forms of cracking, and of correctly identifying areas of fusion by their appearance on the micrograph (sometimes due to difficulties in seeing the detail in some areas of the micrograph because of charging of the specimen while under electron bombardment in the SEM, and sometimes possibly due to inconsistencies in operator judgement during classification). Although randomization does not guarantee that these variables will have no confounding effect on the data, it can be assumed to minimize the effect to some extent.

There are other sources of error for which controls other than randomization were used. Opaque tape was placed over the information bars on the micrographs to minimize the bias in the classification of cracking and fusion and in the actual measurement due to prehand knowledge of the laser exposure parameters used to create any particular impact site. It was unlikely that this precaution was completely successful because of the previously mentioned tell-tale nature of the cracking and fusion characteristics with respect to the general power and pulse durations responsible for that impact site. In addition, the power output of the laser was periodically monitored to prevent major variations in the data. However, it is possible that minute variations occurred between monitorings.

The spot size was approximated by adjusting it so a burn of about 1 millimeter in diameter was produced from an exposure of around 20 Watts and a pulse duration of 0.1 seconds. This approximation potentially introduces a systematic error in the data which is not likely to vary significantly because, once adjusted, the spot size was not changed. Small variations are possible, however, because of the minute differences in distances from the surfaces of the target areas to the lens which might have arisen from inconsistently focusing the binocular scope from one specimen to the next. Any variations in spot size would translate in variations in power density, and therefore temperature, which strongly influences the cracking and fusion.

Measurement reliability was tested by taking one random micrograph and measuring the three dependent variables ten times in succession. More specifically, the length of hairline cracking was measured ten times to give a standard deviation for the measurement of lines, and the areas of wide cracking and fusion coverage were cumulatively measured to give a standard deviation for the measurement of areas in general. The mean value for hairline cracking was 6.501, and the standard deviation was 0.028, or 0.43%. The mean value for area measurement was 1.611 mm^2, with a standard deviation of 0.004 mm^2, or 0.25%. The descriptive statistics for these measurement reliability data are shown in Table XXI.

The Pillai's Criterion (Table XV) is used to determine whether any statistically significant differences exist in the data. It it analogous to the familiar analysis of variance (ANOVA) in function, except that it is often used in conjunction with a multivariate analysis, which is indicated when several dependent variables arising from the same independent variables are to be analyzed. In this context, Pillai's Criterion indicates whether significant differences exist, but it does not indicate between which groups these differences lie. Therefore, the significant result from Pillai's Criterion obtained in this analysis indicates the necessity to do further tests to pinpoint the exact location of those differences. In the case of this investigation, the next test required is a two-way multivariate analysis of variance. It must be a "two-way" analysis because there are two independent variables, power and pulse duration, which may or may not interact to have a significant effect on the dependent variables hairline cracking, wide cracking, and fusion coverage. It should be a "multivariate" analysis because of the relatively large number of dependent variables. An approach which might seem more straight forward would be to run a regular two-way ANOVA three separate times, once for each of the three dependent variables. However, for somewhat abstract statistical reasons, this method results in an accumulation of risk that a significant difference will be found purely by chance, and not because it really exists. In general, when multiple runs of ANOVA (or the Student's t-test, for that matter) are performed to accommodate several groups or variables rather than limiting these tests to just two groups (for which they were designed), the chance for rejecting the null hypothesis when it is in fact true can be approximated by multiplying the original confidence level (e.g. $\alpha = .05$ for this work) by the number of individual runs. This accumulation of error is unacceptable, and can be avoided by using a multivariate analysis of variance (MANOVA). MANOVA has what statisticians refer to as a "hedge" against this accumulation; that is, this test makes it more difficult to find significance as the number of dependent variables increases.

In the analysis of the continuous-wave CO_2 laser data, the two-way MANOVA indicated that the interaction of power and pulse duration had a significant effect on the hairline cracking and fusion coverage, but not the wide cracking (Table XV). It also indicated that power alone as well as pulse duration alone had a significant effect on the wide cracking data. However, it was necessary to know which groups of exposure parameters created significantly different effects within each dependent variable. Therefore, the Duncan's Multiple Range test was performed on those variables shown to hold significant differences by the MANOVA (i.e. hairline cracking and fusion coverage vs. power/pulse duration interaction, and wide cracking vs. power only and vs. pulse duration only). The results of the Duncan's Multiple Range test can be found for the power/pulse duration interaction effect on hairline cracking and fusion coverage in Table XVI and XVII, respectively. Table XVIII and XIX show respectively the results of this test for the effect of power only and pulse duration only on wide cracking. Admittedly, when using such a large number of groups the Duncan's results appear nondescript to cursory examination, but they nevertheless offer precise information regarding where the significant differences lie. A friendlier (and perhaps more relevant) way of presenting the data in which the trends between the laser exposure parameters and their dentinal effects can be visualized is demonstrated in Figures 15-19. These Figures respectively show the mean values for the statistically significant effect of power/pulse duration interaction on hairline cracking, the nonsignificant effect of power/pulse duration interaction on wide cracking, the significant effect of power/pulse duration interaction on fusion coverage, the significant effect of power only on wide cracking, and the significant effect of pulse duration only on wide cracking.

An examination of Figure 15 reveals that the mean values of hairline cracking tend to increase with increasing power, and also with increasing duration.

Remembering that the MANOVA procedure indicated that power/pulse duration interaction had a significant effect on hairline cracking, and also noting that these data produced a Pearson correlation coefficient between energy (energy = power multiplied by pulse duration=Watts X Seconds=Joules) of 0.6046, it can be said with greater than 99% confidence (since the p value in this instance is less than 0.0001) that approximately 37% of the variation seen in the hairline cracking data was due to the amount of energy applied (since the square of the correlation coefficient, $[0.6046]^2=$ 0.3655, represents the proportion of the variance in the data explained by the variation in the independent variable). As Table XX shows, the other independent variables also explain a portion of the variation in the hairline cracking data. The results of the multiple regression procedure are tabulated in a cumulative fashion; that is, in the case of hairline cracking, power explains about 3.5% and pulse duration about 5% of the variation. When energy, power, and pulse duration are considered cumulatively, they explain approximately 45% of the variation seen in the hairline cracking data. (Note that only those independent variables resulting in an R value whose probability of occurring purely by chance was less than a 5% [i.e. $\alpha = .05$] are included). The source(s) of the remainder of the variation (approximately 55%) in the hairline cracking data are not identified here. However, they likely include to some extent those sources, both controlled and uncontrolled, which were elaborated upon earlier in this discussion section. This is also true for the unexplained portion of variation in the wide cracking and fusion coverage data.

Figure 16 presents the effects of power/pulse duration interaction on wide cracking. In this case, the effect was not significant (p=0.5122). A close look reveals that while, in general, the degree of wide cracking increases with increasing power, the relationship of wide cracking with time is less obvious. This is reflected in the lower correlation coefficient of 0.4014 in Table XX. Since the effect of power/pulse duration interaction was not significant, it was necessary to look at the effect of power alone and pulse duration alone (Figures 18 and 19). In this case, both of these variables had a significant effect (p=0.0005 for power alone, and p=0.0029 for pulse duration alone (Table XV)). Figure 18 reveals an obvious trend for mean values of wide cracking to increase with increasing power. However, the relatively low correlation coefficient (R=0.0514) indicates that less than 1% of the variation in the wide cracking data can be explained by power alone. Figure 19 reveals that the minimum mean value for wide cracking occurs at 0.2 seconds. Figure 17 demonstrates the most orderly arrangement of all. Here, the mean area of fusion coverage is seen to increase both with increasing power and with increasing duration. Earlier, MANOVA showed that the interaction of power and pulse duration had a significant effect on fusion coverage (p<0.0001). Moreover, the correlation between energy and area of fusion produce a coefficient of R=0.8290, implying that approximately 69% of the variation in the fusion coverage data can be explained by the total amount of energy applied.

Plates 3 through 6 are scanning electron micrographs which respectively demonstrate examples of no effect, hairline cracking, wide and hairline cracking, fusion along with both kinds of cracking, and the desired effect of glazing with minimal cracking of either kind. It is important to note that the desired effect occurs at 15 Watts and 0.2 seconds. This visual choice is corroborated by the statistical results, which indicate that the minimal mean value of wide cracking occurred at 0.2 seconds. 15 Watts of power seems preferable because of the subjective observation that it both consistently created fusion and minimized the depth of the resulting crater. Powers greater than 15 Watts created craters in the dentin which appear deeper than necessary. With this rationale, the optimum (i.e. minimal) combination of power and pulse duration to give glazing of the dentin surface with minimal cracking was chosen to be 15 Watts at 0.2 seconds.

Detailed speculation regarding the laser/tissue interaction phenomena which are responsible for the observed dentinal effects is best deferred to the numerical modelling section, where it is more in context and better supported by the topic under discussion. However, some general comments may be made here. With the carbon dioxide laser, both the reflected and the transmitted portions of the beam shown in Figure 12 can be assumed to be zero due to the extremely high absorption in biological tissues. All of the energy of the beam can thus be considered to be internally scattered or absorbed by the dentin, with absorption predominating over scattering. The sequence of events upon laser impact can be modelled by 1) surface water evaporation, 2) charring of the organic portion, and 3) melting and recrystallization of the inorganic portion of the dentin. These three steps will be broken down into more detail in the section on numerical modelling. A more precise sequence of events would be 1) a rise in temperature to 100° C; 2) absorption of energy as the latent heat of vaporization of water, which vaporizes the water at 100° C; 3) a rise in temperature to about 600° C; 4) absorption of energy as the latent heat of vaporization of the organic component of dentin, which results in the vaporization of this component; 5) a rise in temperature to about 1300° C; 6) absorption of energy as the latent heat of fusion of the inorganic component of dentin, which melts this material, allowing it to flow and occlude tubules; and 7) conductive and perhaps radiative cooling of the impact site after termination of irradiation, which allows the melted material to recrystallize.

Conclusions

Continuous-wave carbon dioxide laser irradiation can consistently glaze the surface of instrumented root canal wall dentin in human teeth without the occurrence of a significant degree of surface cracking. The optimal exposure parameters were determined to be 15 Watts, 0.2 seconds, and a spot diameter of 1.0 millimeter.

Pulsed CO_2 Laser Effects on Canal Wall Dentin

Introduction

One of the modes of output available on the surgical CO_2 laser used was the pulsed mode. Preliminary, unpublished studies had shown that this mode of operation was capable, in certain circumstances, of melting dentin. However, it was unclear whether the surface of root canal wall dentin could be consistently glazed with minimal surface cracking using this mode of CO_2 laser operation. This part of this work was intended to determine the ability of the pulsed CO_2 laser to consistently and reliably glaze the surface of root canal wall dentin with minimal cracking.

Method and Materials

The experimental method used for this part of this thesis was identical to that which was used for the continuous-wave carbon dioxide laser with two exceptions: 1) eighteen single-rooted teeth were used, resulting in 36 specimens, and 2) the canals were irradiated according to Table XIII, resulting in a total of 216 exposures.

Results

Pillai's multivariate tests ($\alpha=.05$) indicated that very significant differences ($p<0.00001$) existed in the data when the interaction of power and pulse duration was considered (see Table XXII).

The MANOVA procedure (Table XXII) indicated that the interaction of power and duration had a very significant effect on hairline cracking ($p<0.00001$), wide cracking ($p<0.0001$), and fusion coverage ($p<0.0001$). Again, a confidence level of

α=.05 was assumed. The results from the Duncan's multiple range tests for the power/pulse duration interaction effect on hairline cracking, wide cracking, and fusion coverage are shown in Tables XXIII through XXV, respectively.

Graphs of the mean values for hairline cracking, wide cracking, and fusion coverage, along with their corresponding Pearson correlation coefficients can be found in Figures 20 through 22, respectively. The results from the multiple regression procedure are shown in Table XXVI. Scanning electron micrographs of laser impact sites which demonstrate the range of pulsed carbon dioxide laser-induced dentinal effects are shown in Plates 7, 8, and 9. Plate 7 shows only hairline cracking, Plate 8 both wide and hairline cracking, and Plate 9 fusion with both kinds of cracking.

No combination of exposure parameters was found to be able to consistently glaze the surface of the canal wall dentin with minimal cracking.

Discussion

Since the design of each of the three experiments which comprise this work were for the most part identical, most of the comments made in the discussion section of the continuous-wave carbon dioxide laser experiment apply equally as well to the pulsed carbon dioxide and pulsed Nd-YAG laser experiments. However, there were some differences which need to be recognized.

In general, when using a pulsed laser, there are three variables under the control of the clinician: the average power, the pulse rate, and the pulse train duration. The pulsed carbon dioxide laser used for this experiment was unfortunately limited in that it was impossible to vary the power and pulse rate with respect to each other, at least to any large degree. This was related to the fact that the average powers of which this laser was capable in pulsed output mode were comparatively low; for instance, 1.0

Watts at 50 pps and 7.5 Watts or less at 450 pps. Since these small magnitudes of power did not allow for meaningfully large variations within them, it was decided to use maximum available power in all circumstances, and simply vary the pulse rate and pulse train duration as the independent variables. This resulted in a very high correlation between power and pulse rate (R=1), and also effectively lowered the number of independent variables from three (power, pulse rate, and pulse train duration) to two (power, and pulse train duration). It also should be mentioned with respect to the variables compared in the Pearson correlation, that the energy was calculated as before, by multiplying the average power by the pulse train duration. This is a good approximation for the energy in the case of a continuous-wave laser, but is not necessarily so in the case of a pulsed laser where pulse shapes and widths must be taken into account. Even so, the comparison of the variation of the actual energy in the pulsed laser output with the variation in the measured dependent variables is probably quite similar when compared to that as shown because the difference between the true and calculated energies is constant, and does not, therefore, contribute to the variation.

Tables XXIII through XXV show the results from the Duncan's multiple range tests found to be statistically significant by the MANOVA procedure. Here, groups consisting of those impact sites resulting from identical combinations of laser exposure parameters (i.e. independent variables) were tested for significance. These results offer precise information regarding whether any one combination of exposure parameters caused significantly different dentinal effects than another. However, they are not in a form from which the general relationships between the independent and dependent variables can be easily surmised. A friendlier way of conveying this sort of information is demonstrated in Figures 20 to 22. Figure 20 shows the effect of the interaction of power and pulse train duration on the mean values of hairline cracking. This effect was described as being strongly significant by the previously run MANOVA procedure ($p<0.00001$; Table XXII). Figure 21 shows the effect of power/pulse train duration interaction on mean values of wide cracking. Again, this effect was found to be very significant by the MANOVA procedure ($p<0.0001$; Table XXII). Figure 22 shows the effect of power/pulse train duration on mean values of fusion coverage. This effect was also shown to be very significant by the MANOVA procedure ($p<0.0001$; Table XXII). Here, it is important to note that no fusion at all occurs below 5.25 Watts (which corresponds to a pulse rate of 300 pps; Table XIII). When fusion does occur, the means vary in such a way as to cross each other in an almost haphazard fashion. Table XXVI indicates, in a cumulative fashion, the independent variables which have a significant effect on the dependent variables. Here, we see that hairline cracking and fusion coverage depend predominantly on the power, but that wide cracking depends both on the energy and the pulse train duration alone, with the effect of energy dominating. The cumulative effect of energy and pulse train duration on wide cracking accounts for about 59.5% of the variation seen in the wide cracking data. In general, variation of the dependent variables not accounted for by their regression results can be attributed to other sources of error, some of which were mentioned in the discussion section of the continuous-wave CO_2 laser experiment.

Clinically speaking, the most important observation was that none of the combinations of exposure parameters produced the desired result of glazing with minimal cracking. On the surface, this would seem to render all of the other results academic; however, it must be remembered that the energies used in this experiment were admittedly very low, representing only a small portion of the range potentially available with other pulsed CO_2 laser units. Even with this limitation, however, the nature of the appearance of the observed dentinal effects and the consideration of the stresses likely to be induced by the repetitive impact of pulses with high peak powers leads one to expect that the likelihood of being able to create the desired effect with *any* pulsed laser at *any* combination of exposure parameters is small. With higher powers, the correspondingly higher peaks could be expected to induce extremely high surface temperatures for very short periods of time, possibly vaporizing the melted inorganic material before it had a chance to flow and obliterate cracks and tubules. This would result in the formation of a crater which deepened as the pulse train duration was increased. Although this was not observed in this experiment (perhaps due to the relatively low energies used), it was observed in the pulsed Nd-YAG experiment, where much higher energies were possible.

Plates 7, 8, and 9 demonstrate the range of pulsed CO_2 laser-induced dentinal effects seen in this experiment. Note that cracking is a predominant feature in all of these examples, and that when fusion does occur, it does not seem to flow and obliterate cracks very well.

Conclusion

The pulsed carbon dioxide laser does not appear to be able to create glazing of root canal wall dentin in human teeth with negligible cracking at the energies used in this experiment.

Pulsed Nd-YAG Laser Effects on Root Canal Wall Dentin

Introduction

If the laser is to be used for purposes of intracanal heating, then a suitable waveguide must be obtained which can deliver the energy to its intended location. One of the advantages of the CW- and pulsed Nd-YAG lasers in this regard is that they can be delivered quite conveniently and easily using currently available quartz optical fibers. These fibers come in various sizes, the smaller sizes of which have no trouble fitting into a prepared root canal, and are flexible enough to negotiate any curvature likely to occur in the course of routine endodontic treatment of human teeth.

Previous research has indicated that the continuous-wave Nd-YAG laser is unsuitable for fusing root canal wall dentin *in vivo*, in spite of its advantage of being easily delivered through an optical fiber[49]. The problem was that of inconsistency of result, which was attributed to the absorption being dependent on the varying microstructure of the target dentin. The more homogeneous translucent (sclerotic) dentin transmitted a large percent of the incident energy, whereas the relatively inhomogeneous opaque (nonsclerotic) dentin caused more internal scattering and therefore more absorption, leading to thermally induced changes in the dentin.

The effects of the pulsed Nd-YAG laser on root canal wall dentin has yet to be determined. This laser also has the advantage that its energy can be delivered through quartz optical fibers. The objective of this part of this thesis was to determine the ability of the pulsed Nd-YAG laser to consistently glaze the surface of root canal wall dentin.

Method and Materials

The same experimental protocol was used for this experiment as was used in both the continuous-wave and pulsed CO_2 laser experiments, with the following exceptions: 1) 27 single rooted teeth were used, resulting in 54 half-tooth specimens; 2) these specimens were irradiated according to Table XII, resulting in a total of 324 exposures; 3) the measured dependent variables were hairline cracking, wide cracking, area of fusion, and area of vaporized and/or unglazed dentin (i.e. "unfused cratering"). The pulsed laser used for this experiment was an experimental laboratory prototype and was not mounted on a surgical microscope as was the carbon dioxide laser. The average power output was measured with an external power meter*. The physical layout of this device and the experimental setup are shown in Figure 23.

Results

Pillai's multivariate tests indicated (assuming $\alpha = 0.05$) that significant differences existed in the data when considering the interactions of power, pulse rate, and pulse train duration ($p=0.036$); pulse rate and pulse train duration ($p<0.001$); power and pulse rate ($p=0.005$); power and pulse train duration ($p<0.041$); power alone ($p<0.001$); pulse rate alone ($p=0.015$); and pulse train duration alone ($p<0.001$).

---

*A Coherent power meter, model 201, was used.

Interestingly, the MANOVA procedure indicated that the interaction of power, pulse rate, and pulse train duration had no significant effect on any of the variables. Other significant effects included the interaction between pulse rate and pulse train duration on the amount of fusion, and the area of unfused cratering; the interaction of power and pulse rate on the amount of fusion, and the area of unfused cratering; the interaction of power and pulse train duration on all of the dependent variables except wide thermal cracking; power alone on all dependent variables except wide cracking; pulse rate alone on area of fusion coverage and the area of unfused cratering; and pulse train duration on area of fusion and the area of unfused cratering. These results are summarized in Table XXVII. The statistically significant results of the Duncan's multiple range test are shown in Tables XXVIII through XXXV. The Pearson correlation coefficients relating the independent variables with the dependent variables are shown in Table XXXVI. Graphs which relate the relationships between the independent and dependent variables can be found in Figures 24 through 47. The results from the multiple regression procedure are shown in Table XXXVII. Scanning electron micrographs which demonstrate the range of effects of the pulsed Nd-YAG laser on dentin are shown in Plates 10, 11, and 12. Plate 10 demonstrates no effect, Plate 11 crater production with minimal fusion, and Plate 12 crater production to the extent that the root was perforated.

Discussion

As previously mentioned, the general experimental protocol for each of the three experiments which comprise this thesis was the same. Therefore, most of the comments made in the discussion section of the continuous-wave carbon dioxide laser experiment apply equally as well to this experiment. However, there were some differences which should be mentioned.

With the pulsed Nd-YAG laser used in this experiment, the power, pulse rate, and pulse train duration were varied independently of each other according to Table XII, and thus were not under the same limitations as the pulsed carbon dioxide laser, where two of the three variables had a very high correlation. Also, the output of this laser was fixed at a 10% duty cycle, meaning that the on time was 10% of the time between leading edges of the successive pulses. Simple calculations therefore show that the peak power approximates ten times the average power, which is the independent variable controlled by the operator. Furthermore, the value of energy used in the Pearson correlation was calculated as the product of these three independent variables. As before, it should be said that although this formula does not give true value for the total energy delivered, it still maintains the same correlation between the dependent variables because the ratio of the true to the calculated value is constant.

Figures 24 through 47 show the mean values in chart form for all of the relationships between the independent and dependent variables. Because of their number and their relative ambiguity, it is difficult to gain a clear impression of what is happening solely from reviewing these charts. They have been included largely for purposes of completeness. The results of the Duncan's multiple range tests (Tables XXVIII through XXXV) denote those groups (designated by their particular combination of laser exposure parameters, or independent variables) which are significantly different from each other. This is very specific information relating how certain combinations of exposure parameters compare to others with respect to their effects on dentin, and can serve to answer specific questions in regard to these comparisons. However, it is again difficult to glean from these results a clear picture of the trends which may relate the variables in question. What is more informative are the Pearson correlation coefficients shown in Table XXXVI. As always, those coefficients whose corresponding probability is 0.05 or greater should be ignored. This, however, still leaves apparent several significant relationships. First, hairline cracking was shown to have a low correlation with the calculated value of energy (R=0.1478). Fusion coverage was found to correlate lowly with energy and pulse train duration (0.4204 and 0.3024) and even lower with power (0.1902). The highest correlations found in this analysis were between the area of unfused cratering and energy (0.5145), power (0.3259), and pulse train duration (0.4649). As before, squaring these coefficients will indicate the proportion of the variation in the data explained by variation in the corresponding independent variable. Another useful description of these relationships is given in the multiple regression results (Table XXXVII). Here, only those R values which are statistically significant are cumulatively categorized by their dependent variable, showing the total proportion of variation in that dependent variable which can be explained by any singular *or* cumulative effect of the independent variables. For example, the only significant correlation with hairline cracking occurred with energy; with the calculated value of beam energy explaining only about 2% of the variation in hairline cracking. Fusion coverage was found to correlate lowly with energy, and even lower with pulse rate, but taken together, these two independent variables account for almost 20% of the variation seen in the fusion coverage data. The phrase "Unfused Cratering" was intended to describe craters and holes left by pulsed Nd-YAG laser impact which were characterized by a lack of tubule occlusion by melted dentin since the dentin was apparently vaporized before it had a chance to flow into the tubules. The area of these craters (or holes or perforations) demonstrated a moderate correlation with the energy, a low correlation with the pulse rate, and an even lower one with the pulse train duration. However, these three independent variables together accounted for almost 40% of the variation in the area of these craters and holes. In all of the aforementioned cases, the remainder of the variation (i.e. that not explained by variation in the independent variables) can be attributed to other sources of error, many of which were elaborated upon in the discussion section of the continuous-wave CO_2 laser experiment.

Much of the above discussion is rendered academic by the fact that the pulsed-Nd-YAG laser was not able to glaze the surface of the dentin in the desired manner in any single case, much less do so consistently. It can be hypothesized that the high peaks characteristic of pulsed laser output supplies ample energy to heat the dentin to its vaporization temperature and also supply the latent heat of vaporization in exceedingly short (clinically speaking) periods of time.

For reference, Plates 10 through 12 show scanning electron micrographs of pulse Nd-YAG laser impact sites which respectively demonstrate no effect, crater production with minimal fusion, and a root perforation.

Conclusion

The pulsed Nd-YAG laser does not appear to be able to consistently glaze the surface of root canal wall dentin with minimal surface cracking.

Radiometric Surface Temperature Measurement

Direct measurement of the surface temperature of dentin upon laser irradiation is best performed by radiometric means, due to the high temperatures and small surface areas involved. In addition, such measurement serves as a general check of the values resulting from the finite element model analysis. Here, it is of predominant interest to measure the maximum surface temperature upon continuous-wave CO_2 laser irradiation, which is the fusion or melting temperature of the inorganic portion of the dentin. This value, then, could be used in the finite element program to set the temperature at which this phase change occurs in the model.

An IRCON optical pyrometer was used to make the measurements. However, it was necessary to calibrate it to minimize measurement error. This calibration was performed by placing a tooth specimen in an oven along with a K-type thermocouple[*] and comparing readings from the pyrometer with those from the Wahl thermocouple at several temperatures. When a discrepancy was noted, the IRCON pyrometer reading was adjusted to equal that of the Wahl thermocouple by way of the emittance (or emissivity) control on the IRCON unit itself. As a rule, the emittance setting necessary to balance the two readings decreased as the temperature increased (see Table

---

[*] Wahl Precision Portable Thermocouple Calibration Standard, Model C-65, used with K-type NiCr/NiAl thermocouple which has a 0.1°C resolution and an accuracy of ± 1°C at 25 ± 2°C. This unit was calibrated on October 12, 1985.

XXXVIII). Since it was expected that the dentin would melt around 1200°C, an emittance of .80 was chosen to be used for the measurement of the actual laser impact.

After the alignment of both the laser and the pyrometer on the target, five specimens were irradiated and temperatures measured at coronal, central, and apical locations along their canal walls, totalling 15 measurements. The pyrometer was set to display the peak temperature measured. The field of view of the pyrometer was approximately 2 millimeters in diameter, which was larger than the 1 millimeter spot of the laser beam. To account for this area difference, the beam was moved about the field during the exposure in an attempt to register the highest possible temperature on the pyrometer. Once raising the temperature even further became impossible by this method, the exposure was terminated. However, it is still possible that the temperatures registered were slightly low due to this problem. The temperature data and descriptive statistics can be found in Table XXXIX. The mean temperature reading was found to be 1284.5°C with a standard deviation of 31.5°C. This value corroborates the fact that synthetic hydroxyapatite crystals are known to begin decomposition at 1100°C and actually melt around 1600°C. Since the mineral content of dentin is not purely hydroxyapatite, and contains other forms of calcium phosphate as well as several other trace elements, it should be expected that the melting point of dentin would fall below that of synthetic hydroxyapatite in its purely crystalline form.

In the subsequent numerical analysis, the melting point of dentin was assumed to be 1300°C on the basis of these data.

A Numerical Model: Temperature and Stress Analysis by the Finite Element Method

Introduction

It was concluded earlier that the continuous-wave carbon dioxide laser was capable of consistently glazing the surface of root canal wall dentin (with minimal associated cracking) at a power output of 15 Watts, pulse duration of 0.2 seconds, and a spot of 1 millimeter in diameter. This particular scenario, then, becomes of primary interest and it follows that it should be the one which is modelled. The creation of a numerical model is not only necessary to develop an understanding of the phenomena active in the case under study, but it also represents an important step in the development of numerical models which predict the temperature and stress distributions due to laser impact in other tissues and with other geometric configurations.

This particular problem is of the class of problems in which a substance undergoes phase change with a concomitant emission or absorption of heat. Common examples of this are melting and solidification. Early research by Stefan[268] was a study of the increase in thickness of polar ice, and for this reason the problem of freezing is frequently referred to as the 'problem of Stefan'. Stefan's formula presents a simple method for calculating the penetration of a phase change front in a semi-infinite body at the phase change temperature to which a constant step temperature is applied.[269] Stefan's formula is:

$$\chi = \sqrt{\frac{2k(\Delta T)t}{L_v}} \tag{17}$$

where χ is the penetration depth of the phase change front, k is the thermal conductivity of the phase nearest the interface (e.g. of ice in the case of freezing water), ΔT is the temperature difference between the phase change temperature and the applied surface temperature, t is the time, and L_v is the volumetric latent heat (of fusion in the case of liquid-to-solid transition). It is important to note that this formula is one dimensional and ignores heat capacities, conduction in the original phase material, thermal radiation and convection.

The essential feature of phase change problems is the existence of a moving phase boundary. It is important to know the way in which this boundary moves. Heat is liberated or absorbed on it, and the thermal properties of the two phases on different sides of it may be different, so that the problem is one of considerable difficulty. In the 1860's, a more general solution to this problem was given by Franz Neumann in his lectures, and represents the most important exact solution of this problem for a semi-infinite body which is assumed to be homogeneous and isotropic[270-272]. Neumann's theory makes some simplifying assumptions, but remains useful in approximating practical solutions to problems of this kind.

Stefan's and Neumann's solutions represent the most important closed-form solutions to the problem described above, but they cannot be used directly to solve the problem of laser impact on dentin. This is because the heat loading and geometric configuration used in this study add complexities not accounted for by these two methods. Also, the composition of dentin is much more complex, requiring three phase transitions to account for the vaporization of the water content, the vaporization of the organic content, and the melting of the inorganic content. This lack of a specific exact solution makes the use of numerical approximation necessary. The numerical approach chosen for this analysis is the finite element method. The two programs used were ADINA[277] (Automatic Dynamic Incremental Non-linear Analysis) for obtaining stresses and ADINAT[273] for obtaining the temperatures. Working in in an uncoupled manner, ADINAT and ADINA have the capability of performing the required transient analysis and reporting both the resultant temperatures and their corresponding stresses as a function of time.

ADINAT

Simplifying Assumptions

The following approximations and assumptions were used this analysis:

GEOMETRY: The geometry chosen for this analysis was of an axis-symmetric body with the laser beam impinging on its surface perpendicularly (Figure 48). Two-dimensional elements were used in an axisymmetric mesh, thereby reducing computing expenses. In principle, this mesh can be rotated 360° around its axis to form a three-dimensional solid in the shape of a bowl. This configuration would then have the laser beam impinging on the center of the top plane of the bowl. Should this configuration result in temperatures which change very little on the nodal points most distant from the surface area of laser impact, it can then be said to roughly approximate to closed form solutions which pertain to heat flux input on the surface of a semi-infinite solid.

BOUNDARY CONDITIONS: There are several boundary conditions which need be specified, and were as follows:

Temperature Conditions: The temperature may be prescribed at specific points and surfaces of the body. In this study, all nodes were initially set to 20°C (room temperature) because it was approximately at this temperature that the tooth specimens were irradiated.

Heat Flow Conditions: The heat flow input may be prescribed at specific points and surfaces of the body. From the known values of power used (15 Watts) and the cross sectional area of the beam, the power density was calculated and input into ADINAT as an applied heat flux (Figure 48).

Convection Boundary Conditions: ADINAT has the capability of accounting for surface convection. It has been the general consensus in other work of this kind that convection plays a negligible role in influencing temperature when a material is irradiated with a high energy laser, especially when the duration of exposure is relatively short.[274] Thus, for this work, convection was ignored.

Radiation Boundary Conditions: ADINAT can also account for the effects of heat loss due to radiation. As with convection, however, radiative loss of heat is also assumed to be negligible in situations of this kind.[274]

Phase Changes: ADINAT has the capability of modelling multiple phase changes. The program does this by lumping the latent heat for each element (rotated through one radian) at its nodal points.

Three phase change interfaces were modelled into this laser/dentin problem. The first was the vaporization of the water component in dentin at 100°C, the second was the vaporization of the organic component of dentin from 600°C to 800°C, and the third was the melting of the inorganic component of dentin at about 1300°C.

Structure and Composition of Dentin: The dentin was assumed to be structurally homogeneous, although that is clearly not the case on a microscopic level. The composition was assumed to be 10% water, 30% organic, and 60% inorganic (by volume). These percentages were used to calculate the latent heat for each phase change interface. The latent heat of vaporization for water has been experimentally determined. The latent heat of vaporization of collagen (the predominant organic constituent of dentin) has not been experimentally determined. Therefore, the value for another organic material, Toluidine, was substituted. The latent heat of fusion for the mineral phase of dentin (mostly hydroxyapatite) was not available in the literature, so the value for calcium carbonate was used. These latent heat values are listed in Table XXXX.

Laser Absorption Characteristics: As mentioned before, it is usual to assume 100% energy absorption when dealing with the 10.6 μm light of the CO_2 laser. This is implemented by assigning the heat flux loading only to selected surface nodes, and not to any nodes at locations deeper in the finite element grid.

Thermal Properties: Along with the appropriate latent heat values for each phase interface, ADINAT requires the thermal conductivity and volumetric specific heat. The values used were chosen from the literature and are 5.69×10^{-4} W/mm^3°C for the thermal conductivity, and 2.46×10^{-3} J/mm^3°C for the volumetric specific heat.

Sequence of Thermal Events: The *in vitro* sequence of thermal events was assumed to be as follows: a rise in temperature of the dentin to 100°C; while at 100°C, energy is absorbed to vaporize the water in the dentin; another rise in temperature to 600°C; while at temperatures between 600 and 800°C, energy is absorbed to vaporize the organic portion of the dentin; a further rise in temperature from 800 to 1300°C; energy is absorbed to melt the mineral portion of dentin; and a continuation of temperature rise above 1300°C (Figure 49). Vaporization of the inorganic component was not allowed in this model.

Method

The numerical time integration scheme used in this transient analysis was the Euler backward method.[275] This method calculates a temperature change based on the local heat fluxes and material thermal properties (ignoring the latent heats), and then adjusts this temperature to take account of the latent heats. Usually, several of these adjustments must be performed in order for the tolerance requirement, a user defined parameter, to be satisfied. These adjustment cycles are known in ADINAT as *equilibrium iterations* .

The Euler backward method is used as part of a step-by-step time integration scheme, where the total duration of the laser exposure is divided into several smaller time steps. Equilibrium iterations are then performed at each of these time steps to find the temperatures at the nodes for each time step.

To include the effects of phase changes, ADINAT uses the algorithm presented in 1982 by Rolph and Bathe[276]. Pure and complex substances with multiple phase change fronts can be considered in one analysis.

The material thermal properties of dentin are assumed to be constant with respect to temperature in this analysis. A linear transient analysis was performed using ADINAT.

ADINA

ADINA is a computer program for the static and dynamic displacement and stress analysis of solids, structures, and fluid-structure systems. The program can be employed to perform linear and nonlinear analysis. ADINAT is designed to serve as the companion program for ADINA. A summary of the theory used in ADINA can be found in the literature[278] and the program documentation[279].

Simplifying Assumptions

The following assumptions were made to facilitate this analysis:

GEOMETRY: The same two-dimensional grid which was used for the ADINAT temperature analysis was also used for this stress and displacement analysis.

MATERIAL PROPERTIES: The mechanical material properties were assumed to vary with respect to temperature. The values used for the modulus of elasticity (Young's Modulus), coefficient of thermal expansion, and Poisson's ratio are shown in Table XXXXI. The modulus of elasticity was lowered from its relatively high value of 19×10^6 MPa to 1.0 MPa to simulate the drastic drop in stiffness of the material when it makes the solid to liquid phase transition from 1300 to 1310°C. Poisson's ratio was also input to change from .25 to 0 at these temperatures. The coefficient of thermal expansion began at a positive value (8.3×10^{-6} m/m°C), but at temperatures of 600 to 800°C was set at a rather large negative value (-6.65×10^{-4} m/m°C) to accommodate what was assumed to be a 40% overall loss in volume due to the vaporization of the water and the organic content.

BOUNDARY CONDITIONS: The following boundary conditions were imposed on this analysis:

1. **Stresses:** No restrictions were placed on the possible stresses any element might experience in response to thermal loading.

2. **Displacements:** Since this was an axisymmetric analysis, the center axis nodes were fixed horizontally. However, these nodes were free to move vertically (Figure 48). All other nodes were free to displace in response to thermal loading.

Results

The temperatures calculated by ADINAT for selected nodes for the 25 time steps of the analysis are profiled in Figure 50. The ADINAT-calculated depth of melt is compared to that calculated by a modified Stefan's equation in Figure 51. A temperature vs. time profile of selected external-most nodes is given in Figure 52. ADINA-calculated stresses are plotted for each of the time steps in Figures 53 through 77, and deformations for the first five time steps in Figures 78 through 82. The maximum ADINA-calculated stresses are listed with the time step at which they occurred in Table XXXXII.

Discussion

The nodes selected for display in Figure 50 (nodes 96 through 126) were chosen because they lie within and underneath the laser impact area, and will approximate worst-case extremes of temperature. This figure shows that as time increases, so does the surface temperature and the depth of heat penetration. At close inspection, small steps can be observed at 600°C which correspond to the time delay over which the latent heat of vaporization of the organic component is absorbed. The latent heat of vaporization of water and the latent heat of fusion of the inorganic component are small in comparison. Since the time periods over which these two heats are supplied is exceedingly small, they exceed the time-step resolution of this model and are not apparent in Figure 50.

The modulus of elasticity was made to change from 19.3 MPa to 0.001 MPa during the temperature interval from 1300 to 1310°C to model the abrupt drop in the modulus which occurs when a solid melts to become a liquid. This allows the approximated phase change front to be readily observed as the leading edge of a low-stress area near the surface of laser impact in the stress plots of Figures 56 through 77. The melted surface layer becomes deeper with time so long as the laser exposure continues. This phase change front can be considered to approximate the 1300°C isotherm. In reality, however, the melting-temperature isotherm has a width which depends on the latent heat of fusion; the greater the latent heat of fusion, the wider the isotherm (or approximate isotherm, in the case of materials where the latent heat is absorbed over a small range of temperature). The leading edge of this isotherm represents material which has just reached the melting temperature but has absorbed no latent heat; the trailing edge (nearest the laser impact area) represents the material which is also at the melting temperature but has absorbed the total amount of latent heat required to transform to the liquid state. In this model, the latent heat of fusion of the inorganic component was small in comparison to the latent heat of vaporization of the organic component. This is mirrored by the lack of an obvious step in the temperature profiles at 1300°C in Figure 50. It is on this basis that the 1300°C isotherm can be said to approximate the calculated phase change front.

As a check of the model, the ADINAT-calculated phase change front* is compared with a modified Stefan's solution in Figure 51. Here, it can be seen that Stefan's equation generally predicts a greater depth of melting than ADINAT. However, it must be remembered that Stefan's equation does not account for material heat capacity as does ADINAT. In addition, the unmodified Stefan's equation assumed a constant surface temperature. Here, this constant was replaced with the actual ADINAT-calculated surface temperature (at node 96) for each time step. This means that Stefan's equation can be expected to error in an amount which increases with the time. Even so, the Stefan's and ADINAT results are well within one order of magnitude of each other.

Of a more clinical interest is the question of whether the periodontal ligament and bone will see damaging temperatures were this energy to be applied *in vivo* to an intracanal location. A preliminary look into this problem is given by Figure 52, where the temperatures of selected external-most nodes are plotted against time. These nodes are about 0.9 millimeters distant from the laser impact surface, which approximates, in some cases, the amount of dentin between the canal wall and the external root surface in areas very near the apical constriction, and perhaps in other areas where severe external root concavities exist. (In most cases, the dentin thickness is much greater than this). It can be seen that the temperature rise experienced by these external nodes is calculated to be about 4°C or less after 0.2 seconds. Since this analysis did not model the situation where the laser pulse is only of a 0.2 second duration followed by a cool-down period, it is difficult to say precisely what the temperature profiles should be expected to be when the laser is used at the optimal settings for intracanal glazing. A temperature rise from 37°C to 42°C may cause metabolic derangements in cells after "prolonged" periods of time.[182] However, the current concensus is that soft tissue eventually will necrose if it reaches 60°C for even very short periods of time.[181,185,186] The temperatures in Figure 52, however, may well be exaggerated due to the failure of the model to account for radiation and convection at the dentinal surface as well as outward conduction from these external nodes themselves. Although this bodes well for the safe use of lasers in root canals, this issue requires more investigation.

---

* Linear extrapolation was used to calculate the depth of the 1300°C isotherm when this isotherm fell between two ADINAT-calculated temperatures.

In the stress plots of Figures 53 through 77, the convention is to label tensile stresses with double-headed arrows and compressive stresses with straight lines with the length of the line or arrow being indicative of the magnitude of the stress relative to the maximum value given in the upper right of the plot area. The general presence of tensile stresses is to be expected in a situation where such a large volume loss (40%) is incurred. As previously mentioned, this volume loss was attributed to the volatilization of water and the organic content of the dentin, and was modelled in ADINA by the assignment of a relatively large negative coefficient of thermal expansion. This was corroborated by the fact that in previous ADINA runs where the coefficient of thermal expansion was kept positive and constant, only compressive stresses resulted.

At t=0.02 seconds (Figure 53), horizontal tensile stresses are apparent just subjacent to the irradiated surface, with the maximum stress being approximately 10.17 x 10^6 MPa. By t=0.04 seconds (Figure 54), vertical tensile stresses have also appeared in this area, with the maximum stress being around 14.01 x 10^6 MPa. From t=0.06 seconds to t=0.50 seconds (Figures 55 through 77) the stresses in this subjacent area dissipate and disappear in a fashion which progresses deeper and deeper into the dentin. This disappearance of stress is because the program accounts for the drastic drop in the modulus of elasticity of dentin upon melting. The maximum stresses range from 9.46 x 10^6 MPa at t=0.42 seconds to 14.34 x 10^6 MPa at t=0.28 seconds (Table XXXXII), and although they do not surpass the experimentally determined value of the tensile strength of dentin (51.7 x 10^6 MPa[152]), they are all well within one order of magnitude. The stress plots indicate that the maximum stresses are usually adjacent to the melted (i.e. no-stress) zone, and progress downward and outward with time. However, the maximum stresses do not vary greatly with time. This alludes to the possibility that the mechanism of cracking of such a homogeneous material upon such a laser impact may well depend more on the depth to which the maximum stresses occur rather than there being a great increase in the actual maximum stresses themselves with time. It can be hypothesized that cracking may occur almost immediately upon laser impact and propagate downward with time, resulting in an ever-widening surface area. Furthermore, it may be that at 15 Watts, 0.2 seconds, and a 1.0 millimeter spot, enough inorganic material is melted to flow into and obliterate the relatively young and shallow cracks. Durations much longer than 0.2 seconds may well vaporize too much of the melted inorganic material as well as allow the cracks to progress to a volume to great to be obliterated.

The plots of Figures 78 through 81 illustrate the results of the deformation calculations, as well as demonstrate a problem with the model. At t=0.02 seconds (Figure 78) the contraction in the top layer of elements under the laser impact zone is obvious. Again, this is due to the assigned negative thermal coefficient of expansion between 600 and 800°C. At t=0.04 seconds (Figure 79) the top two layers are undergoing this contraction. At t=0.06 seconds (Figure 80) the second and third layers of elements are contracting while the top layer has returned to near its normal dimension. At t=0.08 (Figure 82) the surface portion of the dentin has melted (compare to Figure 56). This is translated into spurious deformations by ADINA.

These surface deformations are extreme enough to in several cases force ADINAPLOT to reduce the plot in order for it to fit within the designated frame area. These erratic and extreme surface deformations occur in all of the plots from t=0.08 to t=0.50 seconds, and are typified by those seen in Figure 81. They are caused by two factors: 1) that no allowance was made in the model for the actual vaporization of the melted inorganic component; that is, no latent heat of vaporization and element death (disappearance of the vaporized element) were allowed and 2) the coefficient of thermal expansion of the melted dentin was assumed to be constant and the same as solid dentin at temperatures outside of the 600 to 800°C range. This resulted in the calculated presence of a superheated liquid which expanded proportionally to its temperature. Figures 56 through 77 demonstrate temperatures ranging from 1800 to 8000°C. In reality, of course, dentin is in the gaseous phase at these temperatures. It is for these reasons that the erratic surface deformations typified by those seen in Figure 81 are meaningless. Since it has been given a finite heat capacity, this superheated surface material may provide some amount "protection" to the underlying solid dentin when compared to the real situation where fresh dentin is exposed to the laser beam upon vaporization of the melted dentin. Therefore, this must be considered to be a potential source of error.

There exist other sources of variation and error within both the temperature analysis and the stress analysis. In ADINAT, these sources include the approximation of the phase change temperatures and latent heat values for the organic and inorganic components; the use of experimentally determined thermal properties such as the coefficient of thermal conductivity and volumetric specific heat which may not precisely reflect the true values of the irradiated material; and the arbitrary choice of a tolerance value by which the accuracy of the computations is decided.

In ADINA, the value of the ultimate tensile strength against which the calculated stresses were compared was experimentally determined using a relatively slow load application rate. This is in contrast to the rapid stress application due to laser heating. The mechanisms involved in the tensile or compressive failure of a complex material such as dentin are probably numerous and may depend on factors such as tubule orientation, the local tubule density, and the macroscopic geometry of the specimen. Due to the variations of these factors with location in any given section of dentin, it is reasonable to assume that the true ultimate tensile strength for any given location may well be different from the chosen value. The compressive properties of dentin have recently been shown to decrease with increasing temperature[280]; this would suggest that the same may also be true for the tensile properties. Also, the chosen value of 51.7 MPa[152] for the tensile strength of dentin was obtained with dentin specimens which were continuously at room temperature, clearly not the case in the present work. This is important in that the elastic modulus of dentin (as with most materials) tends to decrease with increasing temperature[280]. Since the elastic modulus was assumed to remain constant up to 1300°C, and since a value experimentally determined at room temperature was used[152], ADINA should be expected to calculate artificially high values of stress. Furthermore, the true value of the modulus of elasticity may as well depend to some extent on the tubule density and orientation, factors not accounted for here.

Although the coefficient of thermal expansion was assumed to become negative between 600 and 800°C, it remained constant both within and outside this range, and did not account for its variation as a function of temperature. Depending on the material, this coefficient may vary, increase, or decrease with temperature.[281] A search of the literature revealed no data concerning the variation of the thermal coefficient of expansion for dentin with respect to temperature. This and the fact that an experimentally determined value was used in the model represent possible sources of error.

Poisson's ratio was chosen to be 0.25, another approximation which may not be precisely true for all areas of dentin. This value was chosen for simplicity because it best represents a material which has the same elastic properties in all directions.

This model assumes that the incident laser energy is totally absorbed on the dentinal surface (between nodes 1 and 460). Figure 82 displays the results from a Fourier transform infrared (FTIR) analysis on an actual tooth specimen where light of a wavelength from 1 to 17 μm was incident on apical root dentin and its percent transmission was measured. These results show transmission peaks under about 2 μm wavelength, and no peaks above this value. The low level, high frequency variation seen above this level is attributable to system noise. Even though this noise is present, it is still obvious that above approximately 2 μm there is no transmission through this dentin specimen. This specimen was between 1 and 2 millimeters thick in the test area. From this, it can be said that there appears to be a drastic increase in absorption in wavelengths greater than 2 μm. However, this plot does not precisely define the extinction length, although it lends support to the assumption that light at 10.6 μm is absorbed on or very near the surface. With reference to the Nd-YAG laser studies, it is interesting to note that light at 1.06 μm demonstrates a high degree of transmission, which would partly explain our results where no effect on dentin was seen even with very high powers.

Conclusions

The finite element model presented provides insight into the temperature and stress dynamics which occur in dentin upon carbon dioxide laser impact. Cracking is predicted by this model insofar as stresses within experimental error of the empirically determined tensile strengths of dentin were calculated to appear almost immediately upon laser impact, and to endure throughout the period of irradiation. The presence of melted and recrystallized or "fused" dentin was predicted by the model as well, both at durations of 0.2 and 0.5 seconds. From this model, it appears that the following sequence of events may occur *in vitro* : t=0.02 to 0.06 seconds- heating and minor, shallow cracking of the dentinal surface; t=0.08 to 0.20 seconds- increasing depth of cracking and simultaneous filling of the cracks by melted inorganic dentin, creating the clinically desired glazed surface; and t=0.22 to 0.50 seconds- increasing of the depth of the cracks beyond the point where the melted inorganic material can obliterate them, as well as an increasing amount of the inorganic material itself being vaporized.

Summary and Discussion

The research detailed in this thesis has made progress in determining which of the high-power lasers available were capable of altering the surface of root canal dentin such that a continuously-fused fracture-free surface was obtained. It has been determined that the continuous-wave carbon dioxide laser at 15 watts, 0.2 seconds, and a spot size of 1.0 millimeter was capable of producing this effect. The pulsed carbon dioxide laser was found to cause only large degrees of cracking at the energies used. The pulsed Nd-YAG laser was found to inconsistently create either no effect or craters and root perforations with no occlusion of the dentinal tubules. The finite element numerical model of continuous-wave carbon dioxide laser impact on dentin at 15 watts and 1.0 millimeter spot diameter suggests that the following events occur: $t=0.02$ to 0.06 seconds- heating and shallow cracking of the dentinal surface; $t=0.08$ to 0.20 seconds- increasing depth of cracking and simultaneous melting and filling of the cracks by melted inorganic dentin; and $t=0.22$ to 0.50 seconds- increasing of the depth of the cracks beyond the point where the melted inorganic material can obliterate them.

The clinical importance of this work relates to the use of the laser to create a barrier to fluid migration to and from the root canal space primarily through the apical foramen and secondarily through lateral canals and dentinal tubules. The creation of such a barrier is considered widely to be one of the cornerstones of successful endodontic therapy. Surface fusion of intentionally placed apical plugs has been suggested as a means of accomplishing this barrier. This involves the irradiation of the adjacent root canal wall dentin in an attempt to continuously fuse this dentin with the plug surface. That both the plug surface and the dentinal wall fuse well at 15 watts and 0.2 seconds indicate the potential for such a technique to significantly decrease apical leakage. This potential was manifested in an investigation by Zakariasen et al.[282].

The numerical model presented indicates temperatures at depths of 0.9 millimeters under the laser impact site which are potentially tolerable to soft tissue. The clinical relevance of these values must be tempered with the understanding that the geometry of the model was not intended to specifically answer questions regarding heat transfer to the periodontal ligament and beyond; it was designed only to model a relatively small depth of dentin. To more precisely address this important clinical question of whether the intracanal fusion of apical plugs poses a thermal risk to the periradicular tissues, it will be necessary to conduct animal research where the histology of the effects on these periapical tissues can be evaluated as well as to perform additional numerical models where the precise anatomy and varying material properties of the tissues can be more precisely accounted for.

Tables

Table I

Composition of Dentin on the Basis of Weight and Volume[84,85]

	Enamel		Dentin	
	wt%	vol%	wt%	vol%
Inorganic Material	95	86	70	47
Organic Material	1	2	20	33
Water	3	12	10	21

Table II

Ash Composition of Mineralized Tissues as Percent of Weight[99]

	Enamel	Dentin
Ca	37.5	37.0
PO_4	54.2	55.1
CO_2	2.5	4.5
Na	0.6	0.4
K	0.2	0.1
Mg	0.4	1.2
Cl	0.3	0.0
Ca/P Ratio	2.12	2.06

Table III

Median Concentrations of Trace Elements in Enamel[123]

Concentrations > 10 ppm Dry Weight		Concentrations From 1 to 10 ppm Dry Weight		Concentrations From 0.1 to 1.0 ppm Dry Weight	
Fluoride	200	Boron	2.4	Lithium	0.93
Magnesium	1550	Aluminum	5.6	Manganese	0.26
Sulpher	270	Chromium	1.5	Copper	0.45
Chlorine	4400	Iron	2.6	Selenium	0.22
Potassium	370	Molybdenum	6.3	Bromine	0.93
Zinc	190	Barium	3.4	Rubidium	0.32
Strontium	56	Lead	3.6	Niobium	0.24
				Silver	0.16
				Cadium	0.22
				Tin	0.14
				Antimony	0.11

Table IV

Organic Constituents of Dentin[127-129]
(Approximate Percentage of Dry Weight)

Constituent	% of Dentin (Dry Weight)
Collagen	18
Citrate	0.9
Lipid	0.33
Non-Collagenous Matrix	1.6
Total	**20.83**

Non-Collagenous Matrix Consitiuent	% of Non-Collagenous Matrix
GAG's (Glyco-Amino Glycans; mostly chondroitin sulphate)	12
Glycoproteins	46
Peptides	4.2
Serum Proteins	2.6
Unaccounted For	35

Table V

Experimentally Determined Values for the Thermal Conductivity of Dentin

Thermal Conductivity (cals/sec/cm^2/ ° C/cm)		Reference
2.29×10^{-3}		Lisanti and Zander (1950) [133]
2.35×10^{-3}		Simeral (1951) [134]
0.257×10^{-3}		Phillips et al. (1956) [135]
$0.96 - 1.07 \times 10^{-3}$		Soyenkoff and Okun (1958) [136]
1.36×10^{-3}	heat flow parallel to tubules	Craig and Peyton (1961) [137]
1.39×10^{-3}	heat flow perpendicular to tubules	
1.33×10^{-3}	normal dentin before hydration	
1.23×10^{-3}	normal dentin after hydration	Fanibunda and De Sa (1975) [138]
1.88×10^{-3}	reparative and transparent dentin before hydration	
1.82×10^{-3}	reparative and transparent dentin after dehydration	

Table VI

Experimentally Determined Values for the Elastic Modulus of Dentin

Modulus of Elasticity (× 10 psi)^{6}	Reference
0.8	Black (1895)[142]
1.67	Peyton et al. (1952)[143]
1.1-1.7	Neuman and Di Salvo (1957)[144]
2.4-2.7	Craig and Peyton (1958)[145]
1.5-2.2	Stanford et al (1958)[147]
1.79	Tyldesley (1959)[148]
1.4-2.4	Stanford et al. (1960)[150]
2.8	Bowen and Rodriguez (1962)[152]

Table VII

Experimentally Determined Values for the Proportional Limit of Dentin

Proportional Limit (psi)	Reference
23,400	Peyton et al. (1952)[143]
24,200	Craig and Peyton (1958)[145]
25,100	Stanford et al. (1958)[147]
9,600	Tyldesley (1959)[148]
18,100-24,400	Stanford et al. (1960)[150]

Table VIII

Experimentally Determined Values for the Ultimate Tensile Strength of Dentin

Ultimate Tensile Strength (psi)	Reference
5,800 (Std. Dev. 900)	Bowen and Rodriguez (1960)[151]
7,500 (Std. Dev. 1,500)	Bowen and Rodriguez (1962)[152]
Approximately 6000	Lehman (1967)[153]

Table IX

Experimentally Determined Values for the Ultimate Compressive Strength of Dentin

Ultimate Compressive Strength (psi)	Reference
37,200	Black (1895)[142]
36,100	Peyton et al. (1952)[143]
43,100	Craig and Peyton (1958)[145]
50,400	Stanford et al. (1958)[147]
38,800	Tyldelsey (1959)[148]
30,000-44,200	Stanford et al. (1960)[150]

Table X

Experimentally Determined Values for the Thermal Coefficient of Expansion of Dentin

Coefficient of Thermal Expansion (x $10^{-6}/°C$)		Reference
7.5		Barton and Dickenson[161]
8.3	(root dentin)	Sauder and Paffenbarger[162]
11.4	(crown dentin)	

Table XI

Thermogravimetric Analysis of Dentin: A Summary of Results

	Temperature °C			
Thermal Event	**Lim and Loboff (1972)**[95]	**Holager (1970)**[92]	**Holager (1972)**[88]	**Komrska (1972)**[94]
Dehydration	140	100	100	60-150
Protein Decomposition	330	300	350	280-340
Protein Burning	-	-	-	600
Carbonate Decomposition	530	700	750	710
Tricalcium Phosphate	815	-		-

Table XII

Pulsed-Nd-YAG Laser Exposure Parameters

Average Power (Watts)	Pulse Repetition Rate (pps)	Pulse Train Duration (Sec)	No. of Exposures per Combination
10	10	.2, .5, and 1.0	6
	25	"	"
	40	"	"
20	10	"	"
	25	"	"
	40	"	"
30	10	"	"
	25	"	"
	40	"	"
40	10	"	"
	25	"	"
	40	"	"
50	10	"	"
	25	"	"
	40	"	"
60	10	"	"
	25	"	"
	40	"	"

Total Number of Exposures = 324

Table XIII

Pulsed Carbon Dioxide Laser Exposure Parameters

Power (Watts)	Pulse Train Duration (Sec)	Pulse Repetition Rate (pps)	No. of Exposures per Combination
1.00	0.1, 0.2, 0.5, 1.0	50	6
2.00	"	100	"
3.00	"	150	"
4.00	"	200	"
4.75	"	250	"
5.25	"	300	"
6.00	"	350	"
7.00	"	400	"
7.50	"	450	"

Table XIV

Continuous-Wave Carbon Dioxide Laser Exposure Parameters

Power (Watts)	Pulse Duration (Seconds)	Number of Exposures per Combination
5	0.1, 0.2, 0.5, 1.0	6
10	"	"
15	"	"
20	"	"
23	"	"

Table XV

Results of Multivariate Analysis
Continuous-Wave Carbon Dioxide Laser

Effect of Power/Pulse Duration Interaction

	Value	F Ratio	Prob.(p Value)	
Pillais Criterion	1.171	3.486	<.001	(sig.)
Variable				
Hairline Cracking		1.98	.0333	(sig.)
Wide Cracking		.94	.5122	
Fusion Coverage		33.06	<.0001	(sig.)

Effect of Power Alone

	Value	F Ratio	Prob.(p Value)	
Pillais Criterion	1.008	8.511	<.001	(sig.)
Variable				
Hairline Cracking		15.20	<0.0001	
Wide Cracking		5.47	0.0005	(sig.)
Fusion Coverage		999.26	<0.0001	

Effect of Pulse Duration Alone

	Value	F Ratio	Prob.(p Value)	
Pillais Criterion	1.034	13.139	<.001	(sig.)
Variable				
Hairline Cracking		28.49	<0.0001	
Wide Cracking		4.98	.0029	(sig.)
Fusion Coverage		473.96	<0.0001	

Table XVI

Duncan's Multiple Range Test Results
Hairline Cracking
Effect of Power/Pulse Duration Interaction
Continuous-Wave Carbon Dioxide Laser

	5W/.1s	5W/.2s	15W/.1s	10W/.2s	10W/.1s	20W/.1s	10W/1s	20W/.2s	23W/.1s	5W/.5s	10W/.5s	5W/1s	15W/.2s	20W/1s	15W/.5s	23W/.2s	23W/.5s	20W/.5s	15W/1s	23W/1s
5W/.1s																				
5W/.2s																				
15W/.1s																				
10W/.2s																				
10W/.1s																				
20W/.1s																				
10W/1s	*	*	*	*																
20W/.2s	*	*	*	*																
23W/.1s	*	*	*	*																
5W/.5s	*	*	*	*	*	*														
10W/.5s	*	*	*	*	*	*														
5W/1s	*	*	*	*	*	*														
15W/.2s	*	*	*	*	*	*														
20W/1s	*	*	*	*	*	*														
15W/.5s	*	*	*	*	*	*														
23W/.2s	*	*	*	*	*	*														
23W/.5s	*	*	*	*	*	*														
20W/.5s	*	*	*	*	*	*	*													
15W/1s	*	*	*	*	*	*	*													
23W/1s	*	*	*	*	*	*	*	*	*	*	*	*	*	*	*	*	*	*	*	

* Denotes groups which are significantly different

Table XVII

Duncan's Multiple Range Test Results
Area of Fusion Coverage
Effect of Power/Pulse Duration Interaction
Continuous-Wave Carbon Dioxide Laser

	10W/.1s	5W/.1Ss	5W/.5s	5W/.2s	5W/1s	10W/.2s	15W/.1s	10W/.5s	20W/.1s	15W/.2s	20W/.2s	10W/1s	23W/.1s	23W/.2s	15W/.5s	20W/.5s	15W/1s	20W/1s	23W/.5s	23W/1s
10W/.1s																				
5W/.1Ss																				
5W/.5s																				
5W/.2s																				
5W/1s																				
10W/.2s																				
15W/.1s	*	*	*	*	*	*														
10W/.5s	*	*	*	*	*	*														
20W/.1s	*	*	*	*	*	*	*	*												
15W/.2s	*	*	*	*	*	*	*	*	*											
20W/.2s	*	*	*	*	*	*	*	*	*											
10W/1s	*	*	*	*	*	*	*	*	*											
23W/.1s	*	*	*	*	*	*	*	*	*	*	*	*								
23W/.2s	*	*	*	*	*	*	*	*	*	*	*	*								
15W/.5s	*	*	*	*	*	*	*	*	*	*	*	*	*							
20W/.5s	*	*	*	*	*	*	*	*	*	*	*	*	*	*						
15W/1s	*	*	*	*	*	*	*	*	*	*	*	*	*	*	*	*				
20W/1s	*	*	*	*	*	*	*	*	*	*	*	*	*	*	*	*				
23W/.5s	*	*	*	*	*	*	*	*	*	*	*	*	*	*	*	*	*	*		
23W/1s	*	*	*	*	*	*	*	*	*	*	*	*	*	*	*	*	*	*	*	

* = Denotes groups which are significantly different

Table XVIII

Duncan's Multiple Range Test Results
Wide Cracking
Effect of Power Only
Continuous-Wave Carbon Dioxide Laser

5W					
10W					
15W					
20W	*				
23W	*	*	*		
	5W	10W	15W	20W	23W

* = Denotes groups which are significantly different

Table XIX

Duncan's Multiple Range Test Results
Wide Cracking
Effect of Pulse Duration Only
Continuous-Wave Carbon Dioxide Laser

	.2s	.1s	.5s	1s
.2s				
.1s				
.5s	*			
1s	*	*		

* = Denotes groups which are significantly different

Table XX

Results of Multiple Regression Procedure Continuous-Wave Carbon Dioxide Laser

Dependent Variable	Independent Variable	Multiple R	R^2	df	Signif.
Hairline Cracking	Energy	.60459	.36553	1	<.0001
	Power	.63280	.40044	2	<.0001
	Duration	.67205	.45166	3	<.0001
Wide Cracking	Energy	.40139	.16112	1	<.0001
	Power	.45280	.20503	2	<.0001
Fusion Coverage	Energy	.82896	.68717	1	<.0001
	Power	.95463	.91132	2	<.0001

Table XXI

Measurement Reliability Data
Descriptive Statistics

Line Length Measurement: 10 Trials

Minimum	6.468
Maximum	6.557
Range	0.089
Median	6.498
Mean	6.501
Standard Error	0.009
Variance	0.001
Standard Deviation	0.028

Area Measurement: 10 Trials

Minimum	1.067
Maximum	1.619
Range	0.012
Median	1.610
Mean	1.611
Standard Error	0.001
Variance	0.000
Standard Deviation	0.004

Table XXII

Results of Multivariate Analysis
Pulsed Carbon Dioxide Laser

Effect of Power/Pulse Train Duration Interaction

	Value	F Ratio	Prob.(p Value)	
Pillais Criterion	1.324	3.709	<0.00001	(sig.)
Variable				
Hairline Cracking		14.21	<0.00001	(sig.)
Wide Cracking		3.41	<0.0001	(sig.)
Fusion Coverage		2.98	<0.0001	(sig.)

Table XXIII

Duncan's Multiple Range Test Results
Hairline Cracking
Pulsed Carbon Dioxide Laser

	1W/.2s	1W/.1s	2W/.1s	2W/.5s	2W/.2s	1W/1Ss	4W/.1s	1W/.5s	3W/.1s	3W/.2s	7.5W/.1s	6W/1s	4W/.2s	7.5W/.5s	7W/1s	3W/.5s	7.5W/.2s	6W/.5s
1W/.2S																		
1W/.1S																		
2W/.1S																		
2W/.5S																		
2W/.2S																		
1W/1S																		
4W/.1S																		
1W/.5S																		
3W/.1S																		
3W/.2S																		
7.5W/.1S																		
6W/1S																		
4W/.2S	*	*	*	*	*	*	*											
7.5W/.5S	*	*	*	*	*	*	*											
7W/1S	*	*	*	*	*	*	*											
3W/.5S	*	*	*	*	*	*	*											
7.5W/.2S	*	*	*	*	*	*	*											
6W/.5S	*	*	*	*	*	*	*	*										
2W/1S	*	*	*	*	*	*	*	*										
4.75W/1S	*	*	*	*	*	*	*	*	*	*								
4.75W/.1S	*	*	*	*	*	*	*	*	*	*								
5.25W/.1S	*	*	*	*	*	*	*	*	*	*								
6W/.1S	*	*	*	*	*	*	*	*	*	*								
6W/.2S	*	*	*	*	*	*	*	*	*	*								
5.25W/1S	*	*	*	*	*	*	*	*	*	*	*	*	*	*	*			
7.5W/.1S	*	*	*	*	*	*	*	*	*	*	*	*	*	*	*	*	*	*
7W/.2S	*	*	*	*	*	*	*	*	*	*	*	*	*	*	*	*	*	*
4.75W/.2S	*	*	*	*	*	*	*	*	*	*	*	*	*	*	*	*	*	*
7W/.1S	*	*	*	*	*	*	*	*	*	*	*	*	*	*	*	*	*	*
3W/1S	*	*	*	*	*	*	*	*	*	*	*	*	*	*	*	*	*	*
7W/.5S	*	*	*	*	*	*	*	*	*	*	*	*	*	*	*	*	*	*
4.75/.5S	*	*	*	*	*	*	*	*	*	*	*	*	*	*	*	*	*	*
5.25/.2S	*	*	*	*	*	*	*	*	*	*	*	*	*	*	*	*	*	*
4W/1S	*	*	*	*	*	*	*	*	*	*	*	*	*	*	*	*	*	*
5.25W/.5S	*	*	*	*	*	*	*	*	*	*	*	*	*	*	*	*	*	*
4W/.5S	*	*	*	*	*	*	*	*	*	*	*	*	*	*	*	*	*	*

* = Denotes groups which are significantly different

Table XXIII
(Continued)

	2W/1s	4.75W/1s	4.75W/.1s	5.25W/.1s	6W/.1s	6W/.2s	5.25W/1s	7.5W/.1s	7W/.2s	4.75W/.2s	7W/.1s	3W/1s	7W/.5s	4.75/.5s	5.25/.2s	4W/1s	5.25W/.5s	4W/.5s
1W/.2s																		
1W/.1s																		
2W/.1s																		
2W/.5s																		
2W/.2s																		
1W/1s																		
4W/.1s																		
1W/.5s																		
3W/.1s																		
3W/.2s																		
7.5W/.1s																		
6W/1s																		
4W/.2s																		
7.5W/.5s																		
7W/1s																		
3W/.5s																		
7.5W/.2s																		
6W/.5s																		
2W/1s																		
4.75W/1s																		
4.75W/.1s																		
5.25W/.1s																		
6W/.1s																		
6W/.2s																		
5.25W/1s																		
7.5W/.1s																		
7W/.2s	*	*	*	*														
4.75W/.2s	*	*	*	*														
7W/.1s	*	*	*	*														
3W/1s	*	*	*	*														
7W/.5s	*	*	*	*														
4.75/.5s	*	*	*	*	*	*												
5.25/.2s	*	*	*	*	*	*	*	*										
4W/1s	*	*	*	*	*	*	*	*	*	*	*	*	*	*				
5.25W/.5s	*	*	*	*	*	*	*	*	*	*	*	*	*	*				
4W/.5s	*	*	*	*	*	*	*	*	*	*	*	*	*	*	*	*		

* = Denotes groups which are significantly different

Table XXIV

Duncan's Multiple Range Test
Wide Cracking
Pulsed Carbon Dioxide Laser

	1W/.1s	2W/.1s	3W/.2s	4W/.1s	1W/.2s	2W/.2s	3W/.1s	1W/.5s	1W/1s	2W/.5s	4W/.2s	4.75W/.1s	5.25W/.1s	2W/1s	4.75W/.2s	4W/.5s	7W/.1s	7.5W/.1s
1W/.1s																		
2W/.1s																		
3W/.2s																		
4W/.1s																		
1W/.2s																		
2W/.2s																		
3W/.1s																		
1W/.5s																		
1W/1s																		
2W/.5s																		
4W/.2s																		
4.75W/.1s																		
5.25W/.1s																		
2W/1s																		
4.75W/.2s																		
4W/.5s																		
7W/.1s																		
7.5W/.1s																		
3W/.5s																		
6W/.1s																		
5.25W/.2s																		
3W/1s																		
6W/.2s																		
7.5W/.2s																		
5.25W/.5s	*	*	*	*	*	*	*	*										
4W/1s	*	*	*	*	*	*	*	*										
4.75W/.5s	*	*	*	*	*	*	*	*	*	*	*	*	*	*				
7W/.2s	*	*	*	*	*	*	*	*	*	*	*	*	*	*	*	*	*	*
5.25W/1s	*	*	*	*	*	*	*	*	*	*	*	*	*	*	*	*	*	*
7.5W/.5s	*	*	*	*	*	*	*	*	*	*	*	*	*	*	*	*	*	*
6W/.5s	*	*	*	*	*	*	*	*	*	*	*	*	*	*	*	*	*	*
7W/.5s	*	*	*	*	*	*	*	*	*	*	*	*	*	*	*	*	*	*
4.75W/1s	*	*	*	*	*	*	*	*	*	*	*	*	*	*	*	*	*	*
7W/1s	*	*	*	*	*	*	*	*	*	*	*	*	*	*	*	*	*	*
6W/1s	*	*	*	*	*	*	*	*	*	*	*	*	*	*	*	*	*	*
7.5W/1s	*	*	*	*	*	*	*	*	*	*	*	*	*	*	*	*	*	*

* = Denotes groups which are significantly different

Table XXIV
(Continued)

	3W/.5s	6W/.1s	5.25W/.2s	3W/1s	6W/.2s	7.5W/.2s	5.25W/.5s	4W/1s	4.75W/.5s	7W/.2s	5.25W/1s	7.5W/.5s	6W/.5s	7W/.5s	4.75W/1s	7W/1s	6W/1s	7.5W/1s
1W/.1s																		
2W/.1s																		
3W/.2s																		
4W/.1s																		
1W/.2s																		
2W/.2s																		
3W/.1s																		
1W/.5s																		
1W/1s																		
2W/.5s																		
4W/.2s																		
4.75W/.1s																		
5.25W/.1s																		
2W/1s																		
4.75W/.2s																		
4W/.5s																		
7W/.1s																		
7.5W/.1s																		
3W/.5s																		
6W/.1s																		
5.25W/.2s																		
3W/1s																		
6W/.2s																		
7.5W/.2s																		
5.25W/.5s																		
4W/1s																		
4.75W/.5s																		
7W/.2s	*	*	*															
5.25W/1s	*	*	*	*														
7.5W/.5s	*	*	*	*	*													
6W/.5s	*	*	*	*	*	*												
7W/.5s	*	*	*	*	*	*												
4.75W/1s	*	*	*	*	*	*	*	*	*									
7W/1s	*	*	*	*	*	*	*	*	*									
6W/1s	*	*	*	*	*	*	*	*	*	*	*							
7.5W/1s	*	*	*	*	*	*	*	*	*	*	*	*	*	*	*			

* = Denoted groups which are significantly different

Table XXV

Duncan's Multiple Range Test
Fusion Coverage
Pulsed Carbon Dioxide Laser

	1W/1s	2W/1s	3W/1s	4W/1s	4.75W/1s	2W/.2s	2W/.5s	1W/.2s	3W/.1s	3W/.2s	3W/.5s	1W/.5s	4W/.1s	4W/.2s	4W/.5s	1W/.1s	4.75W/.1s	4.75W/.2s
1W/1s																		
2W/1s																		
3W/1s																		
4W/1s																		
4.75W/1s																		
2W/.2s																		
2W/.5s																		
1W/.2s																		
3W/.1s																		
3W/.2s																		
3W/.5s																		
1W/.5s																		
4W/.1s																		
4W/.2s																		
4W/.5s																		
1W/.1s																		
4.75W/.1s																		
4.75W/.2s																		
4.75W/.5s																		
2W/.1s																		
5.25W/.1s																		
5.25W/.2s																		
7W/.1s																		
5.25W/.5s																		
6W/1s																		
6W/.1s																		
7W/.2s																		
7.5W/.1s																		
7W/.5s																		
7W/1s																		
6W/.5s																		
6W/.2s	*	*	*	*	*	*	*	*										
5.25W/1s	*	*	*	*	*	*	*	*										
7.5W/1s	*	*	*	*	*	*	*	*	*	*	*	*	*	*	*	*	*	*
7.5W/.2s	*	*	*	*	*	*	*	*	*	*	*	*	*	*	*	*	*	*
7.5W/.5s	*	*	*	*	*	*	*	*	*	*	*	*	*	*	*	*	*	*

* = Denotes groups which are significantly different

Table XXV
(Continued)

	4.75W/.5s	2W/.1s	5.25W/.1s	5.25W/.2s	7W/.1s	5.25W/.5s	6W/1s	6W/.1s	7W/.2s	7.5W/.1s	7W/.5s	7W/1s	6W/.5s	6W/.2s	5.25W/1s	7.5W/1s	7.5W/.2s	7.5W/.5s
1W/1s																		
2W/1s																		
3W/1s																		
4W/1s																		
4.75W/1s																		
2W/.2s																		
2W/.5s																		
1W/.2s																		
3W/.1s																		
3W/.2s																		
3W/.5s																		
1W/.5s																		
4W/.1s																		
4W/.2s																		
4W/.5s																		
1W/.1s																		
4.75W/.1s																		
4.75W/.2s																		
4.75W/.5s																		
2W/.1s																		
5.25W/.1s																		
5.25W/.2s																		
7W/.1s																		
5.25W/.5s																		
6W/1s																		
6W/.1s																		
7W/.2s																		
7.5W/.1s																		
7W/.5s																		
7W/1s																		
6W/.5s																		
6W/.2s																		
5.25W/1s																		
7.5W/1s	*	*	*	*	*	*	*	*	*	*	*	*	*	*	*			
7.5W/.2s	*	*	*	*	*	*	*	*	*	*	*	*	*	*	*			
7.5W/.5s	*	*	*	*	*	*	*	*	*	*	*	*	*	*	*	*		

* = Denotes groups which are significantly different

Table XXVI

Results of Multiple Regression Procedure Pulsed Carbon Dioxide Laser

Dependent Variable	Independent Variable	Multiple R	R^2	df	Signif.
Hairline Cracking	Power	.36698	.13468	1	<.0001
Wide Cracking	Energy	.74943	.56165	1	<.0001
	Pulse Train Duration	.77162	.59540	2	<.0001
Fusion Coverage	Power	.44307	.19631	1	<.0001

Table XXVII

Results of Multivariate Analysis
Pulsed Nd-YAG Laser

Effect of Power/Pulse Rate/ Pulse Train Duration Interaction

	Value	F-Ratio	Prob. (p Value)	
Pillais Criterion	0.414	1.228	0.036	(sig.)
Variable				
Hairline Cracking		1.45	0.1036	
Wide Cracking		0.97	0.4918	
Fusion Coverage		1.32	0.1679	
Unfused Cratering		1.53	0.0751	

Effect of Pulse Rate/ Pulse Train Duration Interaction

	Value	F-Ratio	Prob. (p Value)	
Pillais Criterion	0.176	2.487	<0.001	(sig.)
Variable				
Hairline Cracking		1.99	0.0958	
Wide Cracking		1.45	0.2187	
Fusion Coverage		4.62	0.0013	(sig.)
Unfused Cratering		4.64	0.0012	(sig.)

Table XXVII

(Continued)

Effect of Power/ Pulse Rate Interaction

	Value	F-Ratio	Prob. (p Value)	
Pillais Criterion	0.280	1.608	0.005	(sig.)
Variable				
Hairline Cracking		1.33	0.2115	
Wide Cracking		1.05	0.3980	
Fusion Coverage		1.96	0.0374	(sig.)
Unfused Cratering		2.47	0.0077	(sig.)

Effect of Power/ Pulse Train Duration Interaction

	Value	F-Ratio	Prob. (p Value)	
Pillais Criterion	0.467	2.790	<0.0414	(sig.)
Variable				
Hairline Cracking		1.93	0.0414	(sig.)
Wide Cracking		1.12	0.3496	
Fusion Coverage		4.13	<0.0001	(sig.)
Unfused Cratering		8.50	<0.0001	(sig.)

Table XXVII

(Continued)

Effect of Power Only

	Value	F-Ratio	Prob. (p Value)
Pillais Criterion	0.362	4.235	0.001 (sig.)
Variable			
Hairline Cracking		2.55	0.0280
Wide Cracking		0.71	0.6190
Fusion Coverage		5.87	<0.0001
Unfused Cratering		15.18	<0.0001

Effect of Pulse Rate Only

	Value	F-Ratio	Prob. (p Value)
Pillais Criterion	0.080	2.240	0.015 (sig.)
Variable			
Hairline Cracking		0.81	0.4455
Wide Cracking		0.64	0.5293
Fusion Coverage		4.82	0.0088
Unfused Cratering		3.56	0.0299

Table XXVII

(Continued)

Effect of Pulse Train Duration Only

	Value	F-Ratio	Prob. (p Value)	
Pillais Criterion	0.421	14.287	0.001	(sig.)

Variable	F-Ratio	Prob. (p Value)
Hairline Cracking	2.05	0.1306
Wide Cracking	0.034	0.7121
Fusion Coverage	23.32	<0.0001
Unfused Cratering	72.36	<0.0001

Table XXVIII

Duncan's Multiple Range Test
Area of Fusion Coverage
Pulse Rate/Pulse Train Duration Interaction
Pulsed Nd-YAG Laser

	.2S/10pps	.2S.40pps	.5S/10pps	.2S/25pps	.5S/25pps	.5S/40pps	1.0S/10pps	1.0S/40pps	1.0S/25pps
.2S/10pps									
.2S.40pps									
.5S/10pps									
.2S/25pps									
.5S/25pps									
.5S/40pps									
1.0S/10pps									
1.0S/40pps	*	*	*	*	*	*	*		
1.0S/25pps	*	*	*	*	*	*	*	*	

Table XXIX

Duncan's Multiple Range Test Results
Area of Unfused Cratering
Pulse Rate/Pulse Train Duration Interaction
Pulsed Nd-YAG Laser

	.2S/40pps	.2S/25pps	.2S/10pps	.5S/40pps	.5S/25pps	.5S/10pps	1.0S/10pps	1.0S/40pps	1.0S/25pps
.2S/40pps									
.2S/25pps									
.2S/10pps									
.5S/40pps									
.5S/25pps	*	*							
.5S/10pps	*	*							
1.0S/10pps	*	*	*	*	*	*			
1.0S/40pps	*	*	*	*	*	*			
1.0S/25pps	*	*	*	*	*	*	*	*	

Table XXX

Duncan's Multiple Range Test Results
Area of Fusion Coverage
Power/Pulse Rate Interaction
Pulse Nd-YAG Laser

	10W/10pps	30W/10pps	10W/40pps	20W/40pps	10W/25pps	20W/10pps	50W/10pps	50W/40pps	30W/40pps	50W/25pps	40W/40pps	20W/25pps	40W/10pps	60W/10pps	40W/25pps	60W/25pps	30W/25pps	60W/40pps
10W/10pps																		
30W/10pps																		
10W/40pps																		
20W/40pps																		
10W/25pps																		
20W/10pps																		
50W/10pps																		
50W/40pps																		
30W/40pps																		
50W/25pps																		
40W/40pps																		
20W/25pps																		
40W/10pps																		
60W/10pps																		
40W/25pps																		
60W/25pps	*	*	*	*	*	*	*	*	*	*	*	*	*					
30W/25pps	*	*	*	*	*	*	*	*	*	*	*	*	*	*				
60W/40pps	*	*	*	*	*	*	*	*	*	*	*	*	*	*	*			

Table XXXI

Duncan's Multiple Range Test Results
Area of Unfused Cratering
Power/Pulse Rate Interaction
Pulsed Nd-YAG Laser

	10W/25pps	10W/40pps	20W/40pps	10W/10pps	30W/40pps	20W/25pps	40W/40pps	20W/10pps	30W/10pps	50W/25pps	60W/10pps	50W/40pps	50W/10pps	30W/25pps	40W/25pps	40W/10pps	60W/40pps	60W/25pps
10W/25pps																		
10W/40pps																		
20W/40pps																		
10W/10pps																		
30W/40pps																		
20W/25pps																		
40W/40pps																		
20W/10pps																		
30W/10pps																		
50W/25pps																		
60W/10pps	*	*	*															
50W/40pps	*	*	*															
50W/10pps	*	*	*	*														
30W/25pps	*	*	*	*														
40W/25pps	*	*	*	*														
40W/10pps	*	*	*	*	*	*												
60W/40pps	*	*	*	*	*	*	*	*	*	*	*	*						
60W/25pps	*	*	*	*	*	*	*	*	*	*	*	*	*	*	*			

Table XXXII

Duncan's Multiple Range Test Results
Hairline Cracking
Power/Pulse Train-Duration Interaction
Pulsed Nd-YAG Laser

	20W/.2s	60W/.2s	20W/.5s	10W/.2s	30W/.5s	30W/.2s	60W/.5s	20W/1.0s	10W/1.0s	50W/.5s	50W/.2s	50W/1.0s	40W/.2s	30W/1.0s	40W/1.0s	10W/.5s	60W/1.0s	40W/.5s
20W/.2s																		
60W/.2s																		
20W/.5s																		
10W/.2s																		
30W/.5s																		
30W/.2s																		
60W/.5s																		
20W/1.0s																		
10W/1.0s																		
50W/.5s																		
50W/.2s																		
50W/1.0s																		
40W/.2s																		
30W/1.0s																		
40W/1.0s																		
10W/.5s																		
60W/1.0s																		
40W/.5s	*	*	*	*	*	*	*	*	*	*	*	*	*	*	*	*		

Table XXXIII

Duncan's Multiple Range Test Results
Area of Fusion Coverage
Power/Pulse Train Duration Interaction
Pulsed Nd-YAG Laser

	50W/.2s	10W/.2s	20W/.5s	20W/.2s	10W/.5s	40W/.5s	10W/.2s	40W/.2s	30W/.2s	60W/.2s	30W/.5s	50W/.5s	20W/1.0s	60W/.5s	50W/1.0s	40W/1.0s	30W/1.0s	60W/1.0s
50W/.2s																		
10W/.2s																		
20W/.5s																		
20W/.2s																		
10W/.5s																		
40W/.5s																		
10W/.2s																		
40W/.2s																		
30W/.2s																		
60W/.2s																		
30W/.5s																		
50W/.5s																		
20W/1.0s																		
60W/.5s																		
50W/1.0s																		
40W/1.0s	*	*	*	*	*	*	*	*	*	*	*	*						
30W/1.0s	*	*	*	*	*	*	*	*	*	*	*	*	*	*				
60W/1.0s	*	*	*	*	*	*	*	*	*	*	*	*	*	*	*	*		

Table XXXIV

Duncan's Multiple Range Test Results
Area of Unfused Cratering
Power/Pulse Train Duration Interaction
Pulsed Nd-YAG Laser

	50W/.2s	10W/.5s	10W/.2s	30W/.2s	60W/.2s	40W/.2s	20W/.5s	10W/1.0s	30W/.5s	20W/1.0s	20W/.2s	50W/.5s	40W/.5s	60W/.5s	30W/1.0s	50W/1.0s	40W/1.0s	60W/1.0s
50W/.2s																		
10W/.5s																		
10W/.2s																		
30W/.2s																		
60W/.2s																		
40W/.2s																		
20W/.5s																		
10W/1.0s																		
30W/.5s																		
20W/1.0s																		
20W/.2s																		
50W/.5s																		
40W/.5s																		
60W/.5s	*	*	*	*	*	*	*	*	*	*								
30W/1.0s	*	*	*	*	*	*	*	*	*	*	*	*	*					
50W/1.0s	*	*	*	*	*	*	*	*	*	*	*	*	*					
40W/1.0s	*	*	*	*	*	*	*	*	*	*	*	*	*	*				
60W/1.0s	*	*	*	*	*	*	*	*	*	*	*	*	*	*	*	*		

Table XXXV

Duncan's Multiple Range Test Results
Hairline Cracking
Effect of Power Only
Pulsed Nd-YAG Laser

	20 W	50 W	30 W	10 W	60 W	40 W
20 W						
50 W						
30 W						
10 W						
60 W						
40 W	*	*	*	*		

Table XXXVI

Pearson Correlation Coefficients
Pulsed Nd-YAG Laser

	Energy	Power	Pulse Train Duration	Pulse Rate
Hairline Cracking	0.1478 (p=.004)	0.0542 (p=.165)	0.0680 (p=.111)	0.0286 (p=.304)
Wide Cracking	0.0269 (p=.315)	0.0302 (p=.294)	0.0344 (p=.268)	0.0582 (p=.148)
Fusion Coverage	0.4204 (p<.001)	0.1902 (p<.001)	0.3024 (p<.001)	0.0688 (p=.108)
Unfused Cratering	0.5145 (p<.001)	0.3259 (p<.001)	0.4649 (p<.001)	0.0601 (p=.140)

Table XXXVII

Results of Multiple Regression Procedure
Pulsed Nd-YAG Laser

Dependent Variable	Independent Variable	Multiple R	R^2	df	Signif.
Hairline Cracking	**Energy**	.14780	.02184	1	.0077
Fusion Coverage	**Energy**	.42044	.17677	1	<.0001
	Pulse Rate	.44688	.19970	2	<.0001
Unfused Cratering	**Energy**	.51453	.26474	1	<.0001
	Pulse Rate	.62216	.38708	2	<.0001
	Pulse Train Duration	.62881	.39540	3	<.0001

Table XXXVIII

IRCON Optical Pyrometer Calibration Data

Temperature, ° C		
Wahl	**IRCON**	**Emittance**
904	912	>1.0
1005	1006	>1.0
1108	1106	.85
1210	1207	.80

Table XXXIX

Measured Temperature Data and Descriptive Statistics Continuous-Wave Carbon Dioxide Laser Irradiation of Dentin

Location	Temperature
Coronal	1269
Central	1253
Apical	1288
Coronal	1268
Central	1255
Apical	1285
Coronal	1272
Central	1299
Apical	1325
Coronal	1243
Central	1314
Apical	1351
Coronal	1315
Central	1245
Apical	1290

Minimum:	1243
Maximum	1351
Range:	108
Median:	1285
Mean:	1284.8
Std. Error:	8.14
Variance:	994.9
Std. Dev.:	31.5
Skewness:	0.54

Table XXXX

Latent Heat Values Used in ADINAT

Latent Heat	Substance	Value (Joules/mm^3)
Vaporization	Water	0.47418
Vaporization	Toluidine	27.7
Fusion	Calcium Carbonate	0.778

Table XXXXI

Mechanical Properties of Dentin Used in the Finite Element Model

Temperature (° C)	Modulus of Elasticity (MPa)	Poisson's Ratio (m/m° C)	Thermal Coefficient of Expansion
20	19.6×10^{6}	.25	8.3×10^{-6}
590	19.6×10^{6}	.25	8.3×10^{-6}
600	19.6×10^{6}	.25	-6.65×10^{-4}
800	19.6×10^{6}	.25	-6.65×10^{-4}
810	19.6×10^{6}	.25	8.3×10^{-6}
1300	19.6×10^{6}	.25	8.3×10^{-6}
1310	1.0	0.0	8.3×10^{-6}
8000	1.0	0.0	8.3×10^{-6}

Table XXXXII

Maximum Stresses Calculated in ADINA

Time	Maximum Stress (x 10^6 MPa)
0.02	10.16
0.04	14.01
0.06	13.45
0.08	13.45
0.10	13.16
0.12	10.08
0.14	13.88
0.16	13.95
0.18	13.98
0.20	13.37
0.22	13.59
0.24	13.73
0.26	13.34
0.28	14.34
0.30	10.24
0.32	12.00
0.34	10.43
0.36	10.08
0.38	12.95
0.40	12.58
0.42	9.46
0.44	9.96
0.46	10.22
0.48	9.57
0.50	10.73

Figures

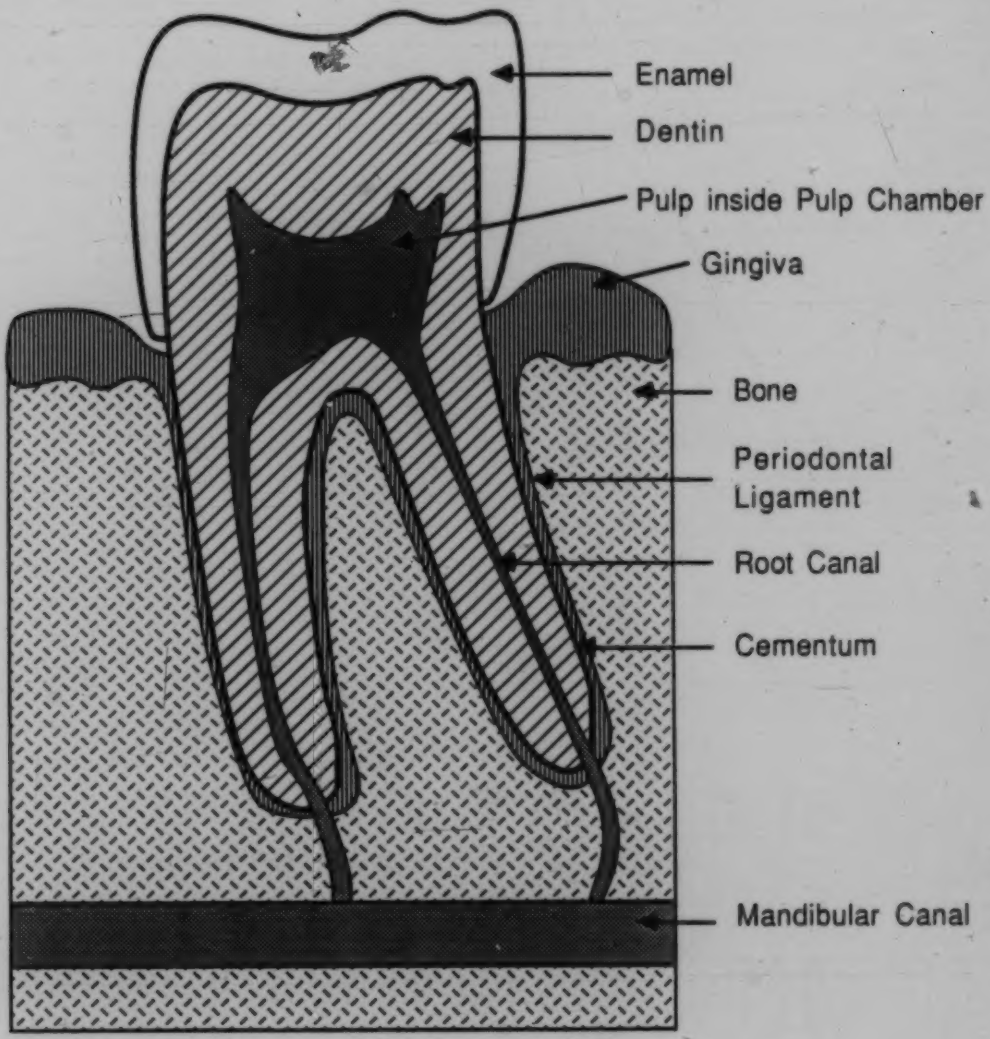
Enamel
Dentin
Pulp inside Pulp Chamber
Gingiva
Bone
Periodontal Ligament
Root Canal
Cementum
Mandibular Canal

Figure 1

Diagram of a human molar and its surrounding structures

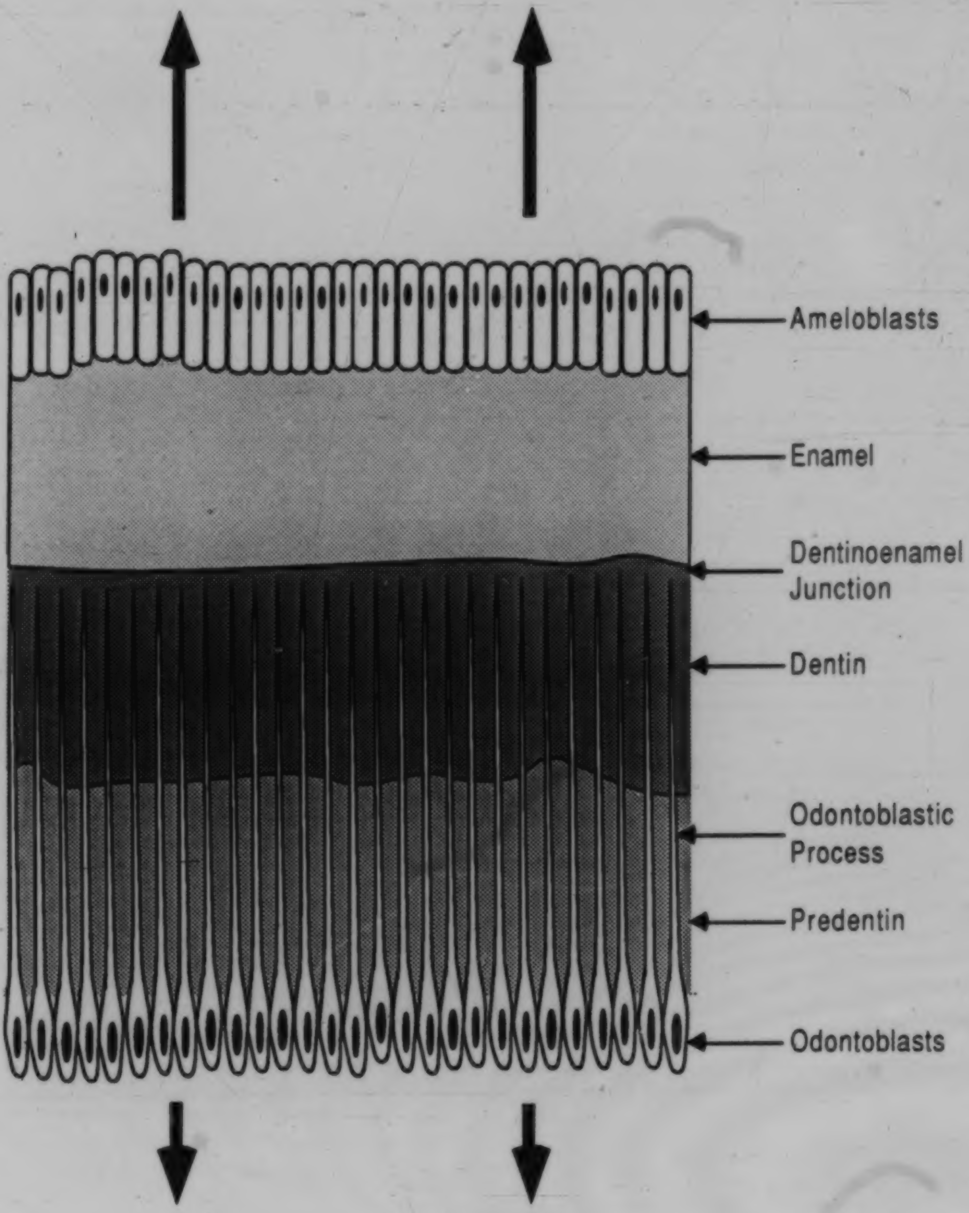
Ameloblasts
Enamel
Dentinoenamel Junction
Dentin
Odontoblastic Process
Predentin
Odontoblasts

Figure 2

Schematic of enamel and dentin development in the crown of the tooth. Note that both the odontoblasts and the ameloblasts (the cells responsible for enamel formation) are moving away from the dentinoenamel junction (DEJ) which was once the boundary at which they met.

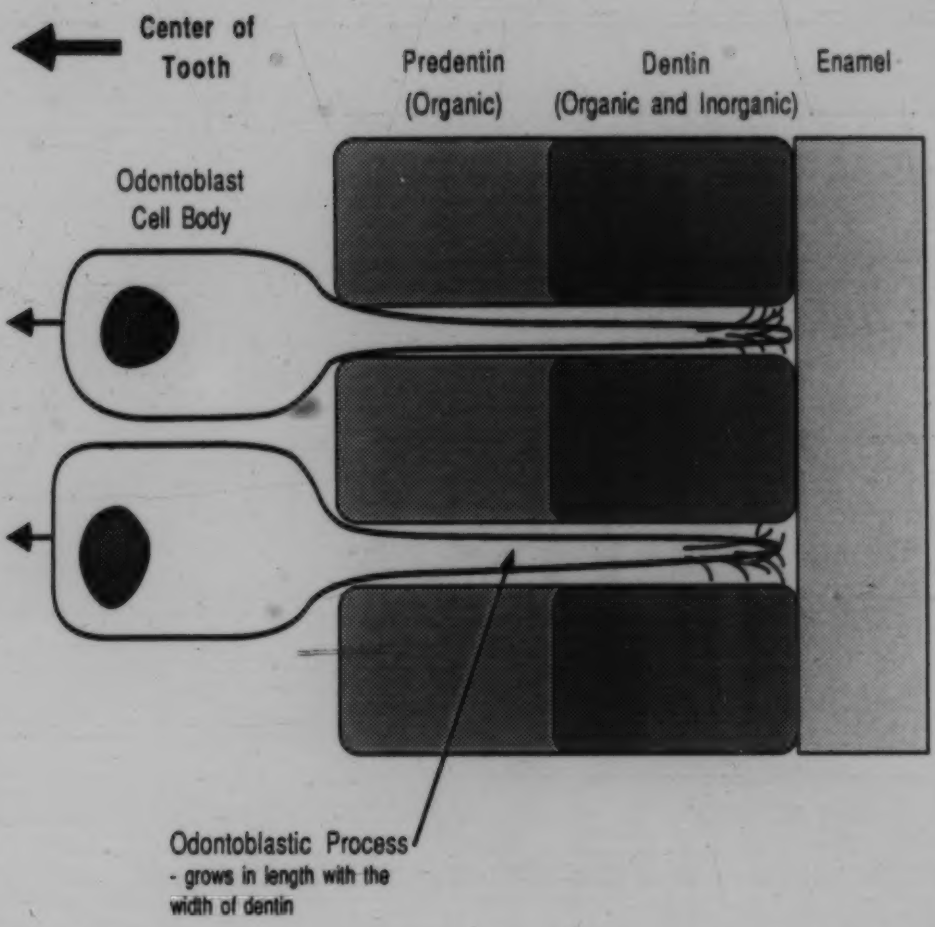
Center of Tooth
Predentin (Organic)
Dentin (Organic and Inorganic)
Enamel
Odontoblast Cell Body
Odontoblastic Process
- grows in length with the width of dentin

Figure 3

Diagram of two odontoblasts during the mineralization phase of dentinogenesis. Note that the cell bodies of the odontoblasts are receding "inwards" toward the center of the developing tooth.

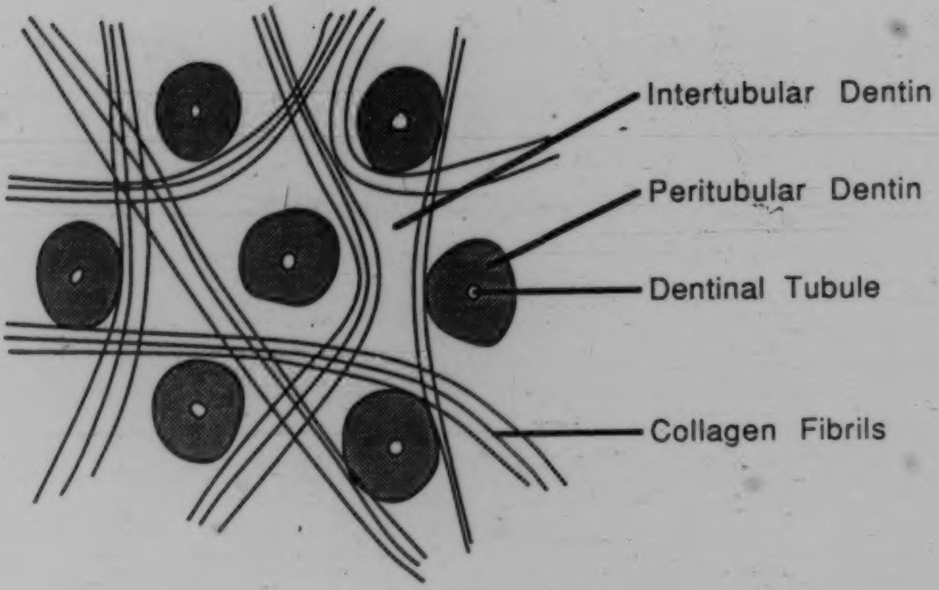
Intertubular Dentin
Peritubular Dentin
Dentinal Tubule
Collagen Fibrils

Figure 4

Diagrammatic representation of a section of dentin cut transversely to the dentinal tubules, showing the peritubular dentin and the collagen fibrils of the intertubular dentin.

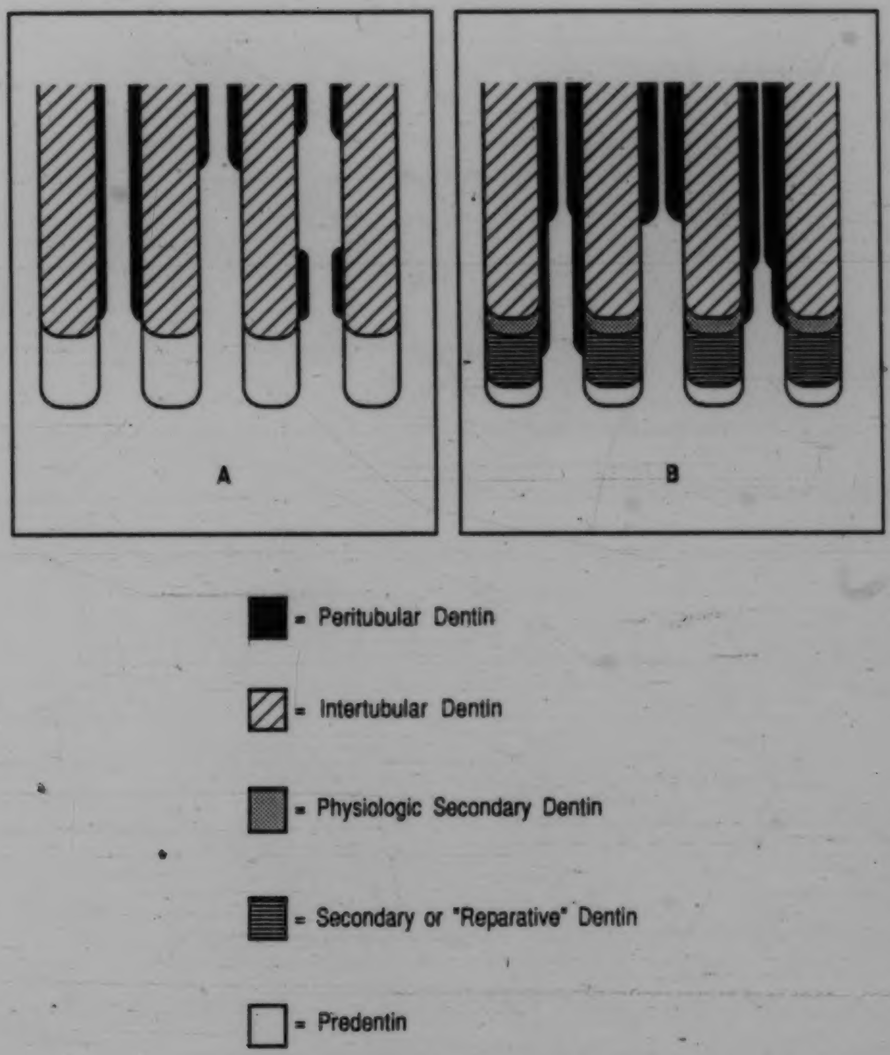
A
B
■ = Peritubular Dentin
▨ = Intertubular Dentin
▩ = Physiologic Secondary Dentin
▤ = Secondary or "Reparative" Dentin
□ = Predentin

Figure 5

Diagrammatic representation of two stages in the deposition of coronal dentin. A) during the formation of the primary dentin, and B) after the tooth has matured and been in the mouth for a number of years.

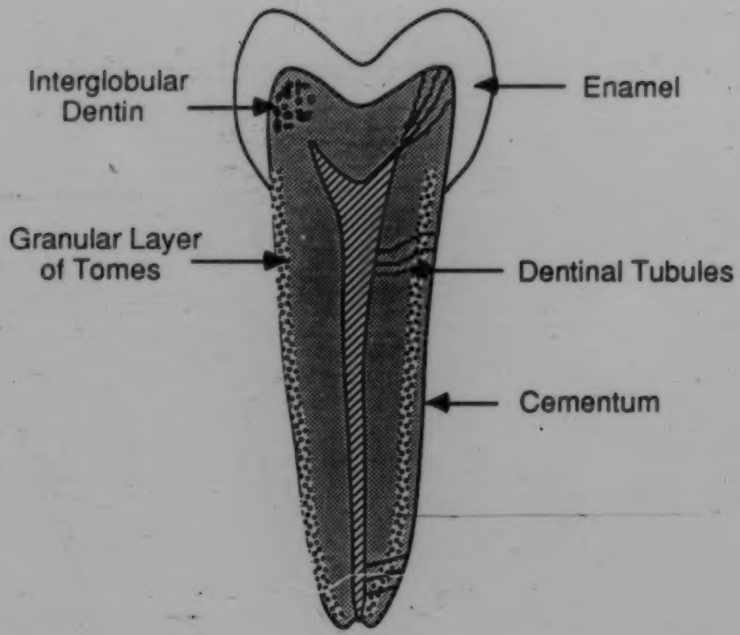
Interglobular Dentin
Enamel
Granular Layer of Tomes
Dentinal Tubules
Cementum

Figure 6

Diagrammatic representation of a vertical section through a tooth to show the arrangement of the dentinal tubules and the granular layer of Tomes.

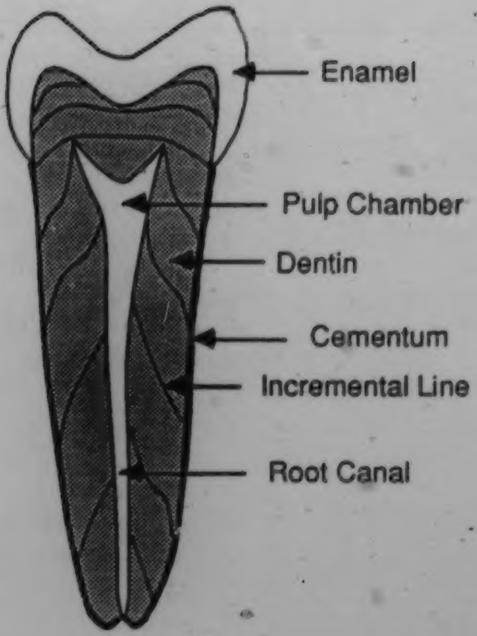
Enamel
Pulp Chamber
Dentin
Cementum
Incremental Line
Root Canal

Figure 7

Diagrammatic representation of a vertical section through a premolar to show the arrangement of the incremental lines (i.e. the "Contour Lines of Owen") in dentin.

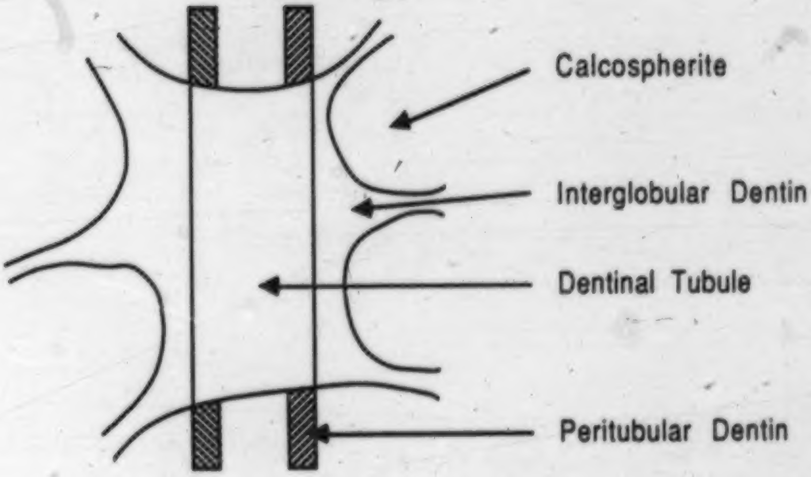
Calcospherite
Interglobular Dentin
Dentinal Tubule
Peritubular Dentin

Figure 8

Diagrammatic representation of an area of interglobular dentin and a dentinal tubule passing through it. The curved lines bounding the interglobular dentin represent the outline of calcospherites.

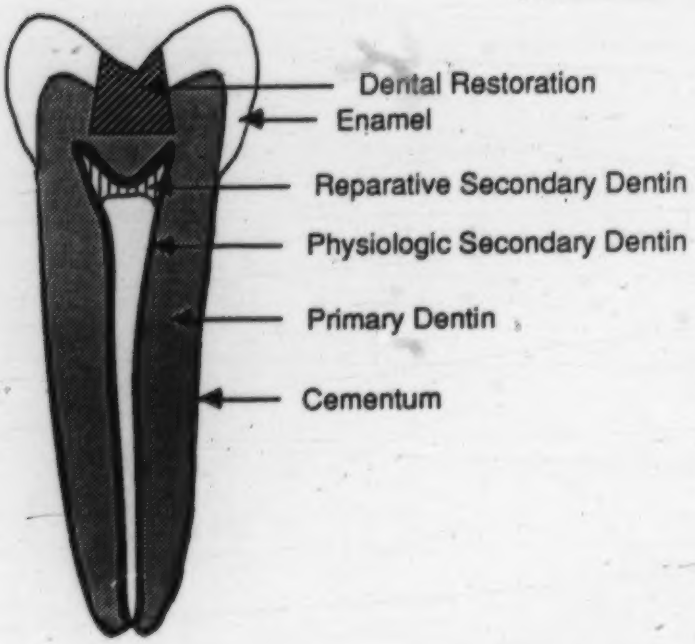
Dental Restoration
Enamel
Reparative Secondary Dentin
Physiologic Secondary Dentin
Primary Dentin
Cementum

Figure 9

Diagrammatic representation of a vertical section through a premolar showing primary dentin, physiologic secondary dentin, and "reparative" secondary dentin formed as a response to irritation caused by restorative dental procedures and caries.

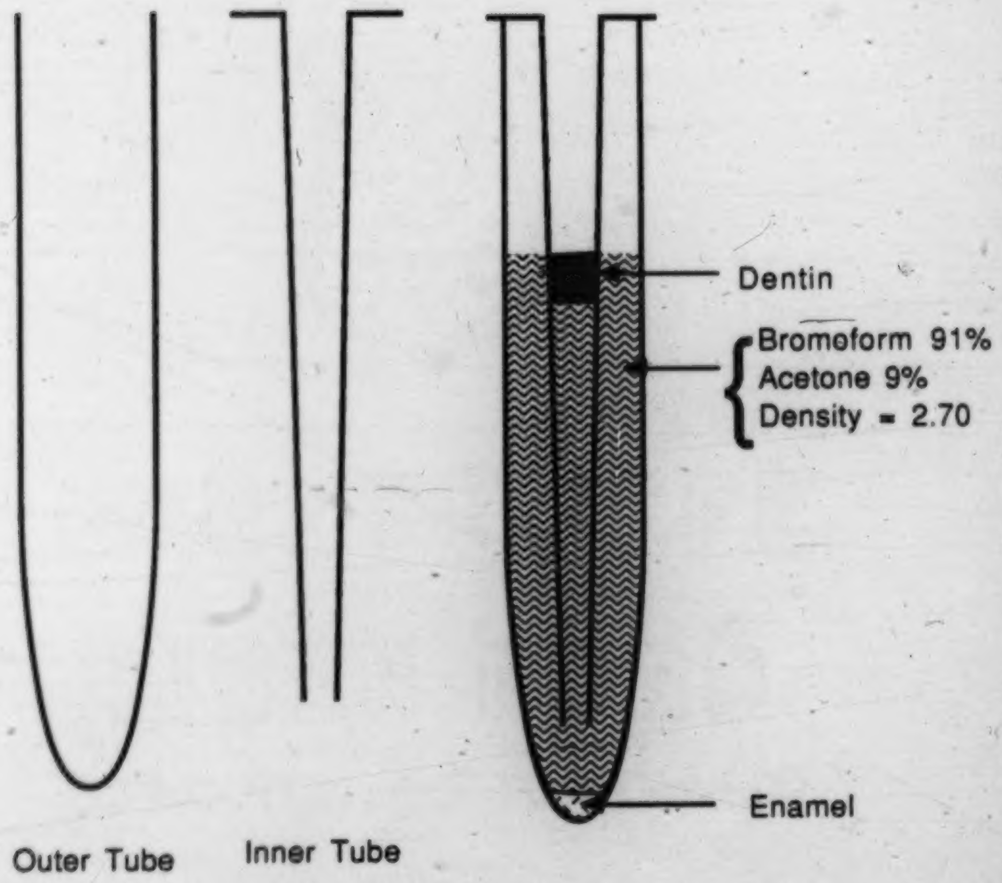
Dentin
Bromoform 91%
Acetone 9%
Density = 2.70
Enamel
Outer Tube
Inner Tube

Figure 10

Diagram of the method used by Manley and Hodge to separate enamel and dentin.

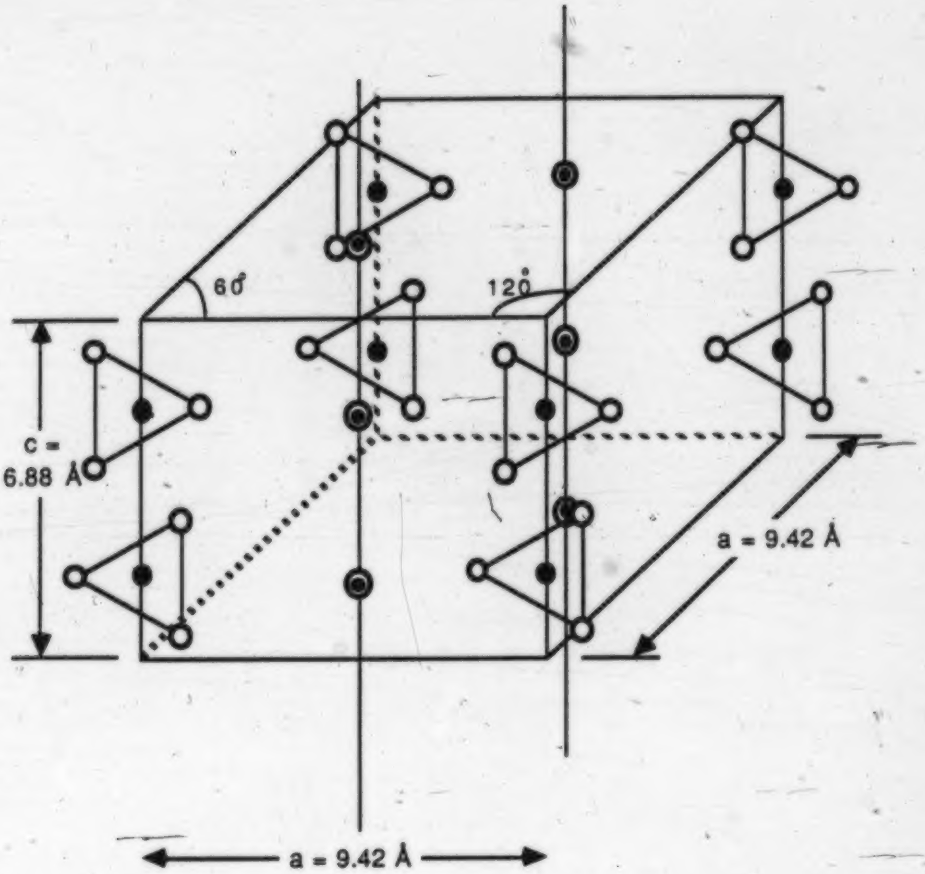

Figure 11

Hydroxyapatite unit cell showing hydroxyl positions (closed circles), calcium positions (open circles), and columnar calcium positions (circles with dot in center). Phosphate positions have been omitted for simplification.

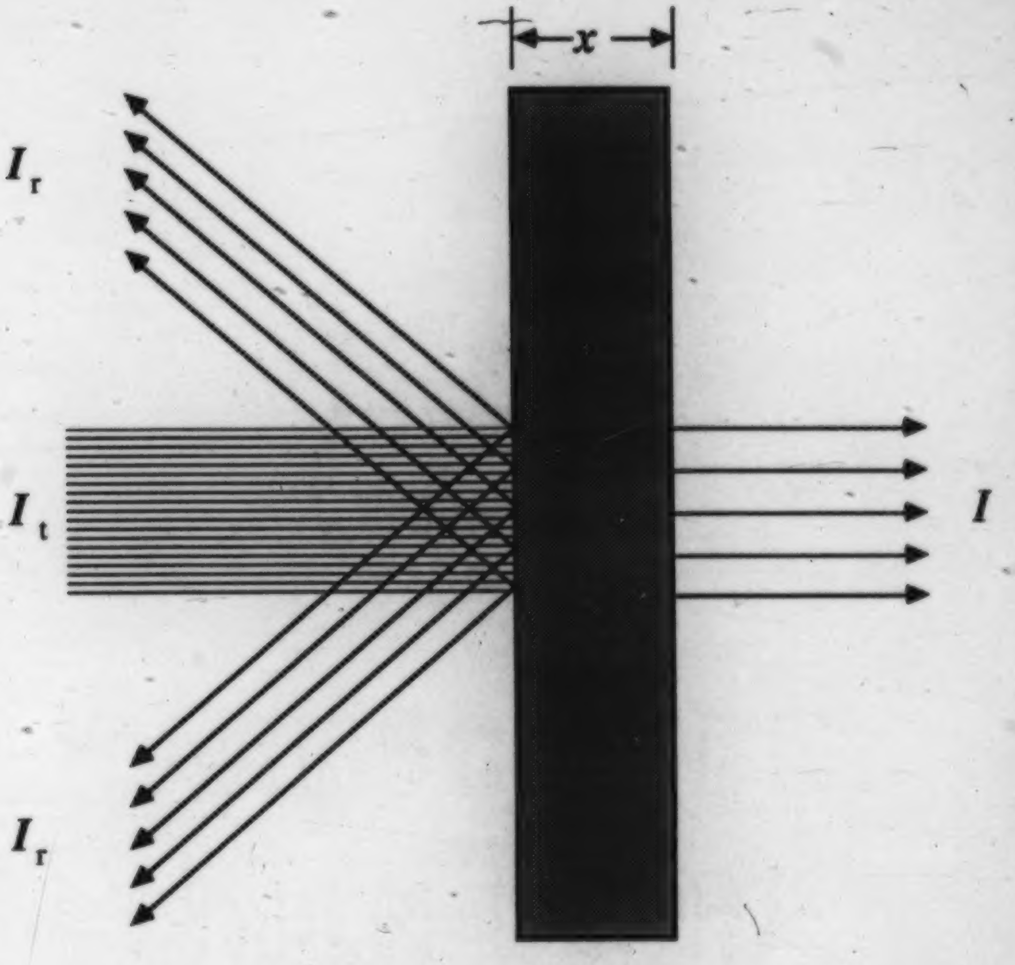

I_t = Intensity of Incident Beam

I_r = Intensity of Reflected Beam

I = Intensity of Transmitted Beam

Figure 12

This diagram is symbolic only and is not intended to demonstrate Snell's Law. Its purpose is only to clarify the most basic relationship between incident, reflected, and transmitted light.

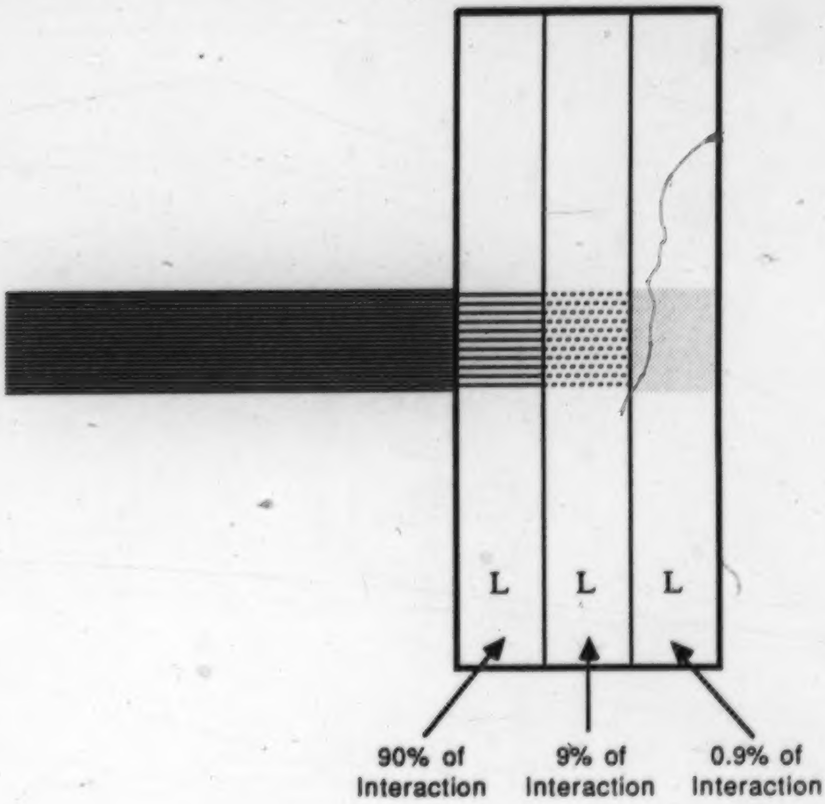

Figure 13

This figure is a highly schematized illustration of the concept of extinction length, and is not drawn to scale for any particular laser. The effects of scattering, nonuniformity of the beam intensity, differences between tissues, the exponential decay of the beam intensity within an extinction length, and exposure time (i.e., of heat conduction) are all neglected in this simplified diagram. Due to differences in absorption and the presence of scattering, the Nd-YAG laser has an extinction length which is substantially larger and an extinction volume which is more symmetrically rounded in shape than that of the carbon dioxide laser.

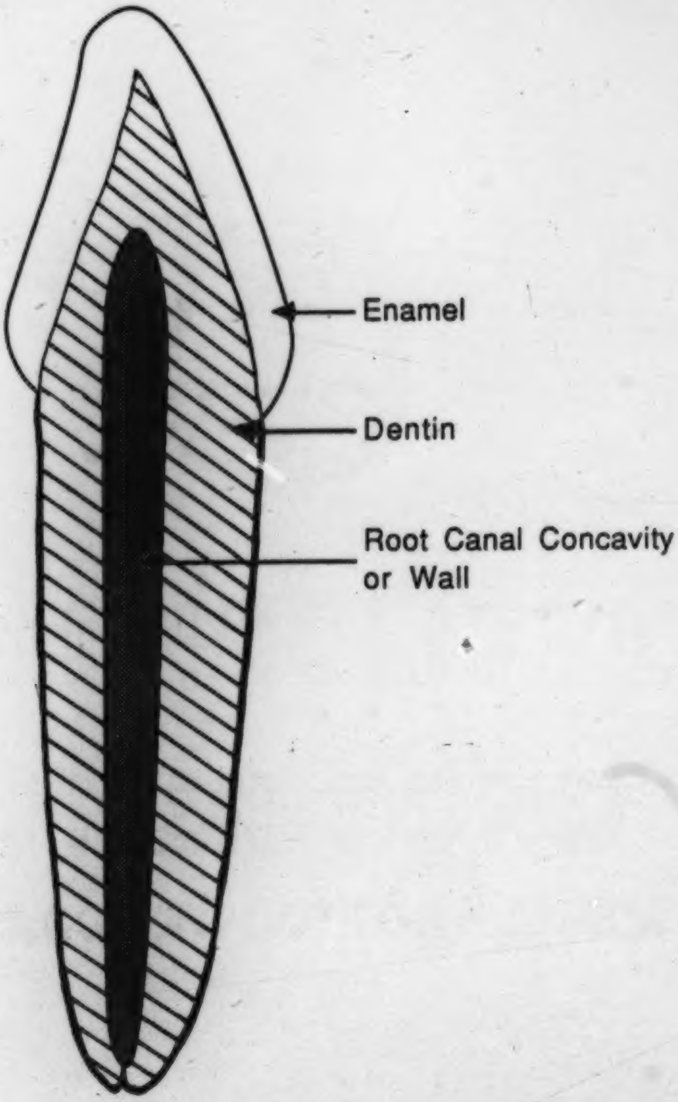
Enamel
Dentin
Root Canal Concavity or Wall

Figure 14

Diagram of a sectioned tooth specimen showing an exposed root canal concavity which has been instrumented in preparation for laser irradiation.

Mean Hairline Cracking
Effect of Power/Pulse Duration Interaction
Continuous-Wave CO_2 Laser

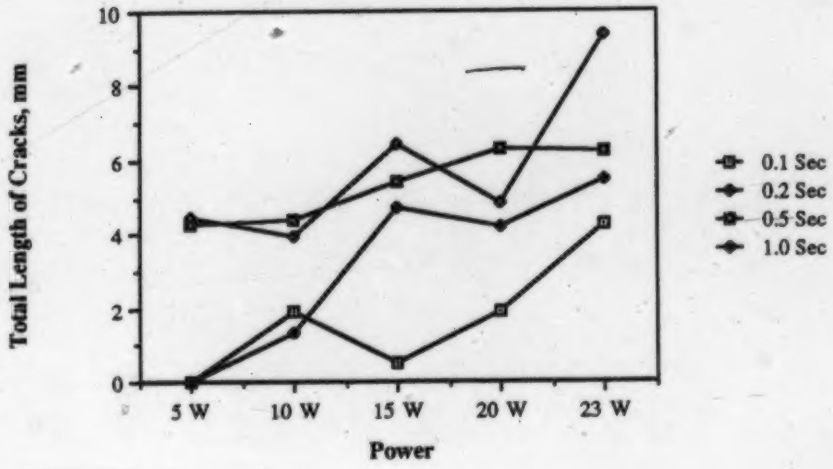

Figure 15

Mean Wide Cracking
Effect of Power/Pulse Duration Interaction
Continuous-Wave CO_2 Laser

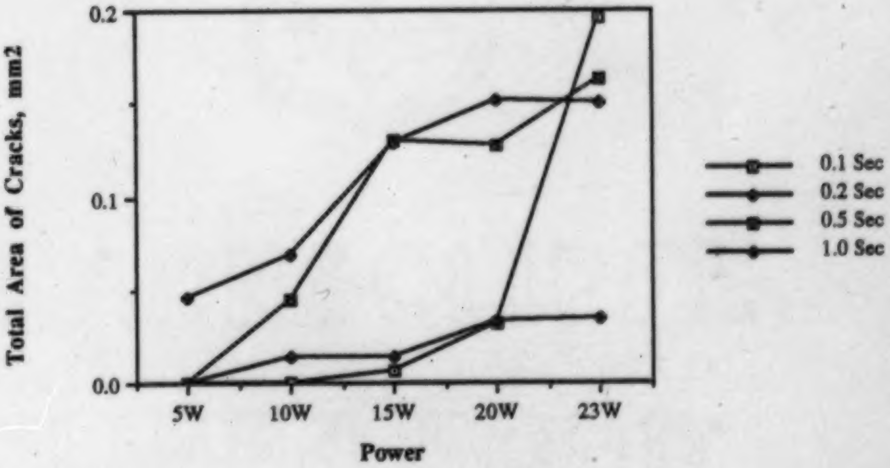

Figure 16

Mean Fusion Coverage
Effect of Power/Pulse Duration Interaction
Continuous-Wave CO_2 Laser

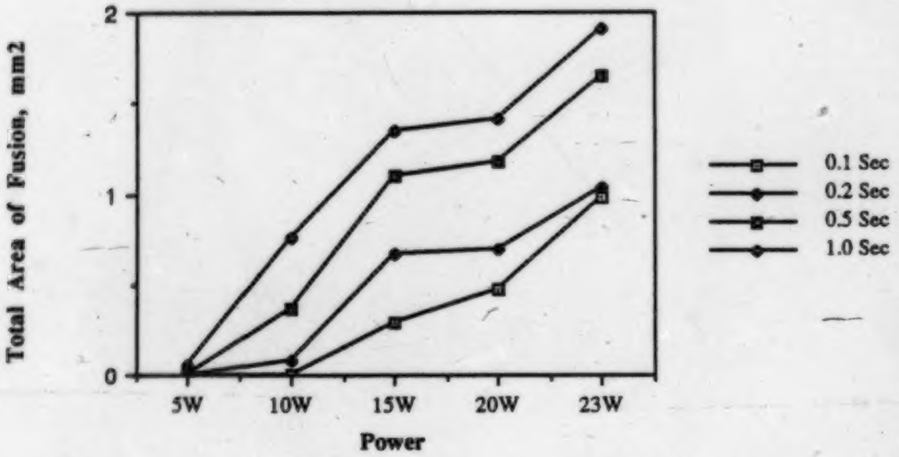

Figure 17

Mean Wide Cracking

Effect of Power Only

Continuous-Wave CO_2 Laser

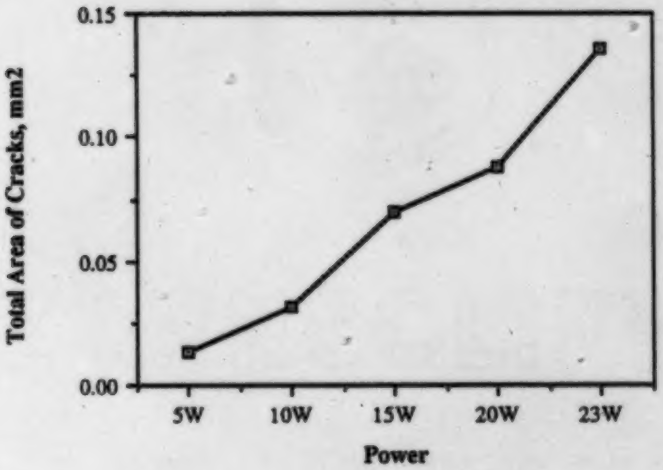

Figure 18

Mean Wide Cracking

Effect of Pulse Duration Only

Continuous-Wave CO_2 Laser

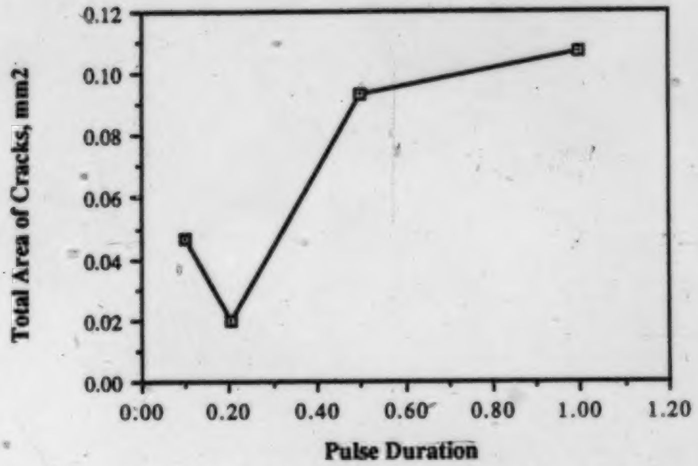

Figure 19

Mean Hairline Cracking

Effect of Power/Pulse Train Duration Interaction

Pulsed CO_2 Laser

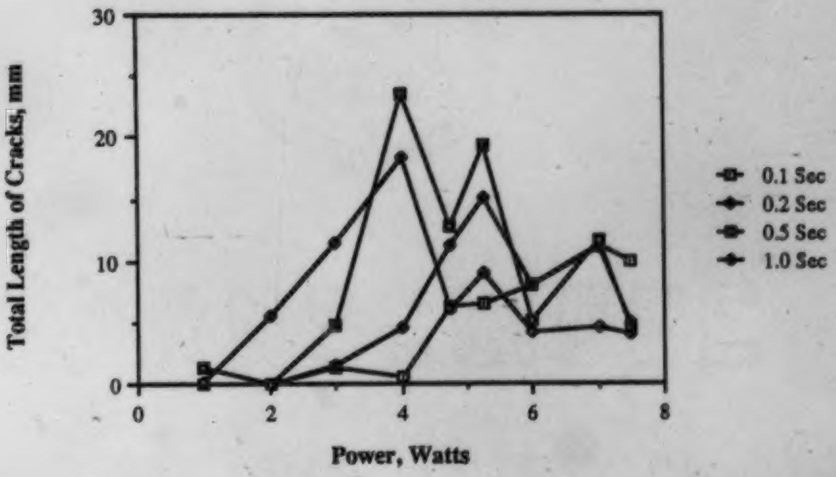

Figure 20

Mean Wide Cracking

Effect of Power/Pulse Train Duration Interaction

Pulsed CO_2 Laser

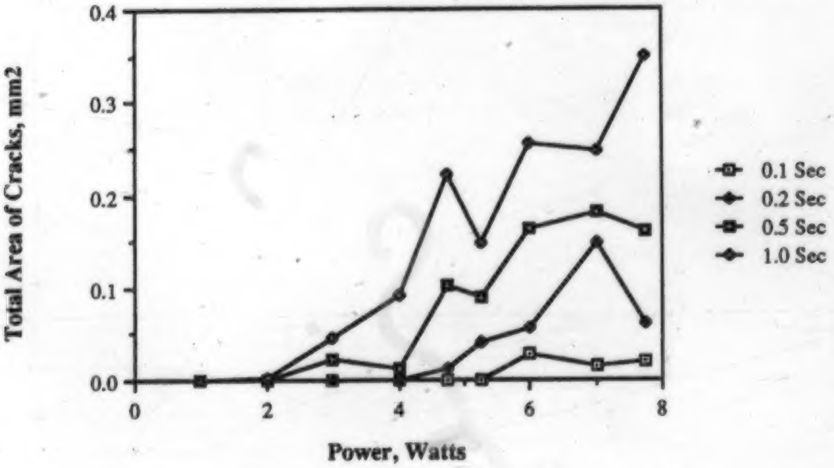

Figure 21

Mean Fusion Coverage

Effect of Power/Pulse Train Duration Interaction

Pulsed CO_2 Laser

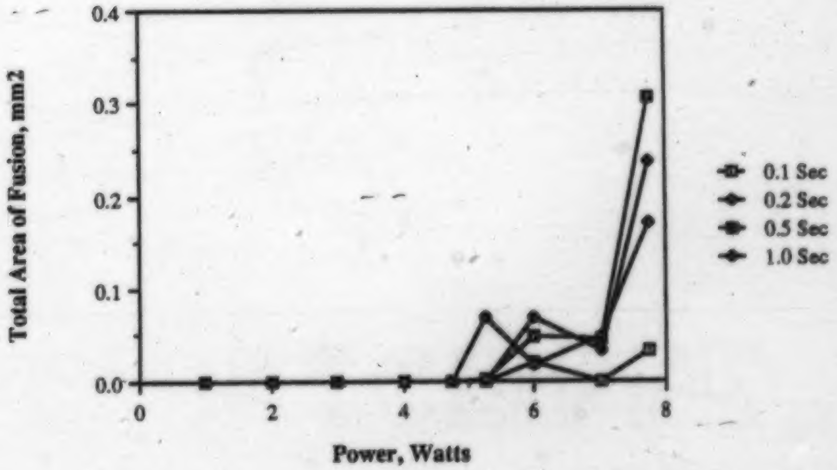

Figure 22

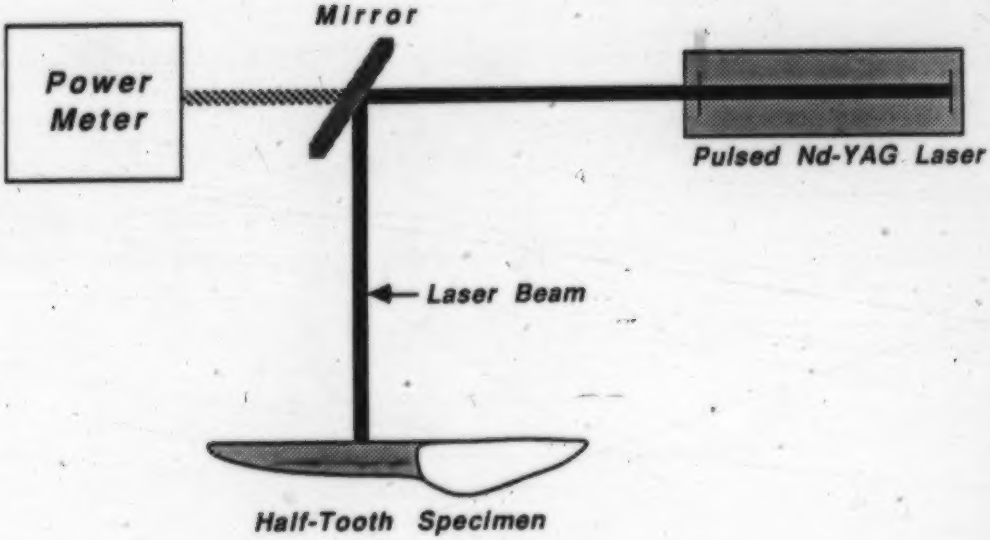
Mirror
Power Meter
Pulsed Nd-YAG Laser
Laser Beam
Half-Tooth Specimen

Figure 23

This diagram illustrates the experimental set-up used to irradiate the tooth specimens with the pulsed Nd-YAG laser. The mirror was positioned as shown for all exposures, and contributed approximately a 4% loss in energy. The mirror was periodically removed in order to allow the beam to strike the meter for purposes of measuring power output.

Mean Hairline Cracking
Effect of Power/Pulse Train Duration Interaction
Pulsed Nd-YAG Laser

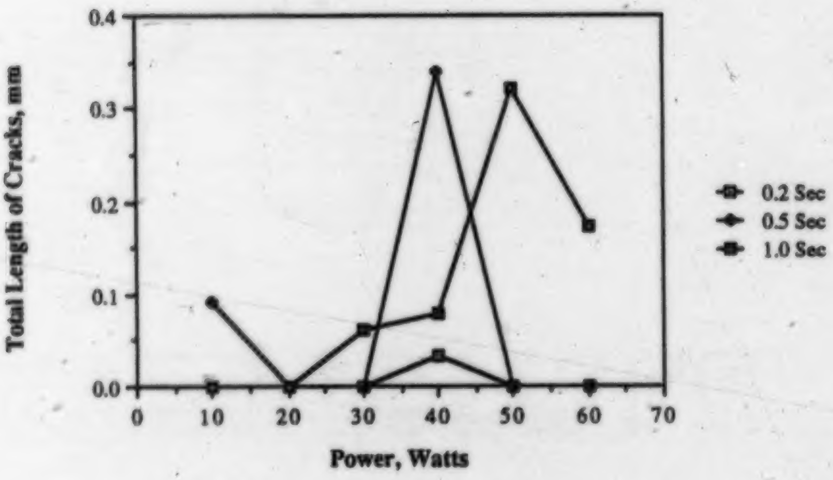

Figure 24

Mean Wide Cracking
Effect of Power/Pulse Train Duration Interaction
Pulsed Nd-YAG Laser

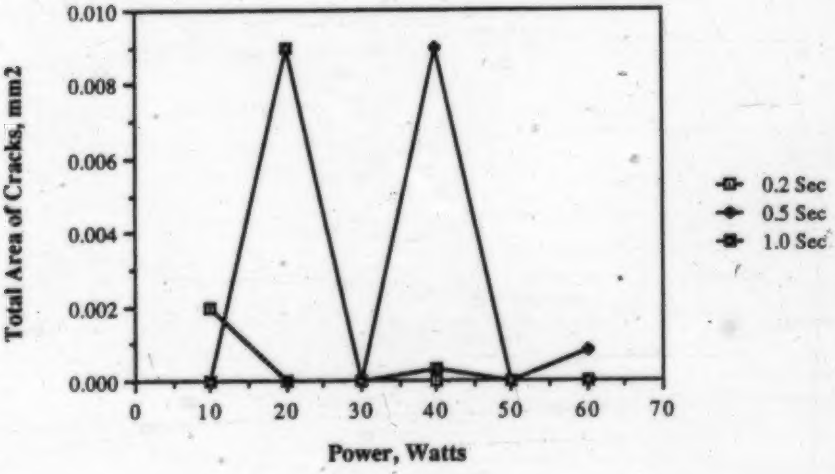

Figure 25

Mean Fusion Coverage

Effect of Power/Pulse Train Duration Interaction

Pulsed Nd-YAG Laser

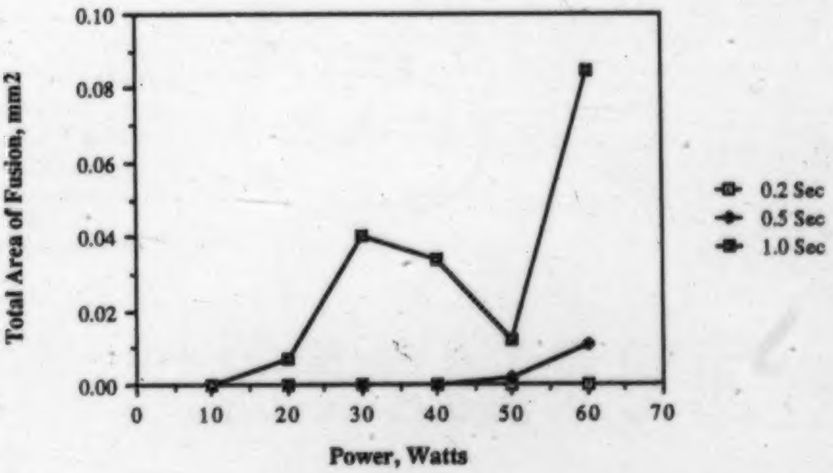

Figure 26

Mean Area of Unfused Cratering
Effect of Power/Pulse Train Duration Interaction
Pulsed Nd-YAG Laser

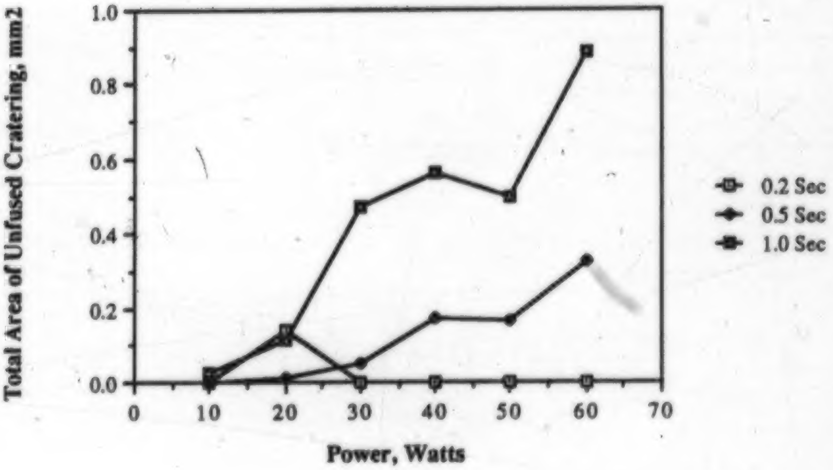

Figure 27

Mean Hairline Cracking

Effect of Power/Pulse Rate Interaction

Pulsed Nd-YAG Laser

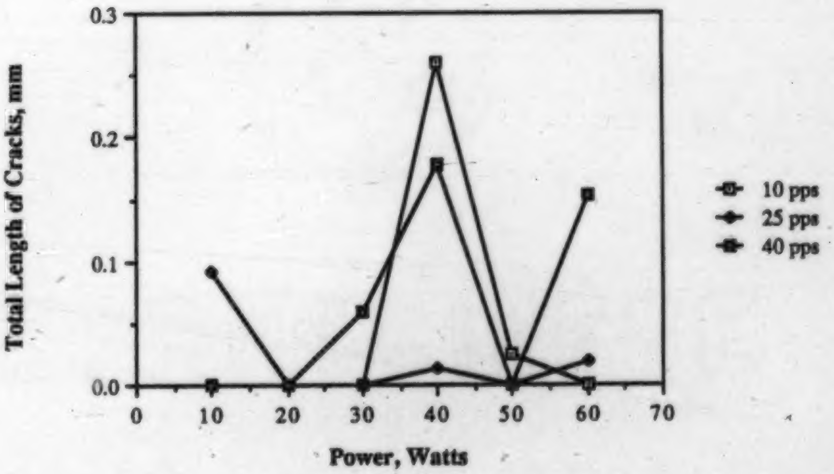

Figure 28

Mean Wide Cracking

Effect of Power/Pulse Rate Interaction

Pulsed Nd-YAG Laser

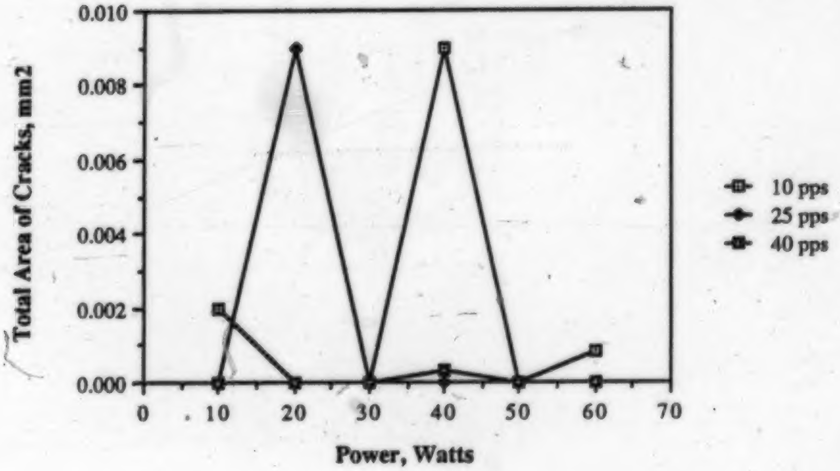

Figure 29

Mean Fusion Coverage
Effect of Power/Pulse Rate Interaction
Pulsed Nd-YAG Laser

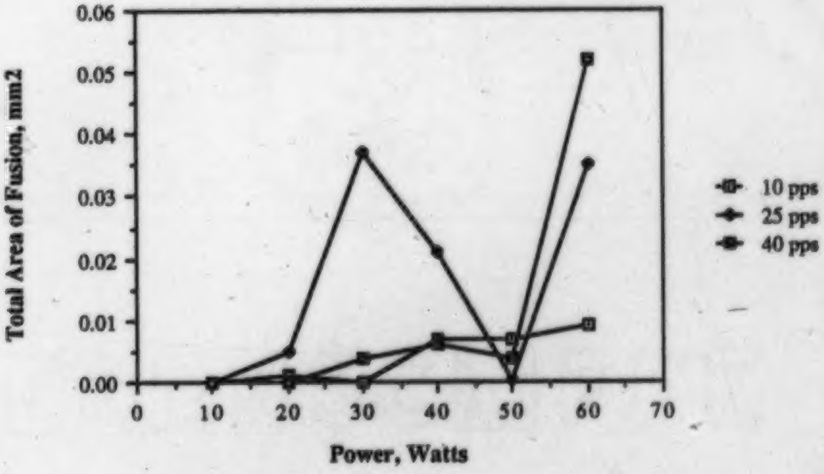

Figure 30

Mean Area of Unfused Cratering
Effect of Power/Pulse Rate Interaction
Pulsed Nd-YAG Laser

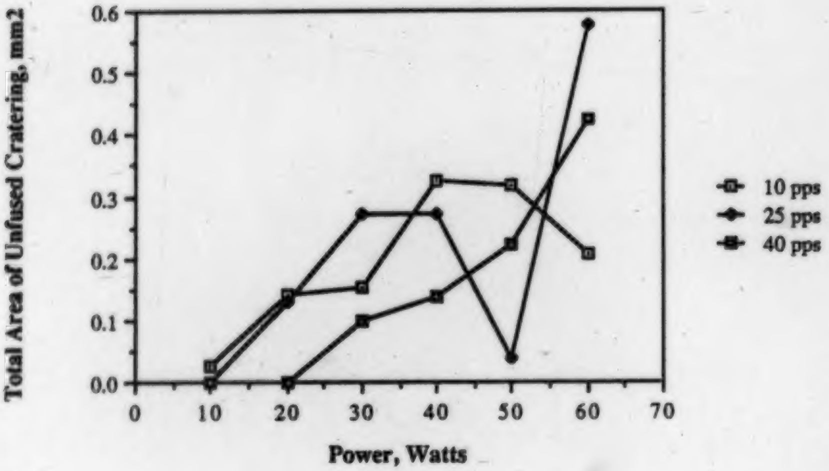

Figure 31

Mean Hairline Cracking

Effect of Pulse Rate/Pulse Train Duration Interaction

Pulsed Nd-YAG Laser

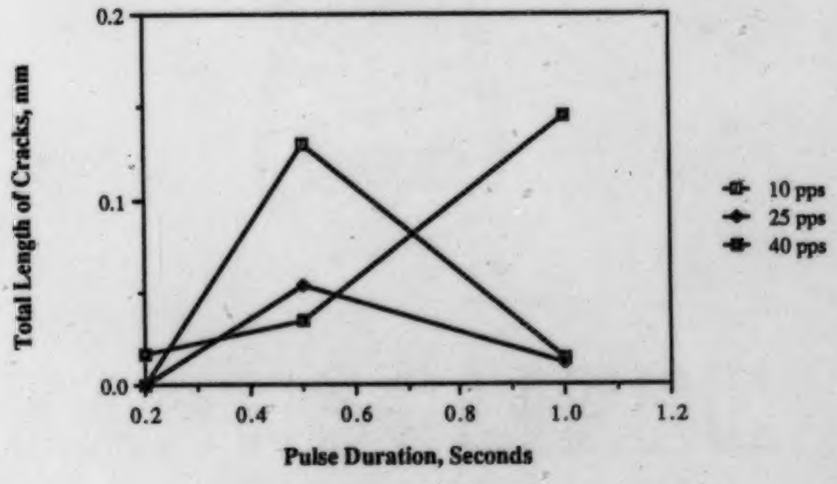

Figure 32

Mean Wide Cracking
Effect of Pulse Rate/Pulse Train Duration Interaction
Pulsed Nd-YAG Laser

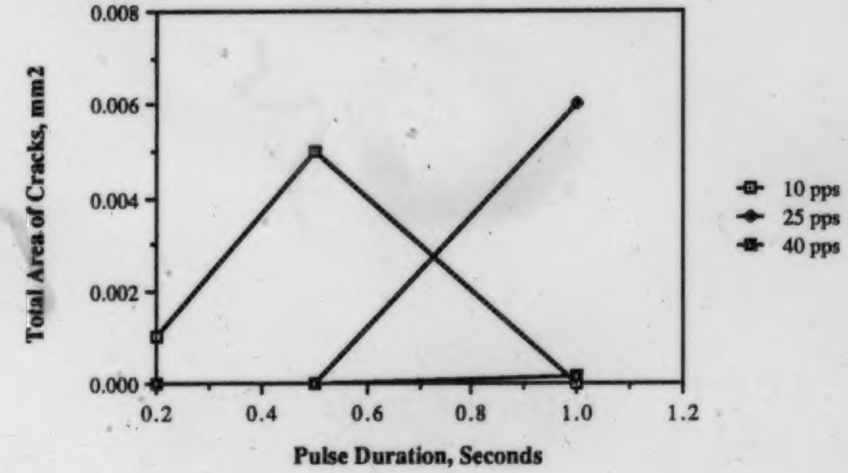

Figure 33

Mean Fusion Coverage

Effect of Pulse Rate/Pulse Train Duration Interaction

Pulsed Nd-YAG Laser

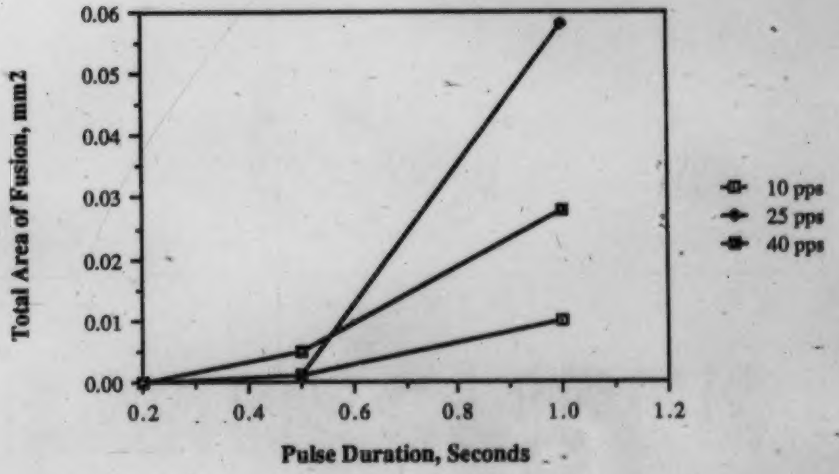

Figure 34

Mean Area of Unfused Cratering

Effect of Pulse Rate/Pulse Train Duration Interaction

Pulsed Nd-YAG Laser

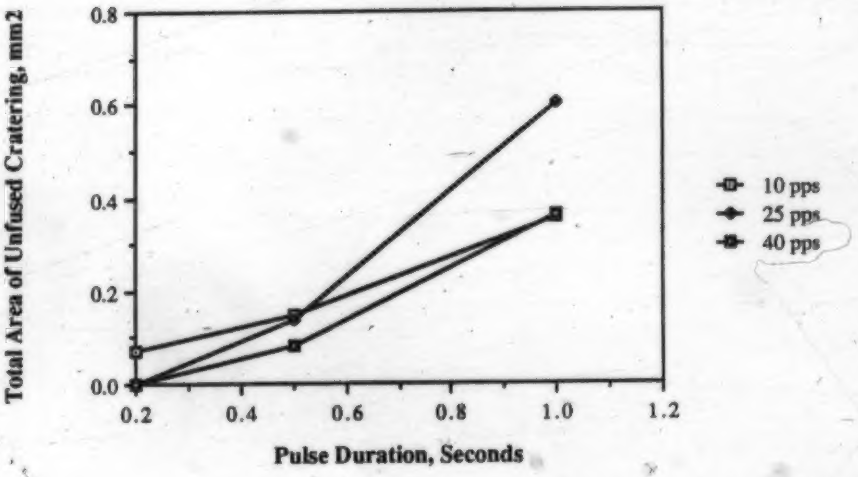

Figure 35

Mean Hairline Cracking
Effect of Power Only
Pulsed Nd-YAG Laser

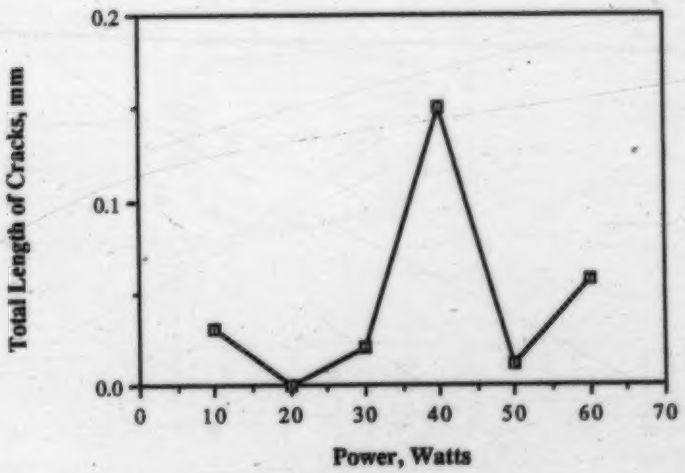

Figure 36

Mean Wide Cracking
Effect of Power Only
Pulsed Nd-YAG Laser

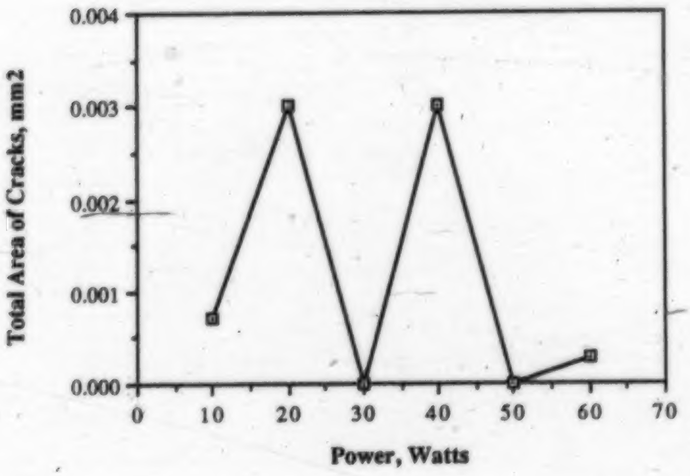

Figure 37

Mean Fusion Coverage
Effect of Power Only
Pulsed Nd-YAG Laser

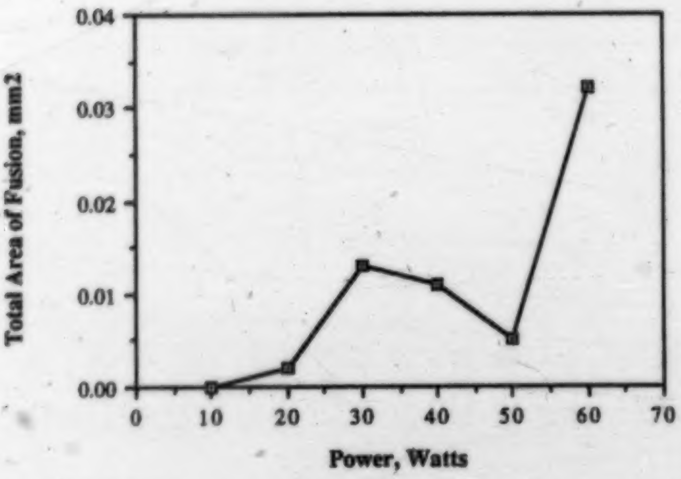

Figure 38

Mean Area of Unfused Cratering
Effect of Power Only
Pulsed Nd-YAG Laser

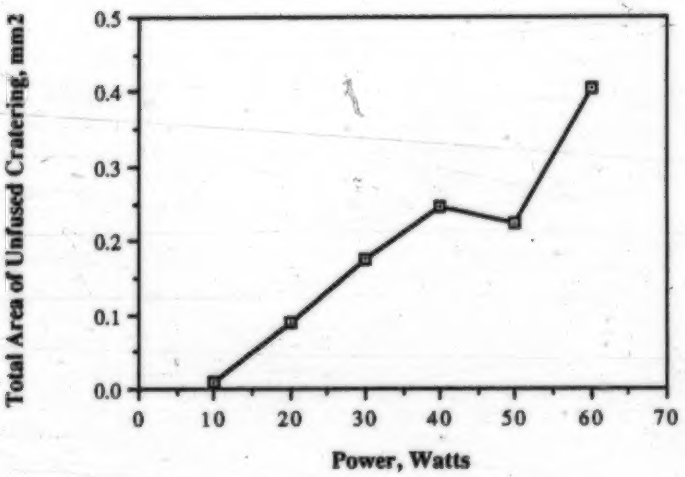

Figure 39

Mean Hairline Cracking

Effect of Pulse Rate Only

Pulsed Nd-YAG Laser

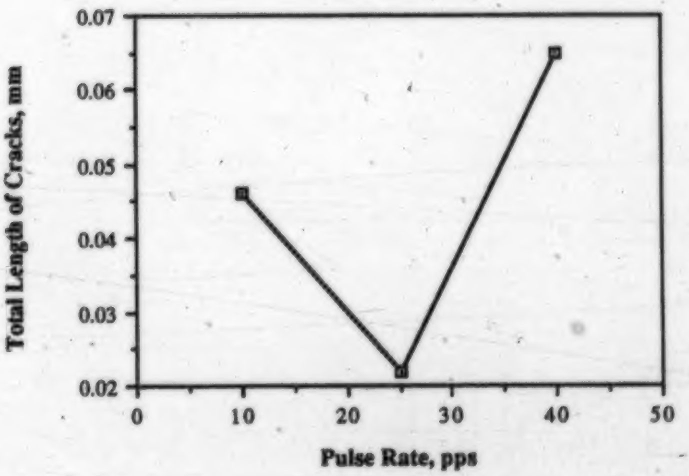

Figure 40

Mean Wide Cracking
Effect of Pulse Rate Only
Pulsed Nd-YAG Laser

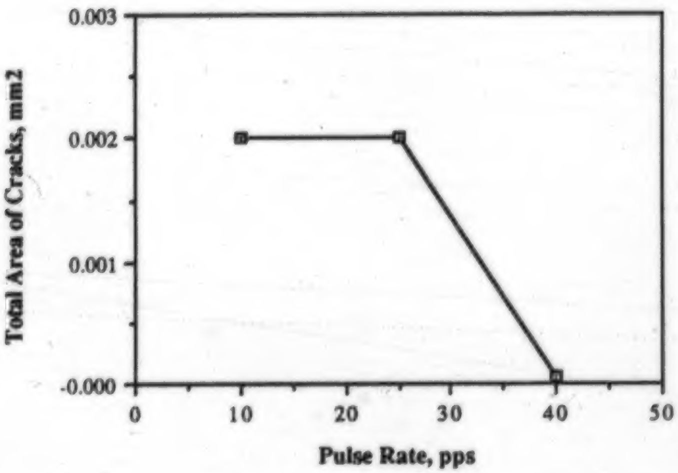

Figure 41

Mean Fusion Coverage

Effect of Pulse Rate Only

Pulsed Nd-YAG Laser

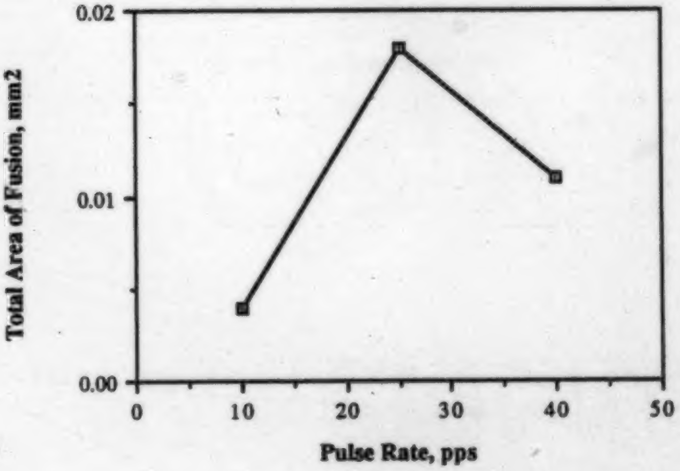

Figure 42

Mean Area of Unfused Cratering
Effect of Pulse Rate Only
Pulsed Nd-YAG Laser

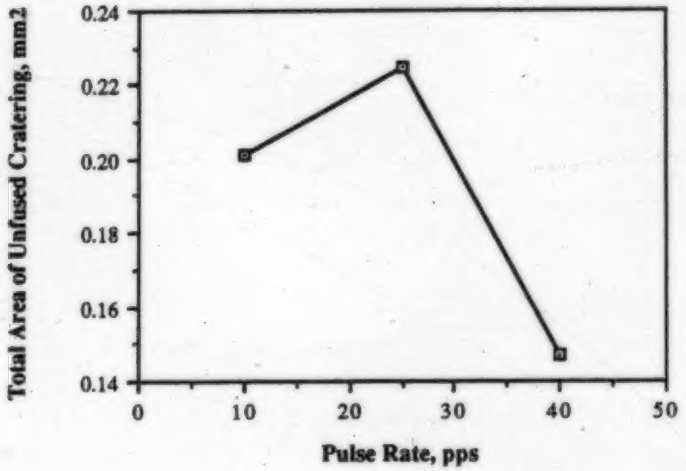

Figure 43

Mean Hairline Cracking

Effect of Pulse Train Duration Only

Pulsed Nd-YAG Laser

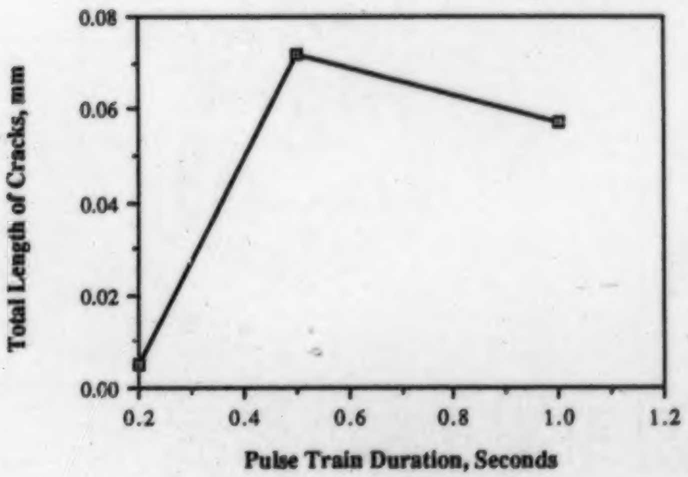

Figure 44

Mean Wide Cracking
Effect of Pulse Train Duration Only
Pulsed Nd-YAG Laser

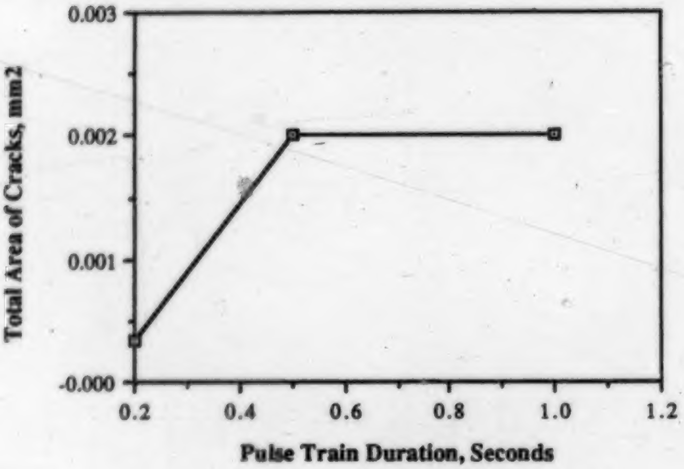

Figure 45

Mean Area of Fusion Coverage

Effect of Pulse Train Duration Only

Pulsed Nd-YAG Laser

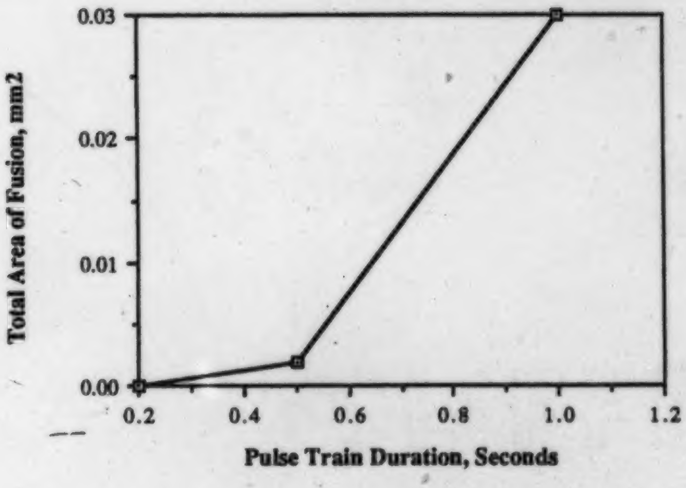

Figure 46

Mean Area of Unfused Cratering

Effect of Pulse Train Duration Only

Pulsed Nd-YAG Laser

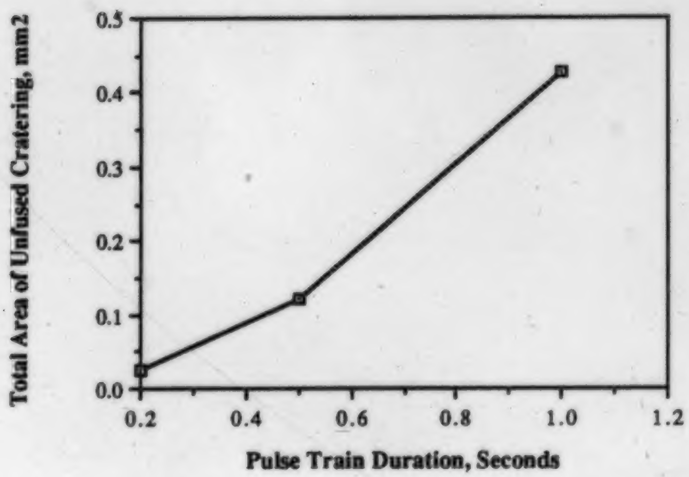

Figure 47

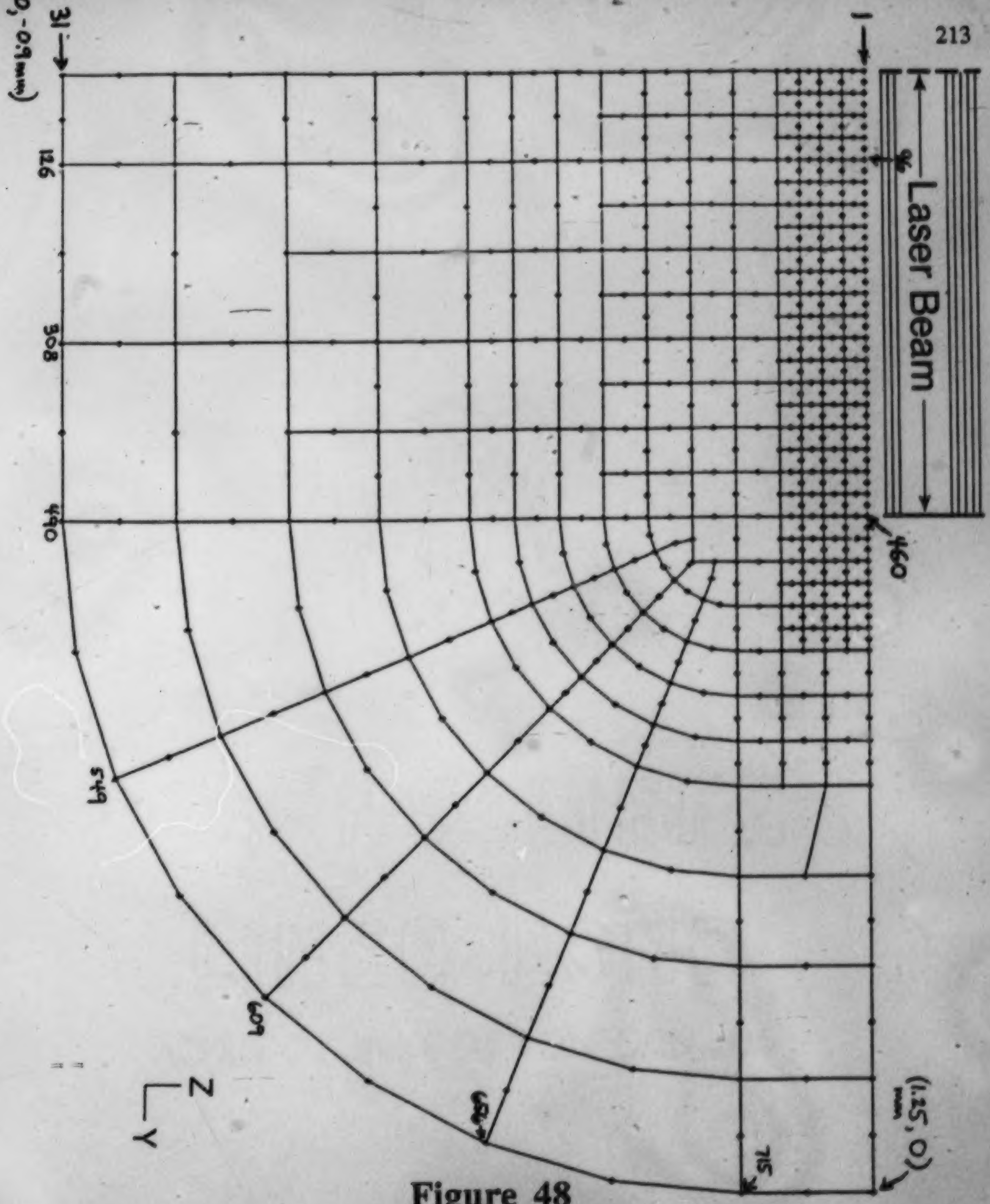
31
(0,-0.9mm)
126
308
490
549
609
715
(1.25, 0) mm
460
1
Laser Beam
Z
Y

Figure 48

Diagram of the laser beam impinging on the finite element mesh. The center axis nodes (1-31) are restricted to vertical movement only. All other nodes can move in the y-z plane.

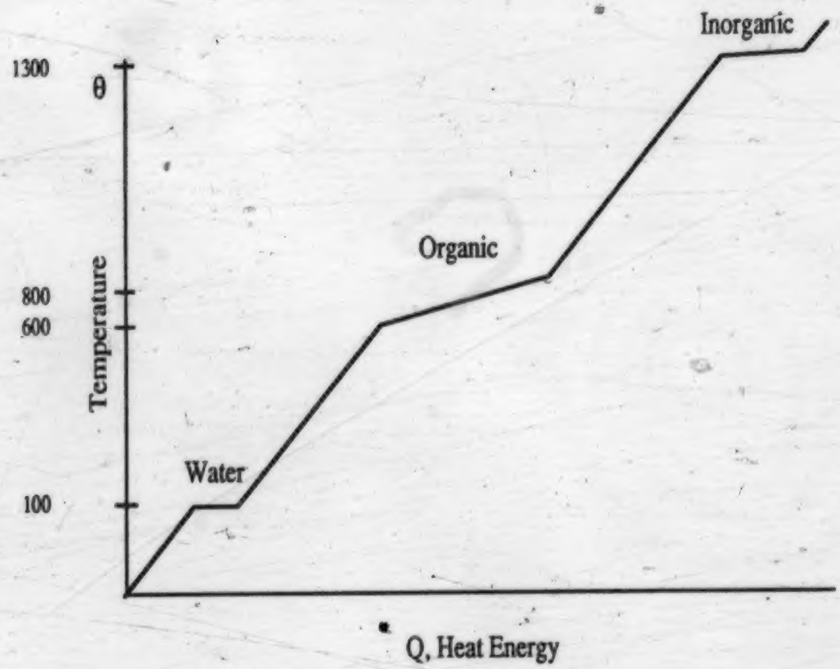

Figure 49

Heat energy versus energy curve for dentin. (Not to scale).

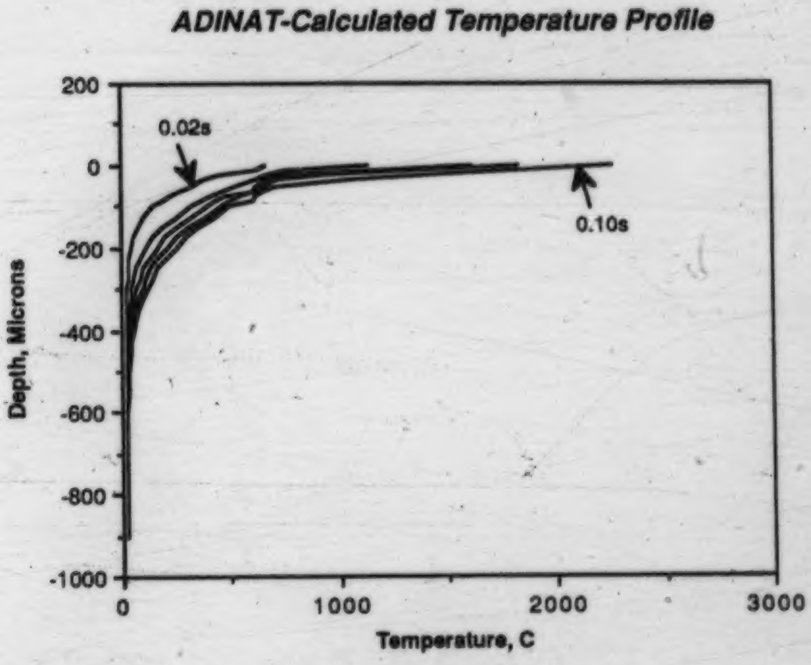

Figure 50

ADINAT-calculated temperature profiles for time steps from 0.02 seconds to 5.0 seconds for nodes 96 to 126.

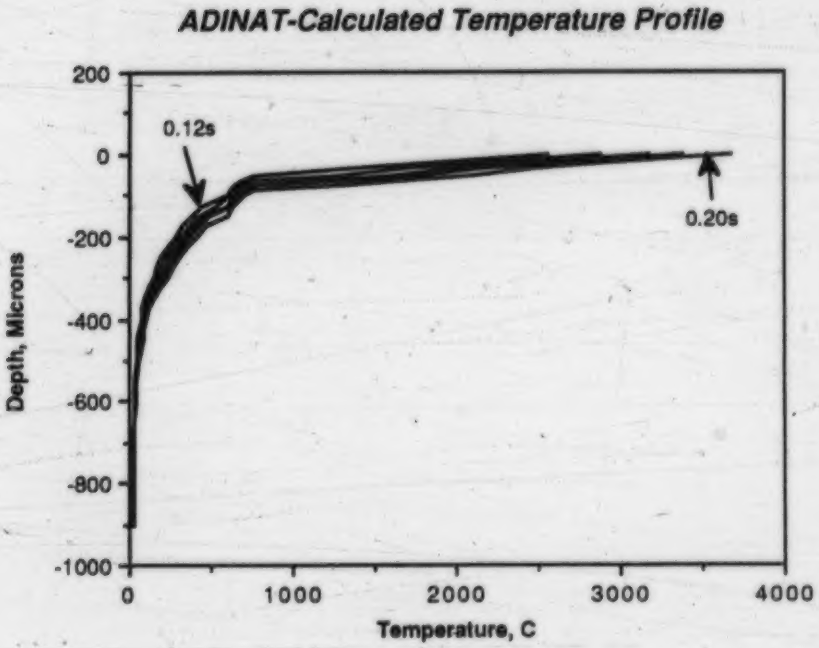

Figure 50

(continued)

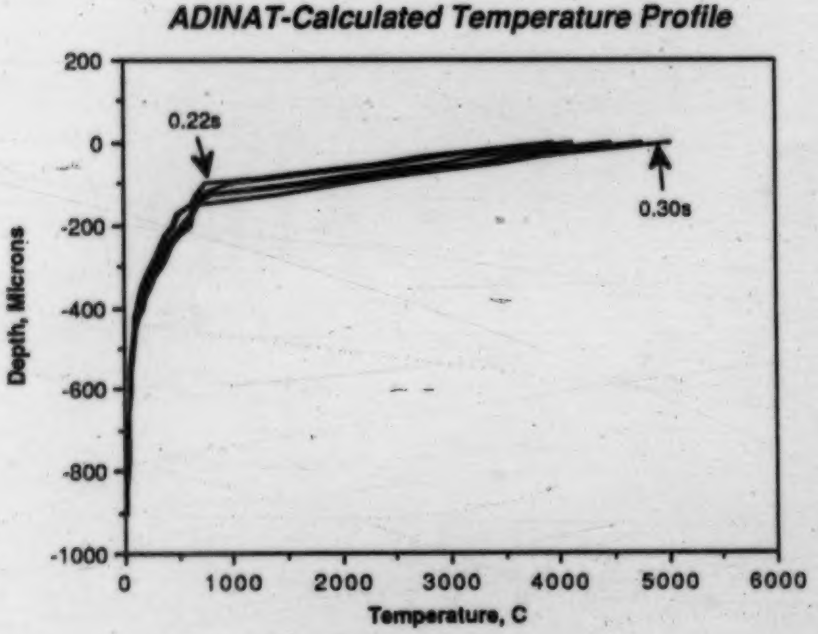

Figure 50

(continued)

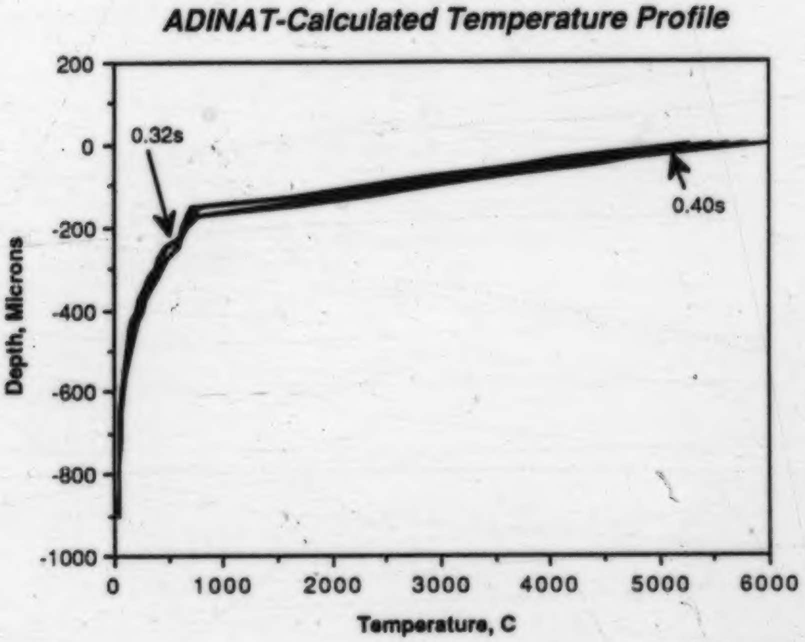

Figure 50

(continued)

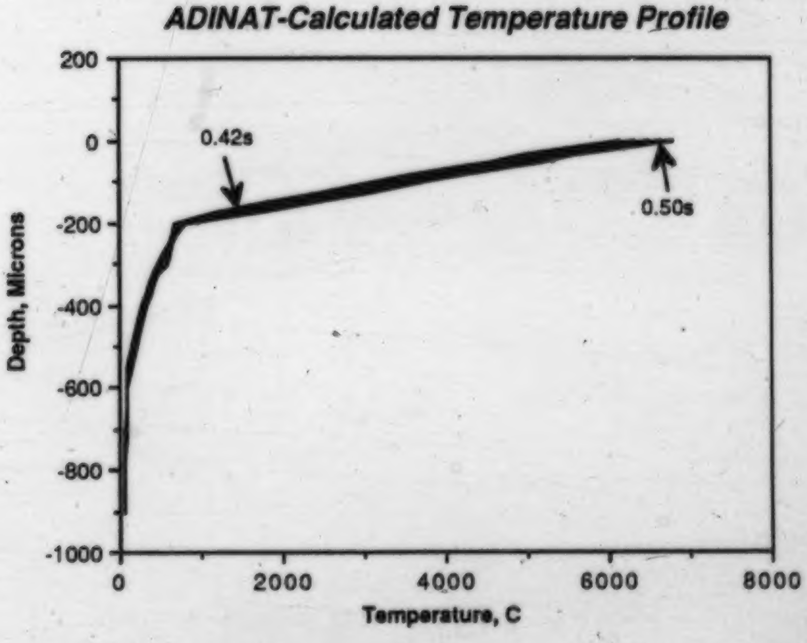

Figure 50

(continued)

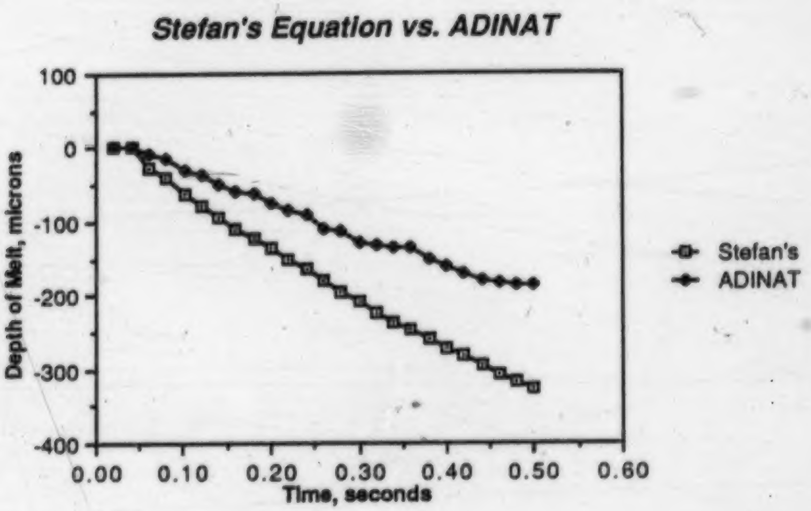

Figure 51

ADINAT-calculated depth of melt versus Stefan's Equation

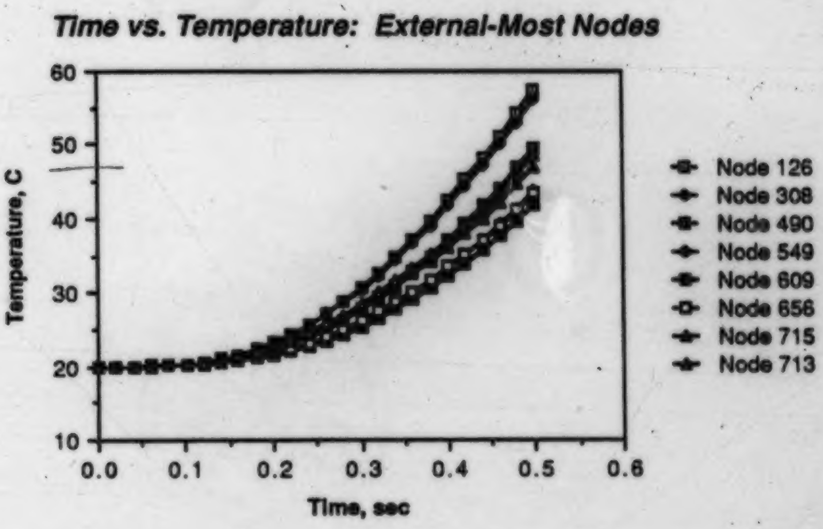

Figure 52

Time versus temperature profile of the external-most nodes

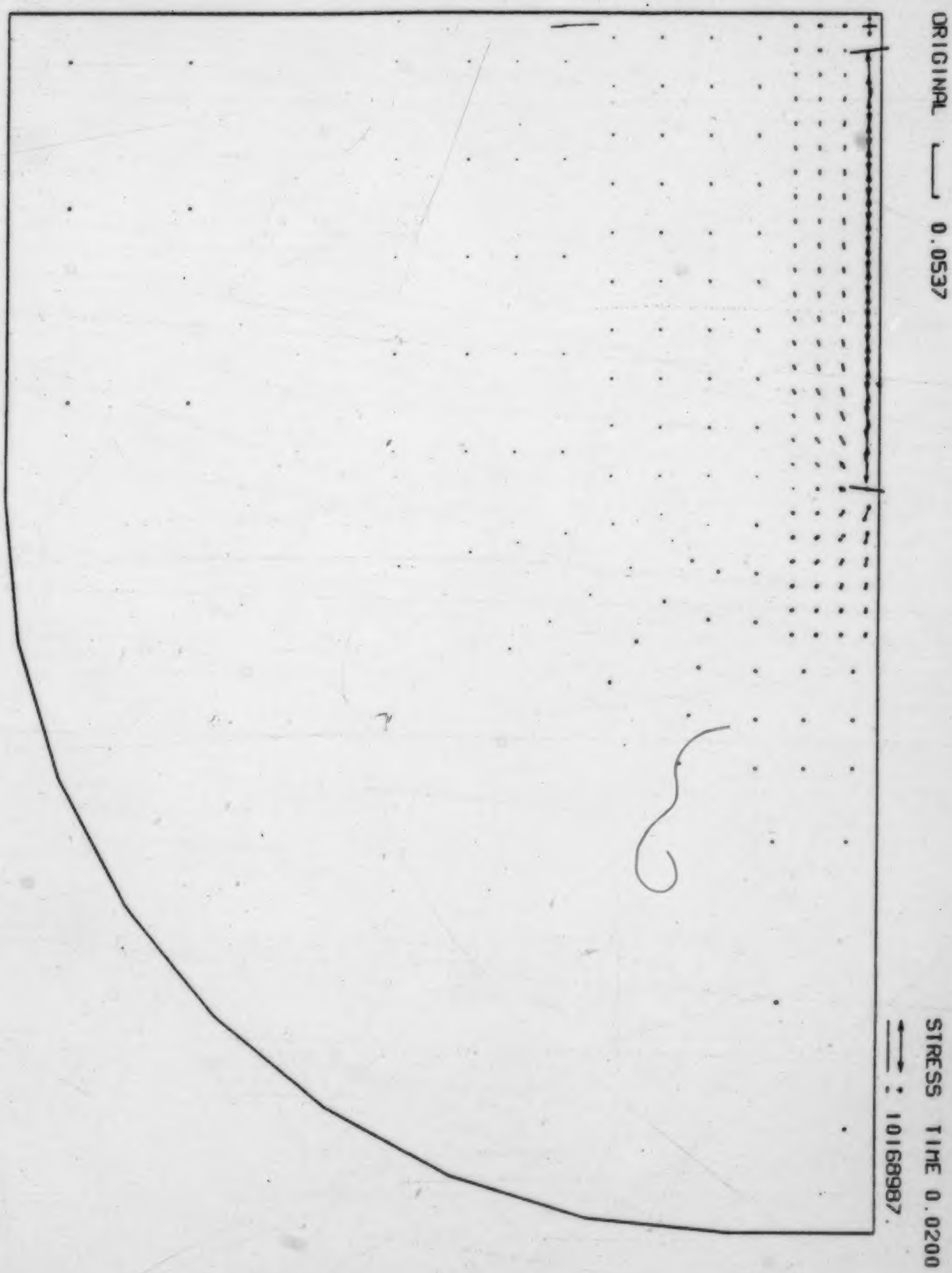

Figure 53

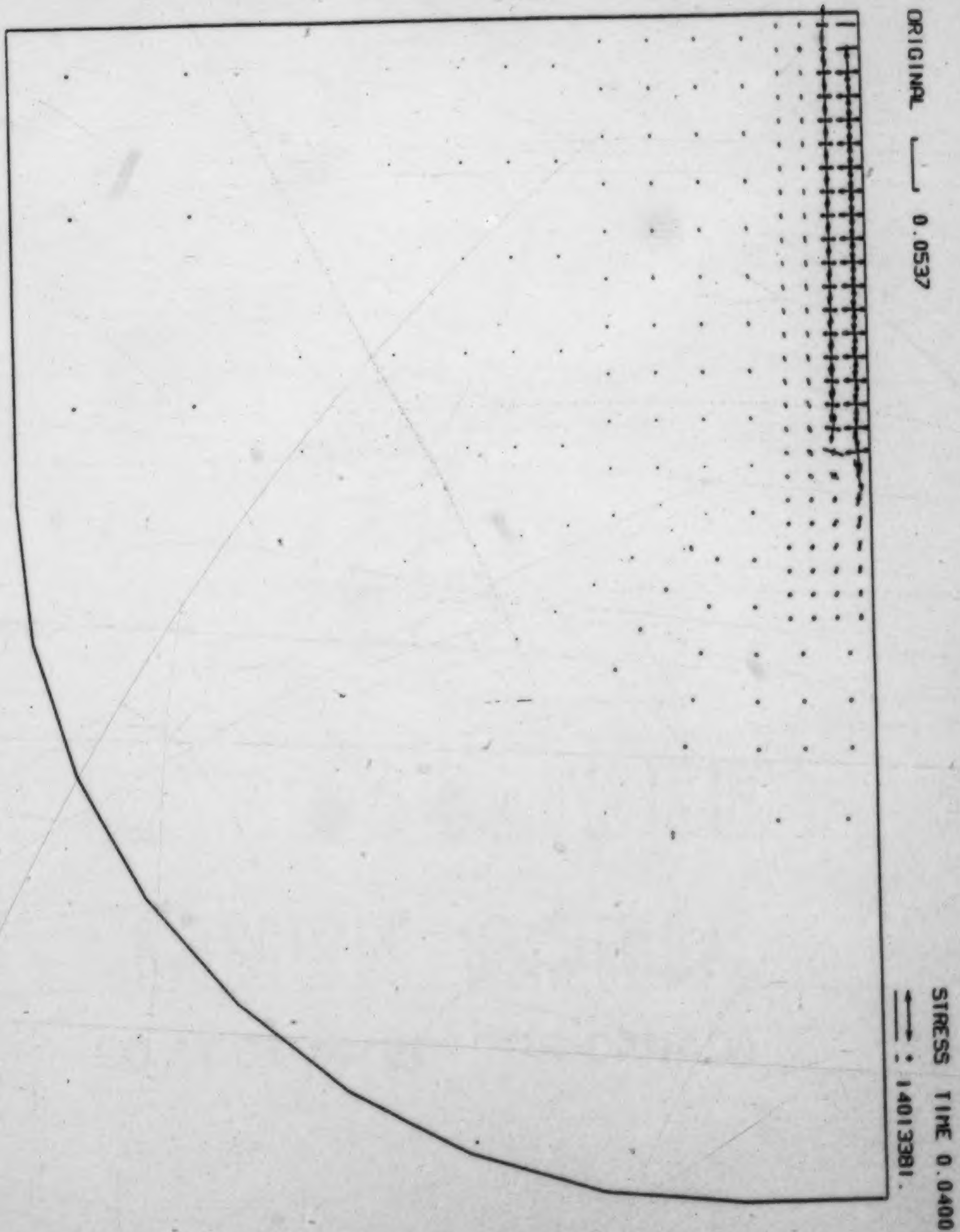

Figure 54

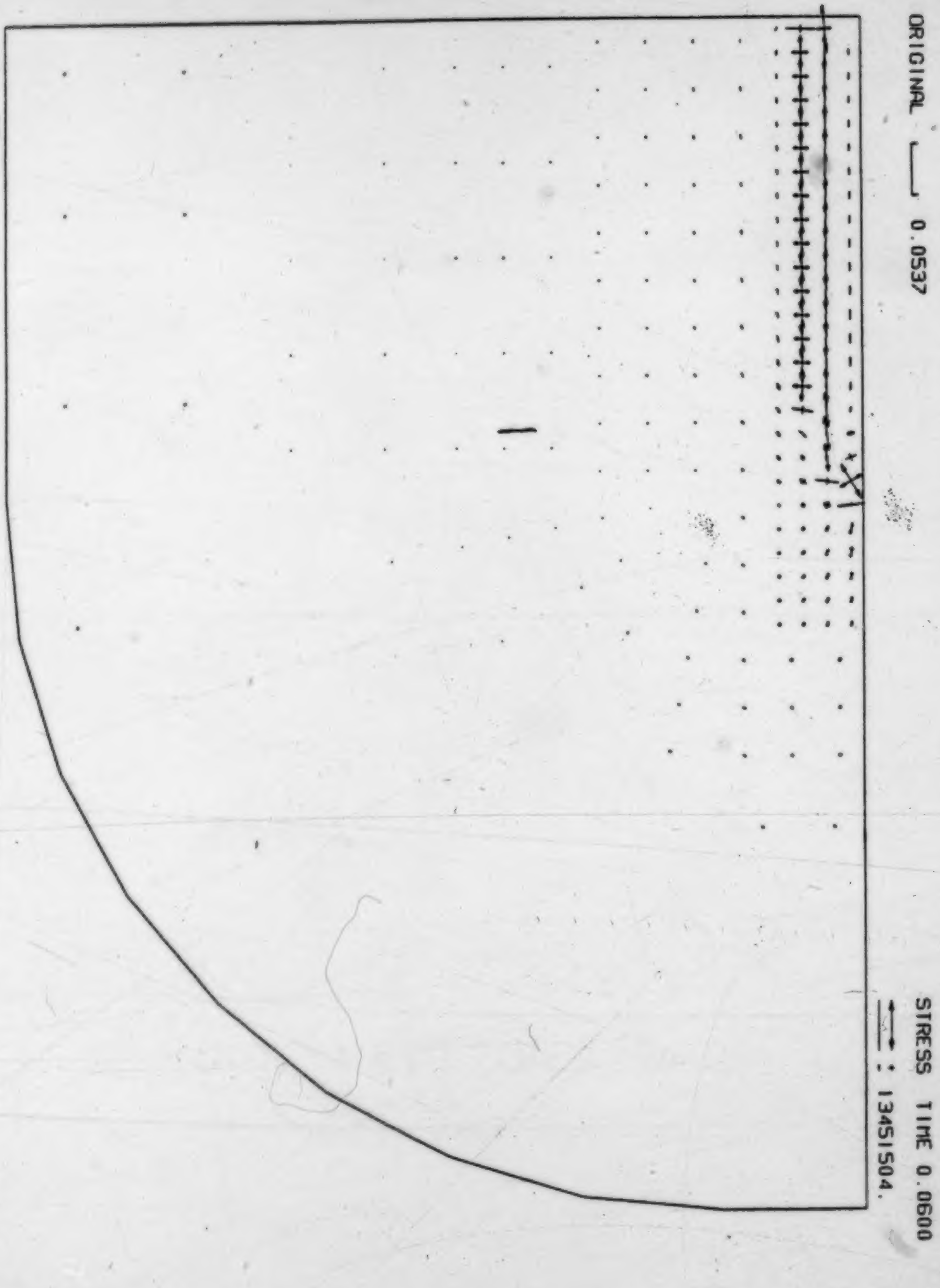

Figure 55

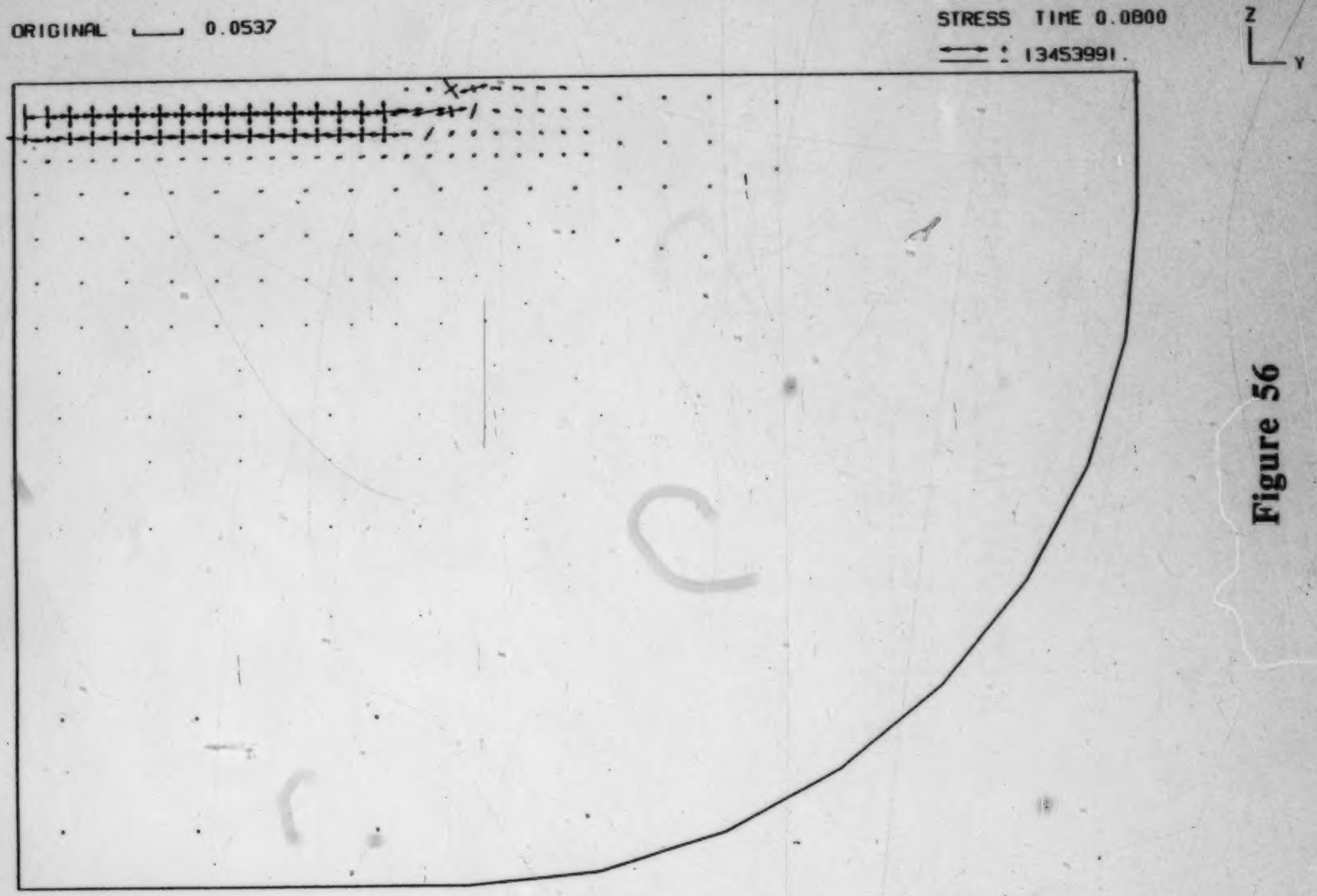

Figure 56

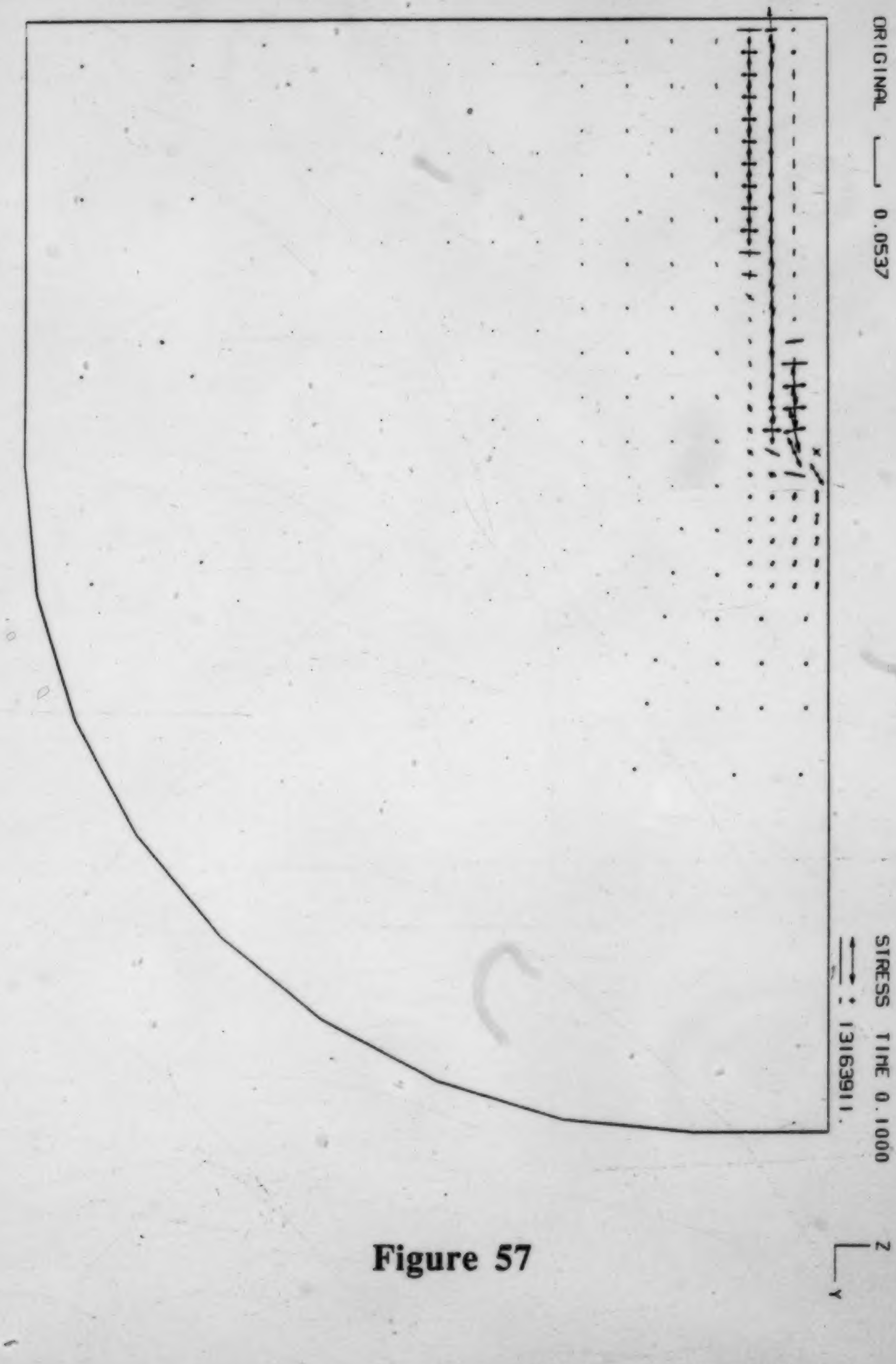

Figure 57

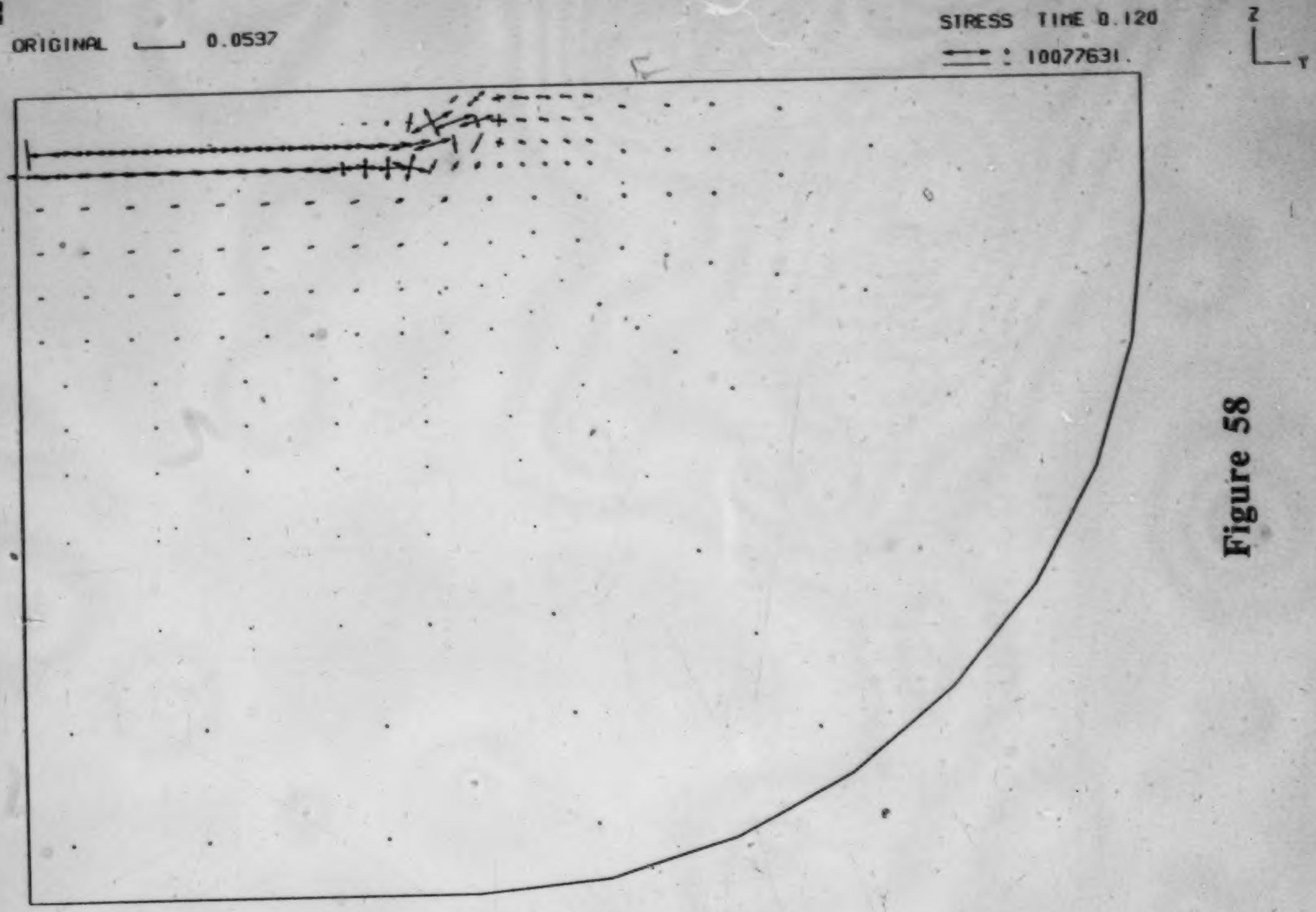

Figure 58

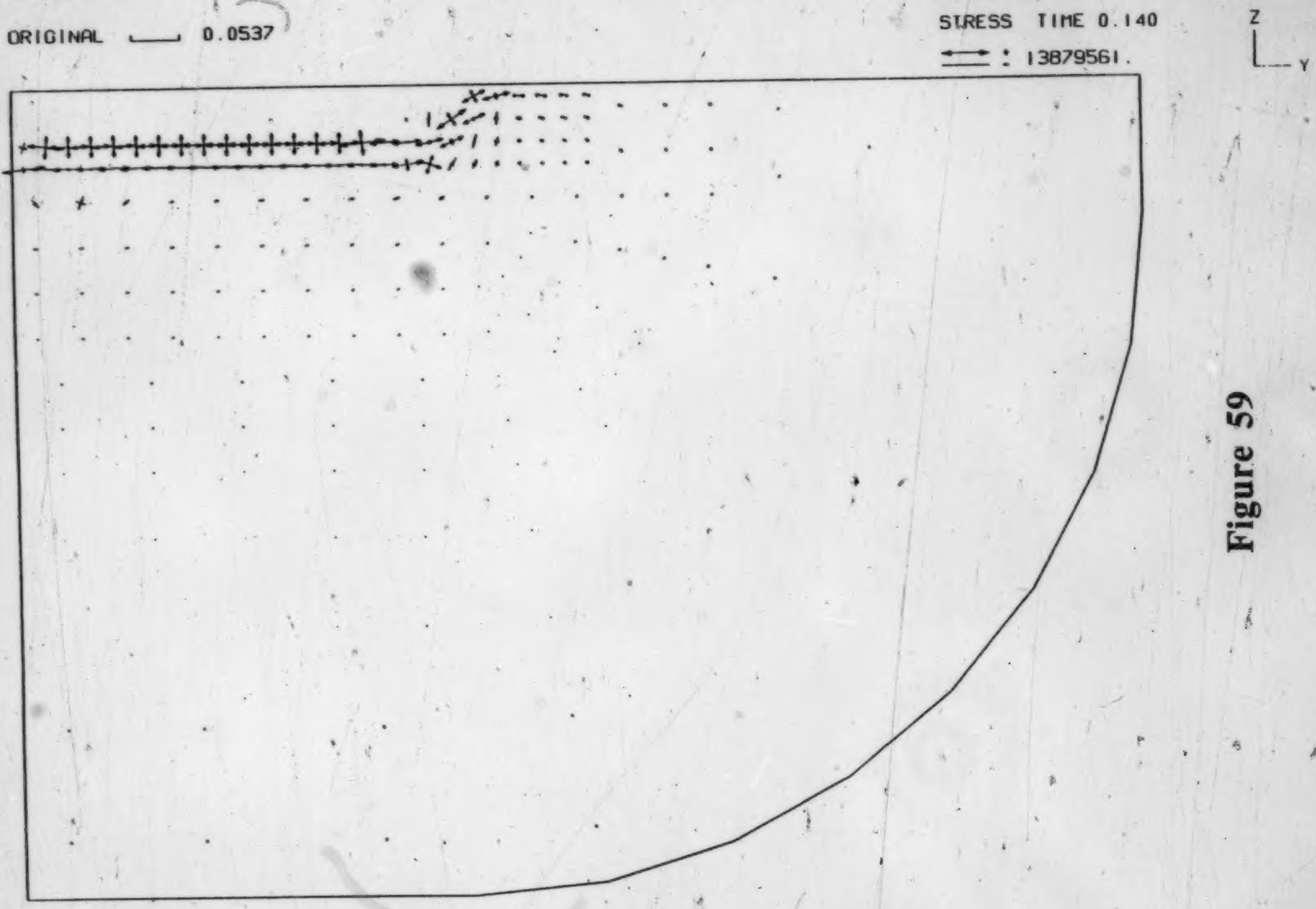

Figure 59

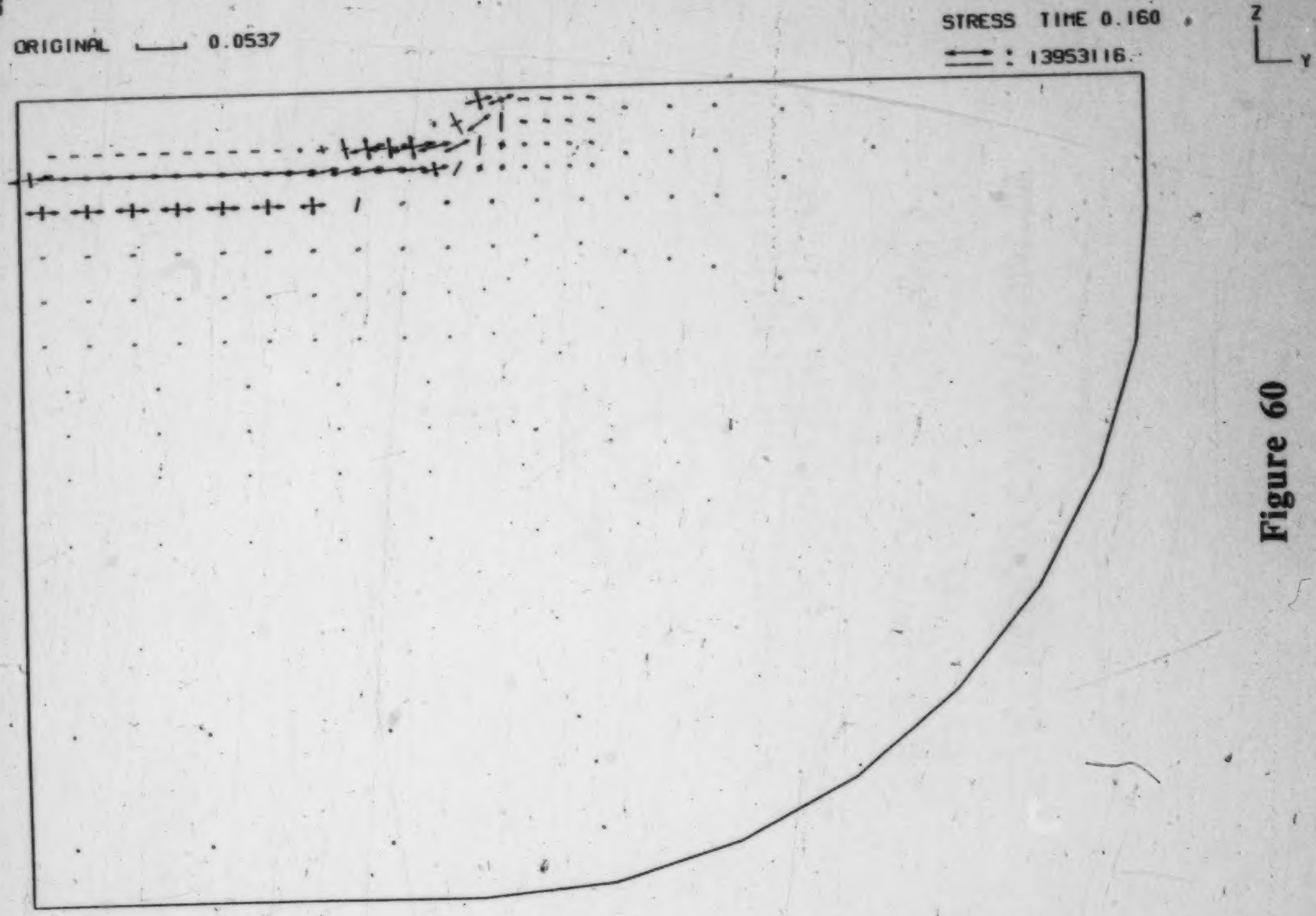

Figure 60

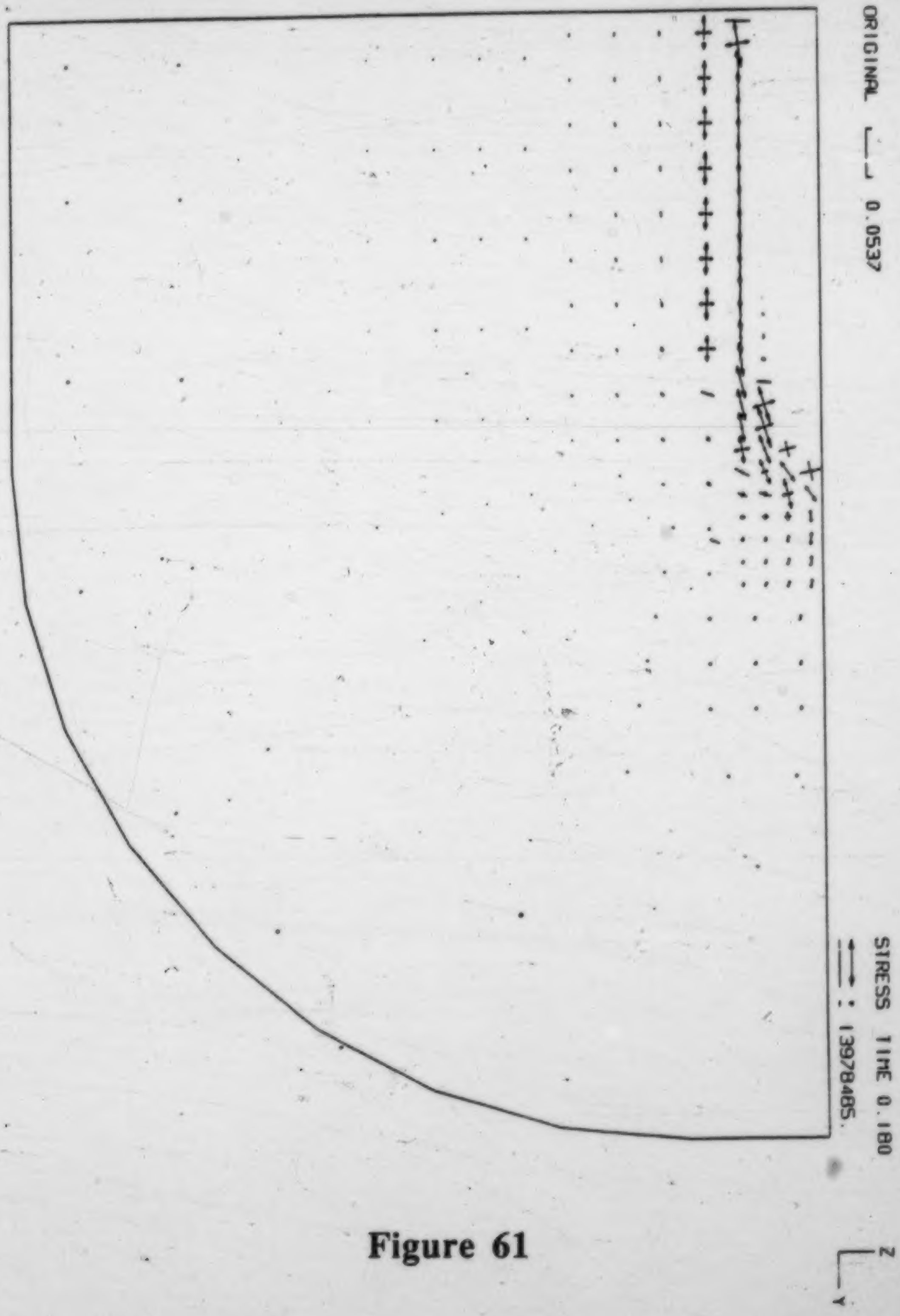

Figure 61

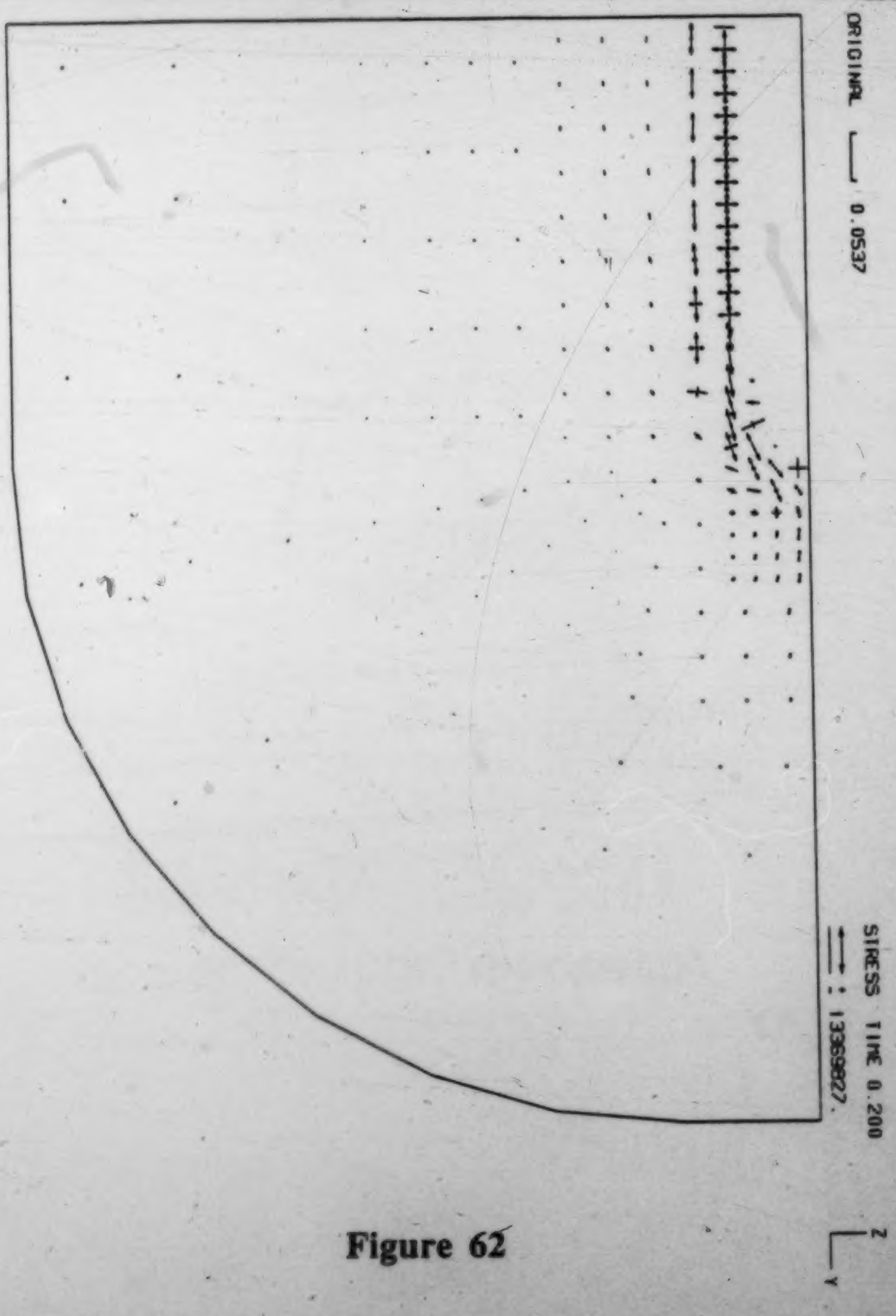

Figure 62

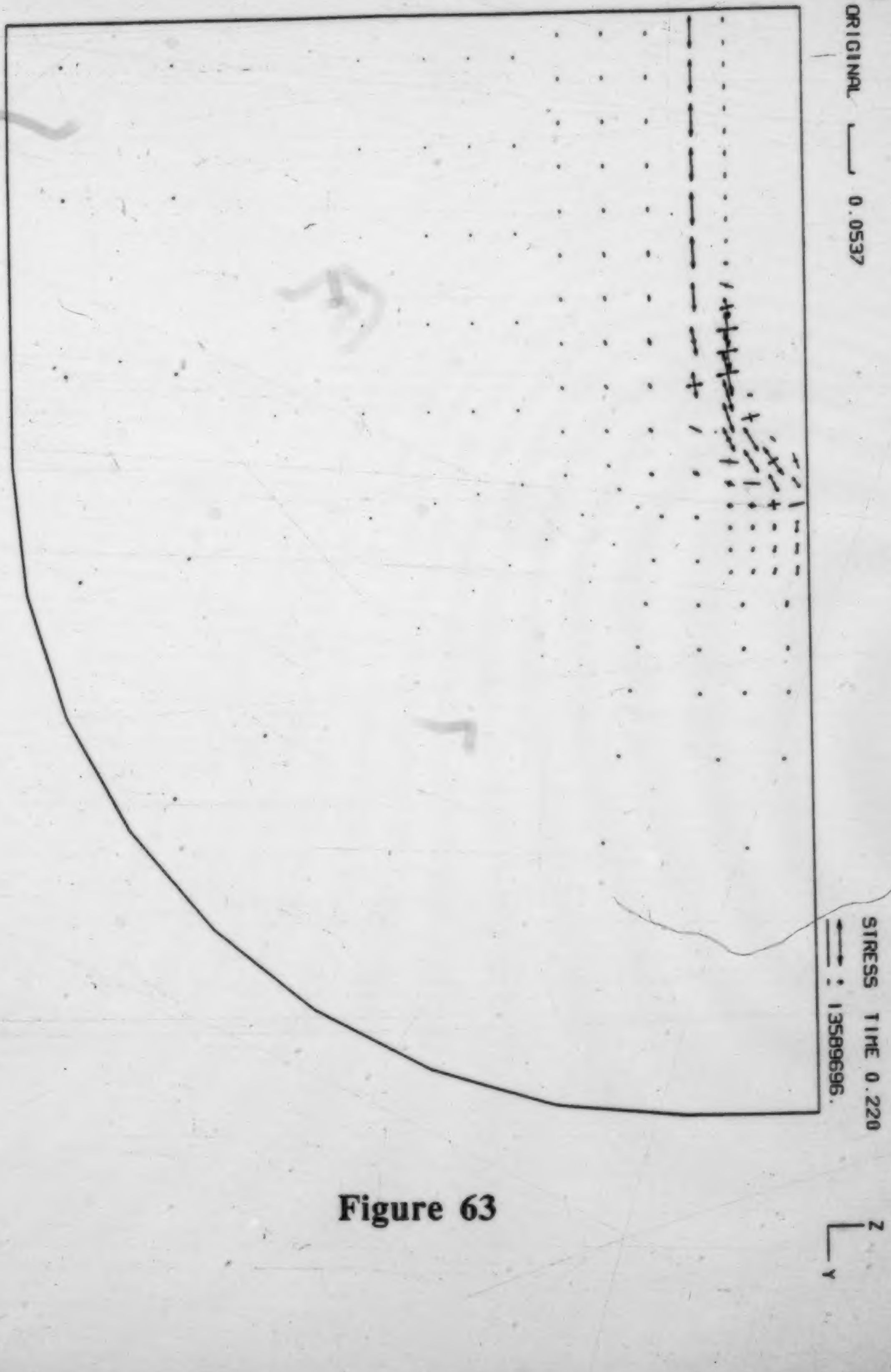
ORIGINAL
0.0537
STRESS TIME 0.220
: 13589696.
Z
Y

Figure 63

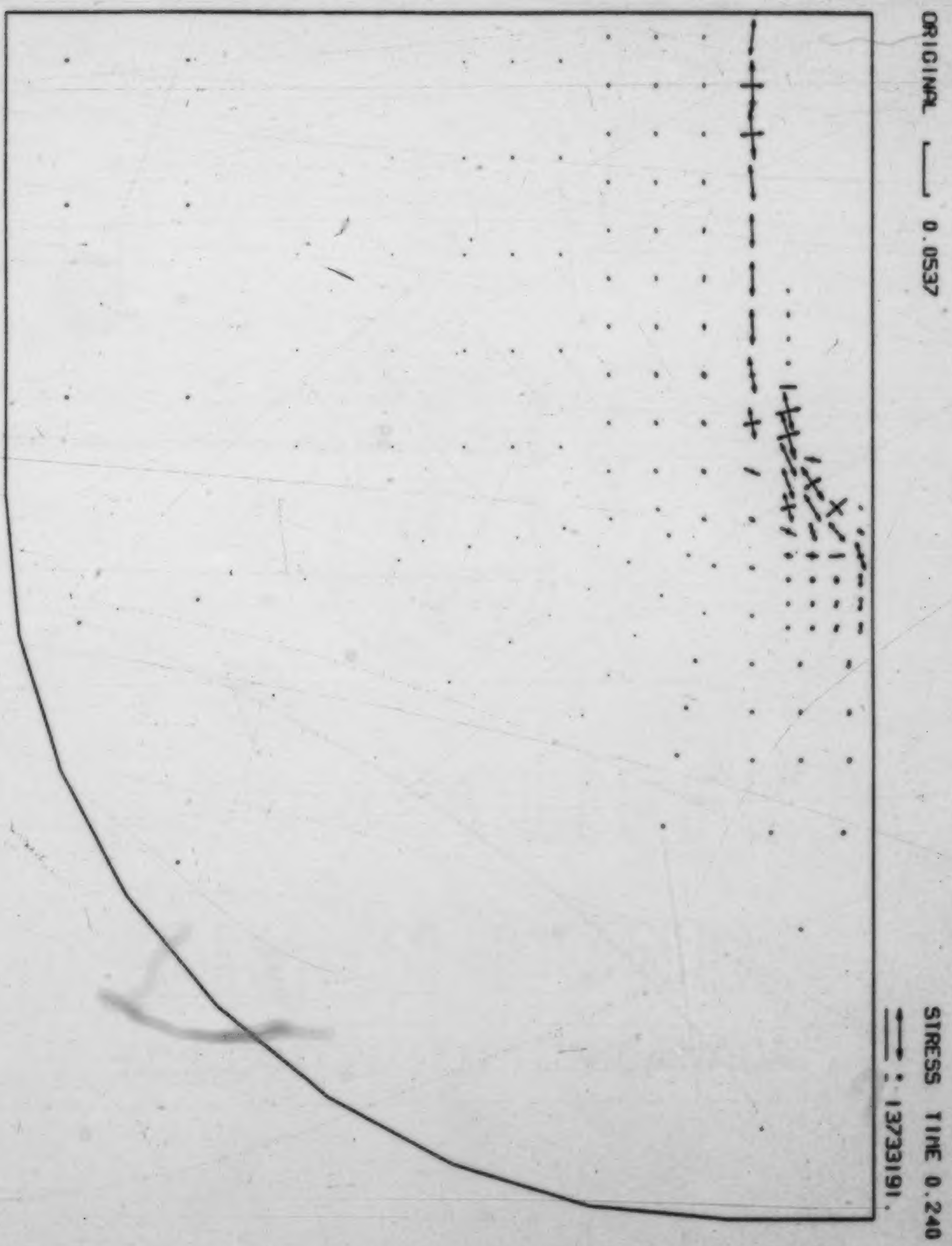

Figure 64

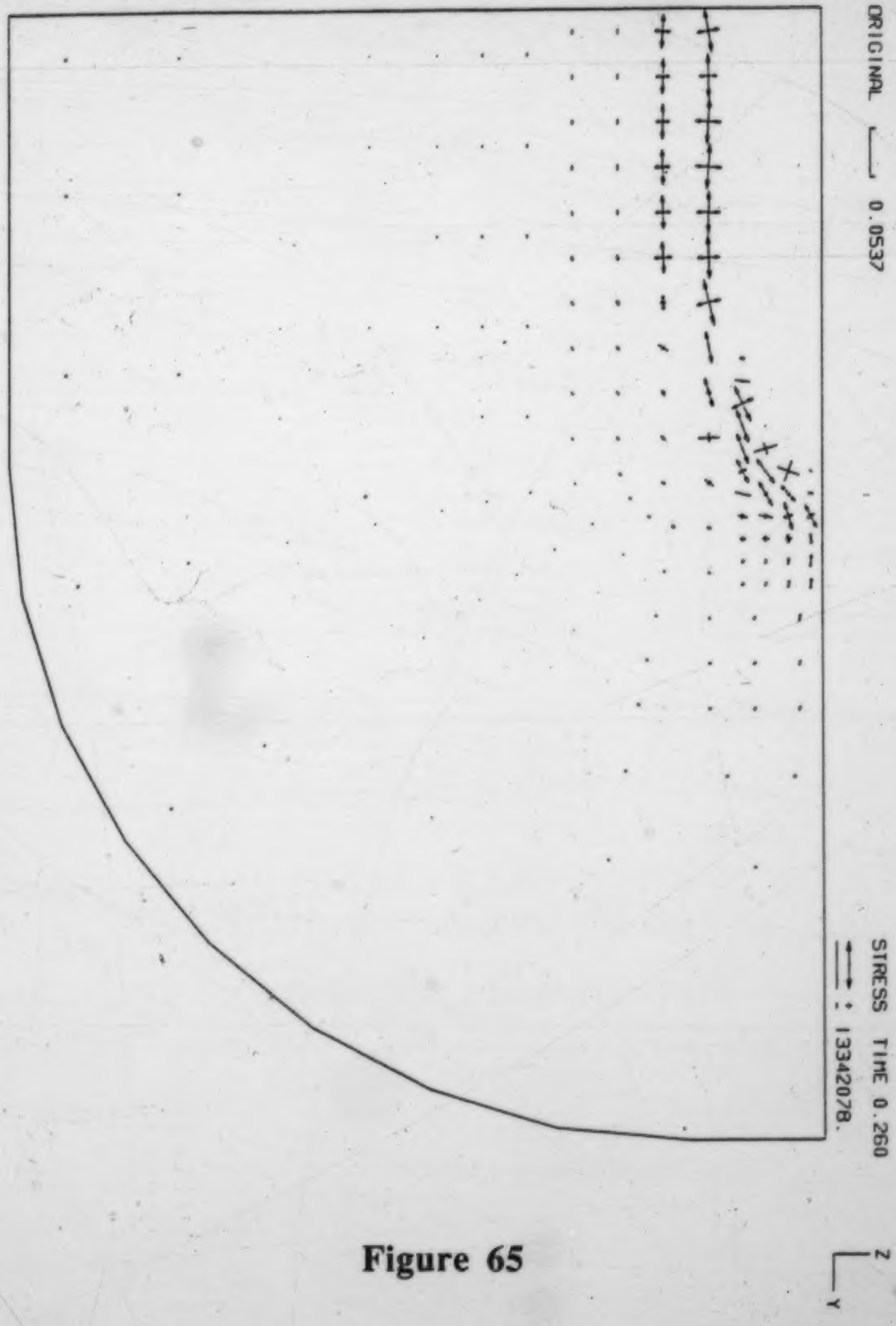
ORIGINAL
0.0537
STRESS TIME 0.260
: 13342078.
Z
Y

Figure 65

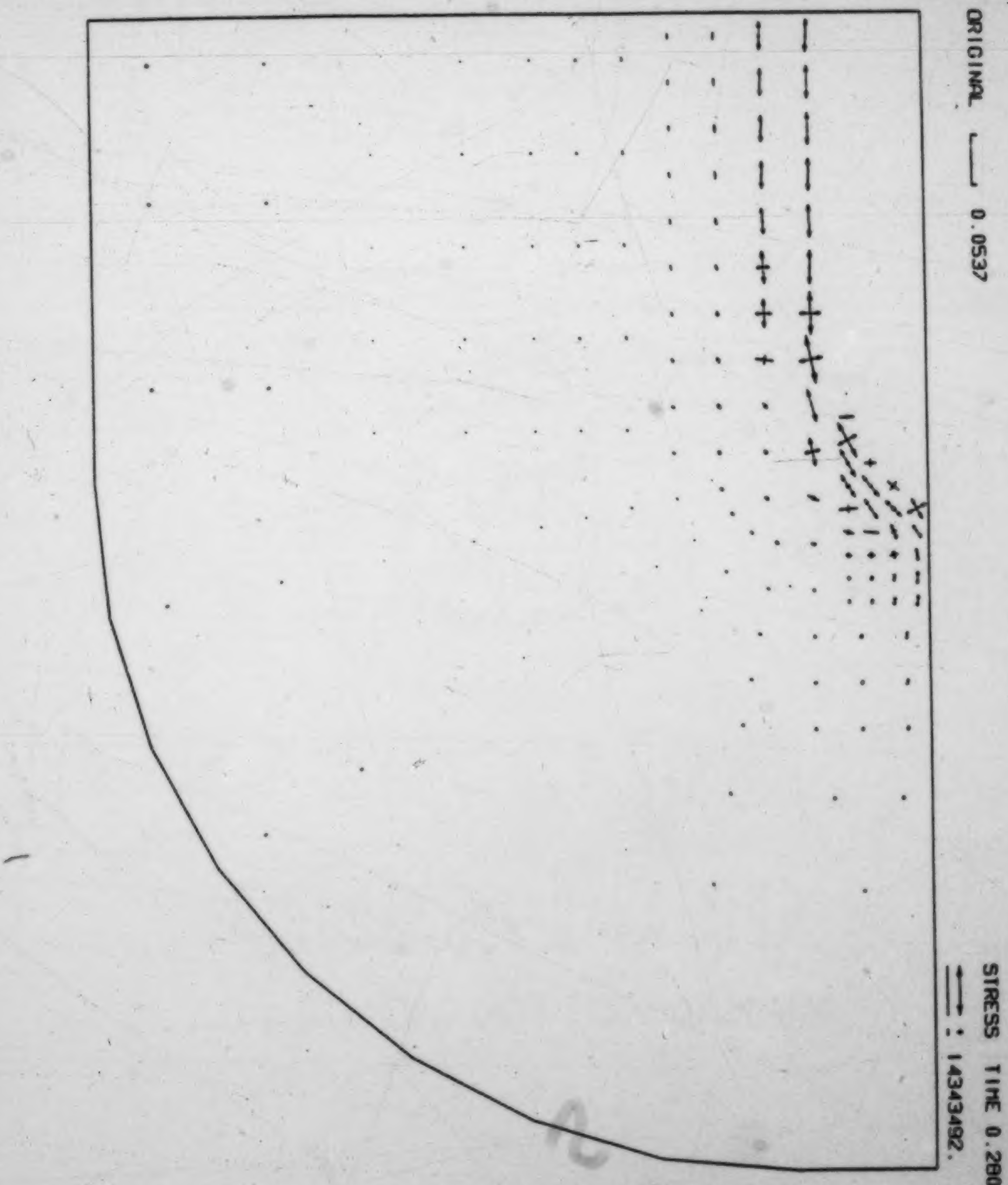

Figure 66

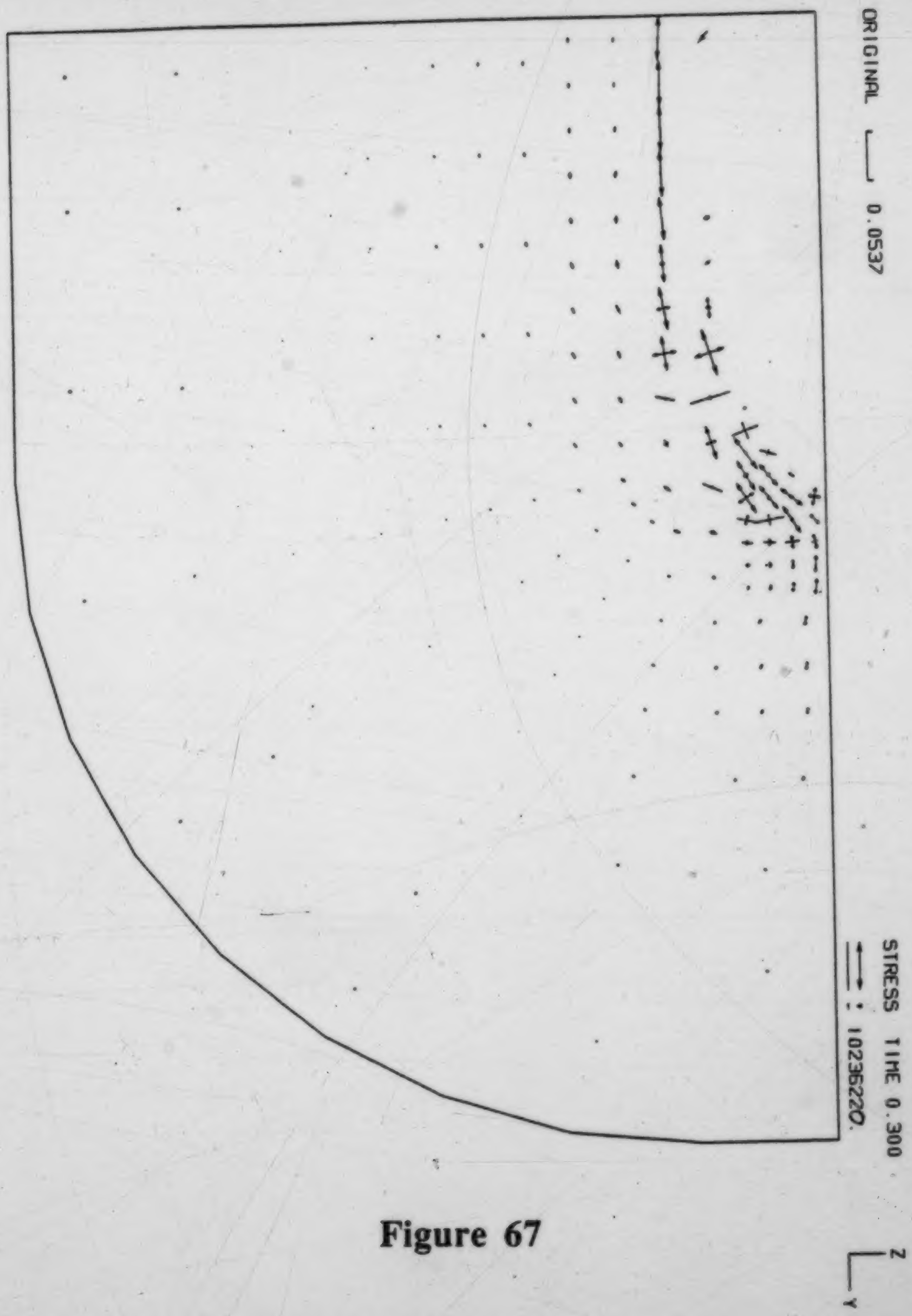

Figure 67

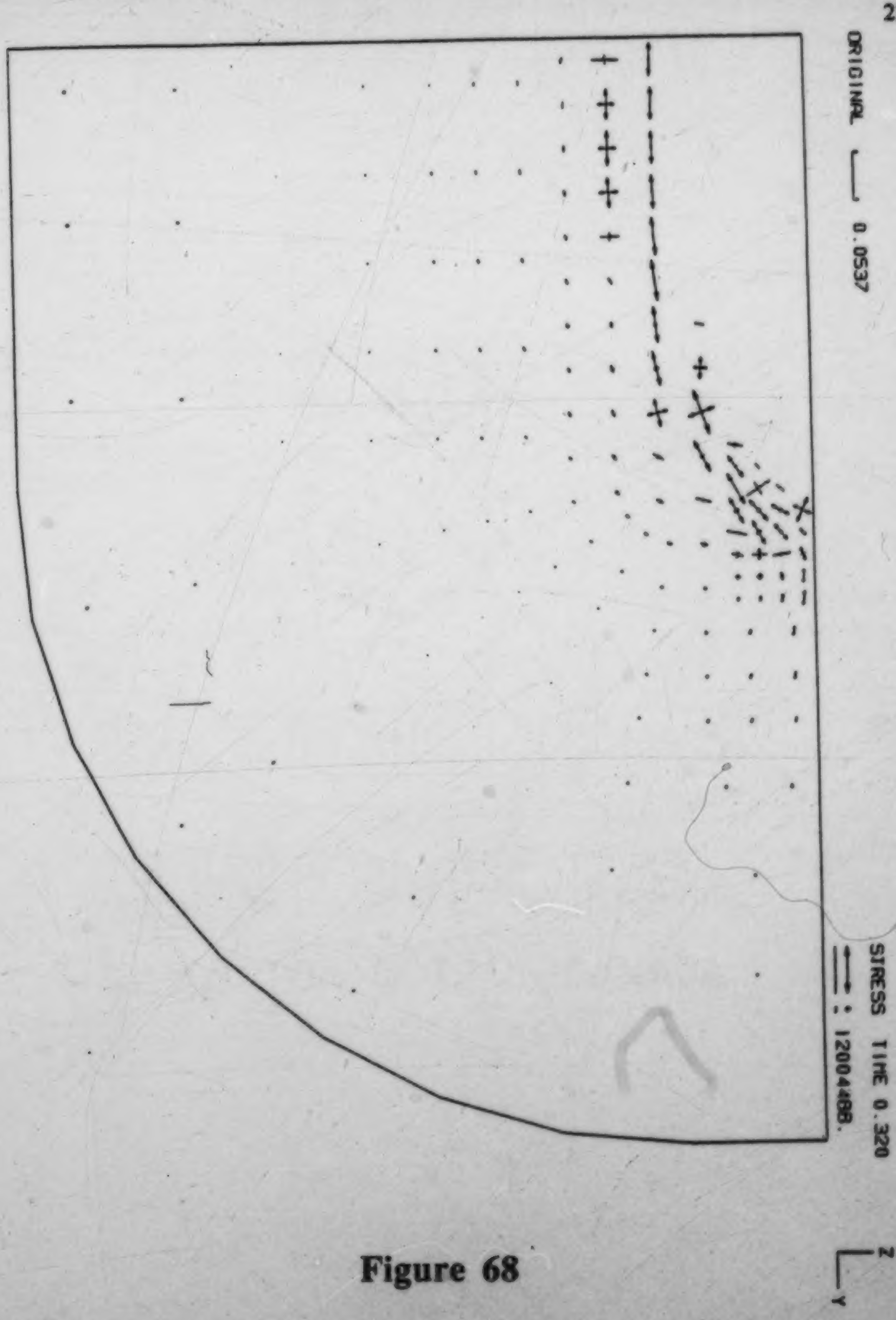
ORIGINAL
0.0537
STRESS TIME 0.320
: 12004488.
Z
Y

Figure 68

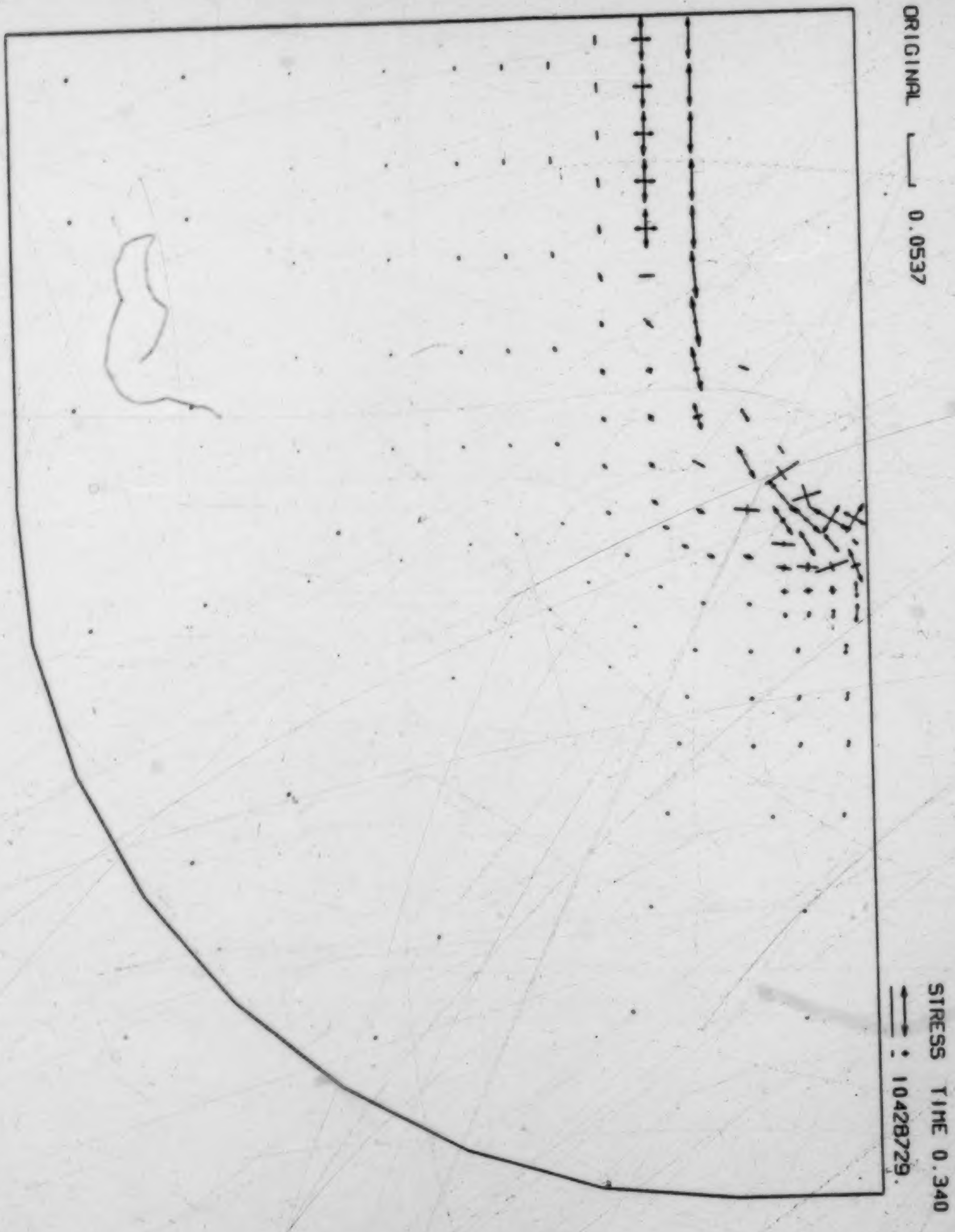

Figure 69

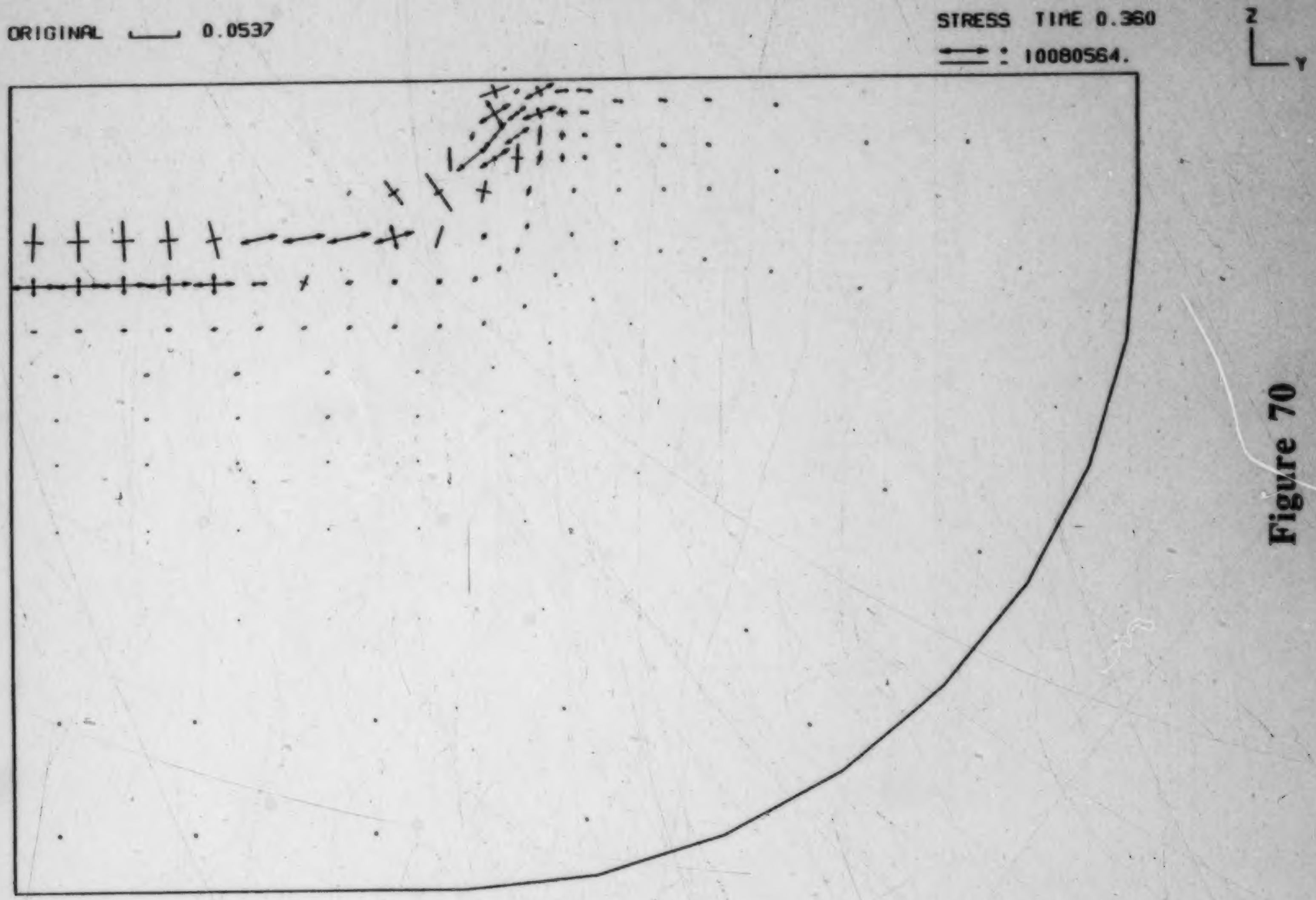
ORIGINAL
0.0537
STRESS TIME 0.360
: 10080564.
Z
Y

Figure 70

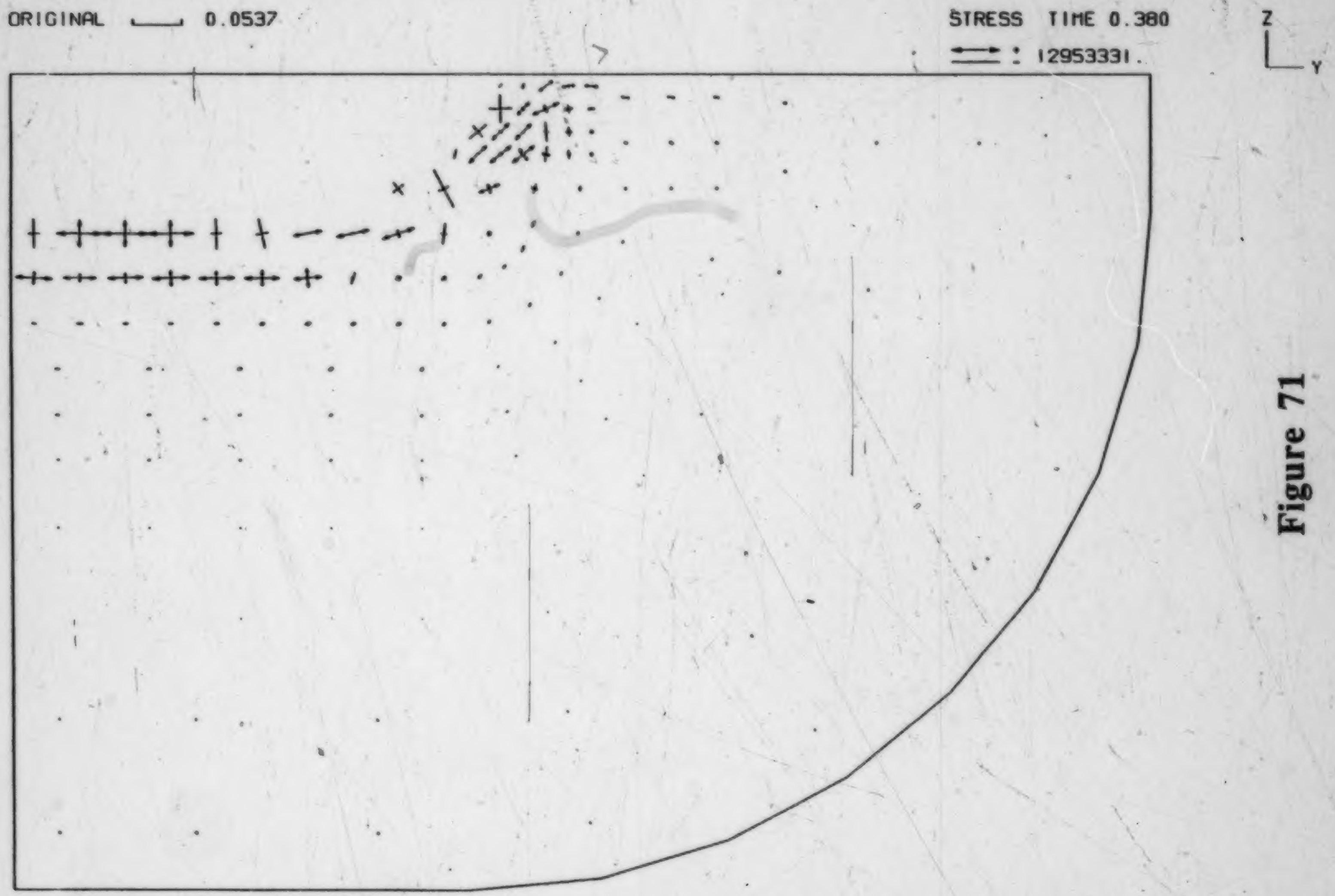

Figure 71

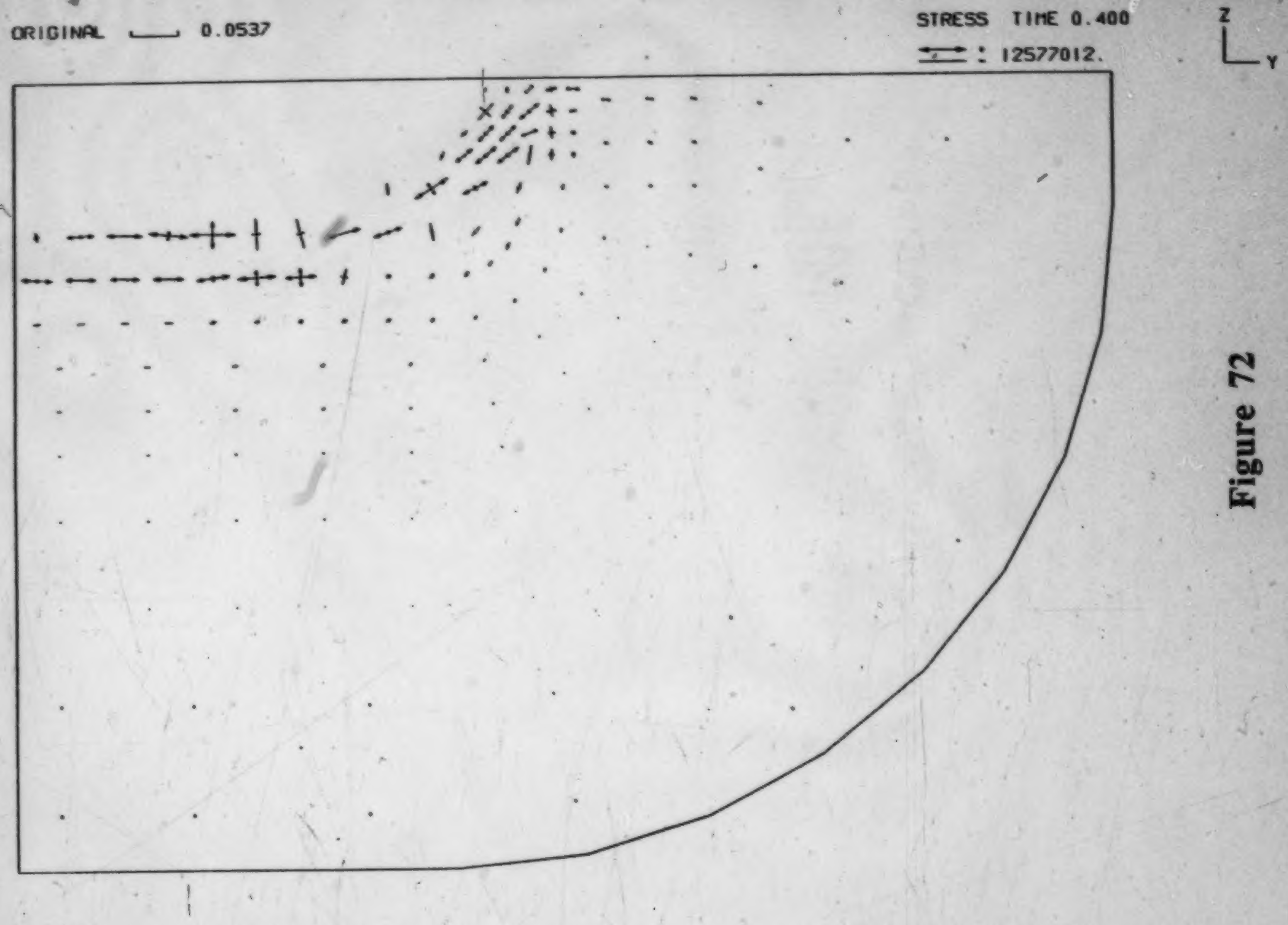

Figure 72

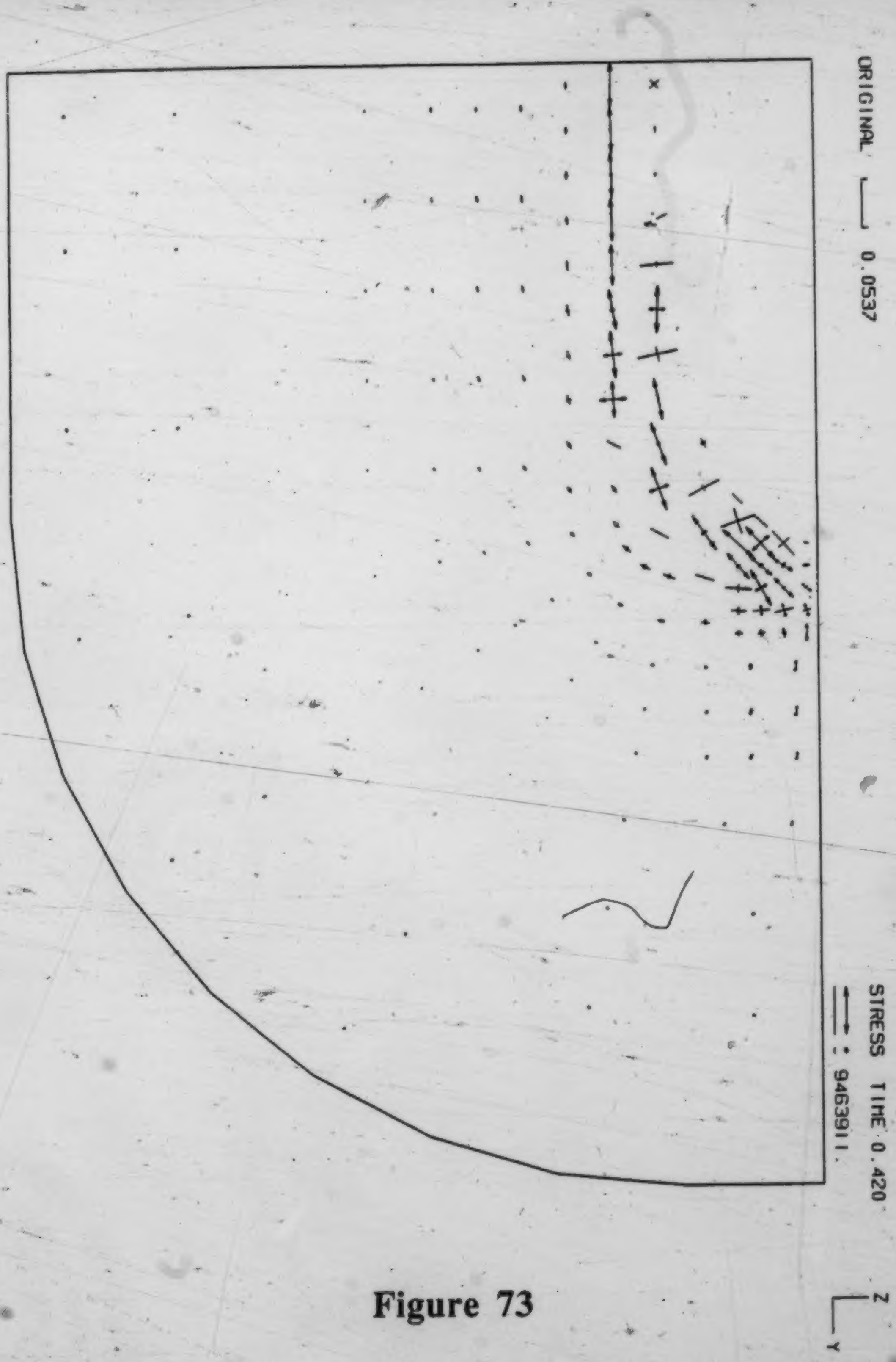

Figure 73

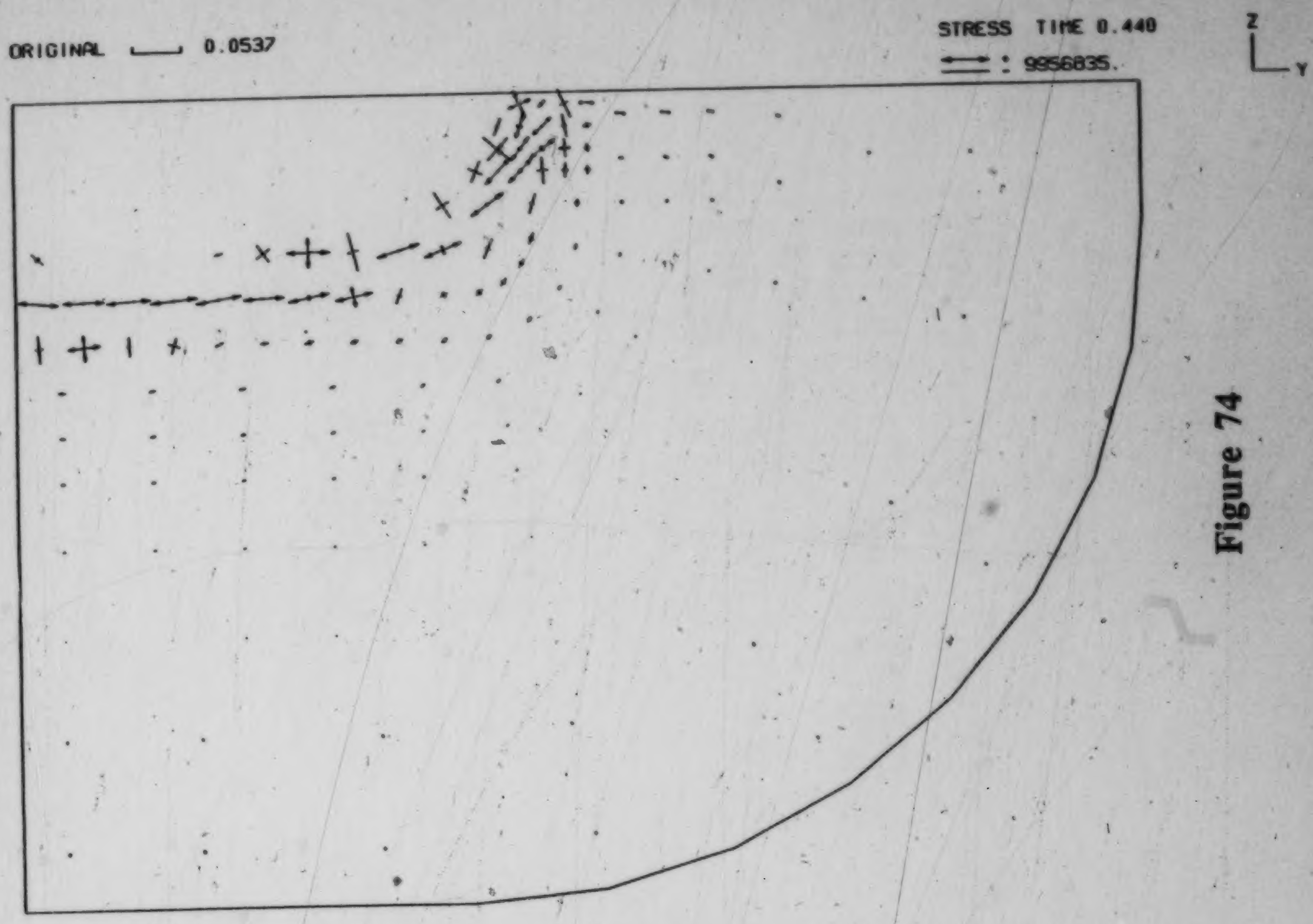

Figure 74

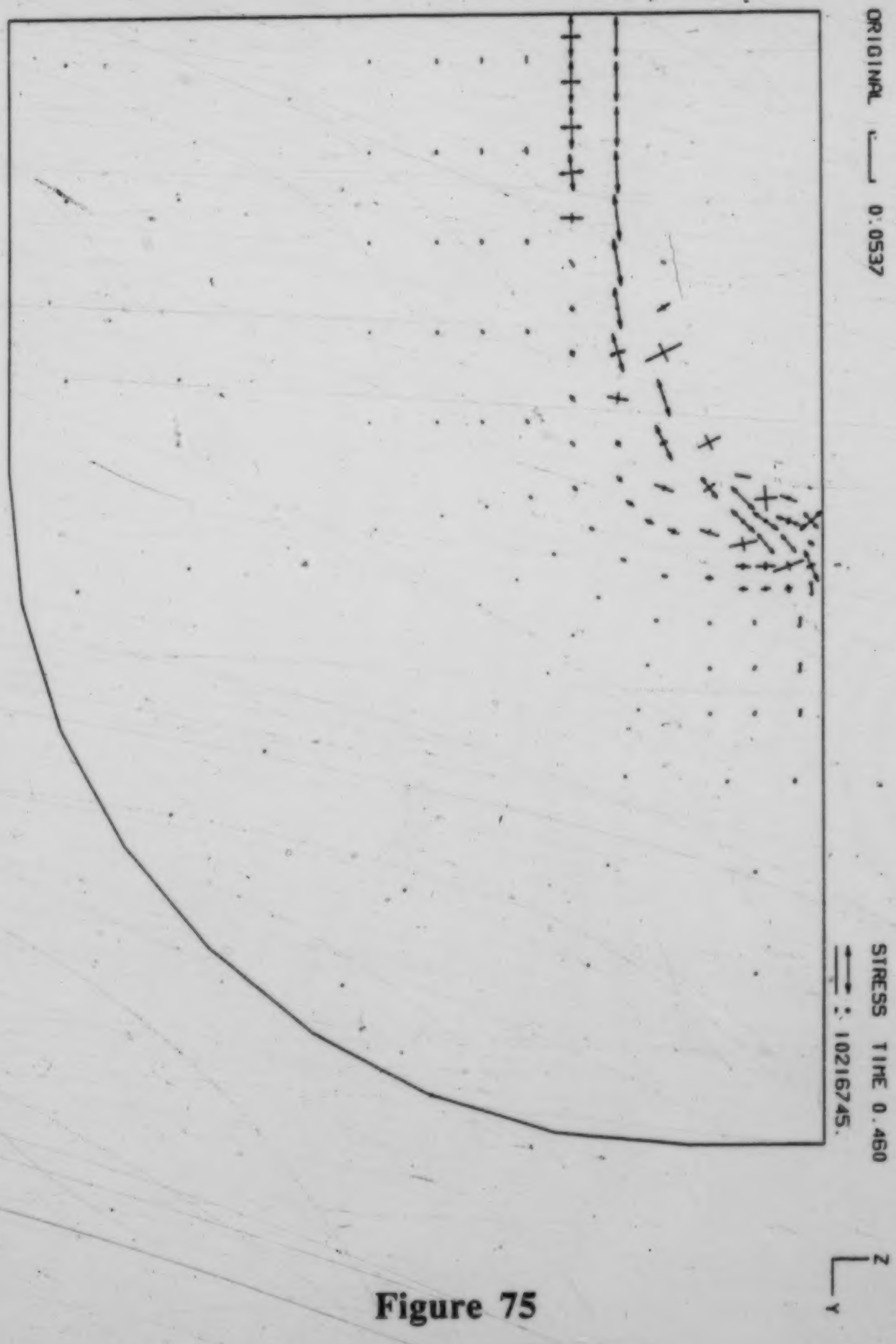

Figure 75

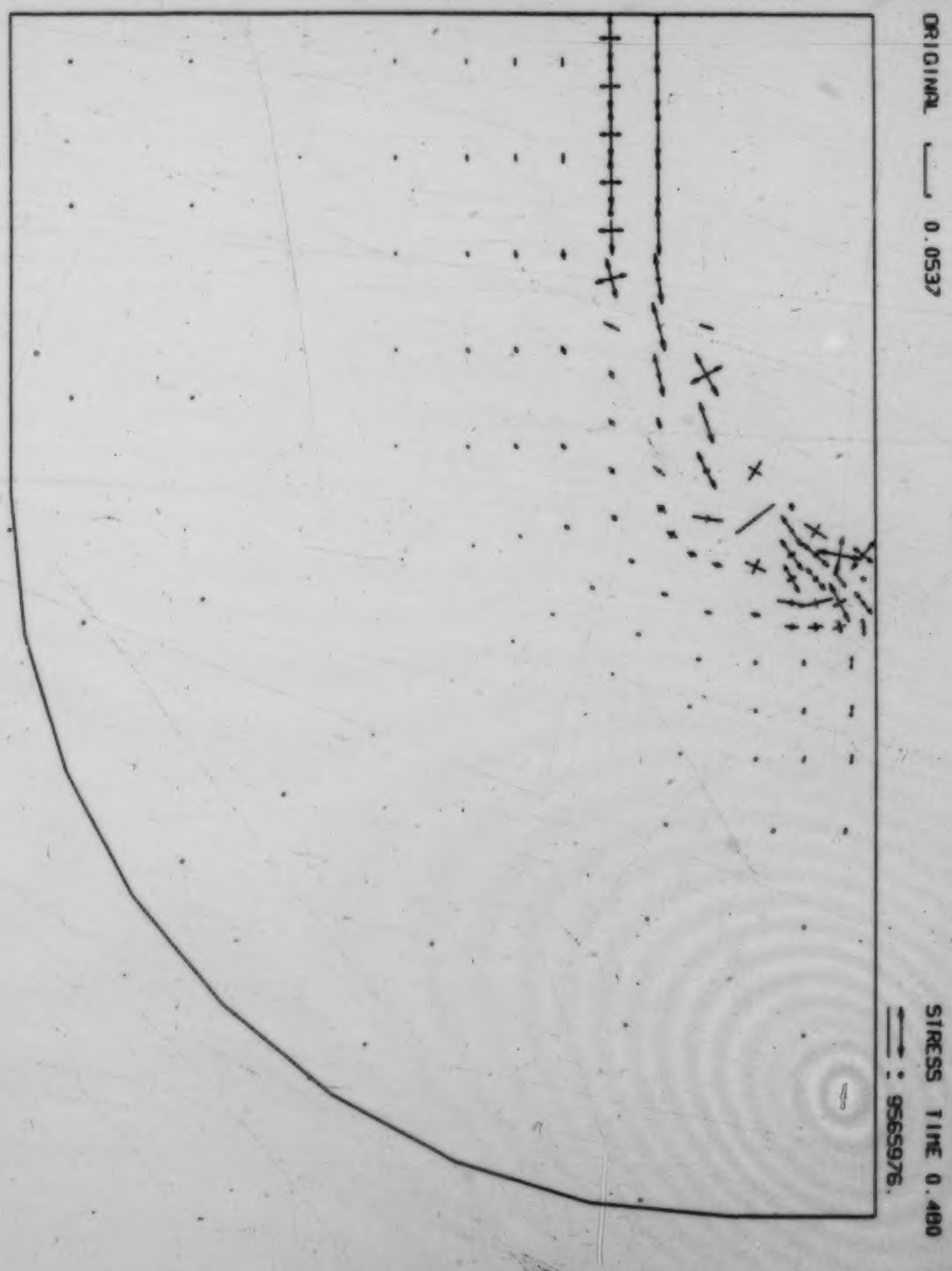

Figure 76

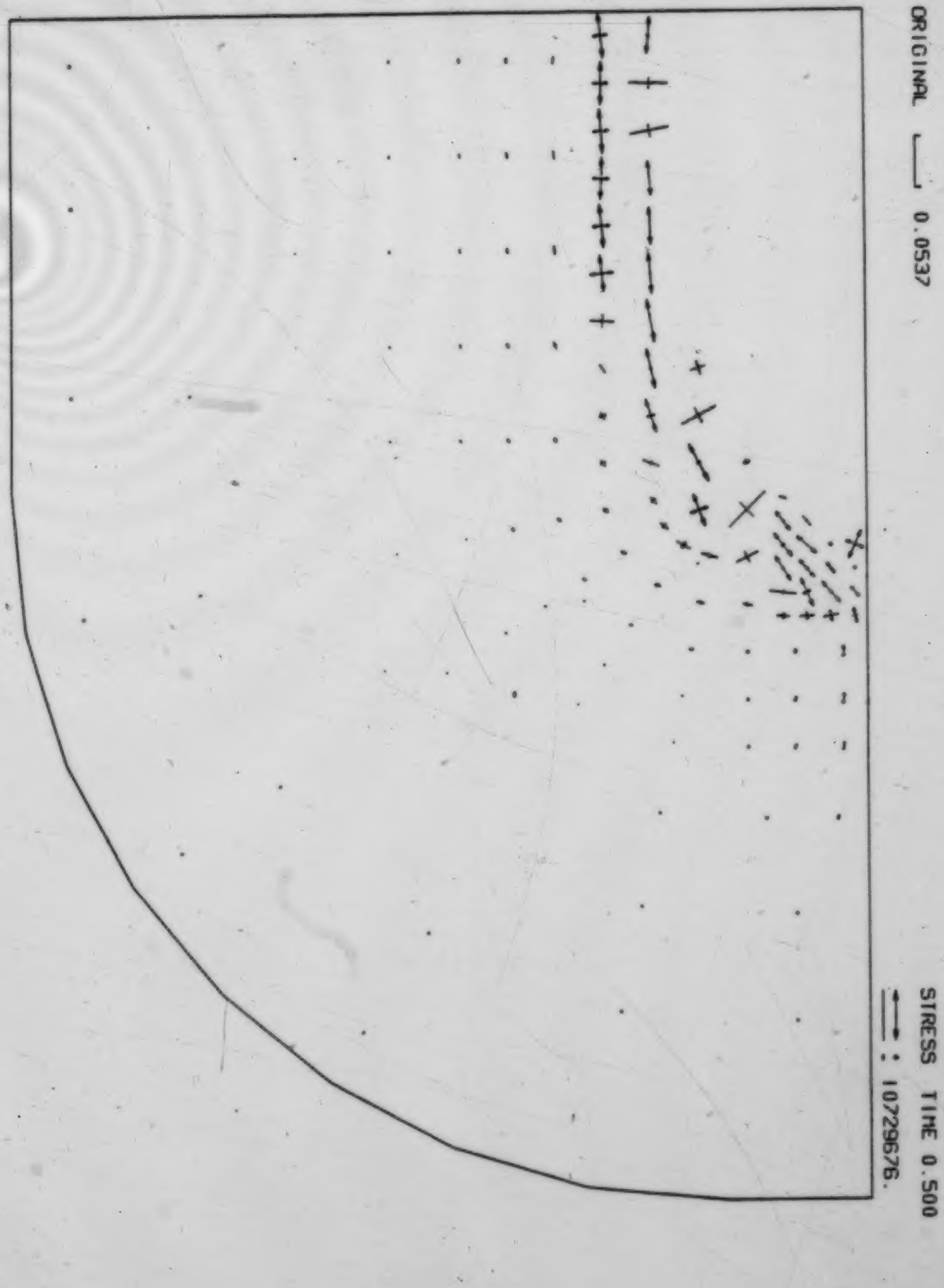

Figure 77

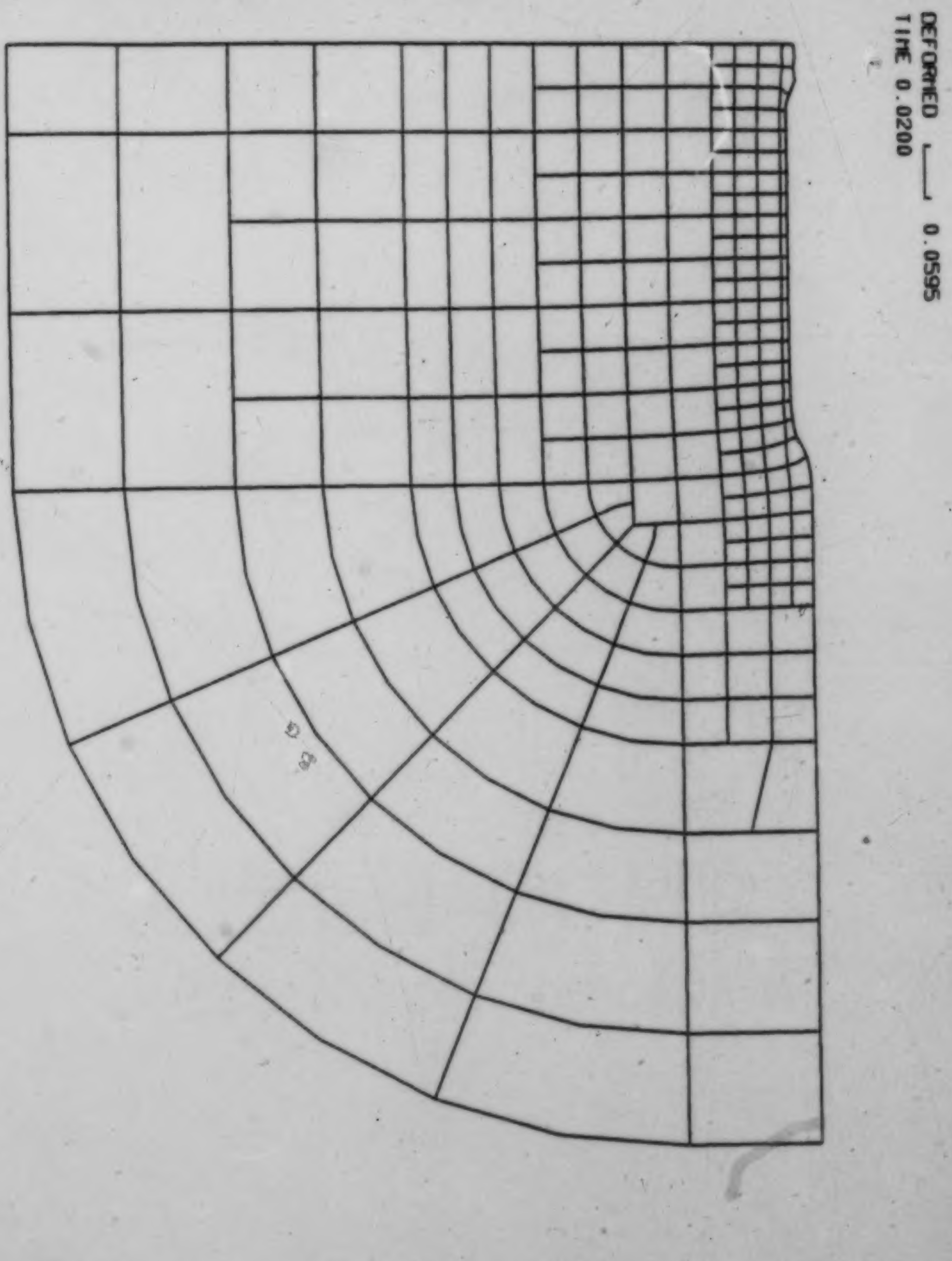
DEFORMED 0.0595
TIME 0.0200
Z
Y

Figure 78

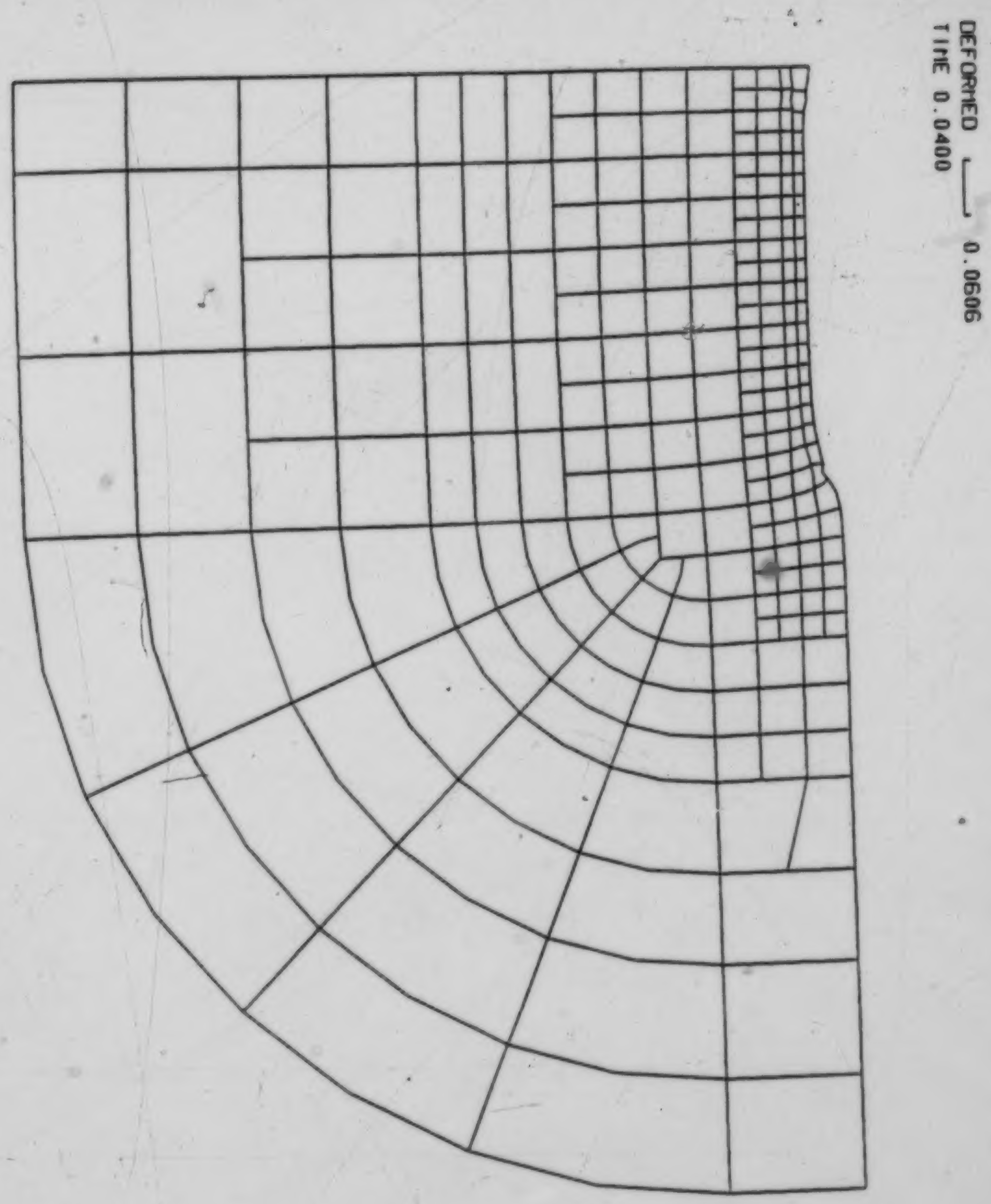
DEFORMED
0.0606
TIME 0.0400
Z
Y

Figure 79

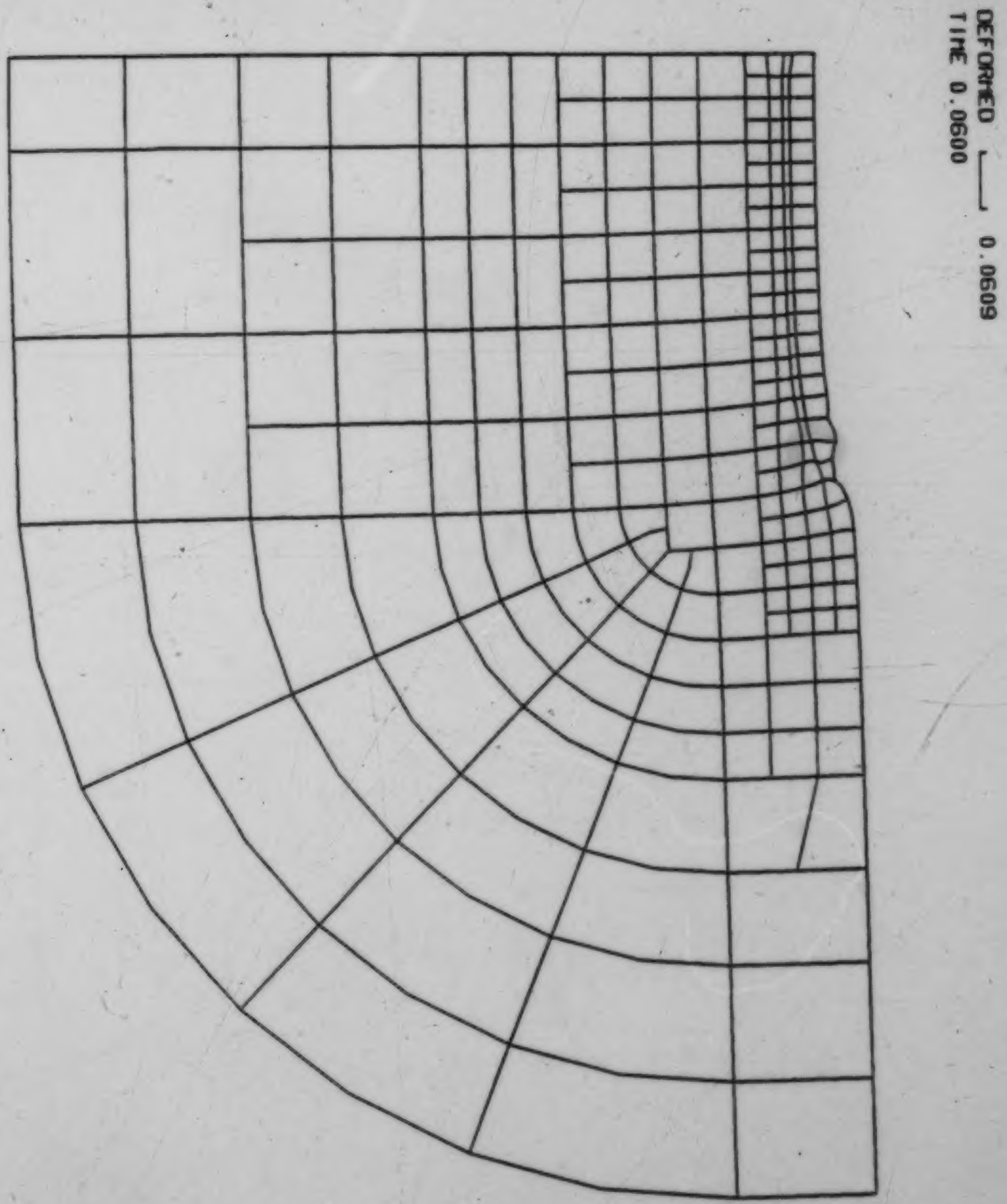
DEFORMED 0.0609
TIME 0.0600
Z
Y

Figure 80

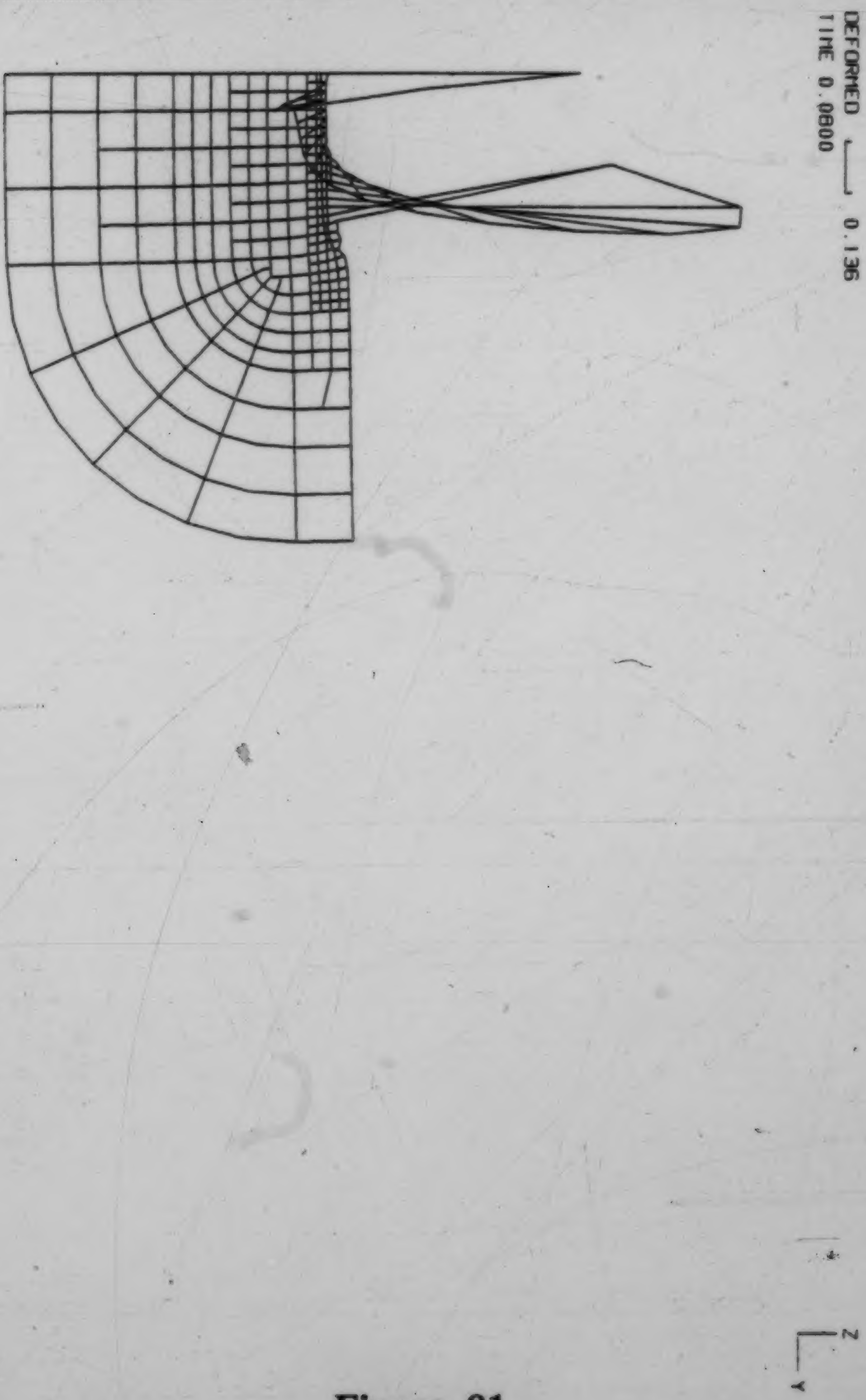
DEFORMED
0.136
TIME 0.0800
Z
Y

Figure 81

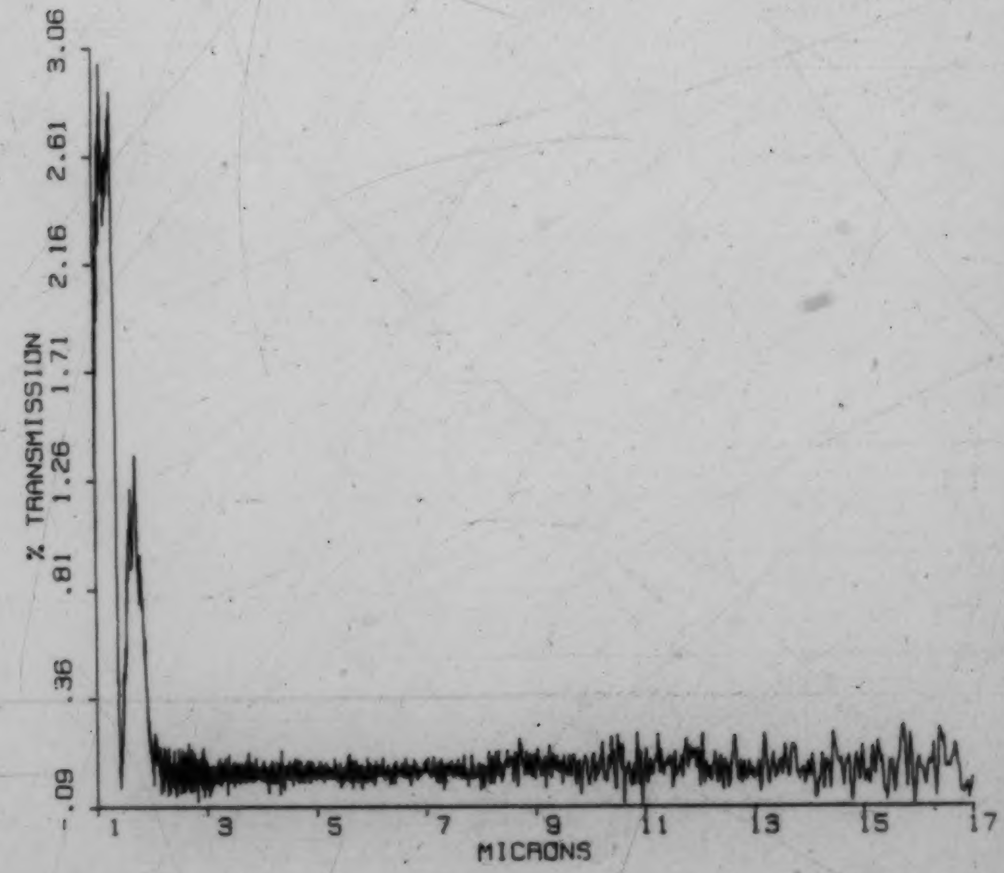

Figure 82

Transmittance Spectra from FTIR Analysis

Plates

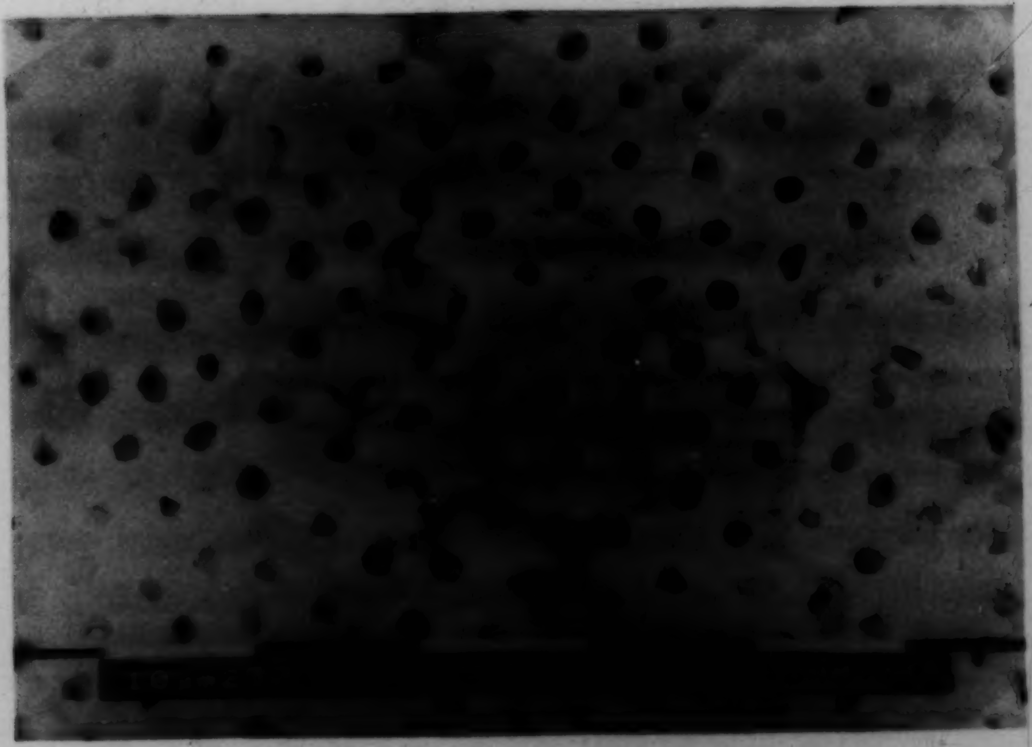

Plate 1

Scanning electron micrograph (55X) of nonsclerotic, opaque root canal wall dentin. Note that the orientation of the tubules at this surface result in roughly circular tubule openings.

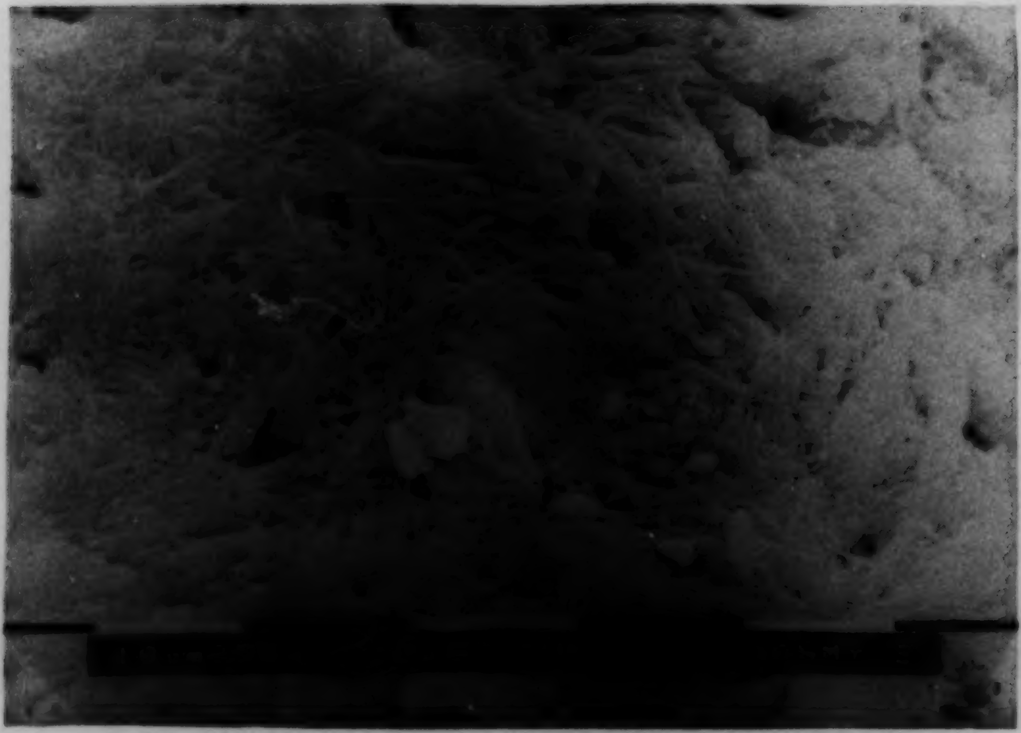

Plate 2

Scanning electron micrograph (55X) of sclerotic, translucent dentin. The tubule openings have been obliterated by sclerosis.

1mm 15.0kV 55.0E1

Plate 3

Scanning electron micrograph (55X) of a continuous-wave carbon dioxide laser impact site on canal-wall dentin which exhibits no effect. The power and duration used here were 5 watts and 0.1 seconds respectively, with a spot diameter of 1.0 millimeter.

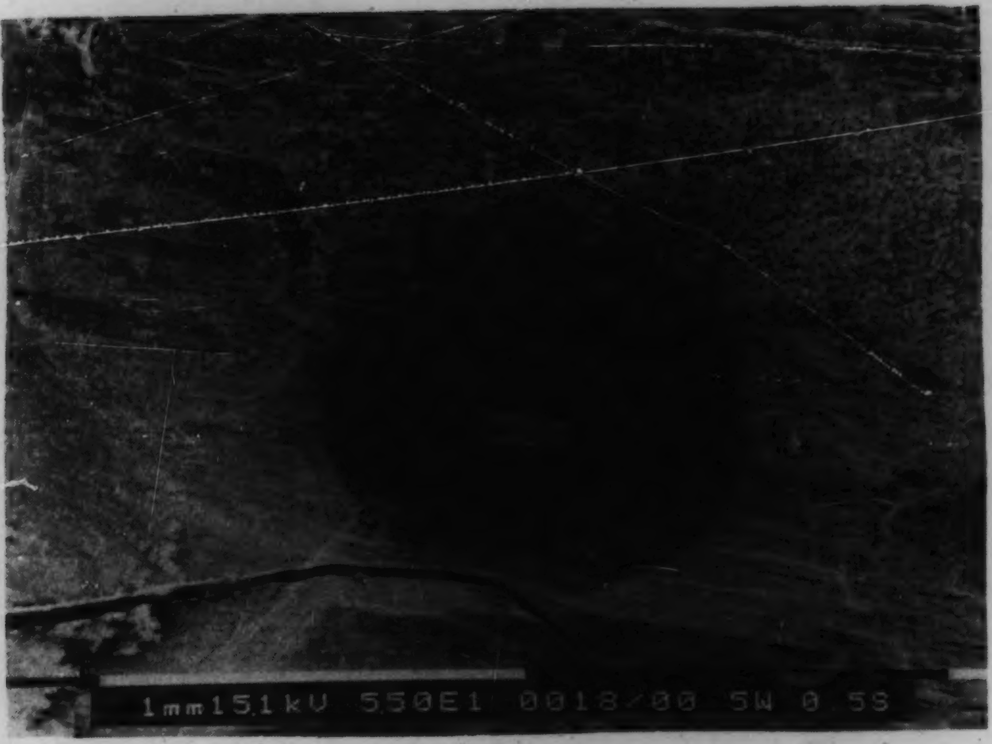

Plate 4

Scanning electron micrograph (55X) of a continuous-wave carbon dioxide laser impact site on canal-wall dentin which exhibits only hairline cracking. The power and duration used here were 5 watts and 0.5 seconds respectively, with a 1.0 spot diameter. A crack typical of that categorized as one due to desiccation is visible in the lower left of the field.

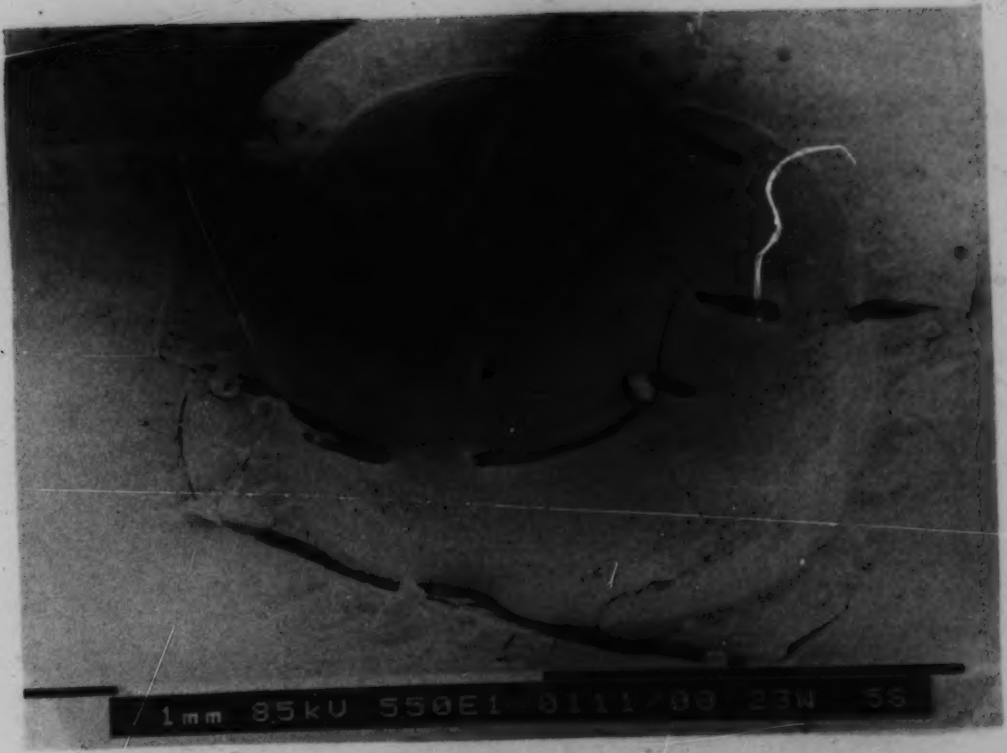

Plate 5

Scanning electron micrograph (55X) of a continuous-wave carbon dioxide laser impact site on canal-wall dentin which exhibits fused dentin as well as both wide and hairline cracking. The exposure was for 23 watts and 0.5 seconds with a spot diameter of 1.0 millimeter.

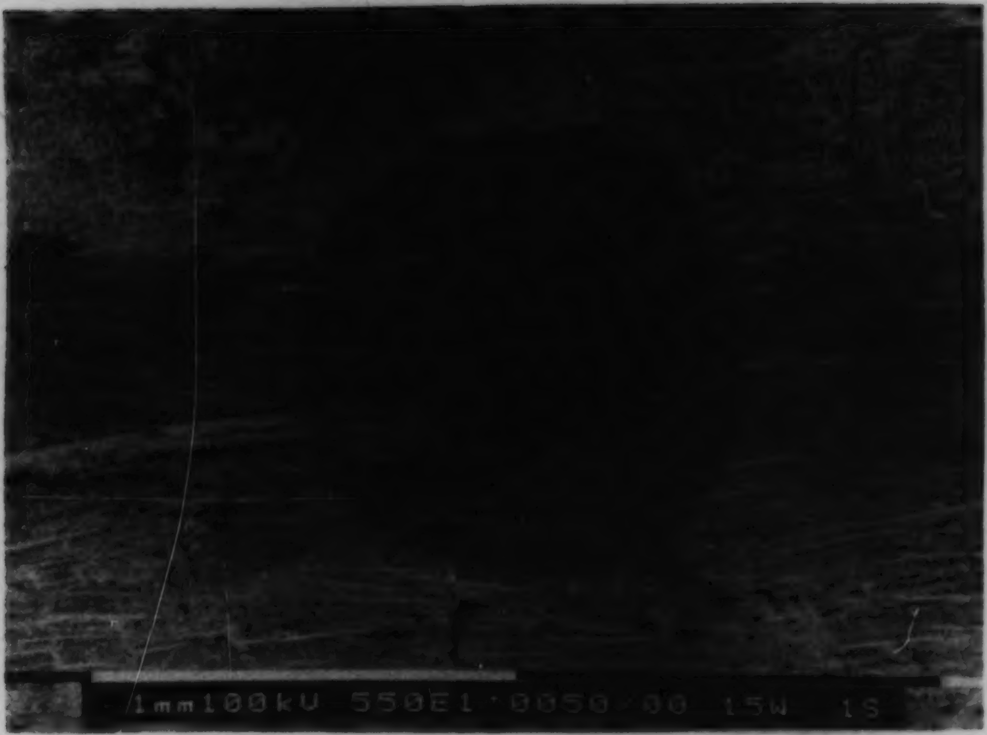
1mm100kU 550E1 0050/00 15W 1S

Plate 6

Scanning electron micrograph (55X) of a continuous-wave carbon dioxide laser impact site on canal-wall dentin which approximates the desired fracture-free surface glazing. A power of 15 watts at 0.1 seconds duration was used for this example.

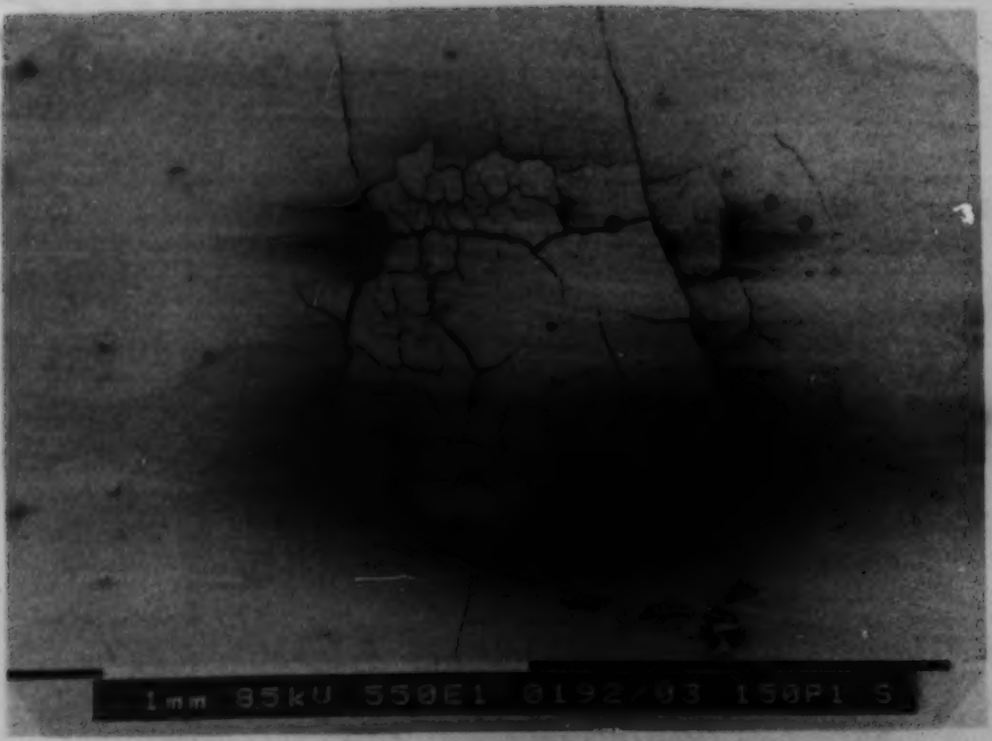
1mm 85kV 550E1 0192/03 150P1 S

Plate 7

Scanning electron micrograph (55X) of a pulsed carbon dioxide laser impact site on canal-wall dentin which exhibits hairline cracking only. The exposure for this example was 3 watts, 150 pps, for 1.0 second duration.

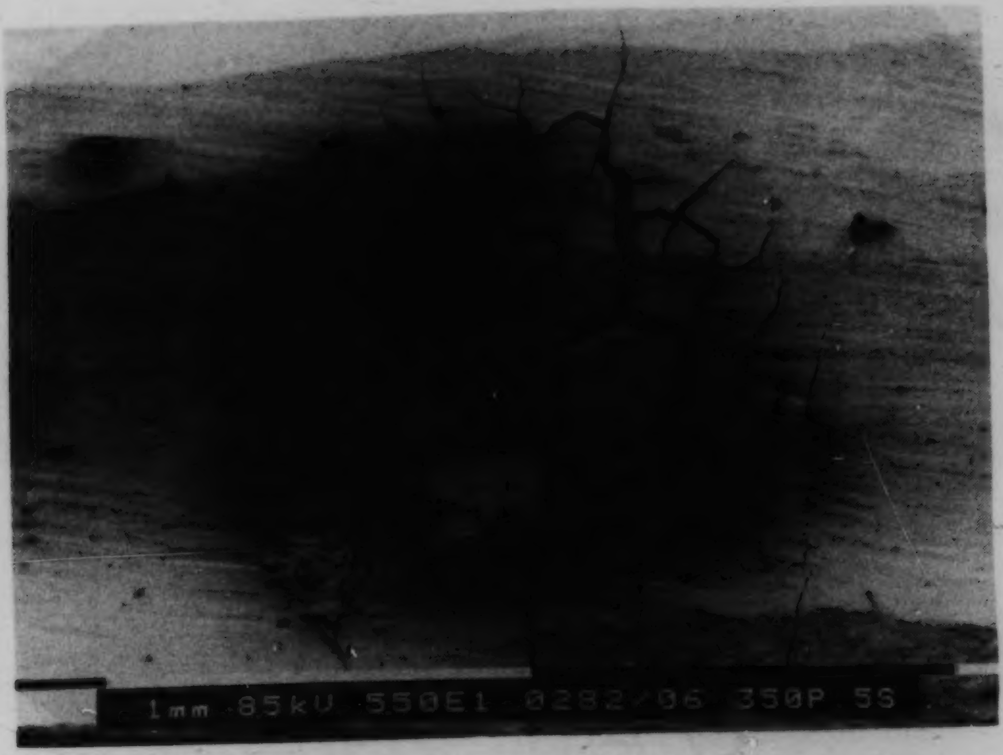
1mm 85kU 550E1 0282/06 350P 5S

Plate 8

Scanning electron micrograph (55X) of a pulsed carbon dioxide laser impact site on canal-wall dentin which exhibits both wide and hairline cracking. The exposure for this example was 6 watts, 350 pps, and 0.5 seconds duration.

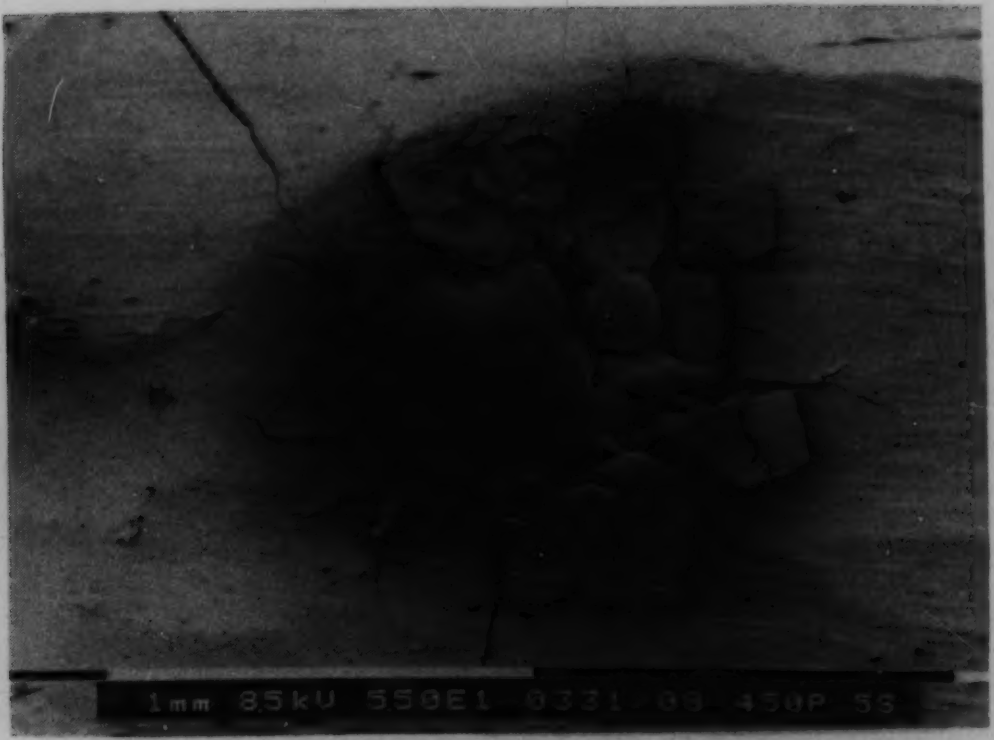
1mm 8.5kU 550E1 0331/88 450P 5S

Plate 9

Scanning electron micrograph (55X) of a pulsed carbon dioxide laser impact site on canal-wall dentin which exhibits fusion and both types of cracking. The exposure for this example was 8 watts, 450 pps, for 0.5 seconds duration.

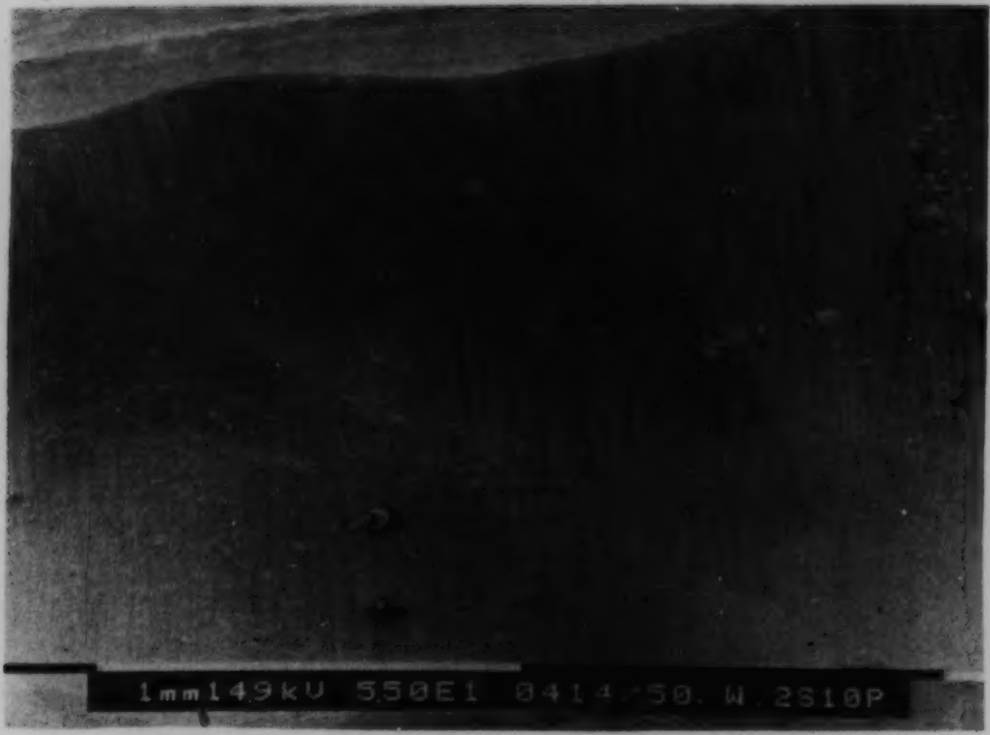
1mm14.9kV 5.50E1 0414/50. W.2S10P

Plate 10

Scanning electron micrograph (55X) of a pulsed Nd-YAG laser impact site on canal-wall dentin demonstrating no effect. The exposure for this example was 50 watts, 10 pps, for 0.2 seconds duration.

1mm150kV 550E1 0371/20 W1 S10P

Plate 11

Scanning electron micrograph (55X) of a pulsed Nd-YAG laser impact site on canal-wall dentin demonstrating crater production with minimal fusion. The exposure for this example was 20 watts, 10 pps, for a duration of 1.0 second.

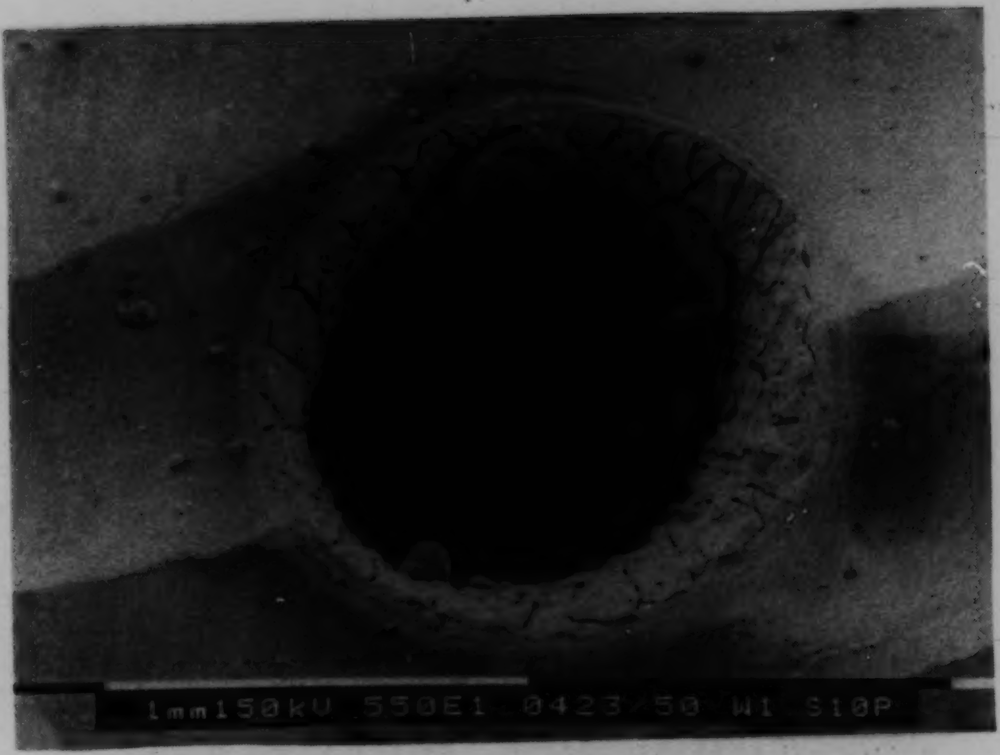
1mm150kV 550E1 0423/50 W1 S10P

Plate 12

Scanning electron micrograph (55X) of a pulsed Nd-YAG laser impact site on canal-wall dentin demonstrating root perforation. The exposure for this example was 50 watts, 10 pps, for 1.0 second duration.

References

1. **Zaret, M.M., Breinin, G.M., Schmidt, H., Ripps, H., Siegel, I.M.:** Ocular lesion produced by an optical maser (laser), ***Science***, 134:1525-1526, November 10, 1961.

2. **Campbell, C.J., Rittler, M.C., Koester, C.J.:** The optical maser as a retinal coagulator: An evaluation, ***Trans. Amer. Acad. Ophthal. Otolaryng.***, 67:58-67, 1963.

3. **Kapany, N.S., Peppers, N.A., Zweng, H.C., Flocks, M.:** Retinal photocoagulation by lasers, ***Nature*** (London), 199:146-149, July 13, 1963.

4. **Fruhmorgen, P., Boden, F., Reidenbach, H.D., Kaduk, B., Demling, L.:** Endoscopic laser coagulation of bleeding gastrointestinal lesions with report of the first therapeutic application in man, ***Gastrointest. Endosc.*** 23:73-75, 1976.

5. **Katon, R.:** Experimental control of gastrointestinal hemorrhage via the endoscope: A new era dawns, ***Gastroenterology*** 70(2):272-277, 1976.

6. **Silverstein, F., Auth, D., Rubin, C., Protell, R.:** High power argon laser treatment via standard endoscopes, ***Gastroenterology*** 71:558-563, 1976.

7. **Goldman, L., Siler, V.E., Blaney, D.:** Laser therapy of melanomas, ***Surg. Gynecol. Obstet.***, 124:49-56, 1967.

8. **Kitzmiller, K.W.:** Laser treatment of tattoos and angiomas, ***J. Med. Assoc. Ga.*** 59:385, 1970.

9. **Kirschner, R.A., Unger, M.:** An introduction to dye lasers and photoradiation therapy, ***Surgical Clinics*** 64(5):939-940, October 1984.

10. **Dougherty, T.J., Grindley, G.B., Fiel, R., Weishaupt, K.R., Boyle, D.G.:** Photoradiation therapy. II. Cures of animal tumors with hematoporphyrin and light, ***J. Natl. Cancer Inst.*** 55:115-121, 1975.

11. **Mester, E. Spiry, T., Szende, B. et al.:** Effect of laser rays on wound healing, ***Am. J. Surg.*** 122:532-535, October 1971.

12. **Mester, E., Korenyi-Both, A., Spiry, T., et al.:** Stimulation of wound healing by means of laser rays. (Clinical and electron microscopial study), ***Acta Chir. Acad. Sci. Hung.*** 14:347-356, 1973.

13. **Mester, E., Nagylucskay, S., Tisza, S., Mester, A.:** Stimulation of wound healing by means of laser rays. Part III - Investigation of the effect on immune competant cells, ***Acta. Chir. Acad. Sci. Hung.*** 19(2);163-170, 1978.

14. **Peled, I., Shohat, B., Gassner, S., Kaplan, I.**: Excision of epithelial tumors: CO_2 lasers versus conventional methods, ***Cancer Let.*** 2:41, 1976.

15. **Andrews, A. Goldenberg, R., Moss, H., Saker, M.**: Carbon dioxide laser for laryngeal surgery, ***Surg. Annu.*** 6:459, 1974.

16. **Lyons, G., Lousteau, R., Mouney, D.**: CO_2 laser laryngoscopy in a variety of lesions, ***Laryngoscope*** 86:1658-1662, 1976.

17. **Coffae, K.P., Brilliant, J.D.**: The effect of serial preparation versus non-serial preparation on tissue removal in root canals of extracted mandibular molars, ***J. Endo.*** 1(6):211-214, June 1975.

18. **Jungmann, C.L., Uchin, R.A., Bucher, J.R.**: Effect of instrumentation on the shape of the root canal, ***J. Endo.*** 1(2):66-69, February 1975.

19. **Littman, S.H.**: Evaluation of root canal debridement by the use of a radiopaque medium, ***J. Endo.*** 3(4):135-138, April 1977.

20. **Walton, R.E.**: Histologic evaluation of different methods of enlarging the pulp canal space, ***J. Endo.*** 2(10):304-311, October 1976.

21. **Bolanos, O.R., Jensen, J.R.**: Scanning electron microscope comparisons of the efficacy of various methods of root canal preparations, ***J. Endo.*** 6(11):815-822, November 1980.

22. **McComb, D., Smith, D.C.**: A preliminary scanning electron microscope study of root canals after endodontic procedures, ***J. Endo.*** 1(7):238-242, July 1975.

23. **Barry, G.N., Heyman, R.A., Elias, A.**: Comparison of apical sealing methods, ***Oral Surg.*** 39(5):806-811, May 1975.

24. **Russin, T.P., Zardiackas, L.D., Reador, A., Menke, R.A.**: Apical seals obtained with laterally condensed, chloroform softened gutta percha and laterally condensed gutta percha and Grossman's sealer, ***J. Endo.*** 6(8):678-682, August 1980.

25. **Mattioff, I.R., Jensen, J.R., Singer, L., Tabibi, A.**: A comparison of methods used in root canal sealability studies, ***Oral Surg.*** 53(2):203-208, February 1982.

26. **Secrist, B., Zakariasen, K.L., Beatty, R.**: Thermomechanical condensation of gutta percha with and without apical plugging, ***J. Dent. Res.*** Program and Abstacts of Papers, Vol. 61, March 1982.

27. **Zakariasen, K.L., Stadem, P.S.**: Microleakage associated with modified eucapercha and chloropercha root canal filling techniques, ***Int. Endo. J.*** 15:67-70, 1982.

28. **Cohen, S., Burns, R.:** ***Pathways of the Pulp***, ed. 2, St. Louis, C.V. Mosby Publishing Co., 1980.

29. **Torneck, C.D.:** Reaction of rat connective tissue to polyethylene tube implants, I., ***Oral Surg.*** 21:379-387, March 1966.

30. **Torneck, C.D.:** Reaction of rat connective tissue to polyethylene tube implants, II., ***Oral Surg.*** 24:674-683, November, 1967.

31. **Shovlin, F.E. et al.:** Reflections on the Sargenti N_2 method of root canal therapy, ***Clin. Prev. Dent.*** 4(5):17, September-October 1982.

32. **Glickman, J.:** Evaluation of the giromatic system, Thesis, Dept. of Endodontics, University of Medicine and Dentistry of New Jersey, Newark.

33. **O'Connell, D.T., Brayton, S.M.:** Evaluation of root canal preparations with two automated handpieces, ***Oral Surg.*** 39(2):298-303, February 1975.

34. **Klayman, S.M., Brilliant, J.D.:** A comparison of the efficacy of serial preparation versus Giromatic preparation, ***J. Endo.*** 1(10):334-337, October 1975.

35. **Russell, D.I. et al.:** Complications of automated root canal treatment, ***Brit. Dent. J.*** 153(11):393-398, December 7, 1982.

36. **Magnusson, B.O.:** Therapeutic pulpotomies in primary molars with the formocresol technique. A clinical and histologic follow-up, ***Acta Odontol. Scand.*** 36(3):157-165, 1978.

37. **Rolling, I. et al.:** Morphologic and enzyme histochemical observations on the pulp of human primary molars 3 to 5 years after formocresol treatment, ***Oral Surg.*** 42(4):518-528, October 1976.

38. **Bender, I.B., Seltzer, S., Turkenkopf, S.:** To culture or not to culture?, ***Oral Surg.*** 18:527-540, October 1964.

39. **Peterson, S.C.:** Endodontic success rates. An analysis comparing culture status at time of fill with a radiographic determination of success versus failure at two year recall, ***Master's thesis***, The University of Iowa, Iowa City, Iowa, 1979.

40. **Ingle, J.:** ***Endodontics***, Lea and Febiger, Philadelphia, Second Edition, 1976.

41. **Zakariasen, K.L., Scott, D.A.:** Silver cones: how have they performed and what is their place in endodontic therapy? Manuscript in preparation, The University of Alberta, Edmonton, Alberta, 1986.

42. **Weichman, J.A., Johnson, F.M.:** Laser use in endodontics, a preliminary investigation, ***Oral Surg.*** 31(3):416-420, March 1971.

43. **Weichman, J.A., Johnson, F.M., Nitta, L.K.:** Laser use in endodontics, Part II, ***Oral Surg.*** 34(5):828-830, November 1972.

44. **Kantola, S.**: Laser-induced effects on tooth structure IV. A study of changes in the calcium and phosphorous contents in dentine by electron probe microanalysis, ***Acta Odont. Scand.***, 30:463, October 1972.

45. **Kantola, S.**: Laser-induced effects on tooth structure VII. X-ray diffraction study of dentine exposed to a CO_2 laser, ***Acta Odont. Scand.*** 31:381-386, December 1973.

46. **Melcer, J., Melcer, F., Hasson, R., Merard, R., Gautier, J., Lancert, J., Benjardin, J.**: Dental structure modification by CO_2 laser beam, Laser Tokyo '81: The Fourth Congress of the Internationsl Society for Laser Surgery, Tokyo, Japan, November 23-27, 1981. Ed. by Atsumi, K., Nimsakul, N.

47. **Hodge, H.C., Finn, S.B., Robinson, H.B.G., Manley, R.S., Manley, M.L., Van Huysen, G., Bale, W.F.**: Heriditary opalescent dentin - III: histological, chemical and physical studies, ***J. Dent. Res.*** 19:521-536, 1940.

48. **Scott, D.A., Zakariasen, K.L., Reeh, E.S., Morela, D.**: Analyzing dentinal tubule morphology as a potential method for reducing leakage variance, ***J. Dent. Res.***, Program and Abstracts of Papers, Vol. 63, March 1984.

49. **Dederich, D.N., Zakariasen, K.L., Tulip, J.**: Scanning electron microscopic analysis of canal wall dentin following neodymium-yttrium-aluminum-garnet laser irradiation, ***J. Endo.*** 10(9):428-437, September 1984.

50. **Dederich, D.N., Zakariasen, K.L., Tulip, J.**: S.E.M. analysis of dyed canal dentin following Nd-YAG laser irradiation, Abstract No. 581, ***J. Dent. Res.*** Program and Abstracts of Papers, Vol. 64, March 1985.

51. **Pashley, D.H., Livingston, M.J., Greenhill, J.D.**: Regional resistances to fluid flow in human dentin, ***in vitro***, Arch. Oral Biol. 23:807-810, 1978.

52. Personal Communication: Dr. John Tulip, Department of Electrical Engineering and The Alberta Laser Institute, The University of Alberta, Edmonton, Alberta, Canada.

53. **Nylen, M.V., Scott, D.B.**: An electron microscopic study of the early stages of dentinogenesis, ***Public Health Serv. Publ.*** 613, U.S. Government Printing Office, Washington, D.C., 1958.

54. **Larsson, A., Bloom, G.D.**: Studies on dentinogenesis in the rat. Fine structure of developing odontoblasts and predentin in relation to the mineralization process, ***Z. Anat. Entwicklungsgesch*** 139:227-246, 1973.

55. **Garant, P.R., Szab, G., Nalbandian, J.**: The fine structure of the mouse odontoblast, ***Arch. Oral Biol.*** 13:857-876, 1968.

56. **Jessen, H.**: The ultrastructure of odontoblasts in perfusion fixed, demineralized incisors of adult rats, ***Acta Odontol. Scand.*** 25:491-523, 1967.

57. **Reith, E.J.:** Collagen formation in developing molar teeth of rats, *J. Ultrastruct. Res.* 21:383-414, 1968.

58. **Sisca, R.F., Provenza, D.V.:** Initial dentin formation in human deciduous teeth. An electron microscope study, *Calcif. Tissue Res.* 9:1-16, 1972.

59. **Bevelander, G., Nakahara, H.:** The formation and mineralization of dentin, *Anat. Rec.* 156:303-324, 1966.

60. **Whittaker, D.K., Adams, D.:** Electron microscopic studies on Von Korff's fibers in the human developing tooth, *Anat. Rec.*;174:175-190, 1972.

61. **Carneiro, J., Leblond, C.P.:** Role of osteoblasts and odontoblasts in secreting collagen of bone and dentine, as shown by radioautography in mice given tritium-labelled glycine, *Exp. Cell Res.* 18:291-300.

62. **Cotton, W.R., Hefferren, S.M.:** An autoradiograph study of tryptophane-H^3 incorporation into rat enamel and dentine matrices, *Arch. Oral Biol.* 11:1027-1037, 1966

63. **Hwang, W.S.S., Tonna, E.A., Cronkite, E.P.:** An autoradiographic study of the mouse incisor using tritiated histidine, *Arch. Oral Biol.* 8:377-385, 1963.

64. **Young, R.W., Greulich, R.C.:** Distinctive graphic patterns of glycine incorporation in rat enamel and dentine matrices, *Arch. Oral Biol.* 8:509-521, 1963.

65. **Belanger, L.F.:** Autoradiographic visualization of the entry and transit of S^{35} methionine and cystine in the soft and hard tissues of the growing rat, *Anat. Rec.* 124:555-579, 1956.

66. **Karpishka, I., Leblond, C.P., Carneiro, J.:** Radio-autographic investigation of the uptake of labelled methionines by the dentine and enamel matrix of growing teeth, *Arch. Oral Biol.* 1:23-28, 1959.

67. **Sundstrom, B.:** New aspects of the utilization of inorganic sulphate during dentin formation, *Histochemie* 26:61-66, 1971.

68. **Weinstock, M., Leblond, C.P.:** Synthesis, migration, and release of precursor collagen by odontoblasts as visualized by radiography after (^3H) proline administration, *J. Cell Biol.* 60:92-127, 1974.

69. **Weinstock, M.:** Collagen formation - Observations on its intracellular packaging and transport, *Z. Zellforsch* 129:455-470, 1972.

70. **Garant, P.R.:** The organization of microtubules within rat odontoblast process revealed by perfusion fixation with glutaraldehyde, *Arch. Oral Biol.* 17:1047-1058, 1972.

71. **Tronstad, L.:** Ultrastructural observations on human coronal dentin, *Scand. J. Dent. Res.* 81:101-111, 1973.

72. **Eisenmann, D.R., Glick, P.L.:** Ultrastructure of initial crystal formation in dentin, *J. Ultrastruct. Res.* 41:18-28, 1972.

73. **Katchburian, E.:** Membrane-bound bodies as initiators of mineralization of dentine, *J. Anat.* 116:285-302, 1973.

74. **Birkedal-Hansen, R., Butler, W.T., Taylor, R.E.:** Isolation and preliminary characterization of bovine cementum collagen, *Calcif. Tissue Res.* 15:325-328, 1974.

75. **Carmichael, D.J., Veis, A., Wang, E.T.:** Dentin matrix collagen: Evidence for a covalently linked phosphoprotein attachment, *Calcif. Tissue Res.* 7:331-344, 1971.

76. **Veis, A., Spector, A.R., Carmichael, D.J.:** The organization and polymerization of bone and dentin collagens, *Clin. Orthop.* 66:188-211, 1969.

77. **Brekhus, P.J., Armstrong, W.D.:** A method for the separation of enamel, dentin, and cementum, *J. Dent. Res.* 15:23-29, 1935.

78. **Manley, R.S., Hodge, H.C.:** Density and refractive index studies of dental hard tissues. I. Methods for separating and determination of purity, *J. Dent. Res.* 18:133-141, 1939.

79. **Neiders, M.E. et al.:** Electron probe microanalysis of cementum and underlying dentin in young permanent teeth, *J. Dent. Res.* 51:122-130, 1972.

80. **Prout, R.E.S., Shutt, E.R.:** Separation of enamel and dentine using cadmium tungstoborate solution, *Arch. Oral Biol.* 15:559-561, 1970.

81. **Yoon, S.H., Brudevold, F., Gardner, D.E., Smith, F.A.:** Distribution of fluoride in teeth from areas with different levels of fluoride in the water supply, *J. Dent. Res.* 39:845-856, 1960.

82. **Coklica, V., Brudevold, F.:** Density fractions in human enamel, *Arch. Oral Biol.* 11:1261-1268, 1966.

83. **Coklica, V., Brudevold, F., Amdur, B.H.:** The distribution and composition of density fractions from human crown dentine, *Arch. Oral Biol.* 14:451-460, 1969.

84. **Armstrong, W.D., Brekhus, P.J.:** Chemical constitution of enamel and dentin. I. Principal components, *J. Biol. Chem.* 120:677-687, 1937.

85. **LeFevre, M.L., Manly, R.S.:** Moisture, inorganic and organic contents of enamel and dentin from carious teeth, *J.A.D.A.* 25:233-242, 1938.

86. **Nordback, L.G., Johansen, E., Parks, H.F.:** Effect of heat on the carbonate content of dentin, Abstr. 177 *J. Dent. Res.* 40:704, 1961.

87. **Olsen, T., Johansen, E.**: Studies on the effect of heat on carbonate content and crystallite morphology of human enamel, ***J. Dent. Res.***, Abstract No. 40, 1965.

88. **Holager, J.**: Thermogravimetric experiments on tooth carbonates, ***J. Dent. Res.*** 51(1):102-106, 1972.

89. **Burnett, G.W., Zenewitz, J.**: The composition of human teeth VI. The composition of syrian hamster enamel and dentin extracted with KOH ethylene glycol, ***J. Dent. Res.*** 36(5):684-689, 1958.

90. **Stack, M.V.**: Organic constituents of dentin, ***Brit. Dent. J.*** 90:173-181, 1951.

91. **Stack, M.V.**: The chemical nature of the organic matrix of bone, dentin, and enamel, ***Ann. N. Y. Acad. Sci.*** 60:585-595, 1955.

92. **Holager, J.**: Thermogravimatric examination of enamel and dentin, ***J. Dent. Res.*** 49(3):546-548, 1970.

93. **Brauer, G.M., Termini, D.J., Burns, C.L.**: Characterization of components of dental materials and components of tooth structure by differential thermal analysis, ***J. Dent. Res.*** 49:100-110, 1970.

94. **Komrska, J.**: Derivatographic analysis of dentin, ***J. Dent. Res.*** 51(1):148-150, 1972.

95. **Lim, J.J., Liboff, A.R.**: Thermogravimetric analysis of dentin, ***J. Dent. Res.*** 51(2):509-514, 1972.

96. **Berendsen, H.J.C.**: Water structure in biological systems, ***Fed. Proc.*** 25:971-976, 1966.

97. **Ramachandran, G.N., Chanrasekhran, R.**: Interchain hydrogen bonds via bound water molecules in the collagen triple helix, ***Biopolymers*** 6:1649-1658, 1968.

98. **Burnett, G.W., Zenewitz, J.**: Studies of the composition of teeth. VII. The moisture content of calcified tooth tissues, ***J. Dent. Res.*** 37:581-589, 1958.

99. **Zipkin, I.**: The chemical composition of bones, teeth, calculus, saliva, and the periodontium of the human, In: Nizel, A.E., Ed., ***The Science of Nutrition and its Application in Clinical Dentistry***, Second Edition, Philadelphia, W.B. Saunders, 1966, pp. 281-295.

100. **McConnell, D.**: The crystal chemistry of dental enamel, ***Arch. Oral Biol.*** 3:28-34, 1960.

101. **Elliot, J.C.**: Interpretation of carbonate bands in infra-red spectrum of dental enamel, ***J. Dent. Res.*** 42:1081-1115, 1963.

102. **Jensen, A.T., Dano, M.**: X-ray crystallographic examination of calculi from salivary glands, ***J. Dent. Res.*** 31:620-626, 1952.

103. **Gron, P., van Campen, G.J., Lindstrom, I.**: Human dental calculus - inorganic chemical and crystallographic composition, ***Arch. Oral Biol.*** 12:829-837, 1967.

104. **LeGeros, R.Z.**: Variations in the crystalline components of human dental calculus. I. Crystallographic and spectroscopic methods of analysis, ***J. Dent. Res.*** 53:45-50, 1974.

105. **Newesely, H., Hohling, H.J.**: Recent findings on the crystal structures of hypomineralized and carious teeth, ***Adv. in Fluorine Res.*** 3:131-135, 1965.

106. **Vahl, V.J., Hohling, H.J., Frank, R.M.**: Elektronenstrahlbeugung an rhomboedrisch aussehenden mineralbildungen in kariosem dentin, ***Arch. Oral Biol.*** 9:315-320, 1964.

107. **Vahl, V.J., Plackova, A.**: Elektronenoptische untersuchungen von braunen schmelzflecken (arretierte karies), ***Dtsch. Zahnaerztl Z.*** 22:620-629, 1967.

108. **LeFevre, R., Frank, R.M., Voegel, J.C.**: Secondary ion microscopy and electron diffraction of human peritubular dentin, Abstr. L429, IADR 53rd General Meeting, London, 1975, p. L107.

109. **Hagen, A.R.**: Structural features of biologically involved phosphates, ***Acta Odontol. Scand.*** 31:149-173, 1973.

110. **Brown, W.E.**: Crystal structure of octacalcium phosphate, ***Nature*** 196:1048-1050, 1962.

111. **Brown, W.E.**: A mechanism for growth of apatite crystals. In: Stack, M.V., Fearnhead, R.W., Eds., ***Tooth Enamel.*** Bristol, John Wright & Sons, 1965, pp. 11-14.

112. **Brown, W.E., Smith, J.P., Lehr, J.R., Frazier, A.W.**: Crystallographic and chemical relations between octacalcium phosphate and hydroxyapatite, ***Nature*** 196:1050-1054, 1962.

113. **Schroeder, H.E.**: ***Formation and inhibition of dental calculus,*** Huber, Bern Eds., 1969.

114. **Dallemagne, M.J., Fabry, C.**: In: ***Bone Structure and Metabolism,*** Ciba Foundation Symposium, Churchill, London, 1956.

115. **Shaw, J.H., Yen, P.K.-J.**: Sodium, potassium and magnesium concentrations in the enamel and dentine of human and rhesus monkey teeth, ***J. Dent. Res.*** 51:95-101, 1972.

116. **Besic, F.C., et al.**: Detailed electron probe micro-analysis of three teeth sections with early enamel caries, ***J. Dent. Res.*** 49:111-118, 1969.

117. **Nixon, G.S. et al.**: Estimation of manganese in human dental enamel by activation analysis, ***Arch. Oral Biol.*** 11:247-252, 1966.

118. **Soremark, R., Gron, P.**: Chloride distribution in human dental enamel as deternimed by electron probe microanalysis, ***Arch. Oral Biol.*** 11:861-866, 1966.

119. **Soremark, R., Samsahl, K.**: Gamma-ray spectrophotometric analysis of elements in normal human dentine, ***J. Dent. Res.*** 41:603-606, 1962.

120. **Nixon, G.S., Smith, H.**: Estimation of arsenic in teeth by activation analysis, ***J. Dent. Res.*** 39:514-516, 1960.

121. **Nixon, G.S., Smith, H.**: Estimation of copper in human enamel by activation analysis, ***J. Dent. Res.*** 41:1013-1016, 1962.

122. **Hardwick, J.L., Martin, C.J.**: A pilot study using mass spectrometry for the estimation of the trace element content of dental tissues, ***Helv. Odont. Acta*** 11:62-70, 1967.

123. **Losee, F.L. et al.**: Natural elements of the periodic table in human dental enamel, ***Caries Res.*** 8:123-134, 1974.

124. **Soremark, R. et al.**: Influence of some dental restorations on the concentrations of inorganic constituents of the teeth, ***Acta Odont. Scand.*** 20:215-224,1962.

125. **Bergenholz, A. et al.**: Studies of the transport of metal ions from gold inlays to the environmental tissues, ***Acta Odont. Scand.*** 23:135-146, 1965.

126. **Levine, R.S.**: The distribution on hydroxyproline in sound coronal dentine, ***Arch. Oral Biol.*** 16-473-478, 1971.

127. **Hess, W.C., et al.**: The lipid content of enamel and dentin, ***J. Dent. Res.*** 35:273-275, 1956.

128. **Dirksen, T.R.**: Lipid components of sound and carious dentin, ***J. Dent. Res.*** 42:128-132, 1963.

129. **Odutuga, A.A., Prout, R.E.S.**: Lipid analysis of human enamel and dentin, ***Arch. Oral Biol.*** 19:729-731, 1974.

130. **Toto, P.D. et al.**: Effect of age on water content in human teeth, ***J. Dent. Res.*** 50:1284-1285, 1971.

131. **Nalbandian, J., et al.**: Sclerotic age changes in root dentine of human teeth as observed by optical, electron, and X-ray microscopy, ***J. Dent. Res.*** 39:598-607, 1960.

132. **Lisanti, V.F., Zander, H.A.**: Thermal conductivity of dentin, ***J. Dent. Res.*** 29:493-497, 1950.

133. **Simeral, W.G.**: Thermal conductivity of dental materials, ***J. Dent. Res.*** 30(4):499, Abstract, 1951.

134. **Phillips, R.W., Johnson, R.J., Phillips, L.J.:** An improved method of measuring the coefficient of thermal conductivity of dental materials, ***J.A.D.A.*** 53:577-583, 1956.

135. **Soyenkoff, B.S., Okun, J.H.:** Thermal conductivity measurements of dental tissues with the aid of thermistors, ***J.A.D.A.*** 57:23-30, 1958.

136. **Craig, R.G., Peyton, F.A.:** Thermal conductivtiy of tooth structure, dental cements and amalgam, ***J. Dent. Res.*** 40:411-418, 1961.

137. **Fanibunda, K.B., De Sa, A.:** Thermal conductivity of normal and abnormal human dentine, ***Arch. Oral Biol.*** 20(7):457-459, 1975.

138. **Peyton, F.A., Simeral, W.G.:** Specific heat of tooth structure, ***Alumni Bulletin of the University of Michigan Dental School*** 56:33, 1954.

139. **Manly, R.S., Hodge, H.C., Ange, L.E.:** Density and refractive index studies of dental hard tissue - II. Density distribution curves, ***J. Dent. Res.*** 18:203-211, 1939.

140. **Braden, M.:** Heat conduction in normal human teeth, ***Arch. Oral Biol.*** 9:479-486, 1964.

141. **Henchel, C.J.:** Heat impact of revolving instruments on vital dentin tubules, ***J. Dent. Res.*** 22:323-333, 1943.

142. **Black, G.V.:** An investigation into the physical characters of the human teeth in relation to their diseases, ***Dent. Cosmos*** 37:353, 469, 553, 637, 737, 1895.

143. **Peyton, F.A., Mahler, D.B., Hershenov, B.:** Physical properties of dentin, ***J. Dent. Res.*** 31:366-370, 1952.

144. **Neumann, H.H., Di Salvo, N.A.:** Compression of teeth under the load of chewing, ***J. Dent. Res.*** 36:286-290, 1957.

145. **Craig, R.C., Peyton, F.A.:** Elastic and mechanical properties of human dentin, ***J. Dent. Res.*** 37:710- 718, 1958.

146. **Craig, R.C., Peyton, F.A. :** Microhardness of enamel and dentin, ***J. Dent. Res.*** 37:661-668, 1958.

147. **Stanford, J., Paffenbarger, G., Kumpula, J., Sweeney, W.:** Determination of some compressive properties of human enamel and dentin, ***J.A.D.A.*** 57:487-496, 1958.

148. **Tyldesley, W.R.:** The mechanical properties of human enamel and dentine, ***Brit. Dent. J.*** 106:269-278, 1959.

149. **Bowen, R.L.:** Tensile strength testing method and values for some dental materials, Abstr. M52, ***J. Dent. Res.*** 39:768, 1960.

150. **Stanford, J., Weigel, K., Paffenbarger, G., Sweeney, W.**: Compressive properties of hard tooth tissue and some restorative materials, ***J.A.D.A.*** 60:746-756, 1960.

151. **Bowen, R., Rodriguez, M.**: Tensile strength, testing method, and values for some dental materials, Abstract M52, ***J. Dent. Res.*** 39:768-769, 1960.

152. **Bowen, R., Rodriguez,M.**: Tensile strength and modulus of elasticity of tooth structure and several restorative materials, ***J.A.D.A.*** 64:378-387, 1962.

153. **Lehman, M.L.**: Tensile strength of human dentin, ***J. Dent. Res.*** 46:197-201, 1967.

154. **Barton, J., Dickenson, G.**: Thermal and hygroscopic dimensional changes of tooth structure, Abstract 673, ***J. Dent. Res.*** 49:217, 1970.

155. **Renson, C.E., Braden, M.**: The experimental deformation of human dentine by indenters, ***Arch. Oral Biol.*** 16:563-572, 1971.

156. **Korostoff, E., Pollack, S.R., Duncanson, M.G.**: Viscoelastic properties of human dentin, ***J. Biomed. Mater. Res.***: 9(6):661-674, 1975.

157. **Duncanson, M.G. Jr., Korostoff, E.**: Compressive visco-elastic properties of human dentin: I. Stress-relaxation behavior, ***J. Dent. Res.*** 54(6):1207-1212, 1975.

158. **Rasmussen, S.T., Patchin, R.E., Scott, D.B., Heuer, A.H.**: Fracture properties of human enamel and dentin, ***J. Dent. Res.*** 55(1):154-164, 1976.

159. **Boehm, R., Rich, J., Webster, J., Janke, S.**: Thermal stress effects and surface cracking associated with laser use on human teeth, Trans. ASME; ***J. Biomech. Eng.*** :189-194, November 1977.

160. **Byars, E.F., Snyder, R.D.**: ***Engineering Mechanics of Deformable Bodies, Third Edition,*** Intext Educational Publishers, New York, © 1975 by Thomas Y. Crowell Company, Inc., p.69.

161. **Barton, J., Dickenson, G.**: Thermal and hygroscopic dimensional changes of tooth structure, Abstract No. 673, ***J. Dent. Res. Program and Abstracts of Papers*** 49:217, 1970.

162. **Sauder and Paffenbarger**: ***Physical Properties of Dental Materials,*** *National Bureau of Standards Circular C433.*

163. **Boehm, R., Baechler, T., Webster, J., Janke, S.**: Laser processes in preventive dentistry, ***Opt. Eng.*** 16:493-496, 1977.

164. **Duley, W.W.**: Laser prodeeding and analysis of materials, ***Plenum***, New York, 1983, p. 79.

165. **Sagi, A., Segal, T., Dagan, J.**: A numerical model for temperature distribution and thermal damage calculations in teeth exposed to a CO_2 laser, ***Mathematical Biosciences*** 71:1-17, 1984.

166. **Pashley, D.H., Michelich, V., Kehl, T.**: Dentin permeability: effects of smear layer removal, ***J. Prosth. Dent.*** 46(5):531-537, 1981.

167. **Ready, J.F.**: ***Effects of High-Power Laser Radiation***, Academic Press, Inc., New York, © 1971, p.5.

168. **Verdeyden, J.T.**: ***Laser Electronics*** , Prentice-Hall, Inc., Englewood Cliffs, N.J., © 1981, pp. 58-61.

169. **Ready, J.F.**: ***Effects of High-Power Laser Radiation***, Academic Press, Inc., New York, © 1971, p. 13.

170. **Hu, Chia-Lun, Barnes, F.S.**: The thermal-chemical damage in biological material under laser irradiation, ***I.E.E.E. Trans. Biomed. Eng.*** 17:220-229, 1970.

171. **Ready, J.F.**: ***Effects of High-Power Laser Radiation***, Academic Press, Inc., New York, © 1971, pp.67-87.

172. **Landry, J., Bernier, J.P., Marceau, N.**: Comparative evaluation of the mammalian cell thermal sensitivity to pulsed CO_2-laser irradiation and hyperthermic water-bath treatment, ***Radiat. Res.*** 71(1):240-250, 1977.

173. **Abela, G.S., Crea, F., Smith, W., Pepine, C.J., Conti, C.R.**: In vitro effects of argon laser radiation on blood: quantitative and morphologic analysis, ***J. Amer. Coll. of Cardiology***, 5(2):231-237 part 1, 1985.

174. **Polanyi, T.G.**: Laser physics, ***Otolaryngol. Clin. North Am.*** 16(4):753-774, 1983.

175. **Halldorsson, T., Langerholc, J.**: Thermodynamic analysis of laser irradiation of biological tissue, ***Appl. Opt.*** 17:3948-3958, 1978.

176. **Hallsworth, R.S., Isenor, N.R.**: Vibrational relaxation of CO_2-laser excited SiF_4 gas in binary mixtures, ***Chem. Phys. Lett.*** 22:283-286, 1973.

177. **Goldman, L., Rockwell, R.J.Jr.**: ***Lasers in Medicine***, Gordon and Breach, Science Publishers, Inc., New York, ©1971, pp. 149-161.

178. **Langerholc, J.**: Moving phase transitions in laser irradiated biological tissue, ***Appl. Opt.*** 18:2286-2293, 1979.

179. **Marchesini, R., Andreola, S., Emanuelli, H., Melloni, E., Schiroli, A., Spinelli, P., Fava, G.**: Temperature rise in biological tissue during Nd:YAG laser girradiation, ***Lasers Surg. Med.*** 5(2):75-82, 1985.

180. **Bonar, L.C., Glimcher, M.J.**: Thermal denaturation of mineralized and demineralized bone collagens, ***J. Ultrastruct. Res.*** 32:545-551, 1970.

181. **Gorisch, W., Boergen, K.P.**: Heat-induced contraction of blood vessels, ***Lasers Surg. Med.*** 2(1):1-13, 1982.

182. **Parrish, J.A., Anderson, R.R., Harrist, T., Paul, B., Murphy, G.F.**: Selective thermal effects with pulsed irradiation from lasers: from organ to organelle, ***J. Invest. Dermatol.*** 80 Suppl.: 75's-80's, 1983.

183. **Gorisch, W., Boergen, K.**: Laser related heat effects on blood vessels, ***Lasers in Medicine and Biology***, Ed. F. Hillenkamp, R. Pratesi, C.A. Sacchi, New York, Plenum Press, pp.99-109, 1980.

184. **Elden, H.R.**: Physical properties of collagen fibers, ***Int. Rev. of Connective Tiss. Res.*** Vol. 4, Ed. D.A. Hall, New York: Academic Press, pp. 283-348, 1968.

185. **Birngruber, R.**: in ***Lasers in Biology and Medicine***, Ed. Hillenkamp et al., New York: Plenum Press, p. 77-97, 1980.

186. **Goldman, L., Rockwell, R.J.**: in ***Lasers in Medicine and Biology***, New York: Gordon and Breach Science Publ. Inc., p.183, 1971.

187. **Hall, R.R., Beach, A.D., Baker, E., Morison, P.C.A.**: Incision of tissue by carbon dioxide laser, ***Nature*** 232:131-132, 1971.

188. **Carome, E.F., Clark, N.A., Moeller, C.E.**: Generation of acoustic signals in liquids by ruby laser-induced thermal stress transients, ***App. Phys. Lett.*** 4(6):95-97, 1964.

189. **Gournay, L.S.**: Conversion of electromagnetic to acoustic energy by surface heating, ***J. Acoust. Soc. Am.*** 40:1233-30, 1966.

190. **Bunkin, F.V., Karlov, N.V., Komissarov, V.M., Kuz'min, G.P.**: Excitation of sound when a surface layer of a liquid absorbs a laser pulse, ***Zh. Eksp. Tior. Fiz. Pis'ma Red.*** 13:479-483, 1971 [JETP Lett. 13:341-343, 1971.

191. **Peck, S., Peck, H.**: Laser radiation: Some specific dental effects and an evaluation of its potential in dentistry, ***J. Prosth. Dent.*** 17:195-203, 1967.

192. **Scheinin, A., Kantola, S.**: Laser-induced effects on tooth structure. I. Crater production with a CO_2 laser, ***Acta Odontol. Scand.*** 27:173-179, 1969.

193. **Mannerberg, F., Kantola, S., Scheinin, A.**: Laser-induced effects on tooth structure. III. Single pulse impacts on surface enamel as observed in shadowed replicas, ***Acta Odont. Scand.*** 27:467-476, 1969.

194. **Yamamoto, H., Okabe, H., Ooya, K., Hanaoka, S.**: Laser effect on vital oral tissues: A preliminary investigation, ***J. Oral Path.*** 1:256-264, 1972.

195. **Gordon, T.E.**: Some effects of laser impacts on extracted teeth, ***J. Dent. Res.*** 45:372-375, 1966.

196. **Varner, R.E., Jarabak, J.P., Phatak, N.M., Kinersley, T.:** Effect of different colored stains on laser microbeam impact sites on tooth enamel, ***J. Dent. Res.*** 46:756, 1967.

197. **Gordon, T.E.:** Single-surface cutting of normal tooth with ruby laser, ***J.A.D.A.*** 74:398-402, 1967.

198. **Myers, T.D., Myers, W.D.:** In vivo caries removal utilizing the YAG laser, ***J. Mich. Dent. Assoc.*** 67:66-69, 1985.

199. **Kimura, H., Sohmura, T., Tsutsumi, N., Okazaki, M.:** Application of laser on dental treatment, ***J. Osaka Univ. Dent. Sch.*** 23:31-42, 1983.

200. **Goldman, L., Gray, J.A., Goldman, J., Goldman, B., Myer, R.:** Effect of laser beam impact on teeth, ***J.A.D.A.*** 70:601-606, 1965.

201. **Adrian, J.C., Bernier, J.L., Sprague, W.G.:** Laser and the dental pulp, ***J.A.D.A.*** 83:113-117, 1971.

202. **Winkler, S., Flynn, K.L., Miller, W.A.:** Neodymium laser fusion of restorative materials to tooth structure - a preliminary report, ***N.Y. State Dent. J.*** 39:614-618, 1973.

203. **Stewart, L., Powell, G.L., Wright, S.:** Hydroxyapatite attached by laser: a potential sealant for pits and fissures, ***Operative Dentistry*** 10:2-5, 1985.

204. **Kinersly, T., Jarabak, J.P., Phatak, N.M., DeMent, J.:** Laser effects on tissue and materials related to dentistry, ***J.A.D.A.*** 70:593-600, 1965.

205. **Van Wazen, J.R.:** ***Phosphorous and its Compounds***, New York: Interscience Pub. Inc., 1:526-527, 1958.

206. **Lobene, R.R., Fine, S.:** Interaction of laser radiation with oral hard tissues, ***J. Prosth. Dent.*** 16:589-597, 1966.

207. **Lobene, R.R., Bhussry, B.R., Fine, S.:** Interaction of carbon dioxide laser with enamel and dentin, ***J. Dent. Res.*** 47:311-317, 1968.

208. **Kantola, S., Laine, E., Tarna, T.:** Laser-induced effects on tooth structure. VI. X-ray diffraction study of dental enamel exposed to a CO_2 laser, ***Acta Odont. Scand.*** 31:369-379, 1973.

209. **Goodman, B.D., Kaufman, H.W.:** Effects of an argon laser on the crystalline properties and rate of dissolution in acid of tooth enamel in the presence of sodium fluoride, ***J. Dent. Res.*** 56(10):1201-1207, 1977.

210. **Newesely, H.:** High temperature behavior of hydroxy- and fluorapatite chrystalchemical implications of laser effects on dental enamel, ***J. Oral Rehabil.*** 4(1):97-104, 1977.

211. **Brune, D.**: Interaction of pulsed carbon dioxide laser beams with teeth in vitro, ***Scand. J. Dent. Res.*** 88(4):301-305, 1980.

212. **Kuroda, S., Fowler, B.O.**: Compositional, structural, and phase changes in in vitro laser-irradiated human tooth enamel, ***Calcif. Tissue Int.*** 36(4):361-369, 1984.

213. **Kantola, S.**: Laser-induced effects on tooth structure. V. Electron probe microanalysis and polarized light microscopy of dental enamel, ***Acta Odont. Scand.*** 30:475-484, 1972.

214. **Scheinin, A., Kantola, S.**: Laser-induced effects on tooth structure. II. Microradiography and polarized light microscopy of dental enamel and dentine, ***Acta Odont. Scand.*** 27:181-192, 1969.

215. **Stern, R.H., Vahl, J., Sognnaes, R.F.**: Lased enamel: ultrastructural observations of pulsed carbon dioxide laser effects, ***J. Dent. Res.*** 51:455-460, 1972.

216. **Nelson, D.G.A., Shariati, M., Glena, R., Shields, C.P., Featherstone, J.D.B.**: Effect of pulsed low energy infrared laser irradiation on artificial caries-like lesion formation, ***Caries Res.*** 20:289-299, 1986.

217. **Sognnaes, R.F.**: Microradiographic observations on demineralization gradients in the pathogenesis of hard-tissue destruction, ***Arch. Oral Biol.*** 1:106-121, 1959.

218. **Sognnaes, R.F., Stern, R.H.**: Laser effect on resistance of human dental enamel to demineralization in vitro, ***J.S. Calif. Dent. Assn.*** 33:328, 1965.

219. **Stern, R.H., Sognnaes, R.F., Goodman, F.**: Laser effect on in vitro enamel permeability and solubility, ***J.A.D.A.*** 73:838-843, 1966.

220. **Borggreven, J.M., Van Dijk, J.W., Driessens, F.C.**: Effect of laser irradiation on the permeability of bovine dental enamel, ***Arch. Oral Biol.*** 25(11-12):831-832, 1980.

221. **Stern, R.H., Sognnaes, R.F.**: Laser inhibition of dental caries suggested by first tests in vivo, ***J.A.D.A.*** 85:1087-1090, 1972.

222. **Yamamoto, H., Ooya, K.**: Potential of yttrium-aluminum-garnet laser in caries prevention, ***J. Oral Path.*** 3:7-15, 1974.

223. **Yamamoto, H., Ooya, K., Matsuda, K., Okabe, H.**: YAG laser effect for acid resistance on tooth enamel, ***J. Dent. Res.*** 53:1093, Abst. No. 7, 1974.

224. **Yamamoto, H., Sato, K.**: Prevention of dental caries by acousto-optically Q-switched Nd:YAG laser irradiation, ***J. Dent. Res.*** 59(2):137, 1980.

225. **Sato, K.**: Relation between acid dissolution and histological alteration of heated tooth enamel, ***Caries Res.*** 17(6):490-495, 1983.

226. **Lenz, P., Gilde, H., Pyttel, U.J.**: Reaktionen der Zahngewebe auf Laserbestrahlung [Reactions of dental tissue to laser radiation], ***Dtsch. Zahnarztl.*** 31(11):884-886, 1976.

227. **Arwill, T., Myrberg, N., Soremark, P.**: Penetration of radioactive isotopes through enamel and dentin. I. Diffusion of Na^{22} in fresh and coagulated dental tissues, ***J. Dent. Res.*** 44:1299-1303, 1965.

228. **Burnett, G.W., Zenewitz, J.**: Studies of the composition of teeth. VII. The moisture content of calcified tooth tissues, ***J. Dent. Res.*** 37:581-589, 1958.

229. **Carlstrom, D., Glas, J.E., Angman, B.**: Studies on the ultrastructure of dental enamel. V. The state of water in human enamel. ***J. Ultrastruct. Res.*** 8:24-29, 1963.

230. **Vahl, J.**: Electron microscopical and X-ray crystallographic investigations of teeth exposed to laser rays, ***Caries Res.*** 2:10-18, 1968.

231. **Goldman, L., Rockwell, R.J.Jr., Richfield, D., Wilson, C., Franzen, M., Smith, P.O., Hyatt, S.R.**: Preliminary investigation of fat embolism from pulsed ruby laser impacts on bone, ***Nature*** 221:361-363, 1969.

232. **Clayman, L.**: Bone response to carbon-dioxide rapid-super-pulse and continuous wave laser osteotomy in albino rabbits, ***Bull. Sinai Hosp. Detroit*** 24:189, 1976.

233. **Clayman, L., Fuller, T., Beckman, H.**: Healing of continuous-wave and rapid superpulsed, carbon dioxide, laser-induced bone defects, ***J. Oral Surg.*** 36(12):932-937, 1978.

234. **Horch, H.H., McCod, R.C., Keiditch, E.**: Histological and longterm results following laser osteotomy, In: Kaplan, I. (Ed.): ***Laser Surgery. II.*** Jerusalem, Academy Press, 1978.

235. **Tauber, C., Farine, I., Horoszowski, H., Gassner, S.**: Fracture healing in rabbits after osteotomy using the CO_2 laser, ***Acta Orthop. Scand.*** 50(4):385-390, 1979.

236. **Allen, G.W., Adrian, J.C.**: Effects of carbon dioxide laser radiation on bone: and initial report, ***Milit. Med.*** 146(2):120-123, 1981.

237. **Neumann, W.F., Neumann, M.W.**: ***The Chemical Dynamnics of Bone Mineral***, Chicago: University of Chicago Press, 1958, p.43.

238. **Goldman, L., Rockwell, R.J.Jr.**: ***Lasers in Medicine***, Gordon and Breach, Science Publishers, Inc., New York, ©1971, p.200-205.

239. **Carslaw, H.S., Jaeger, J.C.**: ***Conduction of Heat in Solids***, Second Edition, Oxford University Press, ©1959, p. 2.

240. **Holman, J.P.:** ***Heat Transfer***, Fifth Edition, McGraw-Hill Book Co., New York, © 1981, p. 4.

241. **Holman, J.P.:** ***Thermodynamics***, Third Edition, McGraw-Hill Book Co., New York, © 1980, p. 350.

242. **Holman, J.P.:** ***Heat Transfer***, Fifth Edition, McGraw-Hill Book Co., New York, © 1981, p. 14.

243. **Ready, J.R.:** Effects due to absorbtion of laser radiation, ***J. Appl. Phys.*** 36:462-468, 1965.

244. **Hayes, J.R., Wolbarsht, M.L.:** Thermal model for retinal damage induced by pulsed lasers, ***Aerospace Med.*** 39:474-480, 1968.

245. **Paek, U.C., Gagliano, F.P.:** Thermal analysis of laser drilling processes, ***J. of Quantum Electronics*** I.E.E.E. AE-8(2):112-119, 1972.

246. **Feiock, F.D., Goodwin, L.K.:** Calculation of laser-induced stresses in water, ***J. Appl. Phys.*** 43:5061-5064, 1972.

247. **Wheeler, C.B.:** Calculation of retinal temperature distributions resulting from laser irradiation of the eye: I. Continuous lasers, ***Phys. Med. Biol.*** 21(4):616-630, 1976.

248. **Priebe, L.A., Welch, A.J.:** Asymptomatic rate process calculations of thermal injury to the retina following laser irradiation, ***J. Biomech. Engr.*** 100:49-54, 1978.

249. **Eichler, J., Knof, J., Lenz, H., Salk, J., Schafer, G.:** Temperature distribution in tissue during laser irradiation, ***Rad. and Environm. Biophys.*** 15:277-287, 1978.

250. **Priebe, L.A., Welch, A.J.:** A dimensionless model for the calculation of temperature increase in biological tissues exposed to nonionizing radiation, ***I.E.E.E. Trans. Biomed. Eng.*** 26(4):244-250, 1979.

251. **Papa, F.F., Sethuraman, R.:** Electromagnetic-wave induced vibrations in the ocular region of the eye, ***Med. Biol. Eng. Comput.*** 20(6):749-755, 1982.

252. **McKenzie, A.L.:** How far does thermal damage extend beneath the surface of CO_2 laser incisions?, ***Phys. Med. Biol.*** 28(8):905-912, 1983.

253. **Laufer, G., Joachims, H.Z., Eliachar, I., Mordechovitz, D.:** Measurement of the laser exposure levels for burn threshold in biological tissue, ***J. Biomech. Eng.*** 106(3):283-284, 1984.

254. **Birngruber, R., Hillenkamp, F., Gabel, V.P.:** Theoretical investigations of laser thermal retinal injury, ***Health Phys.*** 48(6):781-796, 1985.

255. **Laufer, G., Haber, S.:** Numerical analysis of the thermochemical tooth damage induced by laser radiation, ***J. Biomech. Engr.*** 107(3):234-239, 1985.

256. **Mainster, M.A., White, T.J., Tips, J.H., Wilson, P.W.:** Transient thermal behavior in biological systems, ***Bull. Math. Biophys.*** 32:303-314, 1970.

257. **Boehm, R.F., Chen, M.J., Blair, C.K.:** Temperature in human teeth due to laser heating, ***A.S.M.E. Paper*** 75-WA/BIO-8, 1975.

258. **Lloyd, B.A., MacGinley, M.B., Brown, W.S.:** Thermal stress in teeth, ***J. Dent. Res.*** 57:571-582, 1978.

259. **Cummins, L., Navenberg, M.:** Thermal effects of laser radiation on biological tissue, ***Biophys. J.*** 42(1):99-102, 1983.

260. **de Vree, J.H.P., Spierings, Th.A.M., Plasschaert, A.J.M.:** A simulation model for transient thermal analysis of restored teeth, ***J. Dent. Res.*** 62:756-759, 1983.

261. **Laufer, G., Haber, S.:** Numerical analysis of the thermochemical tooth damage induced by laser radiation, Trans. of the A.S.M.E. ***J. Biomech. Engr.*** 107:234-239, 1986.

262. **Zienkiewicz, O.C.:** ***The Finite Element Method in Engineering Science,*** McGraw-Hill, London, 1971.

263. **Bathe, K.J.:** ***Finite Element Procedures in Engineering Analysis,*** Prentice-Hall, Englewood Cliffs, New Jersey, 1982.

264. **Zienkiewicz, O.C., Cheung, Y.K.:** Finite elements in the solution of field problems, ***The Engineer***, September 24, 1964.

265. **Wilson, E.L., Nickell, R.E.:** Application of the finite element method to heat conduction analysis, ***J. Nuclear Engr. and Design*** 4:276-286, 1966.

266. **Wilson, E.L., Bathe, K.J., Peterson, F.E.:** Finite element analysis of linear and nonlinear heat transfer, ***J. Nuclear Engr. and Design*** 29:110-124, 1974.

267. **Van Vlack, L.H.:** ***Elements of Materials Science and Engineering,*** Fourth Edition, Addison-Wesley Publishing Co., Reading, Massachusetts ©1980, p. 14.

268. **Stefan, J.:** ***Ann. Phys. Chem.*** 42:269-286, 1891.

269. **Jumikis, A.R.:** ***Thermal Geotechnics,*** Rutgers University Press, New Brunswick, New Jersey, p.205.

270. **Weber, H.M.:** Die partiellen Differentialgleichungen der Mathematischen Physik nach Riemann's Vorlesungen, 2(49):118-122, Vieweg, Braunshweig, 1901.

271. **Carslaw, H.S., Jaeger, J.C.:** ***Conduction of Heat in Solids***, Second Edition, Oxford University Press, ©1959, p. 282.

272. **Jumikis, A.R.:** ***Thermal Geotechnics***, Rutgers University Press, New Brunswick, New Jersey, p.195.

273. ***Automatic Dynamic Incremental Nonlinear Analysis of Temperatures, Users Manual*** , Report AE 84-2, Adina Engineering, December 1984.

274. **Ready, J.F.:** ***Effects of High-Power Laser Radiation***, Academic Press, Inc., New York, © 1971, p.69.

275. **Bathe, K.J., Khoshgoftaar, M.R.:** Finite element formulation and solution of nonlinear heat transfer, ***J. Nuclear Eng. and Design*** 51:389-401, 1979.

276. **Rolph III, W.D., Bathe, K.J.:** An efficient algorithm for analysis of nonlinear heat transfer with phase changes, ***Int. J. Num Meth. in Eng.*** 18:199-134, 1982.

277. ***ADINA - A Finite Element Program for Autodynamic Incremental Nonlinear Analysis***, Report AE 84-1, ADINA Engineering, December 1984.

278. **Bathe, K.J.:** ***Finite Element Procedures in Engineering Analysis***, Prentice-Hall, Inc., ©1982.

279. ***ADINA Handbook - Theoretical Basis and Modeling Guide***, Report AE 82-4, ADINA Engineering, May 1982.

280. **Watts, D.C., El Mowafy, O.M., Grant, A.A.:** Temperature-dependence of compressive properties of human dentin, ***J. Dent. Res.*** 66(1):29-32, 1987.

281. **Touloukian, Y.S., Kirby, R.K., Taylor, R.E., Desai, P.D.:** ***Thermal Expansion-Metallic Elements and Alloys***, Thermophysical Properties of Matter, The TPRC Data Series, Vol.12, IFI/Plenum Pub., New York ©1975, pp. 3a-31a.

282. **Zakariasen, K.L., McMurray, M., Patterson, S., Dederich, D.N., Tulip, J.:** Apical leakage associated with lased and unlased apical plugs, ***J. Dent. Res.*** Program and Abstracts of Papers, Vol. 65, March, 1986.

Appendix

Experimental Data

Photo No.	Power (Watts)	Pulse Duration (Seconds)	Rate (pps)	Hairline Cracking	Wide Cracking	Area Fused	Unfused Cratering	% Impact Area Fused
CW-CO2 Laser								
1	5.00	0.1	-	0.000	0.000	0.000	-	0.0
2	5.00	0.1	-	0.000	0.000	0.000	-	0.0
3	5.00	0.1	-	0.000	0.000	0.000	-	0.0
4	5.00	0.1	-	0.000	0.000	0.000	-	0.0
5	5.00	0.1	-	0.000	0.000	0.000	-	0.0
6	5.00	0.1	-	0.000	0.000	0.000	-	0.0
7	5.00	0.2	-	0.000	0.000	0.000	-	0.0
8	5.00	0.2	-	0.000	0.000	0.000	-	0.0
9	5.00	0.2	-	0.000	0.000	0.000	-	0.0
10	5.00	0.2	-	0.000	0.000	0.000	-	0.0
11	5.00	0.2	-	0.000	0.000	0.000	-	0.0
12	5.00	0.2	-	0.000	0.000	0.000	-	0.0
13	5.00	0.5	-	5.198	0.000	0.000	-	0.0
14	5.00	0.5	-	5.249	0.000	0.000	-	0.0
15	5.00	0.5	-	2.516	0.000	0.000	-	0.0
16	5.00	0.5	-	0.000	0.000	0.000	-	0.0
17	5.00	0.5	-	7.776	0.000	0.000	-	0.0
18	5.00	0.5	-	4.950	0.000	0.000	-	0.0
19	5.00	1.0	-	0.000	0.025	0.099	-	12.6
20	5.00	1.0	-	2.649	0.075	0.096	-	12.2
21	5.00	1.0	-	9.502	0.044	0.078	-	9.9
22	5.00	1.0	-	3.593	0.049	0.080	-	10.2
23	5.00	1.0	-	5.245	0.045	0.000	-	0.0
24	5.00	1.0	-	6.224	0.000	0.000	-	0.0
25	5.00	1.0	-	4.182	0.086	0.050	-	6.4
26	10.00	0.1	-	2.319	0.000	0.000	-	0.0
27	10.00	0.1	-	3.859	0.000	0.000	-	0.0
28	10.00	0.1	-	5.173	0.000	0.000	-	0.0
29	10.00	0.1	-	0.000	0.000	0.000	-	0.0
30	10.00	0.1	-	0.000	0.000	0.000	-	0.0
31	10.00	0.1	-	0.000	0.000	0.000	-	0.0
32	10.00	0.2	-	0.751	0.014	0.154	-	19.6
33	10.00	0.2	-	1.701	0.000	0.023	-	2.9
34	10.00	0.2	-	1.257	0.037	0.048	-	6.1
35	10.00	0.2	-	0.000	0.022	0.098	-	12.5
36	10.00	0.2	-	2.434	0.000	0.124	-	15.8
37	10.00	0.2	-	1.015	0.013	0.000	-	0.0
38	10.00	0.5	-	4.721	0.043	0.406	-	51.7
39	10.00	0.5	-	4.867	0.039	0.365	-	46.5
40	10.00	0.5	-	2.791	0.023	0.436	-	55.5
41	10.00	0.5	-	3.717	0.082	0.310	-	39.5
42	10.00	0.5	-	4.414	0.053	0.342	-	43.5
43	10.00	0.5	-	6.018	0.026	0.311	-	39.6

44	10.00	1.0	-	0.787	0.020	0.796	-	101.3
45	10.00	1.0	-	5.369	0.015	0.671	-	85.4
46	10.00	1.0	-	6.952	0.045	0.824	-	104.9
47	10.00	1.0	-	1.915	0.072	0.766	-	97.5
48	10.00	1.0	-	3.170	0.079	0.776	-	98.8
49	10.00	1.0	-	5.317	0.184	0.712	-	90.7
50	15.00	0.1	-	1.238	0.000	0.319	-	40.6
51	15.00	0.1	-	0.188	0.000	0.311	-	39.6
52	15.00	0.1	-	1.348	0.010	0.330	-	42.0
53	15.00	0.1	-	0.000	0.017	0.252	-	32.1
54	15.00	0.1	-	0.167	0.017	0.271	-	34.5
55	15.00	0.1	-	0.000	0.000	0.274	-	34.9
56	15.00	0.2	-	4.885	0.006	0.710	-	90.4
57	15.00	0.2	-	5.029	0.015	0.753	-	95.9
58	15.00	0.2	-	6.906	0.000	0.556	-	70.8
59	15.00	0.2	-	2.582	0.003	0.661	-	84.2
60	15.00	0.2	-	5.563	0.010	0.669	-	85.2
61	15.00	0.2	-	3.200	0.053	0.684	-	87.1
62	15.00	0.5	-	5.030	0.123	1.249	-	159.0
63	15.00	0.5	-	5.182	0.058	1.224	-	155.8
64	15.00	0.5	-	4.764	0.076	0.974	-	124.0
65	15.00	0.5	-	7.629	0.060	1.015	-	129.2
66	15.00	0.5	-	5.791	0.142	0.968	-	123.2
67	15.00	0.5	-	4.227	0.323	1.137	-	144.8
68	15.00	1.0	-	2.359	0.092	1.454	-	185.1
69	15.00	1.0	-	8.947	0.076	1.579	-	201.0
70	15.00	1.0	-	6.840	0.043	1.489	-	189.6
71	15.00	1.0	-	10.585	0.099	1.180	-	150.2
72	15.00	1.0	-	6.114	0.158	1.125	-	143.2
73	15.00	1.0	-	3.680	0.304	1.287	-	163.9
74	20.00	0.1	-	0.566	0.024	0.485	-	61.8
75	20.00	0.1	-	0.000	0.038	0.502	-	63.9
76	20.00	0.1	-	2.529	0.030	0.471	-	60.0
77	20.00	0.1	-	0.882	0.045	0.406	-	51.7
78	20.00	0.1	-	3.227	0.036	0.467	-	59.5
79	20.00	0.1	-	4.177	0.020	0.506	-	64.4
80	20.00	0.2	-	2.212	0.019	0.785	-	99.9
81	20.00	0.2	-	5.856	0.048	0.733	-	93.3
82	20.00	0.2	-	6.065	0.026	0.646	-	82.3
83	20.00	0.2	-	4.665	0.023	0.654	-	83.3
84	20.00	0.2	-	3.390	0.012	0.693	-	88.2
85	20.00	0.2	-	3.124	0.073	0.623	-	79.3
86	20.00	0.5	-	7.382	0.109	1.357	-	172.8
87	20.00	0.5	-	5.552	0.092	1.190	-	151.5
88	20.00	0.5	-	6.088	0.149	1.244	-	158.4
89	20.00	0.5	-	7.662	0.141	1.163	-	148.1
90	20.00	0.5	-	4.781	0.170	1.045	-	133.1
91	20.00	0.5	-	6.400	0.110	1.049	-	133.6
92	20.00	1.0	-	6.183	0.116	1.604	-	204.2
93	20.00	1.0	-	2.012	0.084	1.525	-	194.2
94	20.00	1.0	-	5.143	0.089	1.339	-	170.5
95	20.00	1.0	-	5.453	0.126	1.258	-	160.2
96	20.00	1.0	-	4.824	0.168	1.367	-	174.1
97	20.00	1.0	-	5.376	0.323	1.377	-	175.3
98	23.00	0.1	-	4.629	0.002	0.941	-	119.8
99	23.00	0.1	-	1.598	0.000	0.966	-	123.0
100	23.00	0.1	-	4.373	0.026	0.903	-	115.0
101	23.00	0.1	-	6.766	0.037	0.952	-	121.2

102	23.00	0.1	-	6.375	0.095	1.223	-	155.7
103	23.00	0.1	-	1.826	0.015	0.880	-	112.0
104	23.00	0.2	-	2.309	0.042	1.038	-	132.2
105	23.00	0.2	-	6.176	0.050	1.079	-	137.4
106	23.00	0.2	-	5.642	0.071	0.971	-	123.6
107	23.00	0.2	-	6.901	0.049	1.001	-	127.5
108	23.00	0.2	-	7.319	0.000	1.050	-	133.7
109	23.00	0.2	-	4.596	0.000	1.058	-	134.7
110	23.00	0.5	-	4.608	0.131	1.693	-	215.6
111	23.00	0.5	-	9.217	0.124	1.704	-	217.0
112	23.00	0.5	-	7.826	0.244	1.612	-	205.2
113	23.00	0.5	-	6.308	0.168	1.636	-	208.3
114	23.00	0.5	-	4.551	0.130	1.618	-	206.0
115	23.00	0.5	-	5.128	0.180	1.589	-	202.3
116	23.00	1.0	-	10.837	0.274	1.817	-	231.3
117	23.00	1.0	-	11.114	0.115	1.923	-	244.8
118	23.00	1.0	-	12.644	0.067	1.837	-	233.9
119	23.00	1.0	-	12.432	0.029	2.230	-	283.9
120	23.00	1.0	-	5.497	0.199	1.789	-	227.8
121	23.00	1.0	-	3.621	0.216	1.897	-	241.5
Pulsed CO2 Laser								
122	1.00	0.1	50	0.000	0.000	0.000	-	0.0
123	1.00	0.1	50	0.000	0.000	0.000	-	0.0
124	1.00	0.1	50	0.000	0.000	0.000	-	0.0
125	1.00	0.1	50	0.000	0.000	0.000	-	0.0
126	1.00	0.1	50	0.000	0.000	0.000	-	0.0
127	1.00	0.1	50	0.000	0.000	0.000	-	0.0
128	1.00	0.2	50	0.000	0.000	0.000	-	0.0
129	1.00	0.2	50	0.000	0.000	0.000	-	0.0
130	1.00	0.2	50	0.000	0.000	0.000	-	0.0
131	1.00	0.2	50	0.000	0.000	0.000	-	0.0
132	1.00	0.2	50	0.000	0.000	0.000	-	0.0
133	1.00	0.2	50	0.000	0.000	0.000	-	0.0
134	1.00	0.5	50	6.381	0.000	0.000	-	0.0
135	1.00	0.5	50	1.812	0.000	0.000	-	0.0
136	1.00	0.5	50	0.000	0.000	0.000	-	0.0
137	1.00	0.5	50	0.000	0.000	0.000	-	0.0
138	1.00	0.5	50	0.000	0.000	0.000	-	0.0
139	1.00	0.5	50	0.000	0.000	0.000	-	0.0
140	1.00	1.0	50	0.000	0.000	0.000	-	0.0
141	1.00	1.0	50	0.000	0.000	0.000	-	0.0
142	1.00	1.0	50	0.000	0.000	0.000	-	0.0
143	1.00	1.0	50	1.436	0.000	0.000	-	0.0
144	1.00	1.0	50	0.000	0.000	0.000	-	0.0
145	1.00	1.0	50	0.000	0.000	0.000	-	0.0
146	2.00	0.1	100	0.000	0.000	0.000	-	0.0
147	2.00	0.1	100	0.000	0.000	0.000	-	0.0
148	2.00	0.1	100	0.000	0.000	0.000	-	0.0
149	2.00	0.1	100	0.000	0.000	0.000	-	0.0
150	2.00	0.1	100	0.000	0.000	0.000	-	0.0
151	2.00	0.1	100	0.000	0.000	0.000	-	0.0
152	2.00	0.2	100	0.000	0.000	0.000	-	0.0
153	2.00	0.2	100	0.000	0.000	0.000	-	0.0
154	2.00	0.2	100	0.000	0.000	0.000	-	0.0
155	2.00	0.2	100	0.000	0.000	0.000	-	0.0
156	2.00	0.2	100	0.400	0.000	0.000	-	0.0
157	2.00	0.2	100	0.000	0.000	0.000	-	0.0

158	2.00	0.5	100	0.000	0.000	0.000	-	0.0
159	2.00	0.5	100	0.000	0.000	0.000	-	0.0
160	2.00	0.5	100	0.000	0.000	0.000	-	0.0
161	2.00	0.5	100	0.000	0.000	0.000	-	0.0
162	2.00	0.5	100	0.000	0.000	0.000	-	0.0
163	2.00	0.5	100	0.000	0.000	0.000	-	0.0
164	2.00	1.0	100	4.913	0.000	0.000	-	0.0
165	2.00	1.0	100	6.005	0.020	0.000	-	0.0
166	2.00	1.0	100	7.000	0.000	0.000	-	0.0
167	2.00	1.0	100	6.304	0.000	0.000	-	0.0
168	2.00	1.0	100	2.420	0.000	0.000	-	0.0
169	2.00	1.0	100	6.381	0.000	0.000	-	0.0
170	3.00	0.1	150	0.000	0.000	0.000	-	0.0
171	3.00	0.1	150	0.000	0.000	0.000	-	0.0
172	3.00	0.1	150	3.989	0.000	0.000	-	0.0
173	3.00	0.1	150	0.872	0.000	0.000	-	0.0
174	3.00	0.1	150	1.141	0.000	0.000	-	0.0
175	3.00	0.1	150	2.353	0.000	0.000	-	0.0
176	3.00	0.2	150	2.000	0.000	0.000	-	0.0
177	3.00	0.2	150	0.000	0.000	0.000	-	0.0
178	3.00	0.2	150	2.341	0.000	0.000	-	0.0
179	3.00	0.2	150	1.044	0.000	0.000	-	0.0
180	3.00	0.2	150	3.266	0.000	0.000	-	0.0
181	3.00	0.2	150	0.908	0.000	0.000	-	0.0
182	3.00	0.5	150	3.677	0.000	0.000	-	0.0
183	3.00	0.5	150	5.014	0.145	0.000	-	0.0
184	3.00	0.5	150	1.899	0.000	0.000	-	0.0
185	3.00	0.5	150	7.882	0.000	0.000	-	0.0
186	3.00	0.5	150	6.746	0.000	0.000	-	0.0
187	3.00	0.5	150	3.968	0.000	0.000	-	0.0
188	3.00	1.0	150	7.605	0.134	0.000	-	0.0
189	3.00	1.0	150	7.240	0.054	0.000	-	0.0
190	3.00	1.0	150	8.071	0.037	0.000	-	0.0
191	3.00	1.0	150	15.897	0.024	0.000	-	0.0
192	3.00	1.0	150	15.400	0.029	0.000	-	0.0
193	3.00	1.0	150	14.668	0.007	0.000	-	0.0
194	4.00	0.1	200	0.000	0.000	0.000	-	0.0
195	4.00	0.1	200	2.968	0.000	0.000	-	0.0
196	4.00	0.1	200	0.000	0.000	0.000	-	0.0
197	4.00	0.1	200	0.000	0.000	0.000	-	0.0
198	4.00	0.1	200	0.000	0.000	0.000	-	0.0
199	4.00	0.1	200	0.000	0.000	0.000	-	0.0
200	4.00	0.2	200	5.072	0.000	0.000	-	0.0
201	4.00	0.2	200	8.627	0.000	0.000	-	0.0
202	4.00	0.2	200	6.945	0.000	0.000	-	0.0
203	4.00	0.2	200	5.045	0.000	0.000	-	0.0
204	4.00	0.2	200	1.738	0.000	0.000	-	0.0
205	4.00	0.2	200	0.000	0.000	0.000	-	0.0
206	4.00	0.5	200	21.162	0.000	0.000	-	0.0
207	4.00	0.5	200	23.387	0.026	0.000	-	0.0
208	4.00	0.5	200	23.024	0.000	0.000	-	0.0
209	4.00	0.5	200	24.096	0.000	0.000	-	0.0
210	4.00	0.5	200	24.081	0.025	0.000	-	0.0
211	4.00	0.5	200	25.292	0.031	0.000	-	0.0
212	4.00	1.0	200	10.028	0.073	0.000	-	0.0
213	4.00	1.0	200	9.010	0.074	0.000	-	0.0
214	4.00	1.0	200	23.483	0.086	0.000	-	0.0
215	4.00	1.0	200	21.727	0.048	0.000	-	0.0

216	4.00	1.0	200	22.949	0.152	0.000	-	0.0
217	4.00	1.0	200	23.129	0.111	0.000	-	0.0
218	4.75	0.1	250	4.859	0.000	0.000	-	0.0
219	4.75	0.1	250	2.164	0.000	0.000	-	0.0
220	4.75	0.1	250	7.314	0.000	0.000	-	0.0
221	4.75	0.1	250	8.050	0.000	0.000	-	0.0
222	4.75	0.1	250	10.081	0.000	0.000	-	0.0
223	4.75	0.1	250	5.566	0.000	0.000	-	0.0
224	4.75	0.2	250	11.205	0.000	0.000	-	0.0
225	4.75	0.2	250	7.191	0.000	0.000	-	0.0
226	4.75	0.2	250	11.071	0.000	0.000	-	0.0
227	4.75	0.2	250	9.042	0.068	0.000	-	0.0
228	4.75	0.2	250	15.167	0.007	0.000	-	0.0
229	4.75	0.2	250	14.129	0.000	0.000	-	0.0
230	4.75	0.5	250	8.147	0.085	0.000	-	0.0
231	4.75	0.5	250	8.692	0.141	0.000	-	0.0
232	4.75	0.5	250	7.639	0.137	0.000	-	0.0
233	4.75	0.5	250	17.509	0.079	0.000	-	0.0
234	4.75	0.5	250	15.207	0.098	0.000	-	0.0
235	4.75	0.5	250	19.125	0.072	0.000	-	0.0
236	4.75	1.0	250	7.094	0.332	0.000	-	0.0
237	4.75	1.0	250	5.967	0.248	0.000	-	0.0
238	4.75	1.0	250	5.119	0.221	0.000	-	0.0
239	4.75	1.0	250	6.395	0.158	0.000	-	0.0
240	4.75	1.0	250	6.325	0.177	0.000	-	0.0
241	4.75	1.0	250	5.867	0.192	0.000	-	0.0
242	5.25	0.1	300	3.250	0.000	0.000	-	0.0
243	5.25	0.1	300	5.079	0.000	0.000	-	0.0
244	5.25	0.1	300	14,159	0.000	0.000	-	0.0
245	5.25	0.1	300	10.143	0.000	0.000	-	0.0
246	5.25	0.1	300	0.975	0.000	0.000	-	0.0
247	5.25	0.1	300	5.090	0.000	0.000	-	0.0
248	5.25	0.2	300	11.107	0.056	0.000	-	0.0
249	5.25	0.2	300	11.352	0.082	0.000	-	0.0
250	5.25	0.2	300	14.285	0.079	0.000	-	0.0
251	5.25	0.2	300	20.334	0.000	0.000	-	0.0
252	5.25	0.2	300	16.732	0.017	0.000	-	0.0
253	5.25	0.2	300	19.398	0.008	0.000	-	0.0
254	5.25	0.5	300	17.827	0.062	0.000	-	0.0
255	5.25	0.5	300	10.976	0.064	0.011	-	1.4
256	5.25	0.5	300	26.185	0.056	0.000	-	0.0
257	5.25	0.5	300	24.337	0.103	0.000	-	0.0
258	5.25	0.5	300	22.751	0.095	0.000	-	0.0
259	5.25	0.5	300	14.117	0.154	0.000	-	0.0
260	5.25	1.0	300	5.792	0.143	0.061	-	7.8
261	5.25	1.0	300	6.404	0.141	0.242	-	30.8
262	5.25	1.0	300	11.934	0.128	0.110	-	14.0
263	5.25	1.0	300	13.703	0.219	0.000	-	0.0
264	5.25	1.0	300	9.459	0.000	0.000	-	0.0
265	5.25	1.0	300	6.611	0.258	0.000	-	0.0
266	6.00	0.1	350	7.633	0.032	0.000	-	0.0
267	6.00	0.1	350	7.010	0.023	0.000	-	0.0
268	6.00	0.1	350	3.658	0.051	0.019	-	2.4
269	6.00	0.1	350	5.877	0.068	0.099	-	12.6
270	6.00	0.1	350	14.341	0.000	0.000	-	0.0
271	6.00	0.1	350	9.845	0.000	0.000	-	0.0
272	6.00	0.2	350	6.782	0.048	0.177	-	22.5
273	6.00	0.2	350	1.878	0.025	0.149	-	19.0

274	6.00	0.2	350	4.336	0.042	0.083	-	10.6
275	6.00	0.2	350	12.187	0.083	0.000	-	0.0
276	6.00	0.2	350	8.203	0.135	0.000	-	0.0
277	6.00	0.2	350	15.224	0.000	0.000	-	0.0
278	6.00	0.5	350	4.755	0.211	0.000	-	0.0
279	6.00	0.5	350	5.000	0.147	0.123	-	15.7
280	6.00	0.5	350	3.340	0.171	0.133	-	16.9
281	6.00	0.5	350	5.093	0.218	0.040	-	5.1
282	6.00	0.5	350	7.328	0.000	0.000	-	0.0
283	6.00	0.5	350	5.573	0.239	0.000	-	0.0
284	6.00	1.0	350	7.136	0.258	0.107	-	13.6
285	6.00	1.0	350	6.925	0.280	0.000	-	0.0
286	6.00	1.0	350	2.645	0.297	0.000	-	0.0
287	6.00	1.0	350	3.804	0.306	0.000	-	0.0
288	6.00	1.0	350	3.636	0.147	0.000	-	0.0
289	6.00	1.0	350	1.192	0.246	0.000	-	0.0
290	7.00	0.1	400	5.603	0.034	0.000	-	0.0
291	7.00	0.1	400	10.565	0.016	0.000	-	0.0
292	7.00	0.1	400	12.816	0.000	0.000	-	0.0
293	7.00	0.1	400	9.004	0.039	0.000	-	0.0
294	7.00	0.1	400	14.522	0.000	0.000	-	0.0
295	7.00	0.1	400	15.672	0.000	0.000	-	0.0
296	7.00	0.2	400	5.503	0.193	0.052	-	6.6
297	7.00	0.2	400	14.684	0.049	0.000	-	0.0
298	7.00	0.2	400	6.977	0.094	0.044	-	5.6
299	7.00	0.2	400	3.723	0.430	0.099	-	12.6
300	7.00	0.2	400	21.815	0.015	0.000	-	0.0
301	7.00	0.2	400	13.430	0.100	0.000	-	0.0
302	7.00	0.5	400	10.439	0.122	0.165	-	21.0
303	7.00	0.5	400	11.678	0.134	0.000	-	0.0
304	7.00	0.5	400	8.634	0.183	0.116	-	14.8
305	7.00	0.5	400	10.927	0.228	0.000	-	0.0
306	7.00	0.5	400	14.621	0.194	0.000	-	0.0
307	7.00	0.5	400	13.907	0.224	0.000	-	0.0
308	7.00	1.0	400	5.647	0.181	0.295	-	37.6
309	7.00	1.0	400	5.202	0.183	0.000	-	0.0
310	7.00	1.0	400	6.715	0.180	0.000	-	0.0
311	7.00	1.0	400	5.258	0.284	0.000	-	0.0
312	7.00	1.0	400	3.807	0.318	0.000	-	0.0
313	7.00	1.0	400	1.118	0.337	0.000	-	0.0
314	7.50	0.1	450	5.181	0.028	0.065	-	8.3
315	7.50	0.1	450	7.680	0.051	0.123	-	15.7
316	7.50	0.1	450	9.442	0.024	0.011	-	1.4
317	7.50	0.1	450	12.782	0.000	0.000	-	0.0
318	7.50	0.1	450	13.595	0.000	0.000	-	0.0
319	7.50	0.1	450	10.612	0.022	0.000	-	0.0
320	7.50	0.2	450	2.711	0.007	0.251	-	32.0
321	7.50	0.2	450	5.819	0.019	0.177	-	22.5
322	7.50	0.2	450	2.176	0.027	0.347	-	44.2
323	7.50	0.2	450	5.823	0.084	0.233	-	29.7
324	7.50	0.2	450	6.704	0.095	0.226	-	28.8
325	7.50	0.2	450	6.059	0.136	0.195	-	24.8
326	7.50	0.5	450	5.392	0.141	0.409	-	52.1
327	7.50	0.5	450	3.407	0.037	0.020	-	2.5
328	7.50	0,5	450	4.901	0.239	0.377	-	48.0
329	7.50	0.5	450	2.888	0.152	0.558	-	71.0
330	7.50	0.5	450	6.972	0.181	0.168	-	21.4
331	7.50	0.5	450	3.998	0.213	0.301	-	38.3

332	7.50	1.0	450	5.123	0.089	0.155	-	19.7
333	7.50	1.0	450	1.600	0.146	0.443	-	56.4
334	7.50	1.0	450	2.635	0.988	0.327	-	41.6
335	7.50	1.0	450	6.021	0.291	0.000	-	0.0
336	7.50	1.0	450	5.055	0.297	0.000	-	0.0
337	7.50	1.0	450	3.960	0.275	0.099	-	12.6
Pulsed	***Nd-YAG***	***Laser***						
338	10.00	0.2	10	0.000	0.038	0.000	0.000	0.0
339	10.00	0.2	10	0.000	0.000	0.000	0.000	0.0
340	10.00	0.2	10	0.000	0.000	0.000	0.000	0.0
341	10.00	0.2	10	0.000	0.000	0.000	0.000	0.0
342	10.00	0.2	10	0.000	0.000	0.000	0.000	0.0
343	10.00	0.2	10	0.000	0.000	0.000	0.000	0.0
344	10.00	0.5	10	0.000	0.000	0.000	0.000	0.0
345	10.00	0.5	10	0.000	0.000	0.000	0.000	0.0
346	10.00	0.5	10	0.000	0.000	0.000	0.000	0.0
347	10.00	0.5	10	0.000	0.000	0.000	0.000	0.0
348	10.00	0.5	10	0.000	0.000	0.000	0.000	0.0
349	10.00	0.5	10	0.000	0.000	0.000	0.000	0.0
350	10.00	1.0	10	0.000	0.000	0.000	0.000	0.0
351	10.00	1.0	10	0.000	0.000	0.000	0.000	0.0
352	10.00	1.0	10	0.000	0.000	0.000	0.000	0.0
353	10.00	1.0	10	0.000	0.000	0.000	0.000	0.0
354	10.00	1.0	10	0.000	0.000	0.000	0.000	0.0
355	10.00	1.0	10	0.000	0.000	0.000	0.483	0.0
356	20.00	0.2	10	0.000	0.000	0.000	0.716	0.0
357	20.00	0.2	10	0.000	0.000	0.000	0.000	0.0
358	20.00	0.2	10	0.000	0.000	0.000	0.561	0.0
359	20.00	0.2	10	0.000	0.000	0.000	0.510	0.0
360	20.00	0.2	10	0.000	0.000	0.000	0.753	0.0
361	20.00	0.2	10	0.000	0.000	0.000	0.000	0.0
362	20.00	0.5	10	0.000	0.000	0.000	0.000	0.0
363	20.00	0.5	10	0.000	0.000	0.000	0.000	0.0
364	20.00	0.5	10	0.000	0.000	0.000	0.000	0.0
365	20.00	0.5	10	0.000	0.000	0.000	0.000	0.0
366	20.00	0.5	10	0.000	0.000	0.000	0.000	0.0
367	20.00	0.5	10	0.000	0.000	0.000	0.000	0.0
368	20.00	1.0	10	0.000	0.000	0.019	0.000	2.4
369	20.00	1.0	10	0.000	0.000	0.000	0.000	0.0
370	20.00	1.0	10	0.000	0.000	0.000	0.000	0.0
371	20.00	1.0	10	0.000	0.000	0.000	0.000	0.0
372	20.00	1.0	10	0.000	0.000	0.000	0.000	0.0
373	20.00	1.0	10	0.000	0.000	0.000	0.000	0.0
374	30.00	0.2	10	0.000	0.000	0.000	0.000	0.0
375	30.00	0.2	10	0.000	0.000	0.000	0.000	0.0
376	30.00	0.2	10	0.000	0.000	0.000	0.000	0.0
377	30.00	0.2	10	0.000	0.000	0.000	0.000	0.0
378	30.00	0.2	10	0.000	0.000	0.000	0.000	0.0
379	30.00	0.2	10	0.000	0.000	0.000	0.000	0.0
380	30.00	0.5	10	0.000	0.000	0.000	0.000	0.0
381	30.00	0.5	10	0.000	0.000	0.000	0.000	0.0
382	30.00	0.5	10	0.000	0.000	0.000	0.000	0.0
383	30.00	0.5	10	0.000	0.000	0.000	0.000	0.0
384	30.00	0.5	10	0.000	0.000	0.000	0.000	0.0
385	30.00	0.5	10	0.000	0.000	0.000	0.000	0.0
386	30.00	1.0	10	0.000	0.000	0.000	0.865	0.0
387	30.00	1.0	10	0.000	0.000	0.000	0.000	0.0

388	30.00	1.0	10	0.000	0.000	0.000	0.975	0.0
389	30.00	1.0	10	0.000	0.000	0.000	0.000	0.0
390	30.00	1.0	10	0.000	0.000	0.000	0.000	0.0
391	30.00	1.0	10	0.000	0.000	0.000	0.925	0.0
392	40.00	0.2	10	0.000	0.000	0.000	0.000	0.0
393	40.00	0.2	10	0.000	0.000	0.000	0.000	0.0
394	40.00	0.2	10	0.000	0.000	0.000	0.030	0.0
395	40.00	0.2	10	0.000	0.000	0.000	0.000	0.0
396	40.00	0.2	10	0.000	0.000	0.000	0.000	0.0
397	40.00	0.2	10	0.000	0.000	0.000	0.000	0.0
398	40.00	0.5	10	0.000	0.000	0.000	0.440	0.0
399	40.00	0.5	10	0.000	0.000	0.000	0.505	0.0
400	40.00	0.5	10	0.000	0.000	0.000	0.000	0.0
401	40.00	0.5	10	3.233	0.166	0.000	0.000	0.0
402	40.00	0.5	10	1.431	0.000	0.000	0.052	0.0
403	40.00	0.5	10	0.000	0.000	0.000	1.229	0.0
404	40.00	1.0	10	0.000	0.000	0.000	0.658	0.0
405	40.00	1.0	10	0.000	0.000	0.000	0.798	0.0
406	40.00	1.0	10	0.000	0.000	0.000	0.000	0.0
407	40.00	1.0	10	0.000	0.000	0.000	0.791	0.0
408	40.00	1.0	10	0.000	0.000	0.000	0.238	0.0
409	40.00	1.0	10	0.000	0.000	0.119	1.074	15.2
410	50.00	0.2	10	0.000	0.000	0.000	0.000	0.0
411	50.00	0.2	10	0.000	0.000	0.000	0.000	0.0
412	50.00	0.2	10	0.000	0.000	0.000	0.000	0.0
413	50.00	0.2	10	0.000	0.000	0.000	0.000	0.0
414	50.00	0.2	10	0.000	0.000	0.000	0.000	0.0
415	50.00	0.2	10	0.000	0.000	0.000	0.000	0.0
416	50.00	0.5	10	0.000	0.000	0.000	0.653	0.0
417	50.00	0.5	10	0.000	0.000	0.036	0.279	4.6
418	50.00	0.5	10	0.000	0.000	0.000	0.205	0.0
419	50.00	0.5	10	0.000	0.000	0.000	0.681	0.0
420	50.00	0.5	10	0.000	0.000	0.000	0.000	0.0
421	50.00	0.5	10	0.000	0.000	0.000	0.000	0.0
422	50.00	1.0	10	0.000	0.000	0.000	1.046	0.0
423	50.00	1.0	10	0.000	0.000	0.000	1.329	0.0
424	50.00	1.0	10	0.582	0.000	0.000	0.827	0.0
425	50.00	1.0	10	0.000	0.000	0.000	0.000	0.0
426	50.00	1.0	10	0.000	0.000	0.000	0.000	0.0
427	50.00	1.0	10	0.000	0.000	0.000	0.000	0.0
428	60.00	0.2	10	0.000	0.000	0.000	0.000	0.0
429	60.00	0.2	10	0.000	0.000	0.000	0.000	0.0
430	60.00	0.2	10	0.000	0.000	0.000	0.000	0.0
431	60.00	0.2	10	0.000	0.000	0.000	0.000	0.0
432	60.00	0.2	10	0.000	0.000	0.000	0.000	0.0
433	60.00	0.2	10	0.000	0.000	0.000	0.000	0.0
434	60.00	0.5	10	0.000	0.000	0.000	0.108	0.0
435	60.00	0.5	10	0.000	0.000	0.000	0.000	0.0
436	60.00	0.5	10	0.000	0.000	0.000	0.000	0.0
437	60.00	0.5	10	0.000	0.000	0.000	0.000	0.0
438	60.00	0.5	10	0.000	0.000	0.000	0.596	0.0
439	60.00	0.5	10	0.000	0.015	0.000	0.646	0.0
440	60.00	1.0	10	0.000	0.000	0.000	1.388	0.0
441	60.00	1.0	10	0.000	0.000	0.156	0.994	19.9
442	60.00	1.0	10	0.000	0.000	0.000	0.000	0.0
443	60.00	1.0	10	0.000	0.000	0.000	0.000	0.0
444	60.00	1.0	10	0.000	0.000	0.000	0.000	0.0
445	60.00	1.0	10	0.000	0.000	0.000	0.000	0.0

446	10.00	0.2	25	0.000	0.000	0.000	0.000	0.0
447	10.00	0.2	25	0.000	0.000	0.000	0.000	0.0
448	10.00	0.2	25	0.000	0.000	0.000	0.000	0.0
449	10.00	0.2	25	0.000	0.000	0.000	0.000	0.0
450	10.00	0.2	25	0.000	0.000	0.000	0.000	0.0
451	10.00	0.2	25	0.000	0.000	0.000	0.000	0.0
452	10.00	0.5	25	1.653	0.000	0.000	0.000	0.0
453	10.00	0.5	25	0.000	0.000	0.000	0.000	0.0
454	10.00	0.5	25	0.000	0.000	0.000	0.000	0.0
455	10.00	0.5	25	0.000	0.000	0.000	0.000	0.0
456	10.00	0.5	25	0.000	0.000	0.000	0.000	0.0
457	10.00	0.5	25	0.000	0.000	0.000	0.000	0.0
458	10.00	1.0	25	0.000	0.000	0.000	0.000	0.0
459	10.00	1.0	25	0.000	0.000	0.000	0.000	0.0
460	10.00	1.0	25	0.000	0.000	0.000	0.000	0.0
461	10.00	1.0	25	0.000	0.000	0.000	0.000	0.0
462	10.00	1.0	25	0.000	0.000	0.000	0.000	0.0
463	10.00	1.0	25	0.000	0.000	0.000	0.000	0.0
464	24.00	0.2	25	0.000	0.000	0.000	0.000	0.0
465	24.00	0.2	25	0.000	0.000	0.000	0.000	0.0
466	24.00	0.2	25	0.000	0.000	0.000	0.000	0.0
467	24.00	0.2	25	0.000	0.000	0.000	0.000	0.0
468	24.00	0.2	25	0.000	0.000	0.000	0.000	0.0
469	24.00	0.2	25	0.000	0.000	0.000	0.000	0.0
470	24.00	0.5	25	0.000	0.000	0.000	0.089	0.0
471	24.00	0.5	25	0.000	0.000	0.000	0.000	0.0
472	24.00	0.5	25	0.000	0.000	0.000	0.188	0.0
473	24.00	0.5	25	0.000	0.000	0.000	0.000	0.0
474	24.00	0.5	25	0.000	0.000	0.000	0.000	0.0
475	24.00	0.5	25	0.000	0.000	0.000	0.000	0.0
476	24.00	1.0	25	0.000	0.166	0.000	0.613	0.0
477	24.00	1.0	25	0.000	0.000	0.099	0.691	12.6
478	24.00	1.0	25	0.000	0.000	0.000	0.733	0.0
479	24.00	1.0	25	0.000	0.000	0.000	0.000	0.0
480	24.00	1.0	25	0.000	0.000	0.000	0.000	0.0
481	24.00	1.0	25	0.000	0.000	0.000	0.000	0.0
482	30.00	0.2	25	0.000	0.000	0.000	0.000	0.0
483	30.00	0.2	25	0.000	0.000	0.000	0.000	0.0
484	30.00	0.2	25	0.000	0.000	0.000	0.000	0.0
485	30.00	0.2	25	0.000	0.000	0.000	0.000	0.0
486	30.00	0.2	25	0.000	0.000	0.000	0.000	0.0
487	30.00	0.2	25	0.000	0.000	0.000	0.000	0.0
488	30.00	0.5	25	0.000	0.000	0.000	0.000	0.0
489	30.00	0.5	25	0.000	0.000	0.000	0.000	0.0
490	30.00	0.5	25	0.000	0.000	0.000	0.361	0.0
491	30.00	0.5	25	0.000	0.000	0.000	0.181	0.0
492	30.00	0.5	25	0.000	0.000	0.000	0.000	0.0
493	30.00	0.5	25	0.000	0.000	0.000	0.421	0.0
494	30.00	1.0	25	0.000	0.000	0.173	0.806	22.0
495	30.00	1.0	25	0.000	0.000	0.146	0.800	18.6
496	30.00	1.0	25	0.000	0.000	0.174	0.660	22.2
497	30.00	1.0	25	0.000	0.000	0.000	0.781	0.0
498	30.00	1.0	25	0.000	0.000	0.000	0.000	0.0
499	30.00	1.0	25	0.000	0.000	0.169	0.887	21.5
500	40.00	0.2	25	0.000	0.000	0.000	0.000	0.0
501	40.00	0.2	25	0.000	0.000	0.000	0.000	0.0
502	40.00	0.2	25	0.000	0.000	0.000	0.000	0.0
503	40.00	0.2	25	0.000	0.000	0.000	0.000	0.0

504	40.00	0.2	25	0.000	0.000	0.000	0.000	0.0
505	40.00	0.2	25	0.000	0.000	0.000	0.000	0.0
506	40.00	0.5	25	0.000	0.000	0.000	0.000	0.0
507	40.00	0.5	25	0.000	0.000	0.000	0.517	0.0
508	40.00	0.5	25	0.242	0.000	0.000	0.424	0.0
509	40.00	0.5	25	0.000	0.000	0.000	0.000	0.0
510	40.00	0.5	25	0.000	0.000	0.000	0.346	0.0
511	40.00	0.5	25	0.000	0.000	0.000	0.000	0.0
512	40.00	1.0	25	0.000	0.000	0.000	0.960	0.0
513	40.00	1.0	25	0.000	0.000	0.148	1.029	18.8
514	40.00	1.0	25	0.000	0.000	0.237	0.991	30.2
515	40.00	1.0	25	0.000	0.000	0.000	0.988	0.0
516	40.00	1.0	25	0.000	0.000	0.000	0.000	0.0
517	40.00	1.0	25	0.000	0.000	0.000	0.000	0.0
518	50.00	0.2	25	0.000	0.000	0.000	0.000	0.0
519	50.00	0.2	25	0.000	0.000	0.000	0.000	0.0
520	50.00	0.2	25	0.000	0.000	0.000	0.000	0.0
521	50.00	0.2	25	0.000	0.000	0.000	0.000	0.0
522	50.00	0.2	25	0.000	0.000	0.000	0.000	0.0
523	50.00	0.2	25	0.000	0.000	0.000	0.000	0.0
524	50.00	0.5	25	0.000	0.000	0.000	0.000	0.0
525	50.00	0.5	25	0.000	0.000	0.000	0.000	0.0
526	50.00	0.5	25	0.000	0.000	0.000	0.000	0.0
527	50.00	0.5	25	0.000	0.000	0.000	0.178	0.0
528	50.00	0.5	25	0.000	0.000	0.005	0.116	0.6
529	50.00	0.5	25	0.000	0.000	0.000	0.186	0.0
530	50.00	1.0	25	0.000	0.000	0.134	0.840	17.1
531	50.00	1.0	25	0.000	0.000	0.000	0.754	0.0
532	50.00	1.0	25	0.000	0.000	0.000	0.000	0.0
533	50.00	1.0	25	0.000	0.000	0.000	0.000	0.0
534	50.00	1.0	25	0.000	0.000	0.000	0.964	0.0
535	50.00	1.0	25	0.000	0.000	0.000	0.000	0.0
536	60.00	0.2	25	0.000	0.000	0.000	0.000	0.0
537	60.00	0.2	25	0.000	0.000	0.000	0.000	0.0
538	60.00	0.2	25	0.000	0.000	0.000	0.000	0.0
539	60.00	0.2	25	0.000	0.000	0.000	0.000	0.0
540	60.00	0.2	25	0.000	0.000	0.000	0.000	0.0
541	60.00	0.2	25	0.000	0.000	0.000	0.000	0.0
542	60.00	0.5	25	0.000	0.000	0.030	0.766	3.8
543	60.00	0.5	25	0.000	0.000	0.000	0.596	0.0
544	60.00	0.5	25	0.000	0.000	0.000	0.267	0.0
545	60.00	0.5	25	0.000	0.000	0.000	0.162	0.0
546	60.00	0.5	25	0.000	0.000	0.000	0.034	0.0
547	60.00	0.5	25	0.000	0.000	0.000	0.587	0.0
548	60.00	1.0	25	0.000	0.000	0.000	1.398	0.0
549	60.00	1.0	25	0.000	0.000	0.095	1.252	12.1
550	60.00	1.0	25	0.000	0.000	0.000	1.397	0.0
551	60.00	1.0	25	0.000	0.000	0.000	1.401	0.0
552	60.00	1.0	25	0.000	0.000	0.272	1.273	34.6
553	60.00	1.0	25	0.350	0.000	0.240	1.237	30.6
554	10.00	0.2	40	0.000	0.000	0.000	0.000	0.0
555	10.00	0.2	40	0.000	0.000	0.000	0.000	0.0
556	10.00	0.2	40	0.000	0.000	0.000	0.000	0.0
557	10.00	0.2	40	0.000	0.000	0.000	0.000	0.0
558	10.00	0.2	40	0.000	0.000	0.000	0.000	0.0
559	10.00	0.2	40	0.000	0.000	0.000	0.000	0.0
560	10.00	0.5	40	0.000	0.000	0.000	0.000	0.0
561	10.00	0.5	40	0.000	0.000	0.000	0.000	0.0

562	10.00	0.5	40	0.000	0.000	0.000	0.000	0.0
563	10.00	0.5	40	0.000	0.000	0.000	0.000	0.0
564	10.00	0.5	40	0.000	0.000	0.000	0.000	0.0
565	10.00	0.5	40	0.000	0.000	0.000	0.000	0.0
566	10.00	1.0	40	0.000	0.000	0.000	0.000	0.0
567	10.00	1.0	40	0.000	0.000	0.000	0.000	0.0
568	10.00	1.0	40	0.000	0.000	0.000	0.000	0.0
569	10.00	1.0	40	0.000	0.000	0.000	0.000	0.0
570	10.00	1.0	40	0.000	0.000	0.000	0.000	0.0
571	10.00	1.0	40	0.000	0.000	0.000	0.000	0.0
572	20.00	0.2	40	0.000	0.000	0.000	0.000	0.0
573	20.00	0.2	40	0.000	0.000	0.000	0.000	0.0
574	20.00	0.2	40	0.000	0.000	0.000	0.000	0.0
575	20.00	0.2	40	0.000	0.000	0.000	0.000	0.0
576	20.00	0.2	40	0.000	0.000	0.000	0.000	0.0
577	20.00	0.2	40	0.000	0.000	0.000	0.000	0.0
578	20.00	0.5	40	0.000	0.000	0.000	0.000	0.0
579	20.00	0.5	40	0.000	0.000	0.000	0.000	0.0
580	20.00	0.5	40	0.000	0.000	0.000	0.000	0.0
581	20.00	0.5	40	0.000	0.000	0.000	0.000	0.0
582	20.00	0.5	40	0.000	0.000	0.000	0.000	0.0
583	20.00	0.5	40	0.000	0.000	0.000	0.000	0.0
584	20.00	1.0	40	0.000	0.000	0.000	0.000	0.0
585	20.00	1.0	40	0.000	0.000	0.000	0.000	0.0
586	20.00	1.0	40	0.000	0.000	0.000	0.000	0.0
587	20.00	1.0	40	0.000	0.000	0.000	0.000	0.0
588	20.00	1.0	40	0.000	0.000	0.000	0.000	0.0
589	20.00	1.0	40	0.000	0.000	0.000	0.000	0.0
590	30.00	0.2	40	0.000	0.000	0.000	0.000	0.0
591	30.00	0.2	40	0.000	0.000	0.000	0.000	0.0
592	30.00	0.2	40	0.000	0.000	0.000	0.000	0.0
593	30.00	0.2	40	0.000	0.000	0.000	0.000	0.0
594	30.00	0.2	40	0.000	0.000	0.000	0.000	0.0
595	30.00	0.2	40	0.000	0.000	0.000	0.000	0.0
596	30.00	0.5	40	0.000	0.000	0.000	0.000	0.0
597	30.00	0.5	40	0.000	0.000	0.000	0.000	0.0
598	30.00	0.5	40	0.000	0.000	0.000	0.000	0.0
599	30.00	0.5	40	0.000	0.000	0.000	0.000	0.0
600	30.00	0.5	40	0.000	0.000	0.000	0.000	0.0
601	30.00	0.5	40	0.000	0.000	0.000	0.000	0.0
602	30.00	1.0	40	0.000	0.000	0.000	0.563	0.0
603	30.00	1.0	40	0.000	0.000	0.000	0.539	0.0
604	30.00	1.0	40	0.790	0.000	0.066	0.689	8.4
605	30.00	1.0	40	0.289	0.000	0.000	0.030	0.0
606	30.00	1.0	40	0.000	0.000	0.000	0.000	0.0
607	30.00	1.0	40	0.000	0.000	0.000	0.000	0.0
608	40.00	0.2	40	0.581	0.000	0.000	0.000	0.0
609	40.00	0.2	40	0.000	0.000	0.000	0.000	0.0
610	40.00	0.2	40	0.000	0.000	0.000	0.000	0.0
611	40.00	0.2	40	0.000	0.000	0.000	0.000	0.0
612	40.00	0.2	40	0.000	0.000	0.000	0.000	0.0
613	40.00	0.2	40	0.000	0.000	0.000	0.000	0.0
614	40.00	0.5	40	1.213	0.000	0.000	0.050	0.0
615	40.00	0.5	40	0.000	0.000	0.000	0.000	0.0
616	40.00	0.5	40	0.000	0.000	0.000	0.000	0.0
617	40.00	0.5	40	0.000	0.000	0.000	0.000	0.0
618	40.00	0.5	40	0.000	0.000	0.000	0.000	0.0
619	40.00	0.5	40	0.000	0.000	0.000	0.000	0.0

620	40.00	1.0	40	0.000	0.000	0.000	0.772	0.0
621	40.00	1.0	40	1.397	0.006	0.000	0.000	0.0
622	40.00	1.0	40	0.000	0.000	0.000	0.000	0.0
623	40.00	1.0	40	0.000	0.000	0.000	0.773	0.0
624	40.00	1.0	40	0.000	0.000	0.104	0.862	13.2
625	40.00	1.0	40	0.000	0.000	0.000	0.000	0.0
626	50.00	0.2	40	0.000	0.000	0.000	0.000	0.0
627	50.00	0.2	40	0.000	0.000	0.000	0.000	0.0
628	50.00	0.2	40	0.000	0.000	0.000	0.000	0.0
629	50.00	0.2	40	0.000	0.000	0.000	0.000	0.0
630	50.00	0.2	40	0.000	0.000	0.000	0.000	0.0
631	50.00	0.2	40	0.000	0.000	0.000	0.000	0.0
632	50.00	0.5	40	0.000	0.000	0.000	0.000	0.0
633	50.00	0.5	40	0.000	0.000	0.000	0.000	0.0
634	50.00	0.5	40	0.000	0.000	0.000	0.000	0.0
635	50.00	0.5	40	0.000	0.000	0.000	0.000	0.0
636	50.00	0.5	40	0.000	0.000	0.000	0.000	0.0
637	50.00	0.5	40	0.000	0.000	0.000	0.724	0.0
638	50.00	1.0	40	0.000	0.000	0.000	0.752	0.0
639	50.00	1.0	40	0.000	0.000	0.000	0.000	0.0
640	50.00	1.0	40	0.000	0.000	0.000	0.504	0.0
641	50.00	1.0	40	0.000	0.000	0.000	1.061	0.0
642	50.00	1.0	40	0.000	0.000	0.000	0.000	0.0
643	50.00	1.0	40	0.000	0.000	0.076	0.911	9.7
644	60.00	0.2	40	0.000	0.000	0.000	0.000	0.0
645	60.00	0.2	40	0.000	0.000	0.000	0.000	0.0
646	60.00	0.2	40	0.000	0.000	0.000	0.000	0.0
647	60.00	0.2	40	0.000	0.000	0.000	0.000	0.0
648	60.00	0.2	40	0.000	0.000	0.000	0.000	0.0
649	60.00	0.2	40	0.000	0.000	0.000	0.000	0.0
650	60.00	0.5	40	0.000	0.000	0.000	0.185	0.0
651	60.00	0.5	40	0.000	0.000	0.000	0.398	0.0
652	60.00	0.5	40	0.000	0.000	0.000	0.000	0.0
653	60.00	0.5	40	0.000	0.000	0.164	0.890	20.9
654	60.00	0.5	40	0.000	0.000	0.000	0.434	0.0
655	60.00	0.5	40	0.000	0.000	0.000	0.198	0.0
656	60.00	1.0	40	0.000	0.000	0.096	0.952	12.2
657	60.00	1.0	40	1.050	0.000	0.168	1.094	21.4
658	60.00	1.0	40	0.000	0.000	0.000	1.184	0.0
659	60.00	1.0	40	1.506	0.000	0.305	1.166	38.8
660	60.00	1.0	40	0.190	0.000	0.209	1.010	26.6
661	60.00	1.0	40	0.000	0.000	0.090	1.003	11.5